☐ 9月期修了
☑ 3月期修了

博士論文提出届

2023 年　01 月　12 日

神奈川大学大学院

工学　研究科委員長　殿

工学　研究科　工学　専攻

（　経営工学　領域）

博士後期課程　3 年次

学籍番号　202070185

氏　名　モハッマドマスドゥルラホマン　印

指導教授　吉田 稔　印

神奈川大学学位規程第５条第１項第１号の規定に基づき、下記題目の博士論文を提出いたします。

記

論文題名言語：　日本語・(英語)・その他（　　）

論文言語：　日本語・(英語)・その他（　　）

博士論文題目【和文】

主題	**超関数理論を用いた工学的手法による不整脈診断システム**
副題	

博士論文題目【英文】

主題	Arrhythmia Diagnosis System by the Engineering Methods through the Generalized Function Theories
副題	

提出部数　7　部（正本：　2　部、副本：　5　部）

以　上

超関数理論を用いた工学的手法による不整脈診断システム

202070185 モハッマドマスドウルラホマン

要 旨

心臓の異常なリズムを不整脈と言い、深刻な場合は、それにより患者は突然死に至ることがある。自動体外式除細動器（AED）とは、不整脈（自動）診断システムの一つであり、患者の不整脈の検出と、その結果を受けて電気的ショックを与えることにより、心臓の細動（不整脈）を取り除く装置である。正確な診断を下し、迅速な作動の決定を行うアルゴリズムが与えられたAED装置の適用により患者の生存率は高くなる。従って、AEDによる正確な診断と迅速な判断が患者の生存率の向上には、不可欠である。

AEDにおける診断精度の向上には、心電図に含まれる異常信号の特徴量を正確に抽出する必要がある。ガボールウェーブレット変換(GWT) は、正常な信号と異常な信号を適切に区別するための有効な応用数学的”時間-周波数“変換である。いくつかの先行研究では、この変換に基づいて作成される”時間-周波数-振幅（エネルギー）“のグラフ（スカログラム）に基づき、細動（不整脈）を除去するために電気的ショックを当該患者に与えるべきや、否やの判断を行うアルゴリズムが研究されている。しかしながら、例えば、PEAと呼ばれる不整脈と、VFと呼ばれる不整脈については、これらそれぞれに対応する通常のガボールウェーブレット変換に基づくスカログラムは非常に似通っており、両者の区別は困難であった。さらに、深刻な状況としては、PEAの患者に対しては、電気的ショックによる除細動は危険（ショックを与えるべきではない）であり、一方で、VFの患者には速やかに電気的ショックによる除細動を行うべきであることが知られている。

本論文では、上述の識別困難な不整脈の識別精度の向上についての提案を行う。具体的には、AEDによる不整脈診断システムに対し、次の２つの新しい提案を行う。結果として、これにより、不整脈患者の生存率の向上が望まれる。

第１に、擬似微分様演算子と非線形変換関数を組み込んだGWT を提案する。これに基づき、（電気的）ショックを与えるべき不整脈信号とそうすべきでない不整脈信号を、これまでのGWTによるよりも明確に区別で

きる（改良）スカログラムが作成される。ここでは、擬微分作用素を伴うGWTの結果に、適切な非線形関数で変換することにより、上述の改良スカログラムを導出している。

第２に、上記第１により得られたスカログラムから適切な複数の統計的特徴量を抽出し、それに基づき位相的分類機により、異なる種類の不整脈を分類する。ここでは、既存の最近傍法（初等的なユークリッド距離に基づく位相）としてしられる分類機を改良し、当該問題により適した距離関数（非ユークリッド的距離）により定まる分類機を提案し、これを適用している。結果として、既存の最近傍法による分類（特に、上述のPEAとVFとの識別）よりも高精度の分類が可能となっている。
最終的に、異常なクラスにおける（電気的）ショックを与えるべき不整脈とショックを与えるべきではない不整脈とを区別するために本論文において提案された方法の有効性が、データセットに関する数値実験により示された。

キーワード: 心電図, ガボールウェーブレット変換, 疑似微分演算子, スカログラム, 正規化スペクトルインデックス, 正規化時間インデックス, 統計的手法, 位相空間.

Arrhythmia Diagnosis System by the Engineering Methods through the Generalized Function Theories

202070185 MD. MASUDUR RAHMAN

Abstract

Arrhythmia is an abnormal rhythm of the heart which leads to sudden death. The automated external defibrillator (AED) is the arrhythmia diagnosis system, and it requires an accurate and quick decision algorithm to increase the survival rate. Therefore, precision and quick decision by the AED has become essential in improving the survival rate.

To increase the precision of the AED, it is important to extract accurate information (scalogram) from the abnormal ECG signals. The Gabor wavelet transform (GWT) is a powerful time-frequency method that gives a good distinction between normal and abnormal signals. However, it does not achieve enough discrimination between shockable and non-shockable arrhythmias in the abnormal class signals due to generating the same level of coefficient values. The same level of coefficient values over time gives a barrier to getting the best distinction by the decision algorithm. In addition, various decision methods are applied to distinguish the arrhythmias in the decision stage. However, blindly use of such general methods is not the best for considering our problems. For example, the decision becomes changed for selecting the different number of neighbors of the test sample of the Euclidean metric function-based method. Also, many methods require a substantial computation time to generate the decision is not practical for diagnosis purposes. Therefore, an accurate and rapid decision method is the ultimate demand for the safety and performance of an AED.

This dissertation addresses the above issues and proposes two methods to increase the survival rate by enhancing the arrhythmias diagnosis system in the AED.

First, the GWT with pseudo-differential-like operators and non-linear transformation function-based method is proposed to generate an accurate scalogram for shockable and non-shockable arrhythmias signals. Then, we performed qualitative and quantitative evaluations to select the best pair of pseudo-differential-like operators with non-linear transformation function. A good discrimination performance in the decision algorithm is guaranteed through the best pair chosen.

Second, we develop a simple decision method in the general topological space (a new metric function is adopted) to guarantee high accuracy and quick decision between shockable and non-shockable arrhythmias. Numerical experimental results on datasets show the efficiency of the proposed methods for shockable and non-shockable arrhythmias distinction in the abnormal classes.

Keywords: Electrocardiograms, Gabor wavelet transform, pseudo differential operator, scalogram, normalized spectrum index, normalized time index, statistical method, topological space.

Doctoral Dissertation

Arrhythmia Diagnosis System by the Engineering Methods through the Generalized Function Theories

MD. MASUDUR RAHMAN

Field of Industrial Engineering and Management
Course of Engineering
Graduate School of Engineering
Kanagawa University

A thesis submitted in partial fulfillment of the requirements for the degree of
Doctor of Philosophy

March 2023

Arrhythmia Diagnosis System by the Engineering Methods through the Generalized Function Theories

MD. MASUDUR RAHMAN

Abstract

Arrhythmia is an abnormal rhythm of the heart which leads to sudden death. The automated external defibrillator (AED) is the arrhythmia diagnosis system, and it requires an accurate and quick decision algorithm to increase the survival rate. Therefore, precision and quick decision by the AED has become essential in improving the survival rate.

To increase the precision of the AED, it is important to extract accurate information (scalogram) from the abnormal ECG signals. The Gabor wavelet transform (GWT) is a powerful time-frequency method that gives a good distinction between normal and abnormal signals. However, it does not achieve enough discrimination between shockable and non-shockable arrhythmias in the abnormal class signals due to generating the same level of coefficient values. The same level of coefficient values over time gives a barrier to getting the best distinction by the decision algorithm. In addition, various decision methods are applied to distinguish the arrhythmias in the decision stage. However, blindly use of such general methods is not the best for considering our problems. For example, the decision becomes changed for selecting the different number of neighbors of the test sample of the Euclidean metric function-based method. Also, many methods require a substantial computation time to generate the decision is not practical for diagnosis purposes. Therefore, an accurate and rapid decision method is the ultimate demand for the safety and performance of an AED.

This dissertation addresses the above issues and proposes two methods to increase the survival rate by enhancing the arrhythmias diagnosis system in the AED.

First, the GWT with pseudo-differential-like operators and non-linear transformation function-based method is proposed to generate an accurate scalogram for shockable and non-shockable arrhythmias signals. Then, we performed qualitative and quantitative evaluations to select the best pair of pseudo-differential-like operators with non-linear transformation function. A good discrimination performance in the decision algorithm is guaranteed through the best pair chosen.

Second, we develop a simple decision method in the general topological space (a new metric function is adopted) to guarantee high accuracy and quick decision between shockable and non-shockable arrhythmias. Numerical experimental results on datasets show the efficiency of the proposed methods for shockable and non-shockable arrhythmias distinction in the abnormal classes.

Keywords: Electrocardiograms, Gabor wavelet transform, pseudo differential operator, scalogram, normalized spectrum index, normalized time index, statistical method, topological space.

Acknowledgments

First and foremost, praises and thanks to the almighty Allah, for his showers of blessing throughout my research work to complete the research successfully.

With deep sense of gratitude I express my sincere thanks and acknowledge to my esteemed supervisor Professor Minoru W. Yoshida, Graduate School of Engineering, Kanagawa University, who has provided valuable guidance in carrying out this work under his effective supervision, encouragement, enlightenment and cooperation. I was and will be truly honored to be his student for my whole lifetime.

I am extremely grateful for the guidance of co-supervisors, Professor Nobuaki Ishii, and Professor Hideki Katagiri, Department of Industrial Engineering and Management, Graduate School of Engineering, Kanagawa University, and Professor Masanori Akiyoshi and Professor Takamasa Imai, Department of Information Systems Creation, Graduate School of Engineering, Kanagawa University, for their encouragement, support, valuable advice, comments and reliance throughout the research. This thesis is completed through their proper direction and numerous stimulating discussion.

I would like to express my sincere gratitude to professor Sergio Albeverio, Bonn University, Germany, Professor Shuji Kawasaki, Faculty of Science and Engineering, Iwate University, Professor Hidetoshi Oya, Takayuki Okai, Faculty of Information Engineering, Tokyo City University, Professor Yumi Yahagi, Department of Mathematical Informatics, Tokyo University of Information Science, Assistant professor Toshinao Kagawa, Assistant professor Shunya nagai, Department of Information Systems Creation, Kanagawa University for their instructive instruction and fruitful suggestions at the co-author's section meeting.

I am also gratefully acknowledge to professor L. Accardi, Rome University for his valuable suggestions at the QBIC Conference, Tokyo University of Science in October 2020. Also gratefully acknowledge to professor Sergio Albeverio, Bonn University for the instructive comments at the meeting of the operation research society of Japan held at Sofia University in January 2021. I would like to acknowledge to the Japan Society for Simulation Technology (JSST) conference committee held at Kyoto University in 2021 and at Kyushu Institute of Technology in 2022. Also, i would like to say thanks to professor Nagase, physiology of Takarazuka Medical

University, and Dr. Oana, physician of Nishi Saitama chou national hospital for their warm encouragements.

My gratitude also extend to the Ministry of Education, Culture, Sports, Science and Technology (MEXT, Monbukagakusho scholarship) for financial support. The ministry of Japanese government provided scholarship for my Doctoral program.

I would like to say thanks to my friends for their encouraging, help and support during my Doctoral studies.

I am extremely grateful to my parents for their love, prayers, caring and sacrifices for educating and preparing me for my future. I am very much thankful to my wife for her love, understanding, prayers and continuing support to complete this research work. Also I express my thanks to my sisters, brother, and brother in laws for their support and valuable prayers.

Finally, my thanks go to all the people who have supported me to complete the research work directly or indirectly.

Contents

List of Figures

List of Tables

Nomenclature

List of Abbreviations

ACF	Auto-correlation function
ACLS	Advanced cardiac life support
AED	Automatic external defibrillator
AHA	American heart association
AICD	Automatic implantable cardioverter-defibrillator
ANFIS	Adaptive neuro fuzzy interface system
ANN	Artificial neural networks
AR	Autoregressive modeling
BAM	Bin area method
BbNN	Block-based neural network
BSWFM	Bounded sum of weighted fuzzy membership functions
CNN	Convolutional neural networks
CPR	Cardiopulmonary resuscitation
CUDB	Creighton university ventricular tachyarrhythmia database
CVDs	Cardiovascular diseases
CWA	Correlation waveform analysis
CWT	Continuous wavelet transform

DAM	Derivative area method
DNN	Deep neural networks
DWT	Discrete wavelet transform
ECG	Electrocardiogram
EMS	Emergency medical services
FFT	First Fourier Transform
Fs	Sampling frequency
GWT	Gabor wavelet transform
HWT	Haar wavelet transform
ICA	Independent component analysis
IQR	Interquartile range
KNN	K-nearest neighbor
LDA	Linear discriminant analysis
LSTM	Long-short term memory
MITDB	Massachusetts institute of technology database
NC	Normal control
NDOA	Normalized difference of area
NSI	Normalized spectrum index
NTI	Normalized time index
PCA	Principal component analysis
PEA	Pulseless electrical activity
*PNN*50(%)	Adjacent RR intervals that differ by more than 50ms
PNN	Probabilistic neural network
PTABT	percent of time above or below thresholds

PVCs	Premature ventricular contractions
RCWT	Raised cosine wavelet transform
RMS	Root mean square
RMSSD	Root mean square difference between RR intervals of neighboring beats
ROC	Receiver operating characteristic
SCA	Sudden cardiac arrest
SDW	Scale distribution width
SR	Sinus rhythm
STD	Standard deviation
SVD	Singular value decomposition
SVM	Support vector machine
TCI	Threshold crossing interval
TFD	Time-frequency distributions
TVD	Total variation denoising
VF	Ventricular fibrillation
VFDB	Ventricular fibrillation database
VT	Ventricular tachaycardia
WPT	Wavelet package transform

List of Symbols and Variables

$(a+bt)$	Linear term of the signal
$(Wf)(a,b)$	Wavelet transform
$f'(t)$	Differentiation of the signal
$\hat{f}(\xi)$	Fourier transform

λ	Scale factor
μ_{NSI}	Mean of NSI
μ_{NTI}	Mean of NTI
$\psi(t)$	Wavelet function
ρ	Distance
a	Scale parameter
b	shift parameter
$d_p^{(m)}$	Bin width of the histogram
$E(a,b)$	Energy of the scalogram
f	Signal
$F(a)$	Scalogram frequency
$H(\cdot)$	Non-linear transformation function
K_{NSI}	Kurtosis of NSI
K_{NTI}	Kurtosis of NTI
$L(a)$	Pseudo-differential like operators
M_{NSI}	Mode of NSI
M_{NTI}	Mode of NTI
$NSI(a)$	Normalized spectrum index in the time
$NSI(b)$	Normalized spectrum index in the frequency
$NTI(a)$	Normalized time index in the time
$NTI(b)$	Normalized time index in the frequency
$p(t)$	Polynomial coefficients
P_{NSI}	Power of NSI
P_{NTI}	Power of NTI

r	Number of selected feature
S_b	Between-class scatter matrix
S_{NSI}	Slope of NSI
S_{NTI}	Slope of NTI
S_w	Within-class scatter matrix
$T(b)$	Scalogram time
V_{NSI}	Variance of NSI
V_{NTI}	Variance of NTI
$W_p^{(m)}(x)$	Weight of the histogram
$X_{L,\cdot}^G$	Training dataset
$X_{T,\cdot}$	Testing dataset
$\mathcal{F}^{-1}$	Fourier inverse transform
$\mathbb{R}$	Set of Real number
EBI_{NSI}	Entropy-based index of NSI
EBI_{NTI}	Entropy-based index of NTI
SK_{NSI}	Skewness of NSI
SK_{NTI}	Skewness of NTI
t	time

1

Introduction

Arrhythmia is a heart disease when the heart does not beat in the systematic way. Any beat outside of normal or a lack of beat is considered an arrhythmia. Among these arrhythmias, some are shockable, and some are non-shockable arrhythmias with external defibrillation. The shockable arrhythmias lead to sudden death. These rhythms are monitored by the Electrocardiogram (ECG). The ECG is an efficient noninvasive investigative tool that provides useful information on the various states of the heart, and this information is used for the discrimination of diseases and treatment planning of the patients [1]. Over the past decades, many ECG signal analysis algorithms have been developed for the arrhythmia distinction in the automated diagnosis system. The automated external defibrillator (AED) is used as the

automated arrhythmia diagnosis system, and it requires an accurate and quick decision algorithm for the classification of different types of arrhythmias. Despite the improvement of the algorithm, a large number of people die because of the delay or errors in diagnosis by the AED. However, in order to improve the survival rate of the patients presenting with heart attack symptoms, it is important to develop accurate and quick discrimination procedures of typical features of the ECG signals for each of the symptoms.

The rest of this chapter is organized as follows: Section 1.1 presents the research background regarding the necessity of arrhythmia diagnosis by the AED to increase the survival rate of the patients. Section 1.2 shows the research scope and significant issues in the arrhythmia diagnosis system of the AED, followed by section 1.3 briefly introduces the objectives of our entire research work. Section 1.4 highlights the contributions and the list of publications, and conferences generated from our research. Section 1.5 presents proposed structure of the arrhythmia diagnosis system. Finally, the outline of the thesis is presented in section 1.6.

1.1 Motivation

1.1.1 Needs of arrhythmia diagnosis

Arrhythmia diagnosis is essential in the aspect of a healthy life. Arrhythmia can lead to life-threatening complications. The lack of understanding about arrhythmias prevents the doctor for an accurate diagnosis. Different arrhythmias need different treatments, and diagnosing the precise type of arrhythmia is crucially important. Sudden cardiac death is sometimes caused by fatal arrhythmias. With a very high rate of the sudden death, the cardiovascular diseases are observed. Indeed, the statistics reported by World Health Organization indicate clearly that the cardiac arrhythmia is the main reason, with 32% of the sudden death, over the world [2].

In particular, every year more than 50,000 people die due to sudden cardiac arrest (SCA) in Japan [3]; At the same time, 0.65 million of the deaths in USA [4], and 1.8 million of the deaths in Europe are caused by the cardiovascular diseases [5]. Therefore, there is a possibility to increase the survival rate through arrhythmia diagnosis. The country-wise death statistics by cardiovascular diseases (CVDs) are shown in Figure 1.1

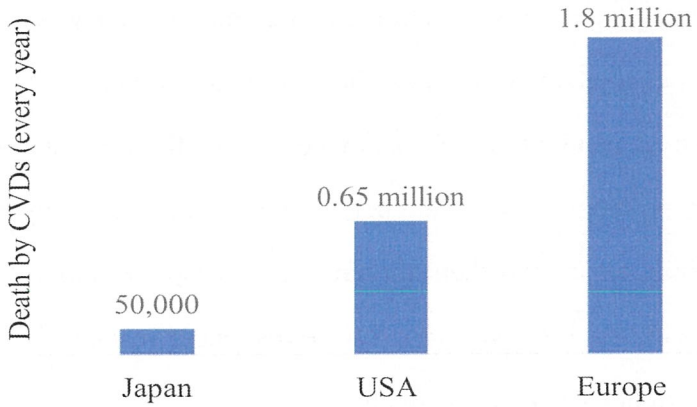

Figure 1.1: The country-wise death statistics by CVDs

1.1.2 The chain of survival

Many research have been conducted about how to improve the generally low survival rates from the sudden cardiac arrest. In early 1990, the American Heart Association established six links in the chain of survival metaphor to describe the sequence of actions for a successful resuscitation in the event of an out-of-hospital cardiac arrest [6]. Also, the International Liaison Committee on Resuscitation introduced the chain of survival concept in early 2000 [7]. Originally it consists of four steps in this order: early access to emergency medical care, early cardiopulmonary resuscitation (CPR), early defibrillation, and early advanced cardiac life support (ACLS). The four main interdependent sequences of the chain of survival are depicted in Figure 1.2.

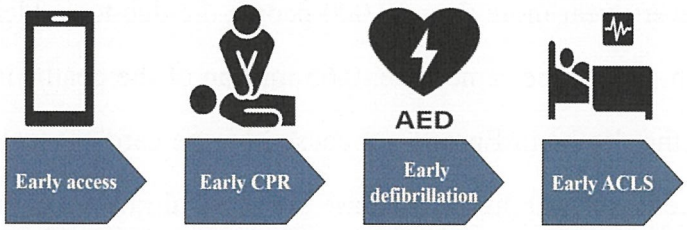

Figure 1.2: The chain of survival, and its four interdependent links based on the AHA guidelines

i) **Early access.** The resuscitation chain starts with early access, which includes all steps between initiating the cardiac arrest and the arrival of emergency medical services (EMS) personnel. First, the treatment of any emergency is to be recognized by the person with symptoms or by a witness that an emergency exists and then phoning the appropriate emergency response number to activate the EMS. Finally, the responder reaches the scene and locates the patient to provide adequate care.

ii) **Early CPR.** The second link in the chain of survival is early CPR. At the time of cardiac arrest, it is possible to start the flow of oxygen in the heart using CPR. CPR consists of chest compressions and ventilations that maintain a minimal blood flow to sustain sufficient perfusion before the arrival of the EMS personnel. Early CPR increases the chances of survival, but it alone cannot save an SCA victim.

iii) **Early defibrillation.** When sudden cardiac arrest occurs, the heart must be restarted by an electrical shock called defibrillation. In an out of hospital setting, the only way to restart the heart is by using an automated external defibrillator (AED). The AED is a portable user-friendly device that analyzes the victim's ECG to determine whether a shockable rhythm is present. When an AED is used and electrodes are placed on the victim's chest, electricity flows from the electrodes through the chest to the heart.

iv) **Early ACLS.** The last link in the sequence of chain of survival is early ad-

vanced cardiac life support (ACLS). The ACLS treatment provided by qualified health care personnel after defibrillation. ACLS includes intubation and the administration of medication.

1.1.3 Importance of accurate and early defibrillation

In the chain of survival, defibrillation is most important for increasing the survival rate. Because defibrillation (i.e., to give a shock) is the only way to restart a heart in cardiac arrest. The automated external defibrillator (AED) is used to the arrhythmia patients for first aid. Accurate and early diagnosis by the AED improves the survival rate [8]. In the AED operation, the ECG signals are analyzed to judge whether the defibrillation by the AED should be applied or not. The vital problem of the AED is distinguishing shockable and non-shockable arrhythmias precisely in the abnormal class of the ECG signals. The abnormal classes of ECG signals, ventricular fibrillation (VF) and ventricular tachycardia (VT) are the shockable arrhythmias which require defibrillation to restart the heart for normal electrical function. In contrast, defibrillation must not be applied for pulseless electrical activity (PEA), which is a non-shockable arrhythmia. If AED applied the shock to the patient with the PEA arrhythmia, then it would harm the patient's heart [9]. Therefore, the accurate discrimination of the shockable and non-shockable arrhythmias in the abnormal classes is crucially important.

Timely treatment can be a matter of saving a life. The survival rates in SCA are explained by two important variables: the time intervals from cardiac arrest to CPR and from cardiac arrest to defibrillation. If CPR and defibrillation are not administered, the survival rates in cardiac arrest decrease by 7% to 10% with every minute [10]. On the contrary, when CPR and defibrillation are provided, the decrease is smaller; it averages 3% to 4% for every minute [11, 12, 13]. When immediate access to defibrillation is available, the survival rates are very high. For

instance, survival rates greater than 90% have been reported for patients defibrillated within the first minute of cardiac arrest [14]. The statistics shown in Figure 1.3 summarize the importance of early defibrillation. After cardiac arrest, if the CPR starts within 5 minutes and defibrillation occurs within 10 minutes, then there is a 37% possibility of survival. The CPR begins within 5 minutes, and the survival rate is decreased rapidly without defibrillation occurring within 10 minutes.

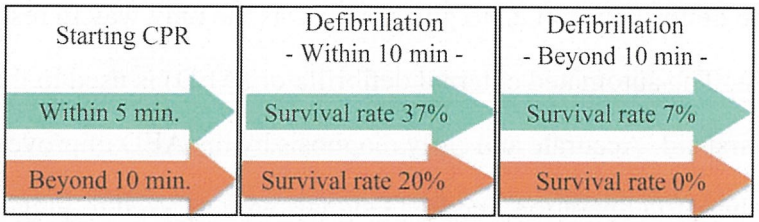

Figure 1.3: The importance of early defibrillation by AED

1.2 Research scope and issues

The scope of this study is to perform arrhythmia diagnosis by the AED in regards to increasing the survival rate from sudden cardiac arrest. Two important aspects related to the design of an arrhythmia diagnosis system of the AED have attracted the attention of this study: how accurately does AED diagnose the shockable and non-shockable arrhythmias in the abnormal classes? and how quickly can make a decision?. Precisely, the most challenging scenario for the AED is the discrimination between non-shockable PEA and shockable VF, VT arrhythmias in the abnormal classes signals, as both signals show an unorganized electrical activity and may have similar visual characteristics. The rapid decision of AED for the application of defibrillation to the arrhythmia patients increases the survival rate. The importance of a rapid decision by the AED to increase the survival rate from SCD is discussed in subsection 1.1.3. From these points of view, there is scope for deep analyses and redesigning an arrhythmia diagnosis system of the AED for the distinction between shockable and non-shockable arrhythmias.

Therefore, this thesis work analyzes the ECG signal to find out the significant gaps in the arrhythmia diagnosis system of the AED. The following research issues are identified in the existing arrhythmia diagnosis system.

i) The Gabor wavelet transform (GWT) is a powerful method for time-frequency representation (scalogram). However, there exists an issue with the abnormal signals representation [15, 16]. During the generation of wavelet coefficient values, the wavelet function is not closely correlated with all the sections of abnormal signal. As a result, the same level of coefficient values is generated for all the sections of the low-frequency signals. The same level of coefficient values over time gives a barrier to getting better distinctions by the decision algorithm.

   Precisely, for non-shockable pulseless electrical activity (PEA), shockable ventricular fibrillation (VF), and ventricular tachycardia (VT) arrhythmias, there seem to be no differences in the scalo-graphic representation when extracting information using the Gabor wavelet transform (see Figures 1.4, 1.5, and 1.6). In the scalograms, energy does not change in frequency over time, and wavelet coefficient values for all scalograms are at the same level, which leads to failure to get the best distinction in the decision algorithm. Therefore, accurately extracting numeric information (scalogram) to improve the discrimination performance in the decision stage for the abnormal signal is an important issue.

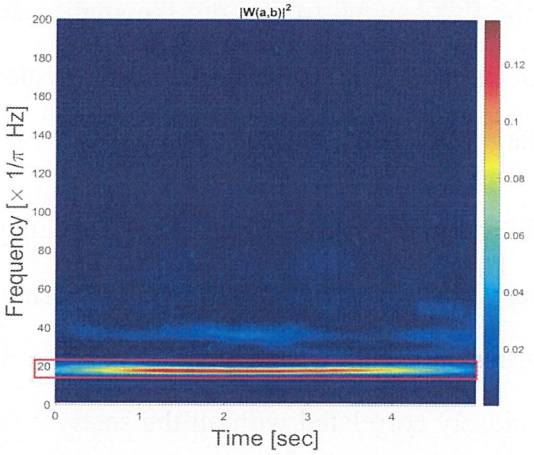

Figure 1.4: Scalogram of PEA (non-shockable arrhythmia)

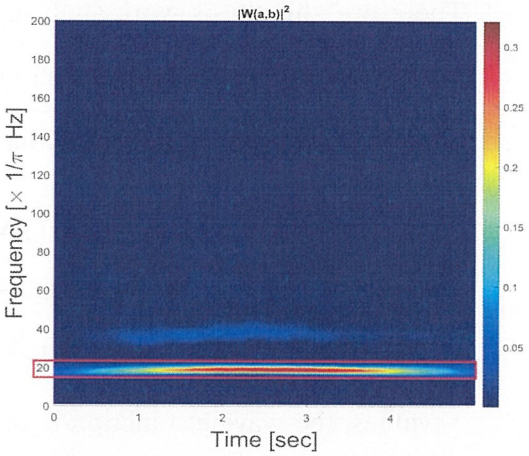

Figure 1.5: Scalogram of VT (Shockable arrhythmia)

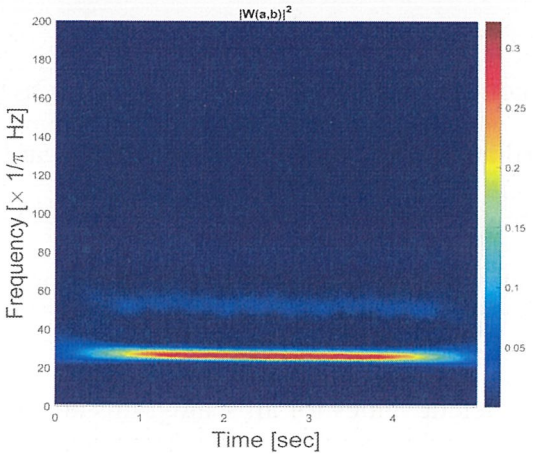

Figure 1.6: Scalogram of VF (Shockable arrhythmia)

ii) Different types of decision algorithms e.g., Mahalanobis distance, nearest neighbor, etc., are used to distinguish the arrhythmias in the decision stage [17, 18]. However, blindly use of such general methods are not the best for considering our problems. For example, the classification through the Mahalanobis distance depends on the concept of an approximation by means of the Gaussian distributions. Although the K-nearest neighbor is a simple, non-parametric decision method, and evaluation is performed by the Euclidean distance, but this Euclidean metric function-based decision method has an

issue for selecting the number of neighbors of the test sample. For example, in figure 1.7, if we consider the three nearest neighbors (K=3) of the test sample, then the test sample is classified under the group of PEA, and if we consider the seven nearest neighbors (K=7) of the test sample, the test sample is classified under the group of VT. Also, overfitting and underfitting occur for selecting the number of one nearest neighbor (K=1) and the total number of data of nearest neighbors (K=N, where the N = total number of data) of the test sample. Therefore, the decision is changing for selecting the different number of nearest neighbors of the test sample.

In addition, researchers use machine learning classifier (A large number of datasets is required) in the decision stage to separate features of shockable and non-shockable arrhythmias [19, 20, 21, 22]. Their focus is put mainly on increasing the precision while the classifier adjusts various parameter values, but not on the quickness. Note that the survival rate decreases from 7% to 10% per minute according to the statistics of the American Heart Association and resuscitation academy [10]. A substantial length of computation time may be taken to generate the optimal feature model in the high dimensional parameter space. Therefore, an accurate and rapid decision-making method for the AED shock and non-shock advice algorithm is the ultimate demand to use the scalogram information properly, and it is a crucial factor in the safety and performance of an AED.

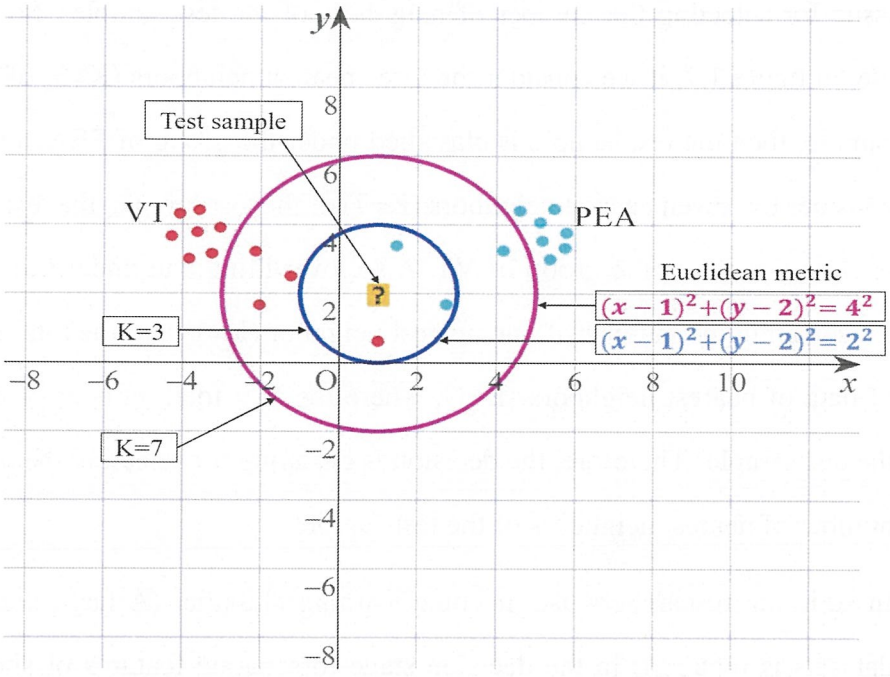

Figure 1.7: Problem of the Euclidean metric function-based decision method

1.3 Research objectives

The main objective of this thesis work is to improvement of survival rate of the patient by enhancing the arrhythmias diagnosis system in the AED. In order to accomplish this objective, a set of specific goals have been defined.

- Derivation of the scalogram. This objective targets at development of a method to generate an exact scalogram for the abnormal classes (non-shockable (PEA), and shockable (VF, and VT) arrhythmias cases). Therefore, it is necessary to generate accurate wavelet coefficients by extracting accurate information from the abnormal ECG signals. The accurate information helps the decision algorithm to get a better distinction.

- Effective characterization of the scalogram in both time and frequency direction. We develop a method how to analyze the scalogram in the time and frequency plane to calculate statistical features effective for the discrimina-

tion.

- Design of the AED shock and non-shock advice algorithm. This objective targets developing an algorithm that guarantees the high accuracy and quick decision between shockable (VF, VT) and non-shockable (SR, PEA) arrhythmias in regard to increasing the survival rate of the patients.

1.4 Research contributions

Following the research issues and objectives described in the foregoing sections, here we summarise the list of our contribution.

- **Derivation of the scalogram.** A method is proposed to generate an accurate scalogram for the abnormal classes (non-shockable (PEA) and shockable (VF, and VT) arrhythmias case) by extracting accurate information from ECG signals. In this context, we apply a new concept of the pseudo-differential like operators to the Gabor wavelet transform (GWT) that solves the issue (i) of section 1.2. We derive the scalogram by applying various settings of pseudo-differential like operators with non-linear transformation function to the GWT. Through the pseudo-differential like operators, we can get much more enlarged fruitful information (fractional order of differentiation of the signal) on the original signals. Moreover, by applying the non-linear transformation functions to the transformed signals, we can make balanced and bigger the part of the transformed signals which has small energy, and amplitude. Through these, we are able to distinguish clearly the signals that have small differences, PEA, VF, and VT and different energies over time lead to get the best discrimination in the decision stage (see Figures 1.8, 1.9, and 1.10). Then, we performed the qualitative and quantitative evaluation to check the intrinsic effect of the pseudo-differential like operators and non-linear trans-

formation function, from which we select the best pair of pseudo-differential like operators with non-linear transformation function.

The main novelty of the proposed method is that the application of pseudo-differential like operators with non-linear transformation function to the GWT does work efficiently and effectively, and generates distinguishable scalograms between shockable and non-shockable arrhythmias in the abnormal class signals, which satisfy visual comparison through scalo-graphic representation (see Figures 1.8, 1.9, and 1.10), and scatter plot observation (see Figures 3.21, 3.22, 3.23, 3.24, 3.25, 3.26, 3.27, and 3.28).

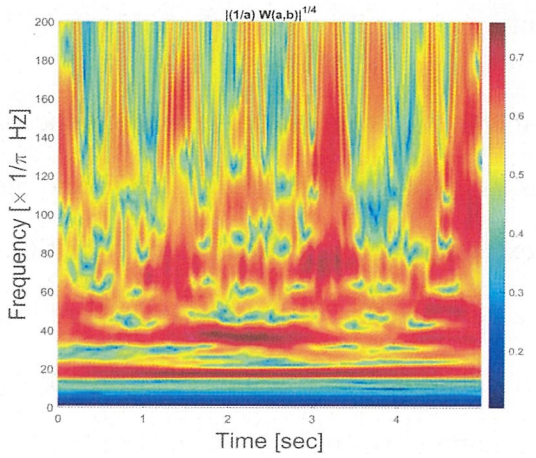

Figure 1.8: Scalogram of PEA (non-shockable arrhythmia)

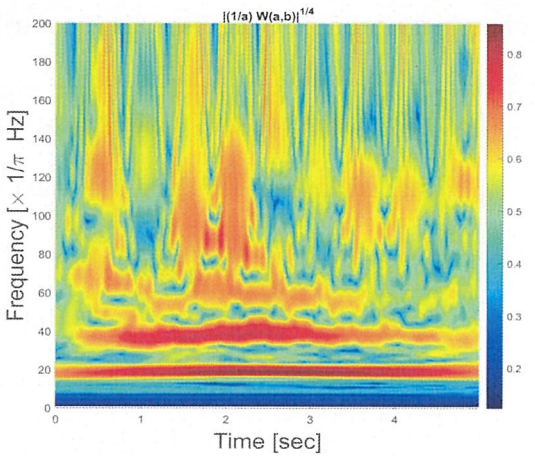

Figure 1.9: Scalogram of VT (Shockable arrhythmia)

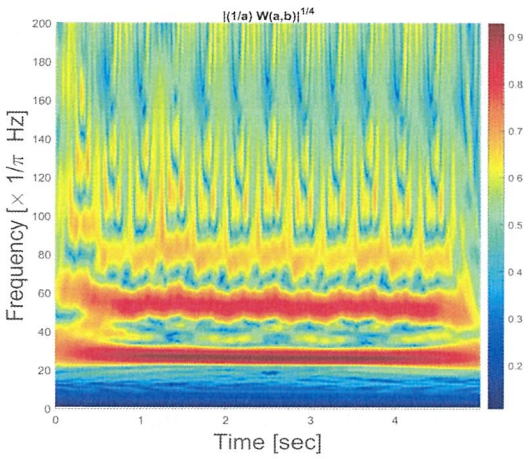

Figure 1.10: Scalogram of VF (Shockable arrhythmia)

- **Effective characterization of the scalogram in both time and frequency direction.** We perform characteristics analysis of the scalogram in the time and frequency plane to calculate statistical features effective for the discrimination. To the best of our knowledge, the scalogram analysis has been mainly considered only along the frequency plane [23, 24, 25, 26]. However, we can draw out more information from the scalogram, which is useful for better discrimination by characterizing the scalogram in the time-frequency plane. In this context, we apply two quality parameters, normalized spectrum index (NSI) and normalized time index (NTI) in the scalogram. The NSI possesses the information in the frequency direction, which has been considered in Rahman et al. [24]. On the other hand, the NTI possesses the information in the time direction, which is a new addition in our study [27, 28] (see Figures 3.29, 3.30, 3.31, 3.32, 3.41, 3.42, 3.43, and 3.44).

- **Design of the AED shock and non-shock advice algorithm.** We propose a simple decision method to mitigate the issue (ii) of section 1.2 in the general topological space to guarantee high accuracy and quick decision between shockable and non-shockable arrhythmias. In this method, we adopt a new metric function, which is defined through adequately chosen topology for the space of scatter plots. We can give the different scales of the metric function to the space of scatter plot through which we can select the open neighborhood of the test sample (see Figure 1.11).

  The main novelty of the proposed decision method is that it effectively discriminates between shockable and non-shockable arrhythmias with low computational time which will help to increase the survival rate of the patients, and the application of the proposed metric function in the decision method achieves the highest accuracy than the application of the Euclidean metric function in the decision method (see Table 4.13 in chapter 4).

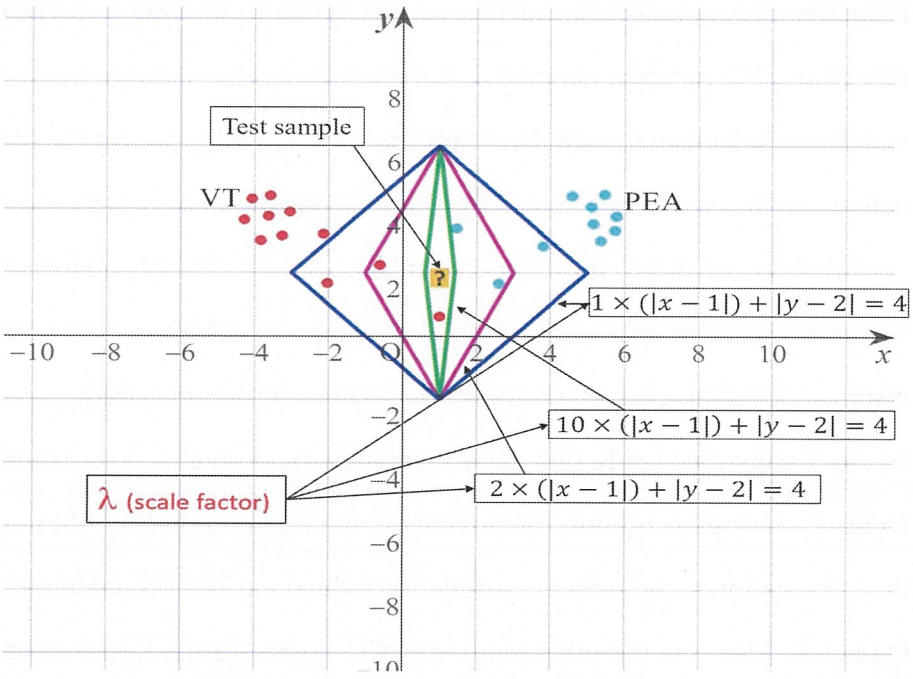

Figure 1.11: Decision strategy based on open neighbourhood topology

Note that the increase in survival rate depends on four interdependent sequences as shown in Figure 1.2. Among these sequences, the arrhythmia diagnosis system in the AED plays the most important role in increasing the survival rate. Therefore, how accurately and early an arrhythmia diagnosis system can diagnose the arrhythmia? Diagnosis accuracy should be 100%, while false diagnosis decisions harm the patients. So, accuracy is a crucial factor, and how much the survival rate could be improved led by accuracy. In addition, I have measured the detailed execution time performance of the proposed method presented in chapter 4. The proposed method takes $3.35 * 10^{-4} s$ second in average to test each sample which is a very short time. I did not perform the time comparison with other methods. This is because it is unfair to directly compare the proposed method's time performance with other methods since the device configurations and the sample duration are different. It is worth mentioning that the proposed distance-based decision method takes the decision in a short time by calculating just a simple distance between the test sample and training samples, while other methods take a substantial length of computation time

to generate the model of the training dataset, and then perform testing. The conventional diagnosis system [29] achieves 86.03% accuracy for the shockable (VF, VT) and non-shockable (PEA) arrhythmias in abnormal class signals, while the proposed arrhythmia diagnosis system increases the accuracy to 97.78% with 11.75% gain. Therefore, the proposed method contributes an additional 11.75% possibility for increasing the survival rate.

The contributions of the research work throughout the thesis have been published as the following list:

Journal

1. Rahman M.M., Kagawa T., Kawasaki S., Nagai S., Okai T., Oya H., Yahagi Y., and Yoshida M.W. : "Various scalographic representation of electrocardiograms through wavelet transform with pseudo-differential operator like operators", Journal of Advanced Simulation in Science and Engineering, vol. 9, issue 1, pp. 96-112, 2022 ([24] in the reference).

2. Rahman M.M., Albeverio S., Kagawa T., Kawasaki S., Okai T., Oya H., Yahagi Y., and Yoshida M.W. : "High accuracy distinction of shockable and non-shockable arrhythmias in abnormal classes through wavelet transform with pseudo differential like operators", Scientific Reports Journal, Springer Nature, Passed revision, January 03 2023 ([28] in the reference).

Conferences and Presentations

1. Rahman M.M., and Yoshida M.W. : "On a detection algorithm for electrocardiogram through the wavelet transforms with pseudo differential operator like operators", QBIC conference, Tokyo University of Science, October 14-16, 2020.

2. Rahman M.M., Kagawa T., and Yoshida M.W. : "Shockable and non-shockable arrhythmias detection using wavelet analysis with pseudo differential operator like operators", Dynamic Decision Models and its Applications of Operations Research Society of Japan, January 23, 2021.

3. Rahman M.M., Kagawa T., Kawasaki S., Nagai S., Okai T., Oya H., Yahagi Y., and Yoshida M.W. : "An analysis of electrocardiograms through the wavelet transform with pseudo-differential operator like operators", Numerical harmonic analysis and signal processing, of the 40th JSST Annual International Conference on Simulation Technology, September 1-3, pp.63-66, 2021 ([23] in the reference).

4. Rahman M.M., Kagawa T., and Yoshida M.W. : "An application of the pseudo differential operators to distinctions of ECG signals", The 3rd Physical Therapy Discussion of Operations Research Society of Japan, October 06, 2021.

5. Rahman M.M., Albeverio S., Kagawa T., Kawasaki S., Okai T., Oya H., Yahagi Y., and Yoshida M.W. : "Improvement of arrhythmias distinction accuracy using suitable combination of features of the Electrocardiograms", Numerical harmonic analysis and signal processing, of the 41st JSST Annual International Conference on Simulation Technology, August 31 – September 2, pp.40-43, 2022 ([27] in the reference).

1.5 The structure of the arrhythmia diagnosis system

The proposed arrhythmia diagnosis system consists of several steps shown in Figure 1.12. This figure describes the overall summary of the distinction process between shockable and non-shockable arrhythmias. In the proposed arrhythmia diagnosis system, the core idea is to derive exact information (scalogram) from the abnormal classes of ECG signals which leads to the decision algorithm for accurate

discrimination between shockable and non-shockable arrhythmias. Following the information, the new quality parameter is adopted to get more information by quantizing the statistical features. Also, a method is proposed in the decision stage to get high accuracy and rapid discrimination which increases the chance of survival. In Figure 1.12, first the pre-processing is performed of the ECG signals for segmenting and detrending. The original ECG signals is separated into pieces of five second signal segments. Then, linear trend is removed from each of the segmented signals to obtain the signals f.

Second, the wavelet transform with pseudo-differential like operators and non-linear transformation is used to accurately generate wavelet coefficients $H(L(a)(Wf)(a,b))$ from f and these coefficients are represented as a scalogram. The definition of the notation $H(L(a)(Wf)(a,b))$ has been defined in chapter 3.

Third, as a basic statistic to quantize the different features over the abnormal class ECG signals of scalogram, we take the normalized spectrum index (NSI) and normalized time index (NTI) which is new addition for more analysis in this study.

Fourth, in order to find out the effective features, we watch at each of the generated features independently and test their discriminatory capabilities by using the class separability technique such as scatter matrices. Also, we examine the individual features with the help of univariate histogram and investigate the best feature combination through the multivariate scatter plot matrix. The procedures help us to select the best feature from the set of features.

The last stage is shockable and non-shockable arrhythmia discrimination which is performed using the proposed decision method. In the method, a test sample is classified based on an open neighbor with the minimum distance by adopting a new metric function.

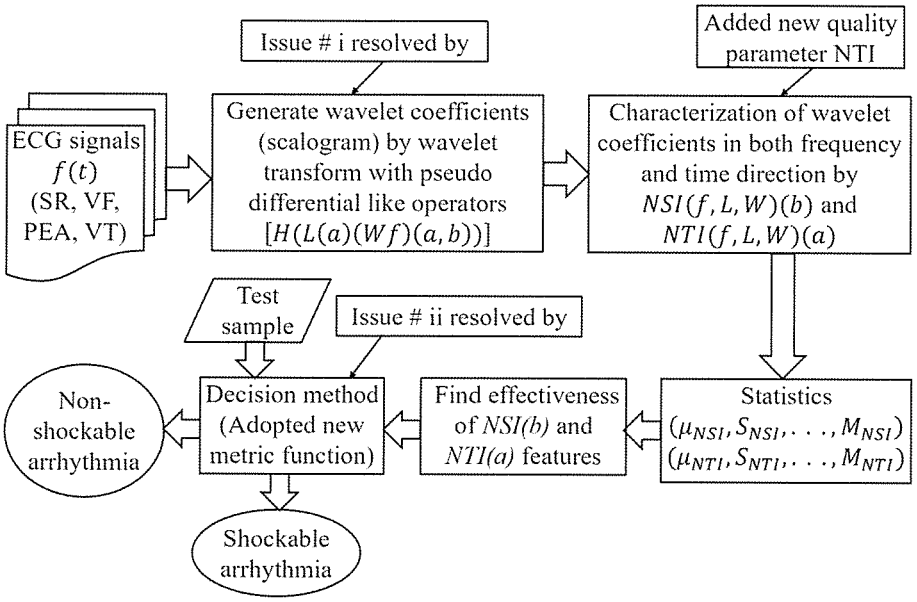

Figure 1.12: The whole scheme of shockable and non-shockable arrhythmia discrimination

1.6 Thesis outlines

The thesis comprises five chapters and it is organized as follows.

Chapter 1 presents the introduction that consists of the motivation, research scope, issues, objectives, proposed methodology of the arrhythmia diagnosis system, and thesis contributions. The importance and necessity of an accurate arrhythmia diagnosis by the AED are explained in this chapter. The main objective of the first chapter is to describe the current issues in the arrhythmia diagnosis system and to define the specific aims of this thesis. Following the research issues and objectives, the proposed methodology in the arrhythmia diagnosis system is outlined, and the research contributions are stated.

Chapter 2 discussed the background and the literature review of the ECG principles, arrhythmia, and as well as arrhythmia diagnosis system. Firstly, the structure of the heart and the activities with the corresponding ECG waves are presented. Secondly, the introduction of four types of arrhythmias is reviewed. Finally, the

literature review of the ECG signal analysis methods and the decision methods are performed, which are related to the arrhythmia diagnosis system.

Chapter 3 presents the method in detail for the derivation of the scalogram. The method is based on the Gabor wavelet transform with pseudo-differential like operators and non-linear transformation. In addition, an analysis of the scalogram in the time and frequency plane to observe the insights of the scalogram is explained in this chapter. The effectiveness of the method for the distinction between shockable and non-shockable arrhythmias is also presented in this chapter.

Chapter 4 presents a new shock and non-shock advice algorithm for the AED. The current issue in the decision method and the importance of an accurate, rapid decision by the AED are explained in this chapter. The proposed design of the algorithm is based on a set of effective features and adopts a new metric function, which is defined through an adequately chosen topology for the space of scatter plots. Numerical experimental results on different updated datasets show the efficiency of shock and non-shock advice algorithm. We also conducted a comparative performance analysis of our proposed algorithm with other state-of-the-art approaches.

Chapter 5 summarises the findings and contributions discussed in this thesis. Future work is also stated in this chapter.

2

Background and Literature review

2.1 The ECG principles

The human heart is a muscular pump organ in the body that serves two main functions: i) To pump blood collected from the lungs to the tissues in the body, ii) To pump blood back to the lungs from tissues in the body. The heart is comprised of four chambers: the two upper chambers, the right and left atria functions, while the two lower chambers, the right and left ventricles functions. Figure 2.1 shows an anterior view of the heart. The right atrium collects used blood from the body and forwards it into the right ventricle, which pumps it into the lung. Similarly, the left atrium receives blood from the lung and pumps it into the left ventricle,

which consequently supplies the body with oxygen-rich blood [30]. This process can be tracked by providing electrical impulses known as action potentials. In general, electrical signal propagation through the heart follows a specific path which is referred to as the electrical conduction system. Therefore, the heart activity can be considered as the propagation of electrical impulses, and any abnormality in heart function is reflected in these electrical impulse propagation characteristics. This could be measured by attaching electrodes to the surface of the body skin and recording the electrical activity by a device. Such recording is generally referred to as ECG and it plays a significant role in day-to-day clinical practice for detecting arrhythmias since the cardiologists can obtain critical signs of malfunction of the heart from ECG signal.

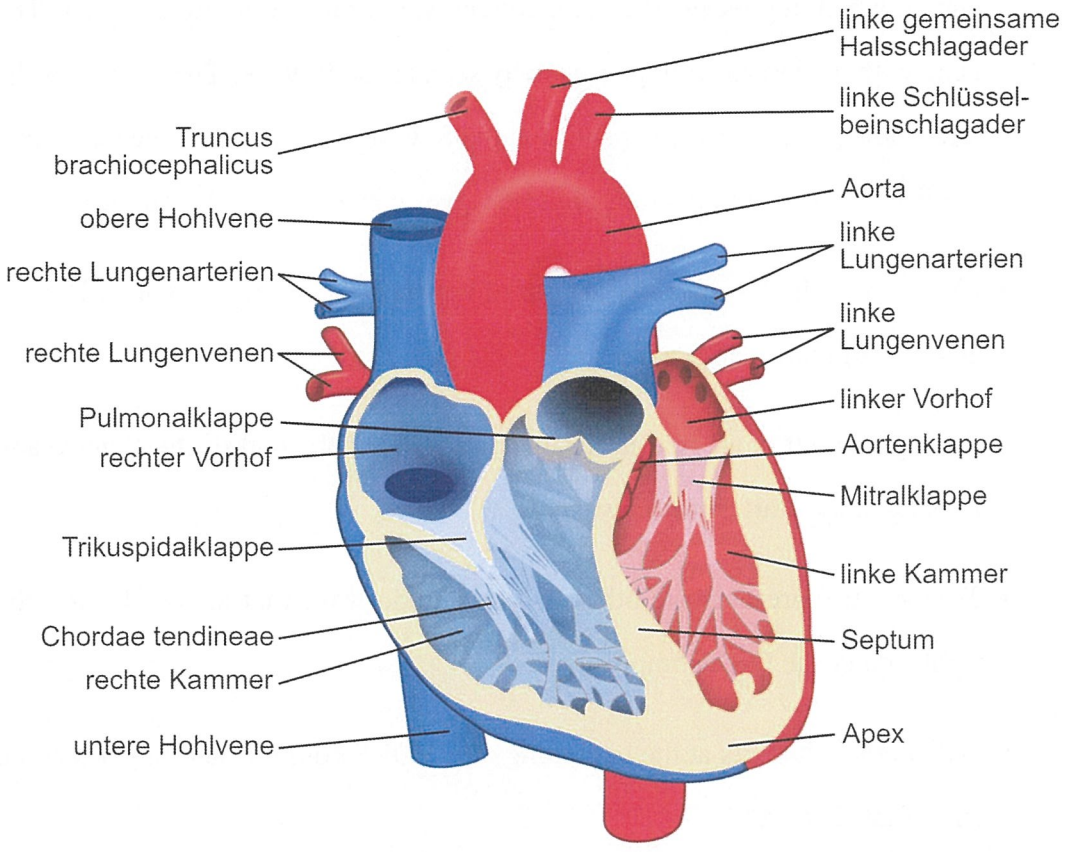

Figure 2.1: Structure of the heart. Downloaded from: https://commons.wikimedia.org/wiki/File:Heart_diagram-de.svg

Figure 2.2 shows a schematic diagram of the normal ECG beat consists of the

P-QRS-T and U waves and the relevant ECG features, such as PR interval, QT interval, QRS complex as well as ST segment, and PR segment. Also, as shown in figure, the straight line between two waves is called the isoelectric line. These lines are the segment that connects two waves together without including either of them. In the following, a separate description of each of the components will be given to summarize their characteristics.

- P wave: It is a positive and slow wave which is the first electrical event that occurs during a heartbeat. Also, this wave has a lower amplitude compared with the R wave which always lies on the left side of QRS complex.
- QRS complex: It is the central and most visually obvious part of the ECG signal, which represents the main voltage variations on the ECG signal. The peak with the largest voltage is usually seen as the R wave. The Q wave is the left saddle point near the R peak, and the S wave is the right saddle point near the R peak. The combination of these waves consists of QRS complex.
- PR interval: It is a duration measured between the starting point of P wave and the beginning of Q wave.
- PR segment: It is an isoelectric line and starts at the end of the P wave and finishes at the start of the Q wave.
- T wave: It represents the other low amplitude wave that always lies on the right side of the QRS complex.
- QT interval: It starts at the beginning of the QRS complex and finishes at the end of the T wave.
- ST segment: It is an isoelectric line and starts at the end of the S wave and finishes at the start of the T wave.

- U wave: It is a positive and small wave that follows the T wave. This wave is not always visible in the record and its absence is not a sign of abnormality.

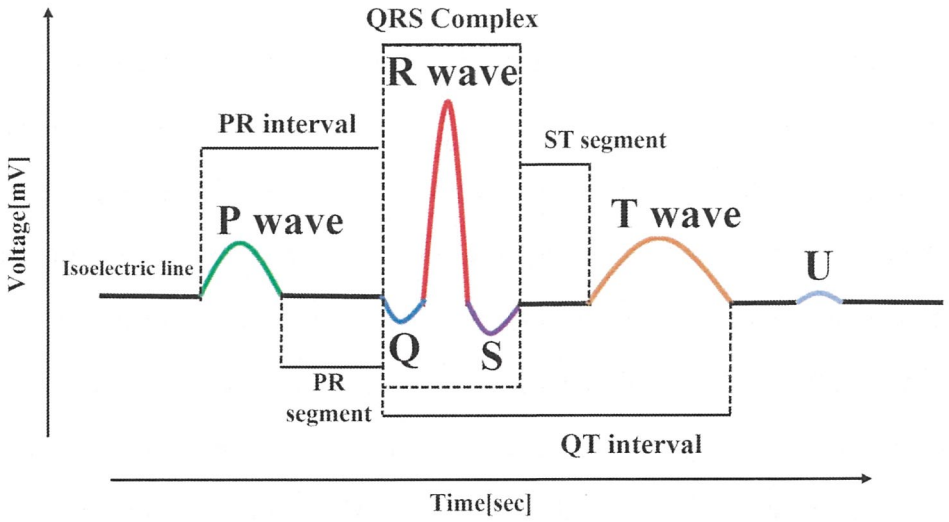

Figure 2.2: Electrocardiogram (ECG) signal and its components

2.2 Arrhythmia

It is well known that a healthy heart supplies the human body with the right amount of blood at the rate needed to work normally. In general, a heartbeat should be 60 to 100 times per minute [31]. However, if disease or injury weakens the human heart or during the cardiac arrest, the rhythm of the heart will be abnormal, which is known as arrhythmia. It is worth mentioning that all generated abnormal signals are not considered fetal arrhythmia for sudden death. Therefore, among these arrhythmias, some are considered shockable arrhythmias, and some are considered non-shockable arrhythmias with an external defibrillators. In the following subsection, we present a discussion about different types of shockable and non-shockable arrhythmias.

2.2.1 Non-shockable arrhythmias

2.2.1.1 Sinus rhythm (SR)

Sinus rhythm is the normal waveform of the heart and results from proper activation of the entire heart in proper sequence that means the electrical conduction along with beating of heart muscle with regards to other variables like timing and voltage is fine. Figure 2.3 shows an example of non-shockable normal sinus ECG. In the figure, the amplitude of the ECG waveform represents the strength of the myocardial movement and the horizontal axis represents the time for the corresponding amplitude. In the normal sinus rhythm, the characteristics waveforms called P wave, QRS complex, and T wave must be appeared [32]. The P wave appears when an electrical impulse is sent from a site called the sinus node, which is a pacemaker of the heart. Since the sinus node should pace the heart, therefore P waves must be round, all of the same shape, and present before every QRS complex. The QRS complex is generated by the propagation of electrical impulse to the ventricles of the heart and this QRS complex should be always a positive wave for the normal sinus rhythm.

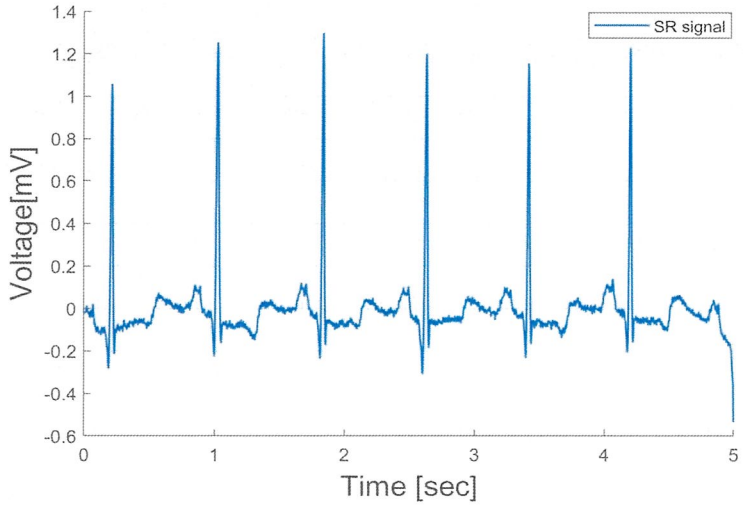

Figure 2.3: An example of non-shockable ECG (SR signal)

2.2.1.2 Pulseless electrical activity (PEA)

Pulseless electrical activity (PEA) is a type of severe arrhythmia, in which the pulse and blood flow are absent despite the presence of an electrocardiogram waveform [33]. In general, in PEA, there is electrical activity but insufficient cardiac output to generate a pulse and supply blood to the organs, whether the heart itself is failing to contract or sometimes leads to sudden death. Figure 2.4 shows an example of a non-shockable pulseless electrical activity ECG. The PEA is a non-shockable heart rhythm, therefore defibrillation should not be applied.

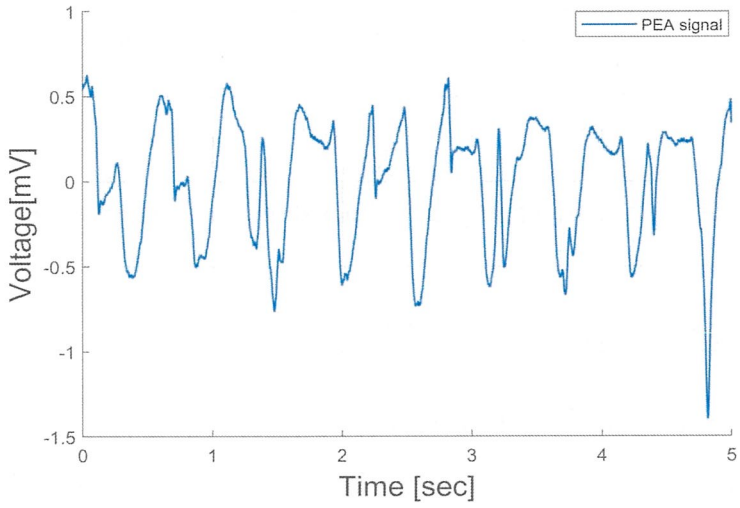

Figure 2.4: An example of non-shockable ECG (PEA signal)

2.2.2 Shockable arrhythmias

2.2.2.1 Ventricular fibrillation (VF)

Ventricular fibrillation (VF) is a life-threatening arrhythmia and it is defined as a chaotic and rapid heart rate with variable speeds up to 300 beats per minute [34]. VF can also be considered as a disorganized electrical signal originating from the ventricle. It causes the ventricle quiver and hence the ventricle cannot pump blood to the body. This situation turns out into sudden cardiac arrest or death within a few minutes. Figure 2.5 shows an example of a shockable ventricular fibrillation

ECG. During ventricular fibrillation, the ECG has no distinctive QRS complex, and also P wave cannot be discerned. The VF is a shockable heart rhythm, therefore defibrillation should be applied as soon as possible after cardiac arrest.

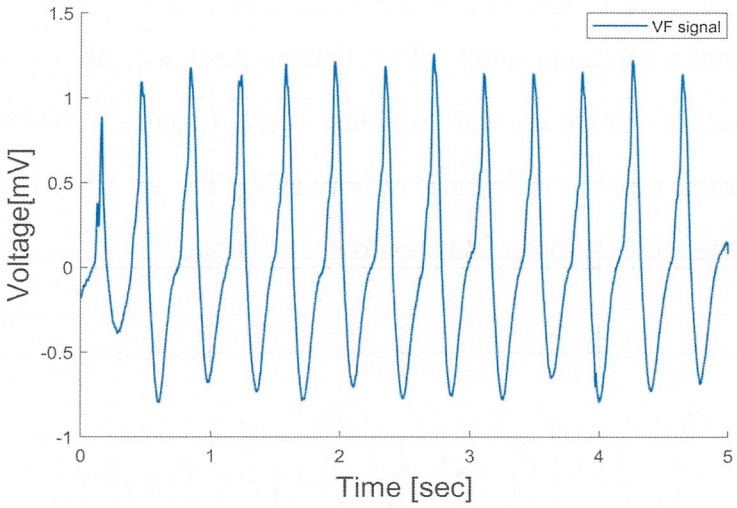

Figure 2.5: An example of shockable ECG (VF signal)

2.2.2.2 Ventricular tachaycardia (VT)

Ventricular tachycardia (VT) is also another type of life-threatening arrhythmia and it is characterized by the wide, bizarre QRS complex, chaotic and rapid heart rate. Figure 2.6 shows an example of a shockable ventricular tachycardia ECG. In general, VT is represented when three or more consecutive heart beats occur in the ventricle with a cycle length larger than 100 beats per minute [34]. In VT, many stimulations are generated in the ventricle. Therefore, there is no constant relationship between the P wave and the QRS complex, and the PQ interval is completely indeterminate. The VT is a shockable heart rhythm, therefore defibrillation should be applied as soon as possible after cardiac arrest.

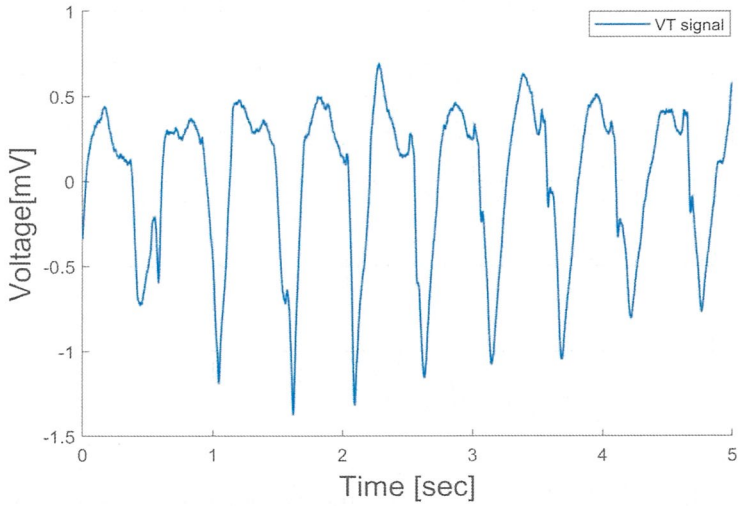

Figure 2.6: An example of shockable ECG (VT signal)

2.3 ECG dataset

In our study, a combination of three accredited databases from Physionet.org [35] has been used. This database provides shockable and non-shockable arrhythmia types. The databases are MIT-BIH arrhythmia database (MITDB) [36], MIT-BIH malignant ventricular ectopy database (VFDB) [37] and Creighton university ventricular tachyarrhythmia database (CUDB) [38]. The MITDB and VFDB databases which are published by Boston's Beth Israel Hospital (now the Beth Israel Deaconess Medical Center) and the Massachusetts institute of technology (MIT). The MITDB database contains 48 ECG waveforms and the VFDB database includes 22 ECG waveforms with their annotations where annotations were made independently by two or more cardiologists. Each ECG waveform is recorded for 30 minutes and the sampling frequency is 360 [Hz]. On the other hand, the CUDB database is collected by Floyd M. Nolle at the Creighton University Cardiac Center and contains 35 ECG waveforms where each ECG waveform is recorded for 8 minutes and the sampling frequency is 250 [Hz]. A total of 1079 ECG samples are collected from these databases, and the data length for each sample is five second. These

ECG samples are grouped into four classes name as Sinus Rhythm (SR), Pulseless Electrical Activity (PEA), Ventricular Fibrillation (VF) and Ventricular Tachycardia (VT). The number of samples for SR signal 491, PEA signal 134. VF signal 299 and VT signal 155. Here SR and PEA signals are non-shockable arrhythmias and VF and VT signals are shockable arrhythmias.

2.4 Detrending ECG data

ECG signals might contain linear and non-linear trends that could be barrier to get the better approximation during signal analysis [39]. Here, the trends of the signals can be roughly understood through the following example: As a mathematical model, suppose that the input signal $f(t), t \geq 0$, is given by

$$f(t) = a + bt + \sin t, \qquad t \geq 0,$$

for some given real numbers a and b. Since, the analysis of the input signal $f(t)$ in the domain of the frequency, therefore, $a + bt$ is the linear term of the signal $f(t)$ which acts worse for the frequency analysis. In this example the term $a + bt$ is understood as the trend of the signal, and it should be removed from the original signal. To eliminate the trend in a signal we apply detrending technique and the detrend signal, $f_{detrend}$ is defined by

$$f_{detrend}(t) \equiv f(t) - (a + bt) = \sin t, \qquad t \geq 0.$$

Generally, for a given signal $f(t)$, for a pre-assumed order of the power n (a natural number), we can find the polynomial $p(t) = a_o + a_1 t^1 + \cdots + a_n t^n$ by which the mean square error (mathematically, the L^2 distance) between $f(t)$ and $p(t)$ is minimized. Then, the polynomial $p(t)$ is understood as the trend (with the n-th order) of the

signal $f(t)$, and the detrended signal, $f_{detrend}$ is defined by

$$f_{detrend}(t) \equiv f(t) - p(t), \qquad t \geq 0.$$

In our study, the input signal (function) is the ECG signal, which is denoted by the same notation ECG, and we adopt the detrend signal, $ECG_{detrend}$, as the one composed by removing the 6-th order trend,

$$ECG_{detrend} - (\text{the 6-th order trend}).$$

Figures 2.7 and 2.8 are showing before detrending and after detrending operations respectively. After detrending, we can easily identify the baseline.

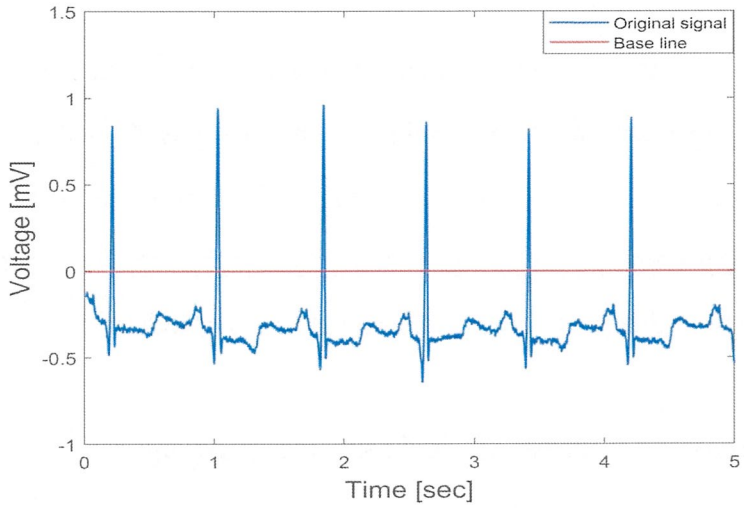

Figure 2.7: ECG signal with trend

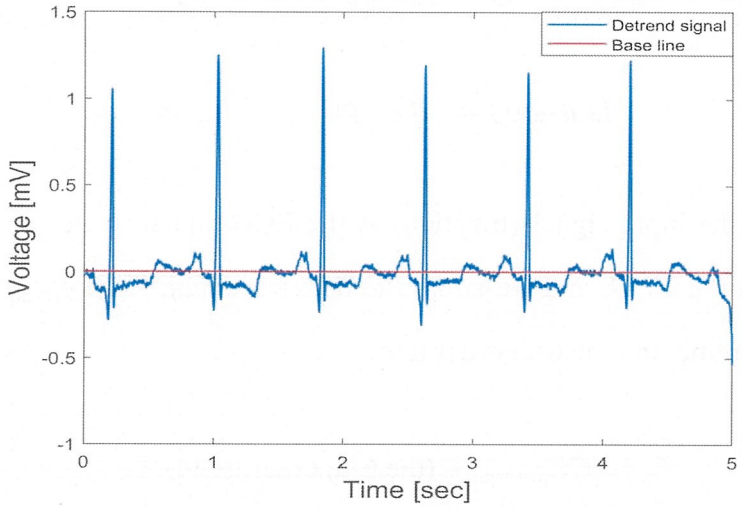

Figure 2.8: ECG signal after removing trend

2.5 Literature review

In this section, the survey begins by reviewing some of the previous studies in ECG signal analysis and discrimination techniques. The survey is divided into two stages, which are the ECG signal analysis stage and the discrimination techniques stage. Section 2.5.1 represent the ECG signal analysis in different approaches, and section 2.5.2 represent different types of discrimination methods.

2.5.1 Literature review of ECG signal analysis

Many researchers have analyzed the ECG signals through different types of approaches. Three types of approaches are commonly used for ECG signal analysis [40, 41]. Section 2.5.1.1 discusses the time-domain based approaches to the analysis of ECG signals, section 2.5.1.2 discusses the frequency-domain based approaches to the analysis of ECG signals, and section 2.5.1.3 discusses the time-frequency domain based approaches to the analysis of ECG signals. Table 2.1, 2.2, and 2.3 presents a summary of the review works in different domain based approaches.

2.5.1.1 Time domain analysis

The ECG signal analysis in the time domain is a simple method for arrhythmia discrimination. The heart rate variability (HRV) analysis such as variation in the mean of RR intervals, QRS widths, and so on, is carried out in the time domain method. The main advantages of this approach is the low complex computations and that analysis is performed directly on the signal. In the time domain method, one can see the signal amplitude over time, but the main disadvantage is that can not take the information of frequency for the corresponding time. Figure 2.9 shows the time domain based ECG analysis approach. First, the raw ECG signals (represented in the time domain) which are collected from the ECG machine. Then, time domain based features (Adjacent RR intervals that differ by more than 50ms (PNN50%), Root mean square difference between RR intervals of neighboring beats (RMSSD), and so on) are directly extracted from the raw ECG signal [42, 43]. Finally, these features are analyzed in the decision stage to distinguish arrhythmia.

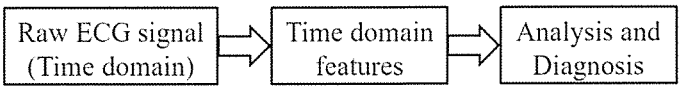

Figure 2.9: Time domain based ECG analysis approach

Researchers have proposed various methods in the time domain for the analysis of ECG signals, selected studies are described as follows.

Murugappan et al. [44] described time domain feature-based arrhythmia prediction. The methodology of this work composes of four stages namely, database description, preprocessing of HRV (Heart rate variability) signals, time domain features extraction, and classification. First, the preprocessing task is performed to remove the noises and other interferences from the ECG signals in MIT/BIT database effectively. Then, a set of time domain features are extracted from HRV signals and classified using two simple machine learning algorithms (KNN and Fuzzy). Murugappan et al. emphasize investigating the time domain features of HRV signals to

predict the SCA (sudden cardiac arrest) before 5 min onset in SCD patients. Among the different types of time domain features, the MeanHR feature is not significant in distinguishing SCA and NC (normal control). The limitation of this work is a smaller number of ECG samples are used to test the methodology.

Arafat et al. [45] proposed time domain method for the detection of ventricular fibrillation in electrocardiogram. The method investigates the ECG signal in the time domain and is basically an improved version of the threshold crossing interval (TCI) algorithm. The ECG signal is preprocessed using the filtering process. Then, each ECG segment is multiplied by a cosine window. The windowed ECG signal is normalized by the absolute maximum value in the segment, and converted into a binary string. Finally, decision is made by counting and comparison of the binary string. The author suggested that this method is very simple and computational cost is very low.

Zhou et al. [46] presents time domain algorithm architecture and define a classification rule for the VF, and VT arrhythmias. Two methods are comprised in the proposed architecture. In the first phase, the QRS detection algorithm suggested by Pan-Tompkins is used, and the beat classification method, the heart beats are detected and classified as normal beats and premature ventricular contractions (PVCs). Subsequently, a computationally efficient method (Lempel and Ziv complexity analysis combined with K-means algorithm for the coarse-graining process) is presented to separate ventricular tachycardia (VT) and ventricular fibrillation (VF). The algorithm architecture, tested on a smart-phone, obtained a good performance level for detection of ECG signal.

Mazomenos et al. [47] proposed an algorithm in the time domain for the extraction of all the fiducial time instances from the ECG waveform. This algorithm extracted the 11 parameters of interest from a single PQRSTcomplex. The first step of the algorithm is to denoising of the ECG signal, and then, the proposed algorithm initially detects the boundaries of the QRS complex by employing an ex-

tended version of the Pan Tompkins detection method. The algorithm is evaluated using QTDB, and PTBDB databases.

Seong et al. [48] proposed a time domain analysis method to detect arrhythmia in real time and implement AED by porting it to programmable gate array and digital signal processor. The analysis of the phase domain improves the detection rate of R-peak using the differentiated electrocardiogram (ECG) waveform rather than the existing ECG waveform and makes it easy to distinguish the normal ECG from the arrhythmia signal in the phase domain. As a consequence, the false alarm is minimized. The algorithm was verified by simulation using Labview and ModelSim, and it was verified that the algorithm works effectively by performing animal experiments using the implemented AED.

The work in [49] aim to contribute to the diagnosis of arrhythmia by introducing a new feature called amplitude difference to heartbeat classification based on two processes. The first process is heartbeat detection and feature extraction, and then, random forest classifier is used to classify heartbeats by their feature. In the heartbeats detection and segmentation from the extracted QRS-complex, the Pan-Tompkins method is used, and a new feature is investigated using the random forest classifier. Finally, evaluations is performed against the MIT-BIH arrhythmia database before and after adding the amplitude difference features through the classification accuracies.

Many time-domain-based analysis methods have been used in the arrhythmia distinction. Tian et al. [50] described arrhythmia detection based on the methods of percent of time above or below thresholds (PTABT), variability of threshold crossing intervals (TCI), and peak similarity in autocorrelation function (ACF). The algorithm offers a way to identify the ventricular fibrillation (VFib), and nonVFib rhythms with several features of ECG signal.

Tsipouras et al. [51] developed a system for the arrhythmias distinction. The distinction is based on heart rate features. The analysis is performed on both time

and time-frequency domains. First, the RR interval duration signal is extracted from the ECG signal and transformed through Short time Fourier transform and several time-frequency distributions (TFD) to extract features. Several combinations of those features are used for training a set of neural networks. The decision is finally obtained using decision rules.

The work in [52] is also an early successful work in the area of arrhythmia diagnosis by the automatic implantable cardioverter-defibrillator (AICD). Their approach is to discriminate probability distributions of interbeat intervals (IBI) in electrogram signals recorded from ventricular leads. The algorithm is comprised of three stages such as, differentiates the signal, averages the sample values within a moving window, and compares the moving window average to an adaptive threshold to detect each beat. In addition, a sequential hypothesis-testing method is proposed to construct the probability distributions of IBI values for several cases of NSR, SVT, VT, and VF.

Table 2.1: Summary of ECG signal analysis in the time domain method.

References	Method / Process	Target / Detected	Note
Schuckers et al. [53]	Variability analysis by CWA, BAM, NDOA and DAM, calculate mean of mean, standard deviation (STD), and interquartile range (IQR)	SR, VF, and VT	reduced sensitivity of VF.
Zhang et al. [54]	Complexity measure by Lempel, and Ziv method, select different window length	SR, VF, and VT	Small dataset (34 SR, 85 VT, and 85 VF)
Anuradha et al. [55]	Four features, Adaptive neuro fuzzy interface system (ANFIS)	NSR, VF, and others	Noise sensitive
Sivanantham et al. [56]	Linear and non-linear feature, Support vector machine (SVM)	Normal, RBBB, and others	Low accuracy
Monte et al. [57]	Morphological filtering, linear interpolation	VF	Only VF detection
Dicarlo et al. [58]	Correlation waveform analysis (CWA), Bin area method (BAM)	SR, and VT	Detection restricted to SR and VT
Lee et al. [59]	feature extraction using Hilbert transforms and phase space reconstruction, neural network with weighted fuzzy membership functions	NSR, and VF	Low accuracy
Roberts et al. [60]	Preprocessing, phase space reconstruction for feature identification, neural network	SR, MVT, PVT, and VF	Low accuracy
Amann et al. [61]	Counting number of boxes on a grid filled by ECG and its delay signals	SR, and VF	No validation
Anas et al. [62]	Calculation of mean absolute value of the signal, and calculation of differences between ECG and first 2 intrinsic mode function	VF, and VT	Requirement of two algorithms
Othman et al. [63]	Feature extraction using semantic mining method, threshold based method	NSR, VF, and VT	No validation
Povinelli et al. [64]	The ECG signal transform into a phase space, extract statistical features, artificial neural networks	SR, MVT, PVT, and VF	Low accuracy regards to VF

2.5.1.2 Frequency domain analysis

Analyzing ECG signals in the frequency domain is an alternative method for arrhythmia discrimination. The frequency properties of the signal are analyzed in the frequency domain method, and the frequency composition of the heart rate can be presented in a graph with power distribution versus frequency. In this method, one can find the distribution of the signal power on different frequencies, but the disadvantage is that not get the time information for the corresponding frequency. The frequency domain based analysis process of the ECG signal is shown in Figure 2.10. First, the raw ECG signals are collected from the ECG machine. Then, transform the input signal from the time domain to the frequency domain. The transformation is performed using Fourier transformation and others. The frequency domain-based features are extracted from the transformed signal in the third phase [65]. Finally, diagnosis is performed in the decision stage by analyzing these features.

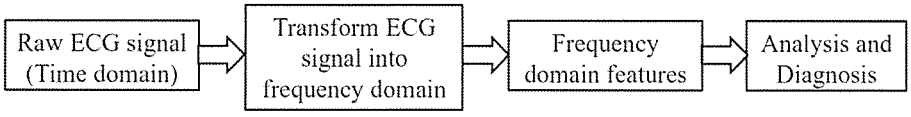

Figure 2.10: Frequency domain based ECG analysis approach

Some frequency domain based analysis methods of arrhythmia discrimination are described as follows.

Temelkov et al. [66] proposed an algorithm for automatic detection of ventricular fibrillation in electrocardiogram records customized for wearable single channel sensors. The algorithm used a sliding window approach and applied the Fast Fourier Transform to convert the data from the time domain to the frequency domain. Then, the decision comes using determination of frequency peaks, calculation of energy around the peak, and its ratio to the overall spectra.

Jekova et al. [67] introduced a real-time detection method of ventricular fibrillation and tachycardia by applying rules to the calculated parameter of the frequency domain. The prepossessing signal filtration with high-pass, low-pass, and notch fil-

ters, is used in this method. The main limitation of this method is the retrospective choice of thresholds.

In [68, 69], the diagnostic procedure consists of two stages: first, the frequency domain based feature was investigated, and then, the grey relational analysis-based classifier was used to discriminate the normal and abnormal signal. The First Fourier Transform (FFT) is used to compute the features. The variations of power spectrum are observed in the range of 0–20 Hz in the frequency domain. This method is tested using MIT-BIH arrhythmia database and compared with the artificial intelligence (AI) methods.

Minami et al. [70] developed a new algorithm to detect VF and VT from ECG signals. This algorithm extracts individual QRS complexes from ECG signals and converts each QRS complex to a spectrum using the Fourier transform. The neural network is used to classify the spectrum into three arrhythmias: SVT, VF, and VT. The key point of the algorithm is to observe only a portion of the QRS complex to improve discrimination accuracy, achieve real-time processing with a compact configuration, and remove heart rate influences.

Chen et al. [71] described some issues in the time domain-based analysis and proposed a method that analyzes the ECG signal in the frequency domain. The raw ECG signal may contain many noises, affecting the diagnosis's accuracy. It usually goes through a series of preprocessing to filter out the noise to get a clean signal. To remove the signal noise, it must transform the input signal from the time domain to the frequency domain and remove the noise. Afterward, the signal will be transformed back to the time domain. The signal transforming process is time-consuming and unsuitable for the real-time ECG analysis system. To reduce the complexity of ECG analysis, The authors extract features directly in the frequency domain, where no need to transform back to the time domain. After transforming the ECG signal to the frequency domain, the signal mostly focuses on the low-frequency region because the frequency of heartbeats is relatively lower than the

noise in the spectrum, which makes it much easier to remove the noise and extract features. Therefore, the preprocessing stage can be simplified. Finally, the neural network is applied to distinguish the arrhythmias using these features.

Gothwal et al. [72] presents a method to analyze electrocardiogram (ECG) signals for the classification of heartbeats according to different arrhythmias. Initially, ECG signals are pre-processed for the removal of power line noise and high-frequency interference. Then, the Fast Fourier transform is used to identify the peaks Q, R, S, and the deflections QRS complex in the ECG signal. These features are very important to identify arrhythmias. Finally, the neural network is trained with 20 datasets containing features of QRS complex which are maximum QRS width, minimum QRS complex width, average QRS width and the heart rate. Once trained, the network is tested on 20 more datasets to identify the arrhythmias. The proposed method is evaluated using accuracy.

The work in [73] is an early work in the frequency domain analysis for arrhythmia detection. The author developed and evaluated a method for use by the CREIGARD computerized arrhythmia monitoring system to detect VF and VT on the surface ECG. The ECG signals sampled at 250 samples per second are filtered with a finite impulse response lowpass filter. Then, performed the FFT in the frequency domain and calculated power amplitude for each frequency component. Also, find the peak component for the maximum power amplitude. Finally, the threshold value is used for the detection of VF and VT.

Ming et al. [74] constructed a robust shockable rhythm detection algorithm based on machine learning, which can distinguish accurately different types of ECG signals even under the condition of severe CPR artifacts interference. In the algorithm, a total of 21 metrics were extracted from the ECG signals by a large number of retrospective studies of the existing shockable detection algorithms. After feature selection, 13 metrics were selected to participate in BP neural network construction. The performance of this network is evaluated through sensitivity and specificity.

Table 2.2: Summary of ECG signal analysis in the frequency domain method.

References	Method / Process	Target / Detected	Note
Aramendi et al. [75]	Apply adaptive filtering to remove artifacts, calculate power spectral density to measure variability	VF	Small dataset
Widman et al. [76]	First fourier transform (FFT), measure power spectra of surface ECG	SVT, VT, and VT	Noise sensitive
Parsi et al. [77]	Preprocessing to remove artifact, Frequency domain features, spectral, bispectrum, and Fourier bessel analysis, support vector machine	VF, VT	Comparative study
Aubert et al. [78]	Preprocessing, digital fast fourier transform (DFFT), spectral analysis	SR,VF, and VT	Small dataset
Clayton et al. [79]	Remove artifact, frequency spectrum analysis by fast fourier transform, extracted four parameters	SR,VF	Sensitive to artifact
Mironovova et al. [80]	Fast Fourier transform, filtering, R-peaks, QRS complex, and heart rate extraction. neural network classifier	Normal and others	No validation
Huikuri et al. [81]	Filtering to remove noise, power spectral densities autoregressive model,	VT	Sustained and non-sustained VT measurement
Ropella et al. [82]	Preprocessing, magnitude squared coherence, ventricular rate, and irregularity analysis	MVT, PVT, and VF	Low accuracy
Minami et al. [83]	extracted individual QRS complexes, Fourier analysis of individual QRS, classification by neural network	SVT, and VF	No validation
Hadhoud et al. [84]	Features extraction using Fourier transform (FFT), autoregressive modeling (AR), and principal component analysis (PCA). artificial neural networks (ANN).	NSR, VF, and VT	small dataset (192 samples)
Owis et al. [85]	Shift invariance transformation, principal component analysis (PCA) and independent component analysis (ICA) based features, nearest neighbor classifier	NR, VC, VB, VF and VT	PCA, and ICA is sensitive to signal shift,

2.5.1.3 Time-frequency domain analysis

The ECG signal analysis methods in the time-frequency domain are used for the distinction of arrhythmias. The benefit of time-frequency representation is to catch the different frequency components present in the signal as well as their evolution in time. There are several methods to represent the ECG signal in the time-frequency domain [86, 87, 88, 89]. The Gabor wavelet transform (GWT) is one of the most important and powerful tools of ECG signal representation [90, 91]. The main advantage of GWT is to observe behaviors of the ECG signals in the time and frequency domain simultaneously, through the scalogram, the time-frequency spectrum. Figure 2.11 represent the time-frequency domain analysis process of the ECG signal. In the process, the raw ECG signals with different amplitudes appearing at different times are transformed into time-frequency distribution using different types of methods. Different types of linear and non-linear features are extracted from the time-frequency distribution. These features are used for the discrimination of normal and abnormal pattern in the ECG signal.

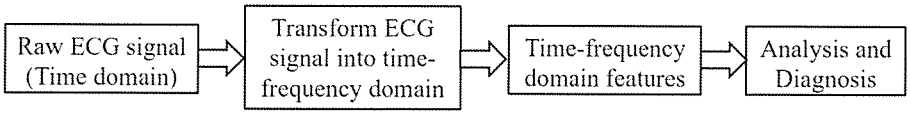

Figure 2.11: Time-frequency domain based ECG analysis approach

Many researchers analyze the ECG signals both in the time-frequency domain that is based on wavelet transform. Selected studies are described as follows.
Okai et al. [15] emphasize to increase the detection performance quickly and accurately for the shockable arrhythmia comparatively as in his previous detection algorithm. In the proposed technique, The Gabor wavelet transform (GWT) is used to extract effective spectrum features from the ECG signal. The proposed recognition algorithm based on spectrum features can achieve good performance compared with the existing results. In this context, a new feature parameter is introduced. On the basis of parameters calculate the Mahalanobis distance and compare them to

find whether the signal is SR or not and the signal is shockable or not. The detection performance of the proposed algorithm can be evaluated by using the receiver operating characteristic (ROC) curve.

In paper [92], the author proposed a continuous wavelet transform-based detection algorithm for ECG such as SR, VF, and so on. Here introduce a new parameter such as variance normalized spectrum index and adopt a threshold crossing sample count to increase the performance of the detection algorithm. After applying threshold crossing sample count to the signal get two binary strings and these binary strings are compared with the threshold value. The author mentioned some indices that are used to make relations among them. From those relations author performed a characteristics analysis and reached a decision.

Balasundaram et al. [93] described wavelet based methodology to discriminate the ventricular arrhythmias especially the VT-VF type signals which are in the overlap zone of VT and VF. The author capture the subtle morphological changes between the three groups of signals using wavelet analysis which lead objectively asses the VT-VF type arrhythmias and compute their affinity towards VT or VF. In the methodology, performed pre-processig, and filtering technique of the ECG signal. Then, analyzed the scalograms for the three groups of signals (VT, VF, and VT-VF) and observed that the energy distribution between VF and VT-VF having distinct patterns in terms of their energy spread over time and scale. The linear discriminant analysis (LDA) based classifier is used to perform the classification.

Meng et al. [94] proposed a method for detection of ventricular fibrillation (VF) and ventricular tachycardia (VT), based upon the Lempel-Ziv complexity and Wavelet transform. Using the wavelet transform, decomposes ECG time series into five scales. The sum of all these scales is equal to the original time series. The components are further subjected to calculate the LZ complexity. After that the got results are as the feature to be sent to SVM classifiers. The method is evaluated using sensitivity and specificity.

Zhou et al. [95] present a detection algorithm of VF, and VT. The algorithm contains 5 steps. In the first step, use the Haar wavelet transform (HWT) to filter ECG signals. Second, the filtered signals are processed with the time-delay transform (TDT) to make the signal more obvious. Third, we extract the initial features from the processed signal. Then, the best six features are selected using bounded sum of weighted fuzzy membership functions (BSWFM), based on NEWFM . Finally, NEWFM trains the six-feature database and outputs the best performance result.

In paper [16] the author emphasizes to increase the detection performance quickly and accurately comparatively as in his previous detection algorithm. In proposed technique, added some feature parameters which is responsible to increase the recognition performance. This algorithm is divided into two part. Firstly, check the signal which is SR or not. Another part is to check shockable ECG for VF and VT. Herewith added newly parameter such as SDW (Scale Distribution width). All statistical parameters value is calculated by using the NSI and SDW but some of parameters are selected for getting the efficient result. To select these parameter check the contribution by using the Mahalanobis distance and chosen two parameters for the two stages. On the basis of two parameters calculate Mahalanobis distance for the two stages and compare them to find the signal is SR or not and signal is shockable or not.

Abdi et al. [96] described cardiac disease classification using total variation denoising and the morlet continuous wavelet transformation of ECG Signals. In the methodology, total variation denoising (TVD) is used to filter ECG signals without smoothing sharp edges, and then, the morlet continuous wavelet coefficient matrices are calculated. Five features were calculated from each row in the coefficient matrix, based on statistical parameters. The classification of cardiac disease versus normal is based on binary logistic regression, and the classification of specific diseases is by multinomial logistic regression.

In the work [97] firstly, applied Gabor wavelet transform to analyze the ECG

signal. Based on characteristics analysis derived some quality parameters and these quality parameters lead to discriminate ECG signal. Finally, on the basis of quality parameters build a discrimination algorithm by using Mahalanobis distance to find the ECG signal is shockable or not. This proposed algorithm is compared with existing algorithm by using the performance parameter.

Kheder et al. [98] present an arrhythmia classification structure using wavelet package transform (WPT) and least square support vector Machine. In the structure, The author is interested in the feature extraction of HRV which includes ventricular fibrillation (VF) and ventricular tachycardia (VT), and find out the efficacy of the signals analysis HRV by WPT compared to the analysis by discrete wavelet transform (DWT). The author presents a new solution using WPT to decompose the HRV signal into HF (high frequency) and LF (low frequency) frequency ranges. The obtained frequency bands are too close to LF and HF bands. The root mean square (RMS) measures the signal power contained in the specified frequency bands LF and HF. The index of sympathovagal balance (LF/HF) is examined by RMS of wavelet coefficients. Finally, LS-SVM is used to classify the extracted features. The performances of the LS-SVM classifier are calculated by ROC (Receiver Operator Characteristic) method.

The work in [99] presents a feature extraction technique based on wavelet decomposition from the ECG to differentiate between VT and VF. A set of Discrete Wavelet Transform (DWT) coefficients, which contain maximum information about the arrhythmias, is selected from the wavelet decomposition. Daubechies 6 wavelet has been used in the decomposition process. The SVM (Support Vector Machine) and the K-nearest neighbor (KNN) classifiers have been deployed to classify the two rhythms and compare the result of the classifiers. The ECG signals for training the classifier and testing purposes are taken from MIT malignant ventricular arrhythmia database. The sensitivity of the SVM and KNN classifier is found to be 91.82% and 92.38% respectively.

Daqrouq et al. [100] proposed a method of arrhythmia classification based on using the continuous wavelet transform (CWT) for analyzing the ECG signal and extracting the desired parameters related to arrhythmia (Heart Rate Variability). In the method, the author introduces two models (piecewise linear (PL) ECG model and analytic (AM) ECG model) to design an artificial ECG signal that is important in signal processing methods testing and evaluation, when the ECG device cannot be available. The PL- model, which is defined in time and amplitude scales, by two vectors of characteristic points, and the AM-model, where the ECG signal is achieved analytically. The models can help in ECG signal processing methods testing without the danger of using people to record different arrhythmias.

In [101], the arrhythmia episodes are investigated to identify recurring signal patterns and develop a methodology to automate the identification process. In the method, the filtering technique, and the energy normalization is applied to the ECG segments for the preparation of the dataset prior to the pattern identification stage. Three types of patterns are calculated from the signal and these patterns are grouped into either local or global pattern. Following the identified patterns, the wavelet analysis is used to detect the occurrence of signal patterns during an arrhythmia segment.

Sun et al. [102] proposed a method for Life-threatening ventricular arrhythmia recognition by the nonlinear descriptor. The multiscale-based non-linear descriptor, the Hurst index "H", is proposed to characterize the ECG episode so that VT and VF can be recognized as different from normal sinus rhythm (NSR) in the descriptor domain. In the method, firstly, perform the wavelet decomposition and computation of its detail coefficients at different scales. Then, compute the Hurst index H, and detect the life-threatening ventricular arrhythmia in the feature space of H.

Table 2.3: Summary of ECG signal analysis in the time-frequency domain method.

References	Method / Process	Target / Detected	Note
Balasundaram et al. [103]	Continuous wavelet transform (CWT), two level binary classification	VT, OVF, and DVF	small dataset (21 VT, 20 OVF and 22 DVF)
Namarvar et al. [104]	Wavelet-singular value decomposition (SVD) analysis, SVM	VF and VT	Low accuracy
Lai et al. [105]	Wavelet transform, investigation of eight 2D CNN structure	NSR, VF, and VT	Time consuming for selection of 2D CNN structure
Shilla et al. [106]	Discrete wavelet transform (DWT), Continuous wavelet transform (CWT), CNN	NSR, VF. and VT	Requirement of two algorithms
Jang et al. [107]	Wavelet transforms, phase space reconstruction , neural network with weighted fuzzy memberships	NSR, and VF	Distinction only NSR versus VF
Khadra et al. [108]	Raised cosine wavelet transform (RCWT), Threshold based decision	NSR, AF, VF, and VT	small dataset
Sumathi et al. [109]	Wavelet transform, Adaptive neuro-fuzzy inference system (ANFIS)	NSR, PVC, AF, VF, and VFL	No validation
Mjahad et al. [110]	Hilbert transform, the pseudo rigner-ville, and the time-frequency representation image (TFRI), multiple classifier, votting method.	SR, vF, VT, and others	Complexity increases for multiple classifier
Werther et al. [111]	Remove artifact by adaptive filtering, time frequency representation by Gabor wavelet transform (GWT)	VF	Test with a small dataset
Zhang et al. [112]	Perform pre-detection process by statistical analysis, extract features using haar wavelet transform, neural fuzzy network	NSR, VF, and VT	Two structures corresponding to VF and VT
Karthika et al. [113]	18 features, filter type feature selection, ANN, and SVM are used for the classification	NSR, VF, and VT	small dataset (15 samples)
Jung et al. [114]	Discrete wavelet transform, used four types of wavelet functions, the relative energy levels are compared for classification	VF, VT, SVT, and VFL	Requirement of inverse discrete wavelet transform

2.5.2 Literature review of decision methods

There are various decision methods that have been utilized for the arrhythmias discrimination in the decision stage. The decision methods can be clustered into several categories based on the classification strategy. Figure 2.12 represents the classification of the test sample by the classifier in the decision stage. In the figure, the classifier learns from the training data and then, this trained classifier model is used for classifying samples from the unknown test set.

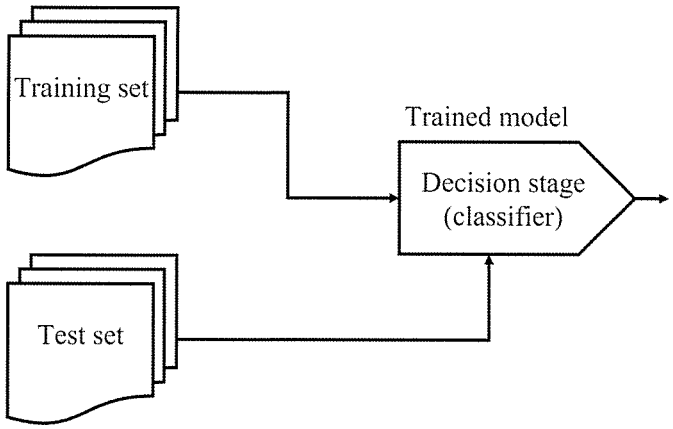

Figure 2.12: The testing process of the classifier in the decision stage

Many researchers have used various decision methods for arrhythmias discrimination in the decision stage. Table 2.4 and 2.5 present summary of some decision methods (Grouped according to decision variant) for arrhythmias discrimination in the decision stage. Here, the application of some decision variants in the context of arrhythmias discrimination are described as follows.

2.5.2.1 Neural network variants

Neural networks are one of the widely employed machine learning techniques and computationally complex due to require large number of dataset for accurate the training model. The neural network is made up of layers of neurons. A basic neural network comprises at least three kinds of layers. The first layer, the input layer picks up the input signals and transfers them to the next layer. The next layers are hidden

layers that take their inputs from the previous nodes to classify a certain input into one of a few predefined categories. The final layer, the output layer, is responsible for producing values based on the input collected from the hidden layers. Those outputs are sent back through the network and may be processed again by other nodes in later layers until they reach their final destination. There are different variants of neural networks such as artificial neural network (ANN), probabilistic neural network (PNN), block-based neural network (BbNN) and so on. The ANN is the most widely used technique to distinguish arrhythmias. One of the works on arrhythmia discrimination by [115], in which ANN is used to detect VT from the ECG signal. On the other hand, the BbNN is a two-dimensional array of neural network blocks with flexible configurations and structures (varying the number of input and outputs and so on) and integer weights. This can be implemented with less complexity on digital hardware. The work in [116] implemented a multi-threaded training mechanism for a 4×4 BbNN to classify the different types of heart arrhythmias.

2.5.2.2 Support Vector Machine (SVM) variants

Support Vector Machine (SVM) is a supervised machine learning algorithm which can be used for both classification or regression challenges. Specially it is design for solving binary classification problems because of its outstanding generalization performance. The main idea of the SVM is to find a maximum margin between the training data and the decision boundary [117]. Support vectors, which are the training samples that are closest to the decision boundary, are used for margin maximization. The SVM can be regarded as either a linear or nonlinear classifier according to the type (variants) of its kernel function. While a linear kernel function makes the SVM a linear classifier, other kernel functions, such as Gaussian radial basis, polynomial, and sigmoid, make it a non-linear classifier. Various approaches with SVM variation have been proposed in the application of arrhythmia classification. The work in [118] proposed a method for multiclass classification of arrhythmia

using ECG records with three different SVM based approaches.

2.5.2.3 Bayesian variants

The Bayesian classifier is a branch of machine-learning techniques that is effective to perform data classification. It is the systems that are based on Bayes decision theory. This theory is a fundamental statistical approach. The idea behind these classifiers is that if the class is known, the values of the other features can be predicted. If the class is not known, then Bayes rule can be used to predict the class label according to the given feature values. In Bayesian classifiers, probabilistic models of the features are built to predict the class label of a new sample. There are different variants of the Bayesian classifiers utilized for arrhythmia classification such as Bayesian network, naive Bayes, Bayes maximum likelihood classifier, and so on. In [119], a naive Bayes based classifier is proposed for ECG arrhythmia detection and classification. However, the performance of Bayesian classifiers for arrhythmia detection is not as effective as neural networks or SVM-based methods. Furthermore, the hardware implementation also incurs higher overheads due to involved computational complexity.

2.5.2.4 Clustering and neighboring variants

Clustering and nearest-neighbor based techniques are relatively low complex techniques which use in the decision stage. Clustering is the process of grouping the data and to detect the outliers as well employed for arrhythmia detection. Similarly, one more low-complex technique to perform classification is to use the distance metrics. The distance based method involves different variants distance metrics such as Euclidean distance, Manhattan distance, Mahalanobis distance, etc. Various approaches with different variation of the distance metrics have been proposed in the application of arrhythmia classification. One of the works [120], in which K-nearest neighbor based method is applied for the classification of arrhythmia. This

method involves calculation of Euclidean distances. For an unknown test sample, the distances from this sample to all samples in the training set are calculated using the Euclidean distance. Then, an unknown test sample is assigned to the class in which the closest k samples mostly belong to. Thus, a kind of majority voting approach is applied. The value of k is a positive integer and is known to be a strongly influencing factor for the accuracy of the classification.

2.5.2.5 Fuzzy logic variants

Fuzzy logic makes use of many-valued logic for true or false, whereas binary logic uses one or zero for true and false. This use of many-valued logic helps in determining confidence levels of true or false in addition to determining accuracy. The major drawback with fuzzy logic is that it is not always possible to have multi-valued logic for true and false values. Fuzzy logic is used in ECG signal analysis as well for arrhythmia detection. Fuzzy logic can be operated together with methods like SVM, neural networks and so on to achieve good accuracy in arrhythmia detection. Various approaches with different variation (e.g., Fuzzy inference model, neuro fuzzy approach, and so on) of the Fuzzy logic have been proposed in the application of arrhythmia classification. The work in [121], where a three step procedure using the fuzzy inference model is proposed for the arrhythmia classification.

2.5.2.6 Deep learning variants

Deep learning is applied in the recent years for the purpose of arrhythmia detection and ECG signal analysis. Various deep learning techniques such as convolutional neural networks (CNN), belief propagation deep neural networks (DNN), long-short term memory (LSTM) networks, etc, are used. The primary advantage with deep learning compared to the traditional machine-learning techniques are the robustness to the noise and other artifacts arising during the signal acquisition. Deep learning is required to be fed with a large amount of samples compared to the tradi-

tional technique for better performance. In addition, deep learning is more suitable for high-end or CPU/GPU-based systems rather than only hardware-based computing systems. In deep learning, large numbers of hidden layers are used. The work in [122], where DNN with 11 hidden layers is used for the myocardial infarction detection using ECG signals. In the method, the computational complexity is much more higher than other traditional methods due to requiring a large number of datasets and the use of large numbers of hidden layers.

In addition to the above-mentioned popular approaches like neural networks, SVM, Bayesian, clustering, Fuzzy logic, and deep learning, there exist other approaches for arrhythmia detection and classification. We refer to these approaches as other decision variants such as statistical discriminant analysis, space search, and so on. These approaches are less complex but have less efficiency in the application of the health care system.

2.6 Summary

In this chapter, we have explained the basic structure of the heart, the ECG with their components as well as four different types of arrhythmia. The collection and preparation of the ECG dataset have also been explained. We have broadly reviewed some of the previous arrhythmia diagnosis system studies, where our review is divided into ECG signal analysis stage and decision technique stage. In the next chapter, we will describe our proposed method for the accurate scalogram generation of the abnormal class ECG signals.

Table 2.4: Summary of decision methods for arrhythmias discrimination in the decision stage (Grouped according to decision variant)

References	Technique	Target / Detected	Note	Decision variant
Joo et al. [123]	Artificial neural networks (ANN, MLP)	VT	Low sensitivity and specificity	Neural network
Rai et al. [124]	Radial basis function neural network(RBFNN)	Normal, LBBB, RBBB, PVC and VT	Required pre-processing	
Ghongade et al. [125]	Probabilistic neural networks (PNN)	10 different arrhythmias	No validation	
Suotsalo et al. [126]	Linear SVM	VFL, VF, and VT	Performed cross-validation	Support vector machine (SVM)
Alonso et al. [127]	Gaussian SVM	NSR, VF, VT, and others	Low accuracy respect to VT	
Jayagopi et al. [128]	Polynomial SVM	16 different arrhythmias	No validation	
Bayasi et al. [129]	Gaussian Naive Bayes	Normal, VF and VT	lower validation performance	Bayesian classifier
Lashgari et al. [130]	Laplacian eigen map with Bayesian	PVC beats	Restricted to one arrhythmia	
Ahmed et al. [131]	One-vs-one error minimization with Bayesian	6 different arrhythmias	Longest learning time	
Abbas et al. [132]	K-nearest neighbors with euclidean distance	NSR, VF, and VT	small dataset	Clustering and neighboring-based classification
Zuo et al. [133]	Kernel difference weighted k-nearest neighbors	15 different arrhythmias	Low accuracy	
Rad et al. [134]	K-local hyperplane distance nearest-neighbors	AS, PES, PR, VF, and VT	Results might be biased due to not using cross-validation	

Table 2.5: Summary of decision methods for arrhythmias discrimination in the decision stage (Grouped according to decision variant) (continued)

References	Technique	Target / Detected	Note	Decision variant
Picon et al. [135]	1D parallel CNN, LSTM and ANN	shockable and non-shockable arrhythmias	No validation	Deep learning
Jaureguibeitia et al. [136]	Fully CNN architecture and ResNet CNN model	Normal, Aystole, VF, and VT	Pre-selected CNN structure	
Kiranyaz et al. [137]	DNN (3 conv. + 2FC)	5 different arrhythmias	Partially fail to detect one arrhythmia	
Acharya et al. [138]	DNN (9 hidden layers)	5 different arrhythmias	Low accuracy	
Sugiura et al. [139]	Neuro fuzzy approach	NSR, VF, and VT	Emphasis on two features	Fuzzy logic
Lim et al. [140]	Neural network with weighted fuzzy membership	PVC beats	Restricted to one arrhythmia	
Lee et al. [141]	Fuzzy support vector machine	NSR, VF, VT, and other	0.25% higher accuracy than the existing method	
Alliche et al. [142]	Higher order statistics and pitch period method	NSR, VF, and VT	Requirement of two methods	Others
Ruiz et al. [143]	Cross correlation	VF and VT	Low sensitivity	
Ramakrishnan et al. [144]	Statistical analysis	NSR, VF, and VT	No validation	

3

Derivation of the Scalogram

3.1 Introduction

Sudden cardiac death is sometimes caused by fatal arrhythmias. The AED identifies these arrhythmias through analysis of ECG signals and plays the most important role in increasing the survival rate from sudden cardiac death. Hence, the most important point of the AED equipment is a reliable judgment of its applicability. In view of the increasing precision of the judgment by the AED equipment, it is necessary to clearly distinguish between shockable arrhythmia (VF and VT), and non-shockable arrhythmia (PEA) in the abnormal classes. A number of researchers [15, 16, 29, 105, 113, 145, 146] analyze the ECG signals both in the

time-frequency domain that is based on wavelet transform, and proposed methods for the AED to discriminate between shockable and non-shockable arrhythmias. The successful works [15, 16, 29] of them applies just a standard Gabor wavelet transform (GWT) to generate a scalogram from the ECG signal, which gives a good distinction between normal and abnormal signals. However, it does not achieve enough discrimination performance between the shockable and non-shockable arrhythmias in the class of abnormal signals (i.e., PEA, VF, and VT). This is because the standard GWT generates the same level of coefficient values for the shockable and non-shockable arrhythmias in the abnormal classes. The same level of coefficient values over time gives a barrier to distinguishing by the decision algorithm. Precisely, for non-shockable arrhythmias such as PEA, and shockable arrhythmias such as VF, and VT, there seem no differences in the scalo-graphic representation when extracting rhythm information using the Gabor wavelet transform (see Figures 3.3, 3.4). In the scalograms, energies do not change in frequency over time, and wavelet coefficient values for all scalograms are at the same level, which leads to failure to get the best distinction in the decision algorithm. It is clear that if we accurately extract numeric information (scalogram) for the abnormal class signals, the discrimination performance could be increased. Therefore, we apply a new concept of the pseudo-differential like operators to the Gabor wavelet transform (GWT) and perform non-linear transformation functions of the transformed signals to generate an accurate scalogram for the abnormal class signals. Through the new concept of pseudo-differential like operators with non-linear transformation functions, we are able to distinguish clearly abnormal class signals which have small differences (see Figures 3.13, 3.14).

After derivation of the scalogram, we look at the generated scalogram to observe the behavior in both time and frequency directions independently. To the best of our knowledge, the scalogram analysis has been mainly considered only along the frequency plane [24, 25, 26]. However, we can draw out more information

from the scalogram, which is useful for better discrimination, by characterizing the scalogram in the time-frequency plane (see section 3.3). This makes it possible to quantify the different statistical features of the abnormal class signals.

The rest of this chapter is organized as follows: in section 3.2, we discuss our proposed algorithm for the derivation of scalogram with the performance results. After that, in section 3.3, we perform characteristics analysis of the scalogram in the time and frequency plane and show the evaluation strategy with their performance results. Finally, the summary of this chapter is drawn in section 3.4

3.2 Methodology

The flow chart of our proposed method generates scalogram using the Gabor wavelet transform (GWT) with pseudo-differential like operators shown in figure 3.1. In the methodology, we refine a conventional procedure of analysis the ECG signals by using the Gabor wavelet transform with the pseudo differential like operators $L(a)$ and applying the non-linear functions $H(\cdot)$ (see equation (3.6) and (3.7)) to the transformed signals, which is a new development in our study. First, the mother wavelet function $\psi(t)$ is convoluted with the signal f. During the generation of wavelet coefficients, we multiply the pseudo-differential like operators $L(a)$ to the GWT defined by equation (3.5) (similar to the case of the pseudo differential operators for the Fourier transform (see equation (3.2), (3.3))), on f to emphasize the low-frequency components of f. As a consequence, we are able to get much more enlarged fruitful information about the (*fractional order of*) differentiations of the input signals $f(t)$, $t \geq 0$. Since the two operations are equivalent to taking a multiplier $L(a)$ on the wavelet transform $Wf(a,b)$, we just substitute this operation by $L(a)(Wf)(a,b)$. Then, we take its non-linear functions $H(L(a)(Wf)(a,b))$ to make balanced and bigger the part of the transformed signals which has a small energy. Finally, these coefficients are represented as a scalogram (see Figures 3.5-3.20).

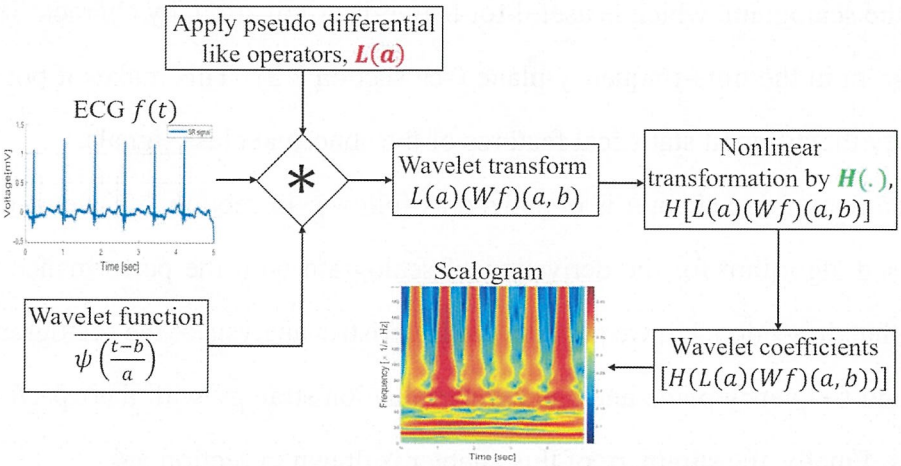

Figure 3.1: Process to generate scalogram using the GWT with pseudo differential like operators and non-linear transformation function

The algorithm 1 shows the implementation for derivation of the scalogram using the Gabor wavelet transform with pseudo differential like operators and non-linear transformation function.

Algorithm 1 Derivation of the scalogram

Require: ECG signal $f(t)$.
Ensure: Scalogram $(Wf)(a,b)$

1: Signal=load $f(t)$
2: Target_time=Signal(: , 1)
3: Target_data=Signal(: , 2)
4: Initialize variables related to Eq. (3.4)
5: Calculate $Fs = 1/(Target\_time(2) - Target\_time(1))$
6: Calculate $dt = 1/Fs$ related to Eq. (3.5)
7: **for** each point in the $f(t)$ along time axis **do**
8: Calculate $\psi(t)$ according to Eq. (3.4)
9: Computes coefficients of wavelet function $\psi(t)$, pseudo differential operator $L(a)$, and the signal $f(t)$ related to Eq. (3.4), (3.5), and (3.7)

$$L(a)(Wf)(a,b) = abs(conv(Target\_dataf(t), \psi(t), L(a)) * dt)$$

10: **end for**
11: Perform non-linear transformation related to Eq. (3.7)

$$(Wf)(a,b) = H[L(a)(Wf)(a,b)]$$

3.2.1 The Gabor wavelet transform (GWT) with pseudo differential like operator

In this subsection, we briefly explain the framework of the wavelet transform with the pseudo differential like operators. The usual pseudo differential operators are defined in the framework of the Fourier analysis. We extend the notion of the pseudo differential operators to the wavelet analysis framework, and call them the pseudo differential like operators, which are defined as follows. We are considering the real-valued functions defined on $\mathbb{R} \equiv (-\infty, \infty)$, denoted by $f(t) \in \mathbb{R}$, as the observable signals. To investigate $f(t)$, $t \in \mathbb{R}$, the Fourier transform of $f(t)$, denoted by $(\mathcal{F}f)(\xi)$ or $\hat{f}(\xi)$ defined below is a fundamental mathematical tool:

$$\hat{f}(\xi) = (\mathcal{F}f)(\xi) = \frac{1}{\sqrt{2\pi}} \int_{-\infty}^{\infty} e^{-it\xi} f(t)\, dt, \qquad \text{for} \quad f \in \mathcal{S}'(\mathbb{R} \to \mathbb{R})$$

where $i \equiv \sqrt{-1}$, and the space $\mathcal{S}'(\mathbb{R} \to \mathbb{R})$ is the space of real Schwartz distributions. Then

$$\mathcal{F} : \mathcal{S}'(\mathbb{R} \to \mathbb{R}) \ni f \longmapsto \hat{f} \in \mathcal{S}'(\mathbb{R} \to \mathbb{R}),$$

[147], and $\hat{f}(\xi)$ corresponds a decomposition of $f(t)$ in the space of the frequency. Correspondingly, let $\mathcal{F}^{-1}$ be the Fourier inverse transform such that

$$(\mathcal{F}^{-1}g)(t) \equiv \frac{1}{\sqrt{2\pi}} \int_{-\infty}^{\infty} e^{i\xi t} g(\xi)\, d\xi, \qquad \text{for} \quad g \in \mathcal{S}'(\mathbb{R} \to \mathbb{R}).$$

We denote $(\mathcal{F}^{-1}\, g)(t) = \check{g}(t)$. It then holds that

$$(\mathcal{F}^{-1}(\mathcal{F}f))(t) = (\mathcal{F}^{-1}\hat{f})(t) = f(t), \qquad \text{for} \quad f \in \mathcal{S}'(\mathbb{R} \to \mathbb{R}).$$

One of an important formula in the framework of the Fourier transform is the following:

$$(\mathcal{F}f')(\xi) = i\xi\, \hat{f}(\xi), \qquad \text{for} \quad f \in \mathcal{S}'(\mathbb{R} \to \mathbb{R}), \tag{3.1}$$

where $f'(t) = \frac{d}{dt}f(t)$ (in the distribution sense).

Equation (3.1) can be generalized to the analysis of the pseudo-differential operators [148]. It is possible to consider, e.g. formally for each $\alpha \in \mathbb{R}$, the pseudo differential operator such that

$$\left(-\frac{d^2}{dt^2}+1\right)^{\alpha} f(t), \qquad t \in \mathbb{R}, \tag{3.2}$$

of which Fourier transform is

$$(\xi^2+1)^{\alpha}\hat{f}(\xi), \qquad \xi \in \mathbb{R}, \tag{3.3}$$

(precisely, equation (3.2) is defined through (3.3)).

In our study, to investigate the ECG signals $f(t)$, $t \in \mathbb{R}$, we use the Gabor wavelet transform with the modifications as follows: Let $L^2 \equiv L^2(\mathbb{R} \to \mathbb{C})$ be the space of the $\mathbb{C}$-valued, complex number valued, square integrable functions on the real line $\mathbb{R}$. For some given $\sigma > 0$ and $\omega_0 \in \mathbb{R}$, take the mother wavelet function $\psi(t)$ in L^2 as follows:

$$\psi(t) \equiv \frac{1}{\sqrt{2\pi\sigma^2}} e^{-\frac{t^2}{2\sigma^2}} e^{i\omega_0 t}, \quad t \in \mathbb{R}, \qquad \text{with } i \equiv \sqrt{-1}. \tag{3.4}$$

Then, for $f \in L^2$, define the Gabor wavelet transform $(Wf)(a,b)$ as follows:

$$(Wf)(a,b) \equiv \frac{1}{\sqrt{a}} \int_{-\infty}^{\infty} f(t)\overline{\psi(\frac{t-b}{a})}dt, \quad a > 0, \quad b \in \mathbb{R}, \tag{3.5}$$

where, the variable $\frac{1}{a} > 0$ corresponds to the frequency of the function f, and b corresponds to the time (shift). Next, we prepare two measurable functions L and H such that

$$L : \mathbb{R}_+ \ni a \longmapsto L(a) \in \mathbb{C}, \qquad H : \mathbb{C} \ni y \longmapsto H(y) \in \mathbb{C}. \tag{3.6}$$

For $f \in L^2$, we then define our wavelet transform with pseudo differential like operator L, and its (non-linear) transform by means of H, which are $\mathbb{C}$-valued measurable functions with the variables $a > 0$ and $b \in \mathbb{R}$, as follows:

$$L(a) \cdot (Wf)(a,b), \qquad H\Big(L(a) \cdot (Wf)(a,b)\Big). \tag{3.7}$$

3.2.2 A suitable choice of the pair $L(a)$ with $H(\cdot)$

In this subsection, we find how the application of the pseudo differential like operators and its non-linear transformation function, is powerful to the delicate distinctions of shockable and non-shockable arrhythmia in abnormal classes. As the first step of the analysis, we derive the various scalograms corresponding to the ECG signals of SR, PEA, VF, and VT by various settings of pseudo differential like operator $L(a)$ with non-linear transformation function $H(\cdot)$ (see Figure 3.2). Then, we perform the qualitative and quantitative evaluation, from which we select the best pair of pseudo-differential like operators with non linear transformation function.

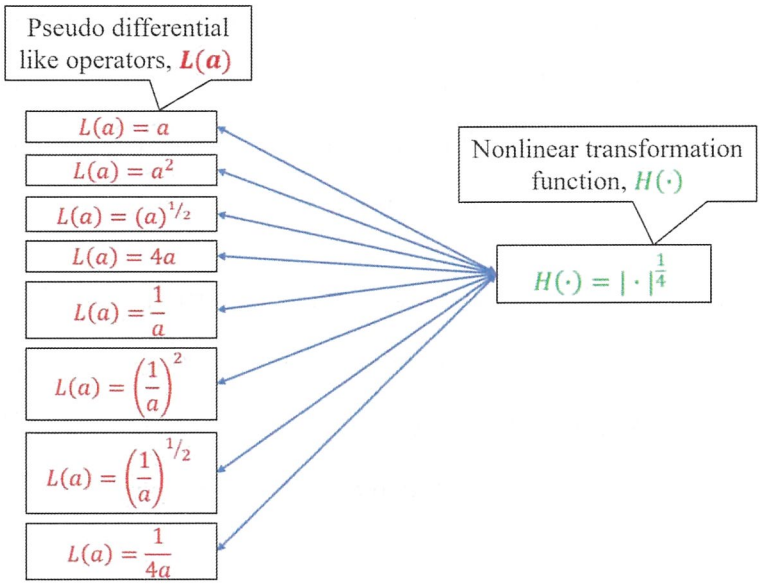

Figure 3.2: The various setting of $L(a)$ with $H(\cdot)$

Here, we presents generated scalograms by the conventional method [15, 16]

and by the proposed method with their qualitative observation.

i) **(Figures 3.3, 3.4)** In these figures the scalograms with $L(a) = 1$ and $H(\cdot) = |\cdot|^2$, which is the conventional setting adopted by [15, 16], where the pseudo differential like operators are not applied. They show a good distinction between the normal and the abnormal signals, but there seem no differences in the scalo-graphic representation between abnormal signals, i.e., PEA, VF, and VT. In the scalograms, energy does not change in frequency over time and wavelet coefficient values for all scalograms are at the same level which leads to failing to get the best distinction in the decision algorithm.

ii) **(Figures 3.5, 3.6)** In these figures the scalograms with $L(a) = a$ and $H(\cdot) = |\cdot|^{\frac{1}{4}}$, which is the setting of pseudo differential like operators and non-linear transformation. By this setting, no significant difference graphically between the abnormal classes signals, i.e., PEA, VF, and VT. The energies corresponding to PEA, VF, and VT are concentrated on the same level.

iii) **(Figures 3.7, 3.8)** In these figures the scalograms with $L(a) = a^2$ and $H(\cdot) = |\cdot|^{\frac{1}{4}}$, which is the setting of pseudo differential like operators and non-linear transformation. By this setting, no significant difference graphically between the abnormal classes signals, i.e., PEA, VF, and VT.

iv) **(Figures 3.9, 3.10)** In these figures the scalograms with $L(a) = (a)^{\frac{1}{2}}$ and $H(\cdot) = |\cdot|^{\frac{1}{4}}$, which is the setting of pseudo differential like operators and non-linear transformation. By this setting, energy has been enlarged slightly, but no significant difference graphically between the abnormal classes signals, i.e., PEA, VF, and VT.

v) **(Figures 3.11, 3.12)** In these figures the scalograms with $L(a) = 4a$ and $H(\cdot) = |\cdot|^{\frac{1}{4}}$, which is the setting of pseudo differential like operators and

non-linear transformation. By this setting, the distinction between abnormal classes exists same as in case ii).

vi) **(Figures 3.13, 3.14)** In these figures the scalograms with $L(a) = \frac{1}{a}$ and $H(\cdot) = |\cdot|^{\frac{1}{4}}$, which is the setting of pseudo differential like operators and non-linear transformation. By this setting, we are able to distinguish clearly between the abnormal class signals, i.e., PEA, VF, and VT. In the scalograms, energy has been changed in frequency over time. In particular, the difference between the maximum frequencies corresponding to PEA and VT is 7.2 (Hz) (randomly selected samples). The different energies over time lead to getting the best discrimination in the decision stage.

vii) **(Figures 3.15, 3.16)** In these figures the scalograms with $L(a) = (\frac{1}{a})^2$ and $H(\cdot) = |\cdot|^{\frac{1}{4}}$, which is the setting of pseudo differential like operators and non-linear transformation. By this setting, energy has been enlarged, but no significant difference graphically between the abnormal classes signals, i.e., PEA, VF, and VT.

viii) **(Figures 3.17, 3.18)** In these figures the scalograms with $L(a) = (\frac{1}{a})^{\frac{1}{2}}$ and $H(\cdot) = |\cdot|^{\frac{1}{4}}$, which is the setting of pseudo differential like operators and non-linear transformation. By this setting, we see the small differences between PEA and VT.

ix) **(Figures 3.19, 3.20)** In these figures the scalograms with $L(a) = \frac{1}{4a}$ and $H(\cdot) = |\cdot|^{\frac{1}{4}}$, which is the setting of pseudo differential like operators and non-linear transformation. By this setting, the distinction between abnormal classes exists same as in case vi). Therefore, we do not have a better distinction than the one of the case vi).

From the experimental results (also cf. subsection 3.2.3, and 3.2.4), for the subsequent considerations we henceforth adopt the pseudo differential like operators

$L(a) = \frac{1}{a}$ with the non-linear transformation $H(\cdot) = |\cdot|^{\frac{1}{4}}$.

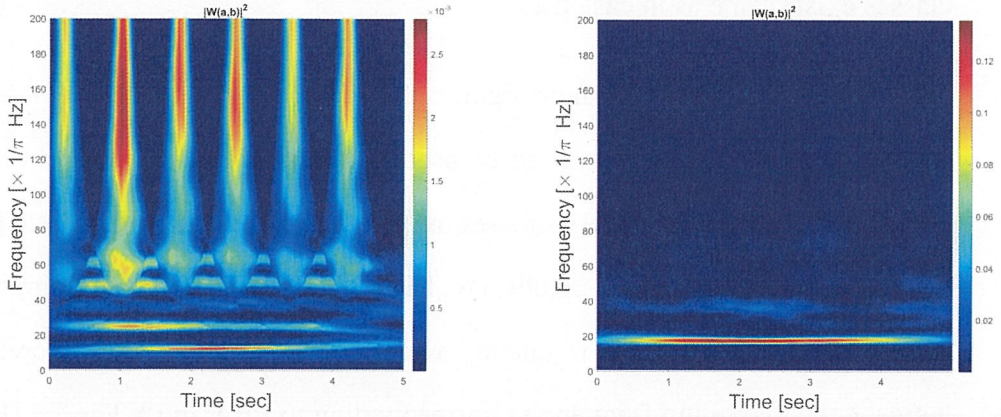

Figure 3.3: Generated scalograms by the conventional method (setting $L(a) = 1$ with $H(\cdot) = |\cdot|^2$) (SR : Left, PEA : Right)

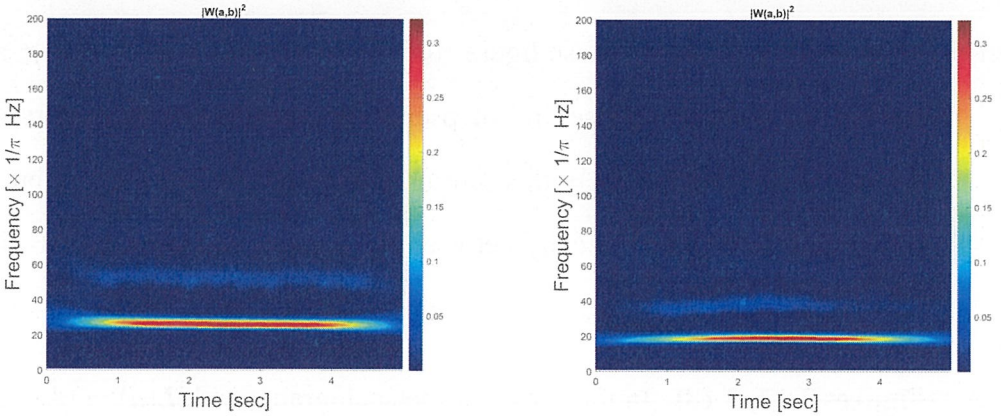

Figure 3.4: Generated scalograms by the conventional method (setting $L(a) = 1$ with $H(\cdot) = |\cdot|^2$) (VF : Left, VT : Right)

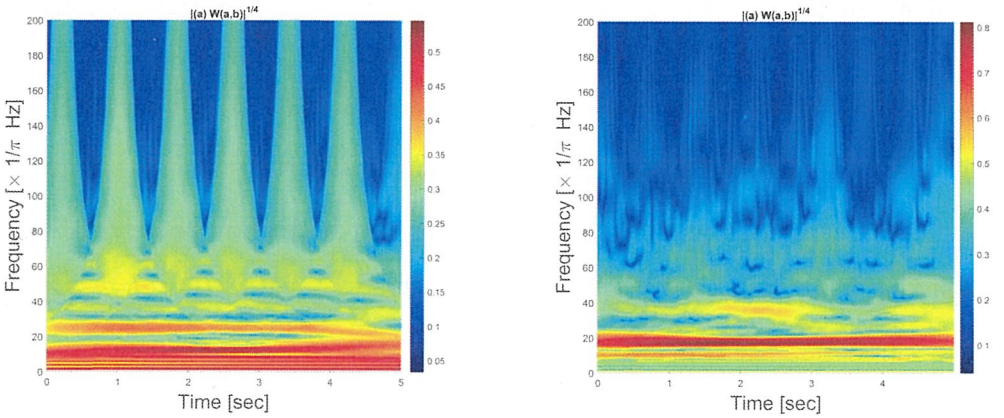

Figure 3.5: Generated scalograms by setting $L(a) = a$ with $H(\cdot) = |\cdot|^{\frac{1}{4}}$ (SR : Left, PEA: Right)

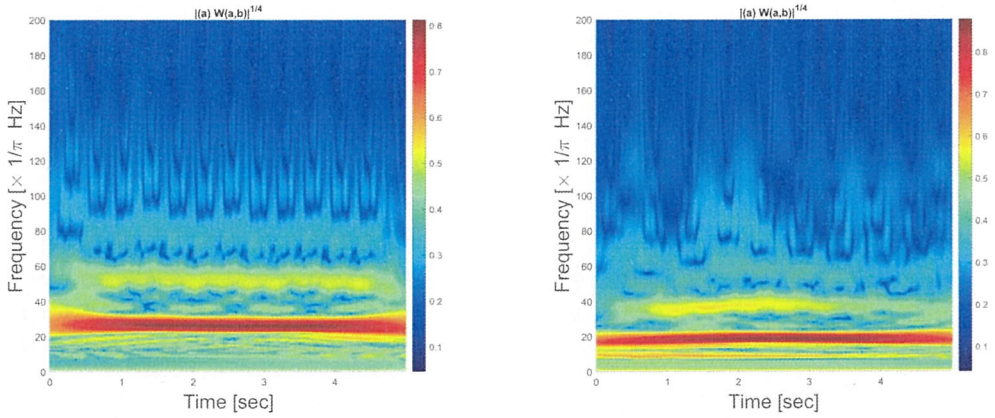

Figure 3.6: Generated scalograms by setting $L(a) = a$ with $H(\cdot) = |\cdot|^{\frac{1}{4}}$ (VF : Left, VT : Right)

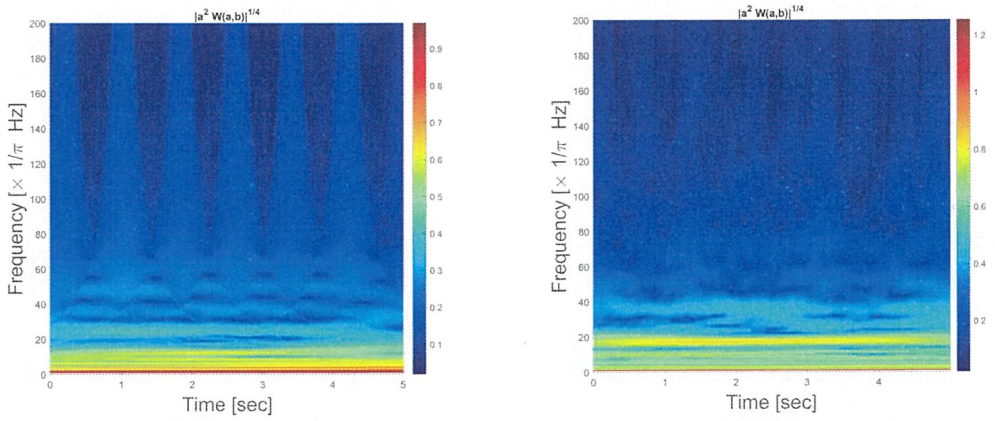

Figure 3.7: Generated scalograms by setting $L(a) = a^2$ with $H(\cdot) = |\cdot|^{\frac{1}{4}}$ (SR : Left, PEA: Right)

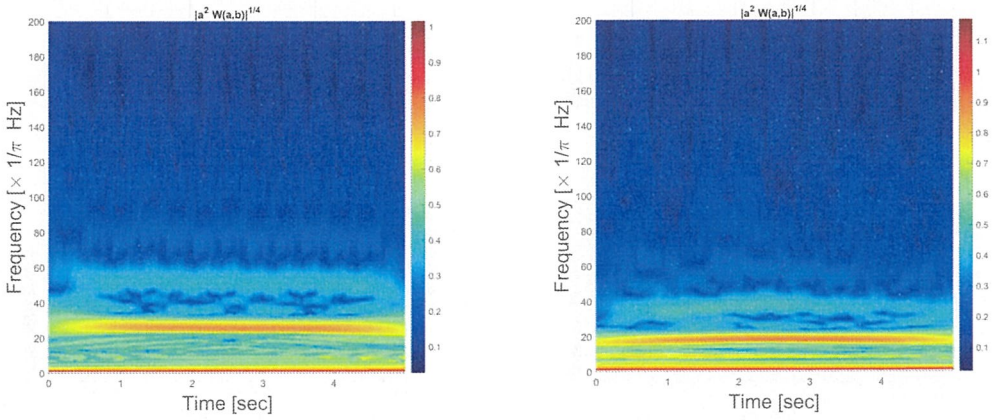

Figure 3.8: Generated scalograms by setting $L(a) = a^2$ with $H(\cdot) = |\cdot|^{\frac{1}{4}}$ (VF : Left, VT : Right)

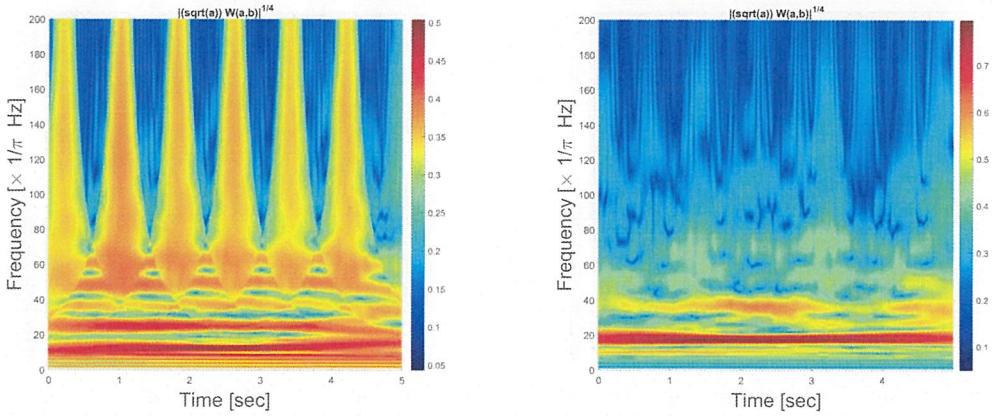

Figure 3.9: Generated scalograms by setting $L(a) = (a)^{\frac{1}{2}}$ with $H(\cdot) = |\cdot|^{\frac{1}{4}}$ (SR : Left, PEA: Right)

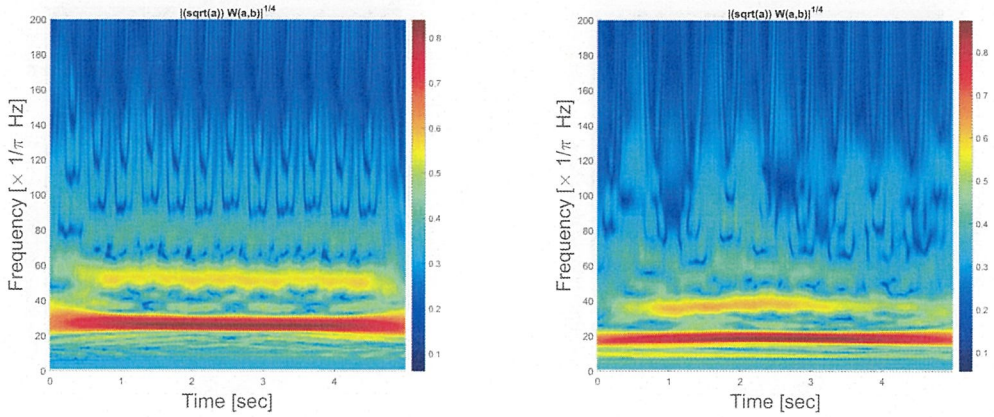

Figure 3.10: Generated scalograms by setting $L(a) = (a)^{\frac{1}{2}}$ with $H(\cdot) = |\cdot|^{\frac{1}{4}}$ (VF : Left, VT : Right)

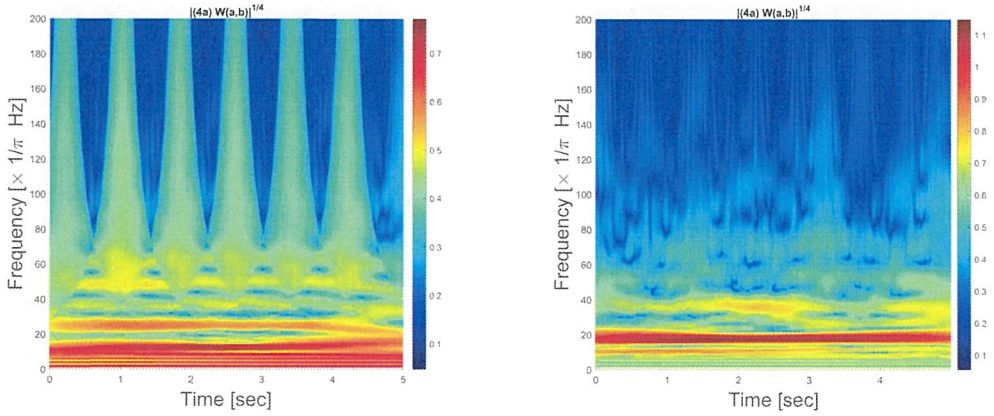

Figure 3.11: Generated scalograms by setting $L(a) = 4a$ with $H(\cdot) = |\cdot|^{\frac{1}{4}}$ (SR : Left, PEA: Right)

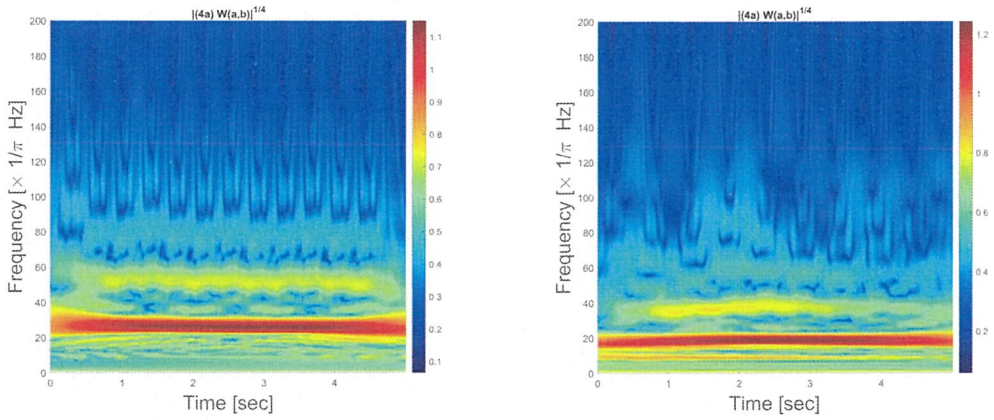

Figure 3.12: Generated scalograms by setting $L(a) = 4a$ with $H(\cdot) = |\cdot|^{\frac{1}{4}}$ (VF : Left, VT : Right)

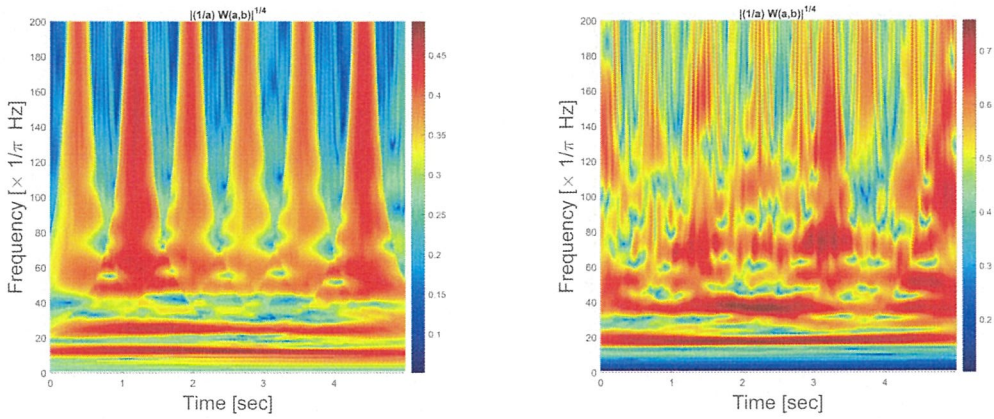

Figure 3.13: Generated scalograms by setting $L(a) = \frac{1}{a}$ with $H(\cdot) = |\cdot|^{\frac{1}{4}}$ (SR : Left, PEA: Right)

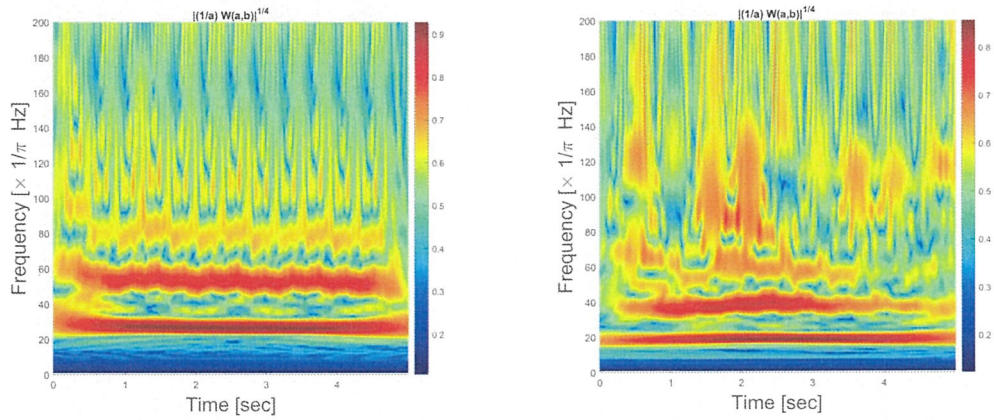

Figure 3.14: Generated scalograms by setting $L(a) = \frac{1}{a}$ with $H(\cdot) = |\cdot|^{\frac{1}{4}}$ (VF : Left, VT : Right)

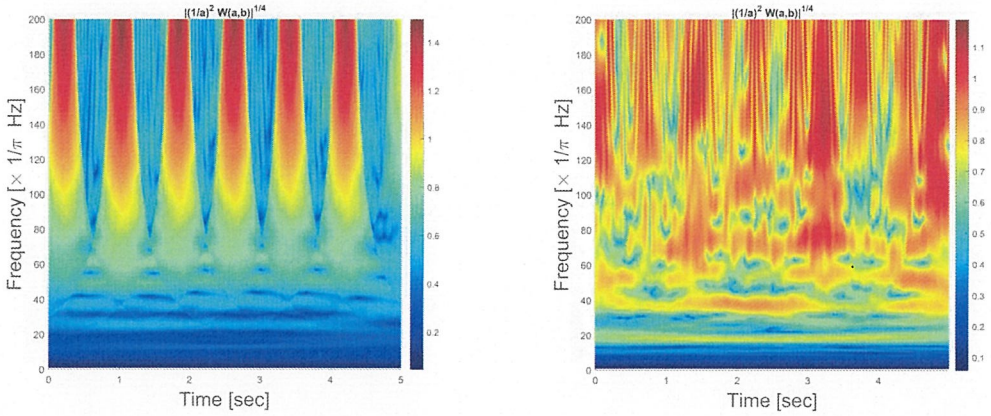

Figure 3.15: Generated scalograms by setting $L(a) = (\frac{1}{a})^2$ with $H(\cdot) = |\cdot|^{\frac{1}{4}}$ (SR : Left, PEA: Right)

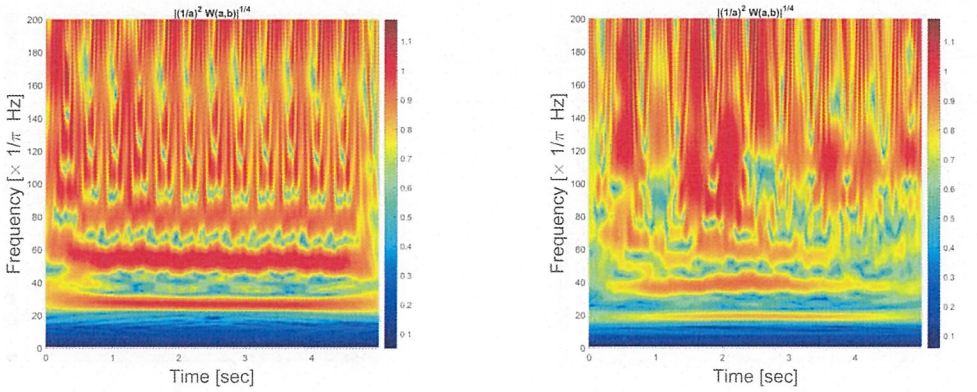

Figure 3.16: Generated scalograms by setting $L(a) = (\frac{1}{a})^2$ with $H(\cdot) = |\cdot|^{\frac{1}{4}}$ (VF : Left, VT : Right)

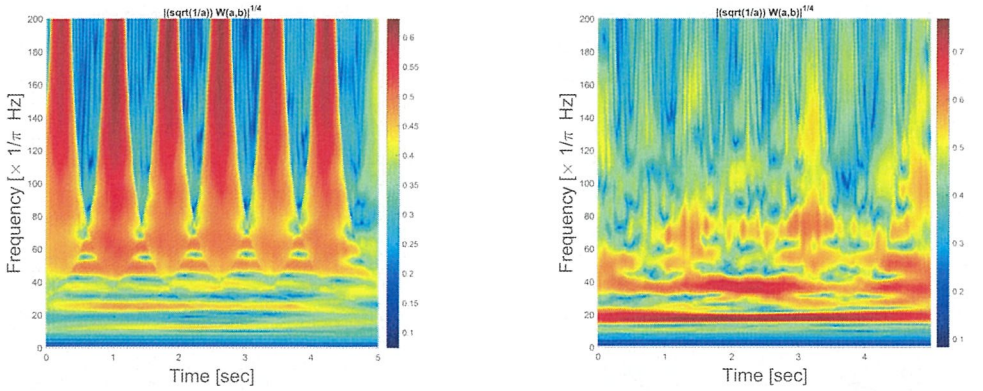

Figure 3.17: Generated scalograms by setting $L(a) = (\frac{1}{a})^{\frac{1}{2}}$ with $H(\cdot) = |\cdot|^{\frac{1}{4}}$ (SR : Left, PEA: Right)

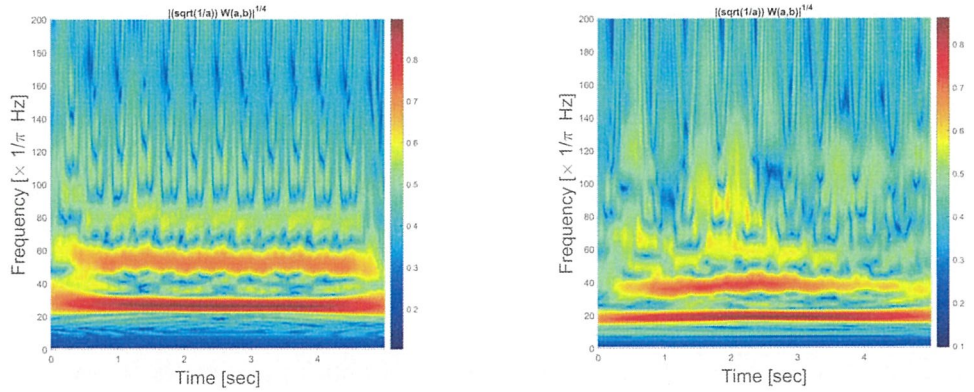

Figure 3.18: Generated scalograms by setting $L(a) = (\frac{1}{a})^{\frac{1}{2}}$ with $H(\cdot) = |\cdot|^{\frac{1}{4}}$ (VF : Left, VT : Right)

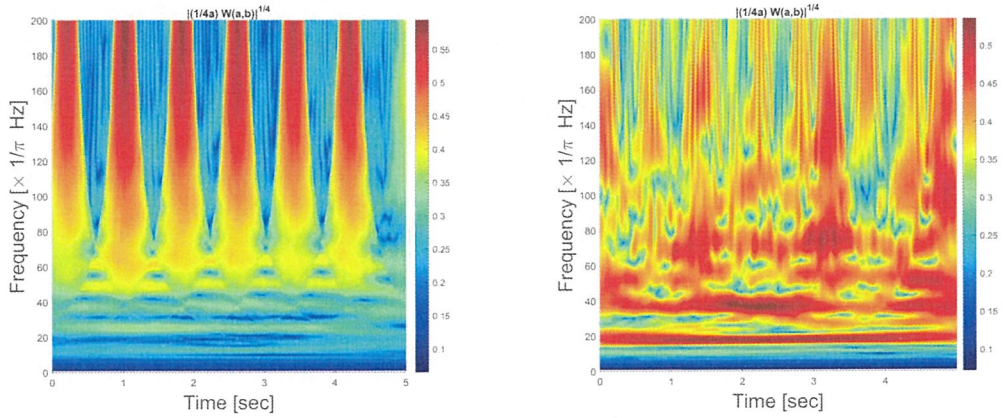

Figure 3.19: Generated scalograms by setting $L(a) = \frac{1}{4a}$ with $H(\cdot) = |\cdot|^{\frac{1}{4}}$ (SR : Left, PEA: Right)

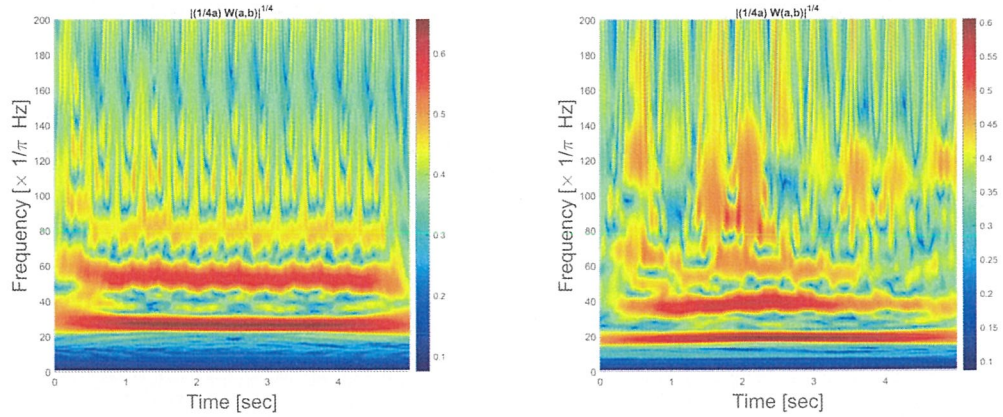

Figure 3.20: Generated scalograms by setting $L(a) = \frac{1}{4a}$ with $H(\cdot) = |\cdot|^{\frac{1}{4}}$ (VF : Left, VT : Right)

3.2.3 General observations

We demonstrate an intrinsic effect of $L(a)$ with $H(\cdot)$ using qualitative evaluation before the numerical decision. We thus select the qualitatively best two-variable scatter plot with histogram for the 1079 samples from all the setting of $L(a)$ with $H(\cdot)$, as in Figures 3.21, 3.22, 3.23, 3.24, 3.25, 3.26, 3.27 and 3.28, respectively. In the figures, we observe that the distribution of abnormal signals (PEA, VF, and VT) are quite different from that of normal signal (SR), where the distribution of abnormal signals is at close distances for all settings of $L(a)$ with $H(\cdot)$. Among the different setting, $L(a) = \frac{1}{a}$ with $H(\cdot) = |\cdot|^{\frac{1}{4}}$ shows better distribution with respect to mean of NSI and the combination of mean of NSI with variance of NSI. In the scatter plot with histogram for this setting, the distribution of the abnormal class signals (PEA, VF, and VT) is quite far from that of normal class signal (SR), where the distribution of the abnormal class signals (PEA, VF, and VT) is isolated from each other. For example, the distribution of VF is isolated from the VT and far from the PEA, where little regions of VT and PEA overlap with each other. Also, the histogram of the abnormal class is slightly interdependent with each other. Therefore, the highest separation exists for this setting in the abnormal class signals.

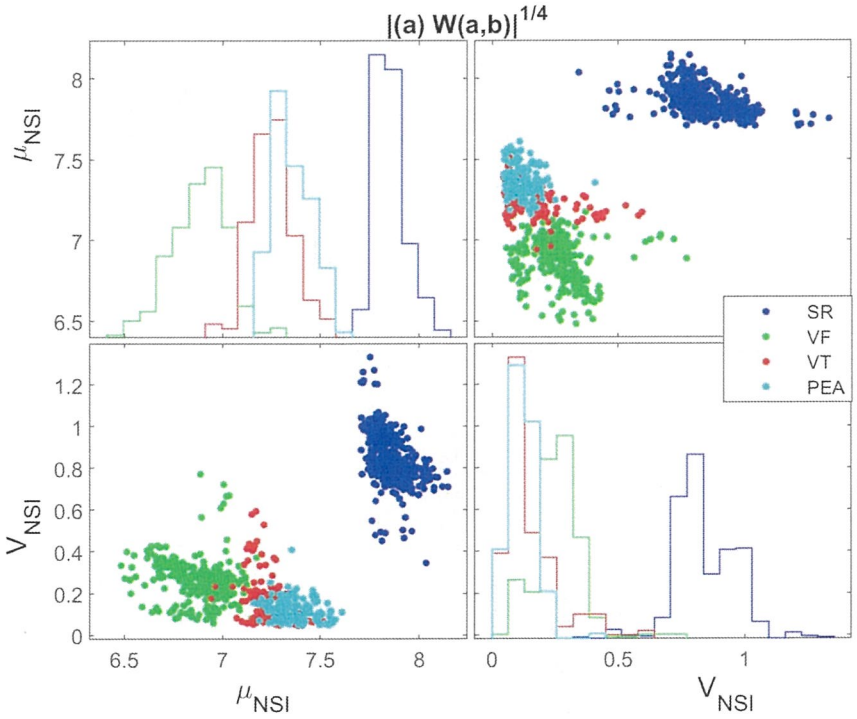

Figure 3.21: Effect of pseudo-differential operator $L(a)$ with nonlinear function $H(\cdot)$ on the setting $L(a) = a$ with $H(\cdot) = |\cdot|^{\frac{1}{4}}$

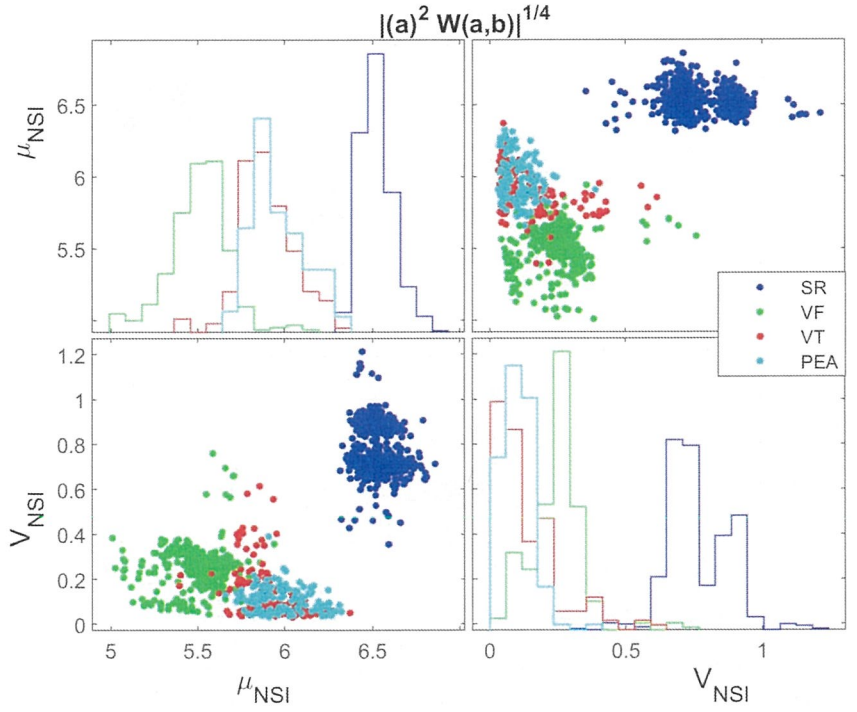

Figure 3.22: Effect of pseudo-differential operator $L(a)$ with nonlinear function $H(\cdot)$ on the setting $L(a) = a^2$ with $H(\cdot) = |\cdot|^{\frac{1}{4}}$

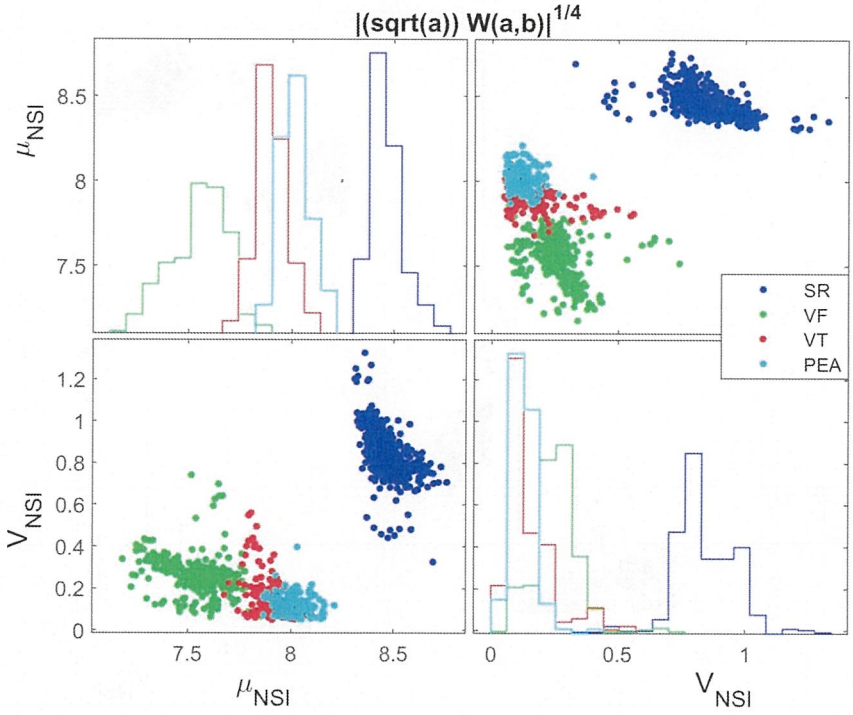

Figure 3.23: Effect of pseudo-differential operator $L(a)$ with nonlinear function $H(\cdot)$ on the setting $L(a) = (a)^{\frac{1}{2}}$ with $H(\cdot) = |\cdot|^{\frac{1}{4}}$

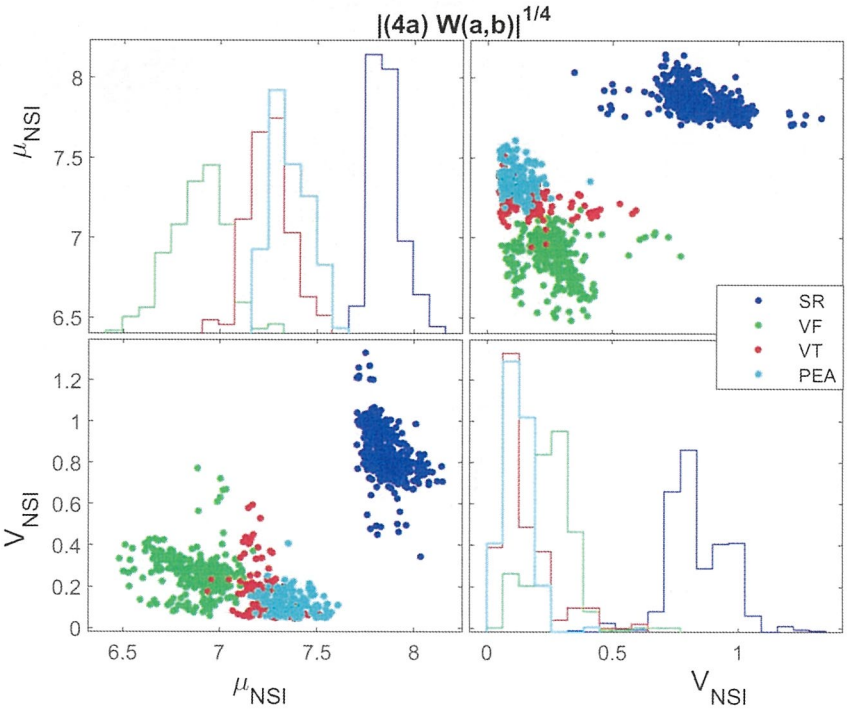

Figure 3.24: Effect of pseudo-differential operator $L(a)$ with nonlinear function $H(\cdot)$ on the setting $L(a) = 4a$ with $H(\cdot) = |\cdot|^{\frac{1}{4}}$

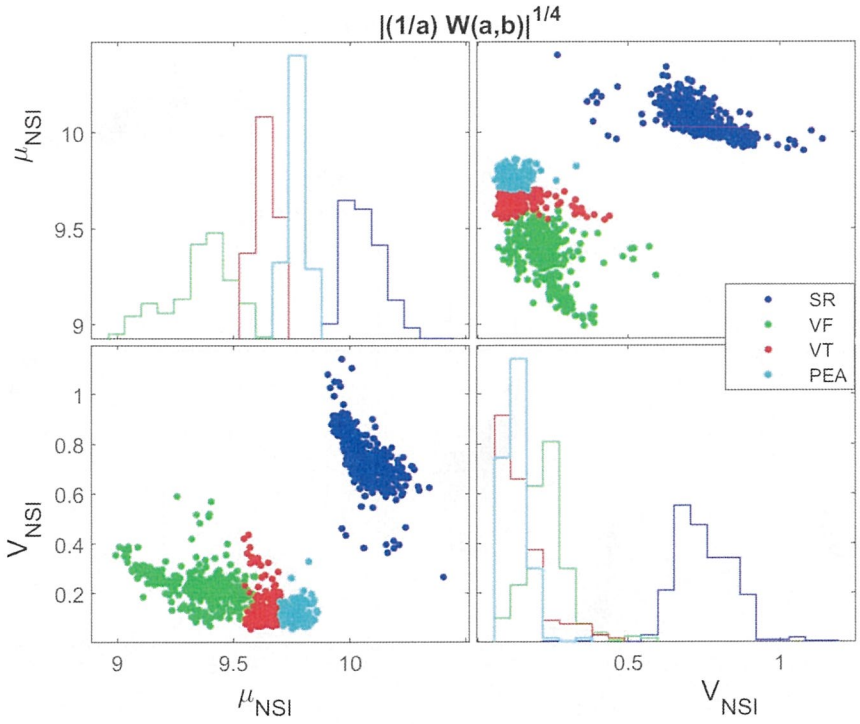

Figure 3.25: Effect of pseudo-differential operator $L(a)$ with nonlinear function $H(\cdot)$ on the setting $L(a) = \frac{1}{a}$ with $H(\cdot) = |\cdot|^{\frac{1}{4}}$

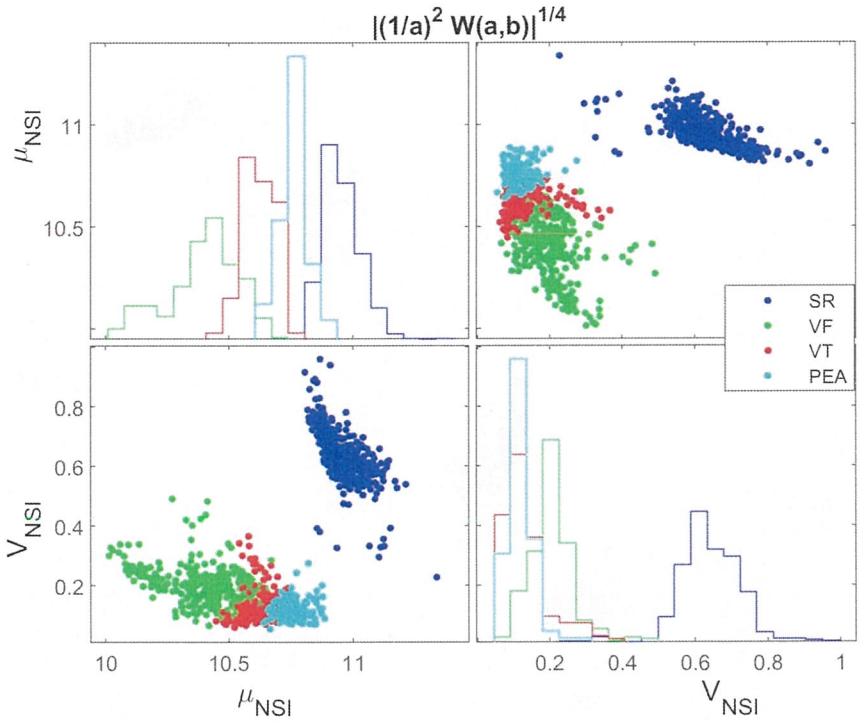

Figure 3.26: Effect of pseudo-differential operator $L(a)$ with nonlinear function $H(\cdot)$ on the setting $L(a) = (\frac{1}{a})^2$ with $H(\cdot) = |\cdot|^{\frac{1}{4}}$

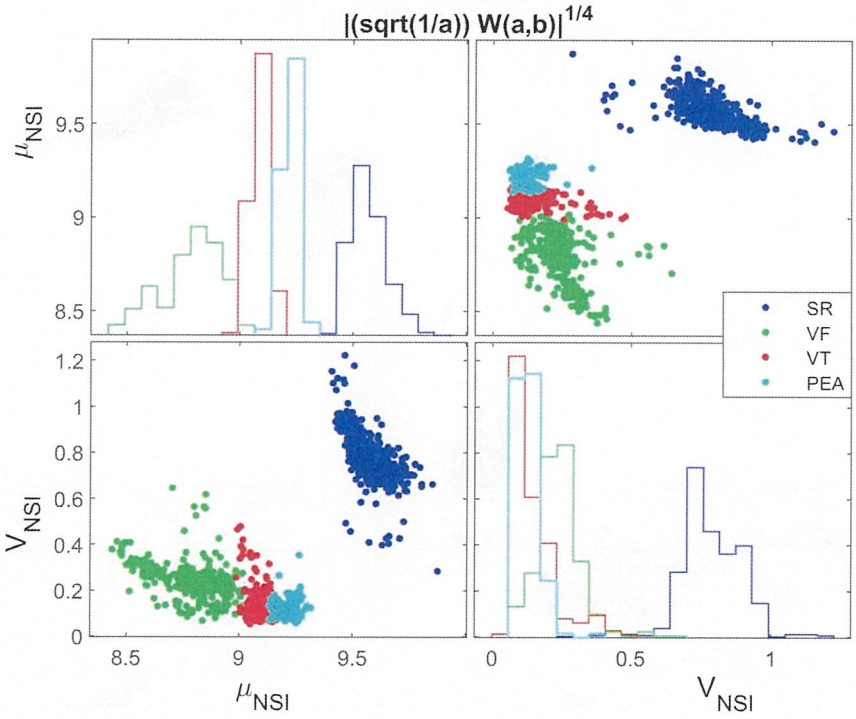

Figure 3.27: Effect of pseudo-differential operator $L(a)$ with nonlinear function $H(\cdot)$ on the setting $L(a) = (\frac{1}{a})^{\frac{1}{2}}$ with $H(\cdot) = |\cdot|^{\frac{1}{4}}$

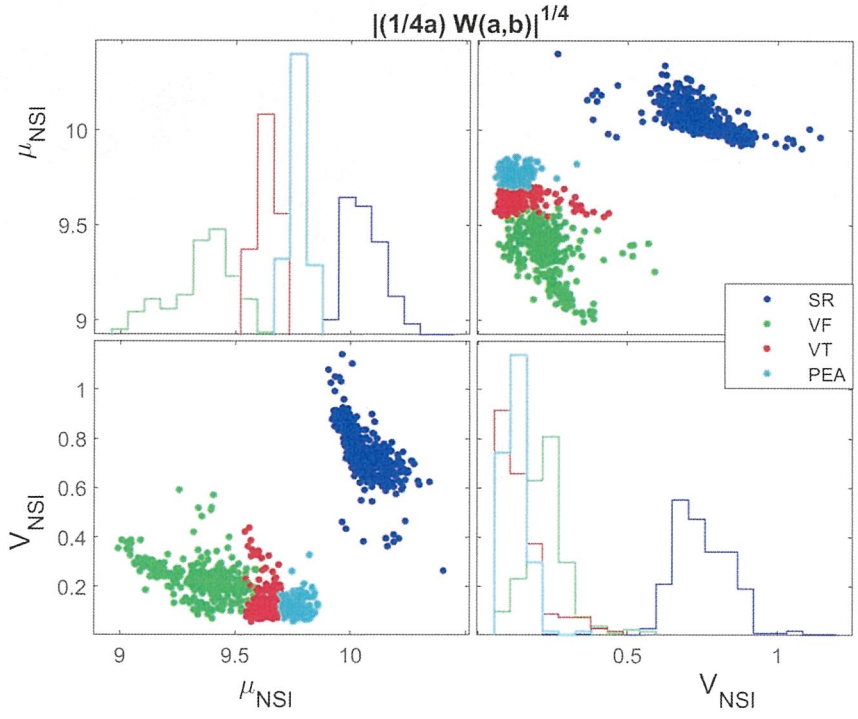

Figure 3.28: Effect of pseudo-differential operator $L(a)$ with nonlinear function $H(\cdot)$ on the setting $L(a) = \frac{1}{4a}$ with $H(\cdot) = |\cdot|^{\frac{1}{4}}$

3.2.4 Quantitative observation

We perform the numerical experiments for various setting of pseudo differential like operators $L(a)$ with non-linear transformation function $H(\cdot)$ and compared the proposed method with the conventional method. In the experiments, we follow the cross validation process (see subsection 3.3.1.4.2), and use macro-and micro-average precision, recall, F1-score (F-measure) and accuracy, as performance indices which are commonly used in multi-class classification measurement (see subsection 3.3.1.4.1), and adopt the histogram as a classifier of the groups to make the decision (see subsection 3.3.1.3). Tables (3.1-3.4) show fold-wise and group-wise individual precision, recall, F1-score (F-measure) and accuracy and macro- and micro-average precision, recall, F1-score for the various settings of pseudo-differential like operators $L(a)$ with nonlinear transformation function $H(\cdot)$. On the other hand, Table 3.5 shows the experimental discrimination accuracy for the various setting of pseudo-differential like operators with nonlinear transformation function and the proposed method keeps the better performance of the discrimination than the conventional method which is conducted by Okai et al [16, 29]. As shown in the Tables 3.5, the ratio of the successful discrimination between normal signals (SR) and abnormal signals (PEA, VF, and VT) is 100% for all setting of pseudo-differential like operators and nonlinear transformation functions and for the conventional approaches. How about the discrimination performance between shockable (VF, and VT) and non-shockable (PEA) arrhythmias for the different setting of pseudo-differential like operators with nonlinear transformation functions and for the conventional approaches? The setting $L(a) = a$ with $H(\cdot) = |\cdot|^{\frac{1}{4}}$ is able to achieves 85.37% accuracy, while 84.52% accuracy is obtained for the setting $L(a) = a^2$ with $H(\cdot) = |\cdot|^{\frac{1}{4}}$. Similarly, the setting $L(a) = (a)^{\frac{1}{2}}$ with $H(\cdot) = |\cdot|^{\frac{1}{4}}$ is able to achieves 87.41% accuracy, while 85.37% accuracy is obtained for the setting $L(a) = 4a$ with $H(\cdot) = |\cdot|^{\frac{1}{4}}$. On the other hand, the setting $L(a) = \frac{1}{a}$ with

$H(\cdot) = |\cdot|^{\frac{1}{4}}$ is able to achieves 91.58% accuracy, while 86.73% accuracy is obtained for the setting $L(a) = (\frac{1}{a})^2$ with $H(\cdot) = |\cdot|^{\frac{1}{4}}$. Similarly, the setting $L(a) = (\frac{1}{a})^{\frac{1}{2}}$ with $H(\cdot) = |\cdot|^{\frac{1}{4}}$ is able to achieves 90.62% accuracy, while 91.58% accuracy is obtained for the setting $L(a) = \frac{1}{4a}$ with $H(\cdot) = |\cdot|^{\frac{1}{4}}$. Therefore, among the various setting, $L(a) = \frac{1}{a}$ with $H(\cdot) = |\cdot|^{\frac{1}{4}}$ shows (91.58% accuracy) the better distinction performance. On the other hand, from the precise numerical results given of section 4.2 in [16] and in part A, section III of [29], we can derive 84.86% and 86.03% accuracy for the shockable (VF, VT) versus non-shockable (PEA) arrhythmia cases, while present proposed method increases the accuracy to 91.58%, with 6.72% and 5.55% gain.

The performance is improved of the proposed method because, the proposed method effectively (generate distinguishable scalogram for the shockable and non-shockable arrhythmia cases in abnormal class signals) enlarge energies over time which lead in decision algorithm to get the best distinction (see Figures 3.13, 3.14). This is the main advantage of the proposed method. On the other hand the performance is low of the conventional method for shockable vs non-shockable cases because, the conventional method generates same level of energy over time which gives a barrier to distinguish in the decision algorithm (see Figures 3.3, 3.4).

Table 3.1: Fold-wise and group-wise performances for the various settings of pseudo-differential like operators $L(a)$ with nonlinear transformation function $H(\cdot)$

Setting	Fold no.	Group	Precision	Recall	F1-score	Accuracy (%)
$L(a) = a$ with $H(\cdot) = \lvert\cdot\rvert^{\frac{1}{4}}$	Fold-1	PEA	0.8710	0.8438	0.8571	96.34
		SR	1.0	1.0	1.0	100.0
		VF	0.9710	0.9155	0.9420	96.74
		VT	0.7568	0.8750	0.8116	94.71
		Macro avg.	0.8995	0.9086	0.9027	
		Micro avg.	0.9390	0.9390	0.9390	
	Fold-2	PEA	0.7813	0.8065	0.7937	95.23
		SR	1.0	1.0	1.0	100.0
		VF	0.9467	0.9221	0.9342	96.33
		VT	0.7692	0.7895	0.7792	93.77
		Macro avg.	0.8743	0.8795	0.8768	
		Micro avg.	0.9267	0.9267	0.9267	
	Fold-3	PEA	0.7429	0.8125	0.7761	94.71
		SR	1.0	1.0	1.0	100.0
		VF	0.9714	0.8718	0.9189	95.77
		VT	0.7174	0.8049	0.7586	92.60
		Macro avg.	0.8579	0.8723	0.8634	
		Micro avg.	0.9155	0.9155	0.9155	
	Fold-4	PEA	0.8049	0.8462	0.8250	94.92
		SR	1.0	1.0	1.0	100.0
		VF	0.9130	0.8630	0.8873	94.20
		VT	0.7174	0.7500	0.7333	91.30
		Macro avg.	0.8588	0.8684	0.8614	
		Micro avg.	0.9022	0.9022	0.9022	
$L(a) = a^2$ with $H(\cdot) = \lvert\cdot\rvert^{\frac{1}{4}}$	Fold-1	PEA	0.8485	0.8000	0.8235	95.50
		SR	1.0	1.0	1.0	100.0
		VF	0.9375	0.8824	0.9091	94.38
		VT	0.6957	0.8205	0.7529	92.13
		Macro avg.	0.8704	0.8757	0.8714	
		Micro avg.	0.9101	0.9101	0.9101	
	Fold-2	PEA	0.7568	0.8235	0.7887	94.20
		SR	1.0	1.0	1.0	100.0
		VF	0.8947	0.8947	0.8947	95.36
		VT	0.7907	0.7391	0.7640	91.89
		Macro avg.	0.8605	0.8643	0.8619	
		Micro avg.	0.9073	0.9073	0.9073	
	Fold-3	PEA	0.8000	0.7742	0.7869	95.03
		SR	1.0	1.0	1.0	100.0
		VF	0.9697	0.8889	0.9275	96.18
		VT	0.6286	0.7857	0.6984	92.74
		Macro avg.	0.8496	0.8622	0.8532	
		Micro avg.	0.9198	0.9198	0.9198	
	Fold-4	PEA	0.8529	0.8529	0.8529	96.56
		SR	1.0	1.0	1.0	100.0
		VF	0.9167	0.9059	0.9112	94.84
		VT	0.7674	0.7857	0.7765	93.47
		Macro avg.	0.8843	0.8861	0.8852	
		Micro avg.	0.9244	0.9244	0.9244	

Table 3.2: Fold-wise and group-wise performances for the various settings of pseudo-differential like operators $L(a)$ with nonlinear transformation function $H(\cdot)$ (continue)

Setting	Fold no.	Group	Precision	Recall	F1-score	Accuracy (%)
$L(a) = (a)^{\frac{1}{2}}$ with $H(\cdot) = \lvert\cdot\rvert^{\frac{1}{4}}$	Fold-1	PEA	0.8125	0.8966	0.8525	96.59
		SR	1.0	1.0	1.0	100.0
		VF	0.9733	0.9241	0.9481	96.96
		VT	0.8372	0.8571	0.8471	95.07
		Macro avg.	0.9058	0.9194	0.9119	
		Micro avg.	0.9432	0.9432	0.9432	
	Fold-2	PEA	0.9333	0.8485	0.8889	97.35
		SR	1.0	1.0	1.0	100.0
		VF	0.9275	0.8889	0.9078	95.09
		VT	0.7381	0.8611	0.7949	93.96
		Macro avg.	0.8997	0.8996	0.8979	
		Micro avg.	0.9321	0.9321	0.9321	
	Fold-3	PEA	0.7941	0.8710	0.8308	96.11
		SR	1.0	1.0	1.0	100.0
		VF	0.9452	0.9079	0.9262	96.11
		VT	0.8085	0.8085	0.8085	93.63
		Macro avg.	0.8870	0.8968	0.8914	
		Micro avg.	0.9293	0.9293	0.9293	
	Fold-4	PEA	0.8684	0.8049	0.8354	95.13
		SR	1.0	1.0	1.0	100.0
		VF	0.9559	0.9028	0.9286	96.25
		VT	0.6486	0.8000	0.7164	92.88
		Macro avg.	0.8682	0.8769	0.8701	
		Micro avg.	0.9213	0.9213	0.9213	
$L(a) = 4a$ with $H(\cdot) = \lvert\cdot\rvert^{\frac{1}{4}}$	Fold-1	PEA	0.9000	0.8710	0.8852	97.29
		SR	1.0	1.0	1.0	100.0
		VF	0.9552	0.9275	0.9412	96.91
		VT	0.7692	0.8333	0.8000	94.20
		Macro avg.	0.9061	0.9080	0.9066	
		Micro avg.	0.9421	0.9421	0.9421	
	Fold-2	PEA	0.7750	0.7949	0.7848	93.68
		SR	1.0	1.0	1.0	100.0
		VF	0.9420	0.9155	0.9286	96.28
		VT	0.7381	0.7561	0.7470	92.19
		Macro avg.	0.8638	0.8666	0.8651	
		Micro avg.	0.9108	0.9108	0.9108	
	Fold-3	PEA	0.7714	0.7714	0.7714	94.13
		SR	1.0	1.0	1.0	100.0
		VF	0.9437	0.8590	0.8993	94.50
		VT	0.6667	0.8000	0.7273	92.30
		Macro avg.	0.8454	0.8576	0.8495	
		Micro avg.	0.9048	0.9048	0.9048	
	Fold-4	PEA	0.7647	0.8966	0.8254	96.04
		SR	1.0	1.0	1.0	100.0
		VF	0.9595	0.8765	0.9161	95.32
		VT	0.7778	0.8140	0.7955	93.52
		Macro avg.	0.8755	0.8968	0.8842	
		Micro avg.	0.9245	0.9245	0.9245	

Table 3.3: Fold-wise and group-wise performances for the various settings of pseudo-differential like operators $L(a)$ with nonlinear transformation function $H(\cdot)$ (continue)

Setting	Fold no.	Group	Precision	Recall	F1-score	Accuracy (%)
$L(a) = \frac{1}{a}$ with $H(\cdot) = \lvert\cdot\rvert^{\frac{1}{4}}$	Fold-1	PEA	0.9048	0.9048	0.9048	97.19
		SR	1.0	1.0	1.0	100.0
		VF	0.9610	0.9250	0.9427	96.84
		VT	0.8095	0.8718	0.8395	95.43
		Macro avg.	0.9188	0.9254	0.9217	
		Micro avg.	0.9474	0.9474	0.9474	
	Fold-2	PEA	0.9714	0.9444	0.9577	98.86
		SR	1.0	1.0	1.0	100.0
		VF	0.9692	0.9545	0.9618	98.10
		VT	0.8485	0.9032	0.8750	96.96
		Macro avg.	0.9473	0.9506	0.9486	
		Micro avg.	0.9697	0.9697	0.9697	
	Fold-3	PEA	0.8421	0.9143	0.8767	96.85
		SR	1.0	1.0	1.0	100.0
		VF	0.9730	0.8780	0.9231	95.80
		VT	0.7959	0.8864	0.8387	94.75
		Macro avg.	0.9027	0.9197	0.9096	
		Micro avg.	0.9371	0.9371	0.9371	
	Fold-4	PEA	0.8750	1.0	0.9333	98.77
		SR	1.0	1.0	1.0	100.0
		VF	0.9851	0.9296	0.9565	97.54
		VT	0.8810	0.9024	0.8916	96.31
		Macro avg.	0.9353	0.9580	0.9454	
		Micro avg.	0.9631	0.9631	0.9631	
$L(a) = (\frac{1}{a})^2$ with $H(\cdot) = \lvert\cdot\rvert^{\frac{1}{4}}$	Fold-1	PEA	0.8919	0.8462	0.8684	96.21
		SR	1.0	1.0	1.0	100.0
		VF	0.9324	0.8961	0.9139	95.07
		VT	0.7500	0.8571	0.8000	94.31
		Macro avg.	0.8936	0.8999	0.8956	
		Micro avg.	0.9280	0.9280	0.9280	
	Fold-2	PEA	0.8571	0.9231	0.8889	97.73
		SR	1.0	1.0	1.0	100.0
		VF	0.9701	0.8667	0.9155	95.47
		VT	0.7556	0.8718	0.8095	93.96
		Macro avg.	0.8957	0.9154	0.9035	
		Micro avg.	0.9358	0.9358	0.9358	
	Fold-3	PEA	0.8500	0.8718	0.8608	96.08
		SR	1.0	1.0	1.0	100.0
		VF	0.8873	0.8873	0.8873	94.30
		VT	0.7561	0.7381	0.7470	92.52
		Macro avg.	0.8734	0.8743	0.8738	
		Micro avg.	0.9146	0.9146	0.9146	
	Fold-4	PEA	0.8387	0.8667	0.8525	96.65
		SR	1.0	1.0	1.0	100.0
		VF	0.9306	0.8816	0.9054	94.79
		VT	0.8095	0.8718	0.8395	95.16
		Macro avg.	0.8947	0.9050	0.8993	
		Micro avg.	0.9331	0.9331	0.9331	

Table 3.4: Fold-wise and group-wise performances for the various settings of pseudo-differential like operators $L(a)$ with nonlinear transformation function $H(\cdot)$ (continue)

Setting	Fold no.	Group	Precision	Recall	F1-score	Accuracy (%)
$L(a) = (\frac{1}{a})^{\frac{1}{2}}$ with $H(\cdot) = \lvert\cdot\rvert^{\frac{1}{4}}$	Fold-1	PEA	0.8750	0.8750	0.8750	96.53
		SR	1.0	1.0	1.0	100.0
		VF	0.9610	0.9136	0.9367	96.53
		VT	0.7959	0.8667	0.8298	94.46
		Macro avg.	0.9080	0.9138	0.9104	
		Micro avg.	0.9377	0.9377	0.9377	
	Fold-2	PEA	0.8621	0.9259	0.8929	97.53
		SR	1.0	1.0	1.0	100.0
		VF	0.9844	0.9545	0.9692	98.35
		VT	0.8824	0.8824	0.8824	96.70
		Macro avg.	0.9322	0.9407	0.9361	
		Micro avg.	0.9630	0.9630	0.9630	
	Fold-3	PEA	0.8611	0.9118	0.8857	97.23
		SR	1.0	1.0	1.0	100.0
		VF	0.9872	0.9059	0.9448	96.88
		VT	0.7907	0.8947	0.8395	95.50
		Macro avg.	0.9097	0.9281	0.9175	
		Micro avg.	0.9481	0.9481	0.9481	
	Fold-4	PEA	0.9355	0.8788	0.9063	97.67
		SR	1.0	1.0	1.0	100.0
		VF	0.9403	0.9403	0.9403	96.89
		VT	0.8250	0.8684	0.8462	95.34
		Macro avg.	0.9252	0.9219	0.9232	
		Micro avg.	0.9496	0.9496	0.9496	
$L(a) = \frac{1}{4a}$ with $H(\cdot) = \lvert\cdot\rvert^{\frac{1}{4}}$	Fold-1	PEA	0.8333	0.9677	0.8955	97.41
		SR	1.0	1.0	1.0	100.0
		VF	0.9861	0.8987	0.9404	96.67
		VT	0.8333	0.8750	0.8537	95.57
		Macro avg.	0.9132	0.9354	0.9224	
		Micro avg.	0.9483	0.9483	0.9483	
	Fold-2	PEA	0.8889	0.9600	0.9231	98.50
		SR	1.0	1.0	1.0	100.0
		VF	0.9722	0.8974	0.9333	96.25
		VT	0.7955	0.8750	0.8333	94.75
		Macro avg.	0.9141	0.9331	0.9224	
		Micro avg.	0.9476	0.9476	0.9476	
	Fold-3	PEA	0.9524	0.9091	0.9302	97.84
		SR	1.0	1.0	1.0	100.0
		VF	0.9697	0.9552	0.9624	98.20
		VT	0.8462	0.9167	0.8800	96.77
		Macro avg.	0.9421	0.9452	0.9432	
		Micro avg.	0.9642	0.9642	0.9642	
	Fold-4	PEA	0.9118	0.9118	0.9118	97.70
		SR	1.0	1.0	1.0	100.0
		VF	0.9589	0.9333	0.9459	96.94
		VT	0.8537	0.8974	0.8750	96.18
		Macro avg.	0.9311	0.9356	0.9332	
		Micro avg.	0.9542	0.9542	0.9542	

Table 3.5: Overall quantitative evaluation for the various settings of pseudo-differential like operators $L(a)$ with nonlinear transformation function $H(\cdot)$, and comparison with the conventional approaches.

Method	Setting	Distinction scheme	Accuracy(%)
The GWT with pseudo-differential like operators and nonlinear transformation function (Proposed)	$L(a)=a$ with $H(\cdot)=\lvert\cdot\rvert^{\frac{1}{2}}$	Normal (SR) vs Abnormal (PEA, VF and VT)	100.0
		Shockable (VF, VT) vs non-shockable (PEA)	85.37
	$L(a)=a^2$ with $H(\cdot)=\lvert\cdot\rvert^{\frac{1}{2}}$	Normal (SR) vs Abnormal (PEA, VF and VT)	100.0
		Shockable (VF, VT) vs non-shockable (PEA)	84.52
	$L(a)=(a)^{\frac{1}{2}}$ with $H(\cdot)=\lvert\cdot\rvert^{\frac{1}{2}}$	Normal (SR) vs Abnormal (PEA, VF and VT)	100.0
		Shockable (VF, VT) vs non-shockable (PEA)	87.41
	$L(a)=4a$ with $H(\cdot)=\lvert\cdot\rvert^{\frac{1}{4}}$	Normal (SR) vs Abnormal (PEA, VF and VT)	100.0
		Shockable (VF, VT) vs non-shockable (PEA)	85.37
	$L(a)=\frac{1}{a}$ with $H(\cdot)=\lvert\cdot\rvert^{\frac{1}{2}}$	Normal (SR) vs Abnormal (PEA, VF and VT)	100.0
		Shockable (VF, VT) vs non-shockable (PEA)	91.58
	$L(a)=(\frac{1}{a})^2$ with $H(\cdot)=\lvert\cdot\rvert^{\frac{1}{4}}$	Normal (SR) vs Abnormal (PEA, VF and VT)	100.0
		Shockable (VF, VT) vs non-shockable (PEA)	86.73
	$L(a)=(\frac{1}{a})^{\frac{1}{2}}$ with $H(\cdot)=\lvert\cdot\rvert^{\frac{1}{2}}$	Normal (SR) vs Abnormal (PEA, VF and VT)	100.0
		Shockable (VF, VT) vs non-shockable (PEA)	90.62
	$L(a)=\frac{1}{4a}$ with $H(\cdot)=\lvert\cdot\rvert^{\frac{1}{4}}$	Normal (SR) vs Abnormal (PEA, VF and VT)	100.0
		Shockable (VF, VT) vs non-shockable (PEA)	91.58
Conventional [16]	$L(a)=1$ with $H(\cdot)=\lvert\cdot\rvert^2$	Normal (SR) vs Abnormal (PEA, VF and VT)	100.0
		Shockable (VF, VT) vs non-shockable (PEA)	84.86
Conventional [29]	$L(a)=1$ with $H(\cdot)=\lvert\cdot\rvert^2$	Normal (SR) vs Abnormal (PEA, VF and VT)	100.0
		Shockable (VF, VT) vs non-shockable (PEA)	86.03

* The accuracy has been calculated according their predicted result given of section 4.2 in ([16], and see part A of section III in [29]).

3.3 Effective characterization of the scalogram

In this section, we explore the insights of scalogram in the time and frequency direction and calculate the statistical features using the quality parameters.

3.3.1 Characterization of scalogram along with the frequency

For the analysis of scalogram along the frequency, we adopt quality parameter "normalized spectrum index (NSI)" [24] and take the center of gravity of energies over frequencies of the scalogram. For given H and L, let $H(L(a)(Wf)(a,b))$ be the function defined in section 3.2.1. To derive the characteristics, we take $NSI(f,L,W)(b)$ with respect to frequency. The definition of the NSI is given by (the continuous variable case)

$$NSI(f,L,W)(b) \equiv \frac{\int_0^\infty a \cdot H\big(L(a)\cdot(Wf)(a,b)\big)da}{\int_0^\infty H\big(L(a)\cdot(Wf)(a,b)\big)da}. \tag{3.8}$$

In the numerical treatments by means of MATLAB for the discretized wavelet transforms, we have to modify the formula (3.8) as follows. For simplicity, for given H and L, let us denote, $E(a,b) \equiv H(L(a)(Wf)(a,b))$ and $NSI(b) \equiv NSI(f,L,W)(b)$. Then, for the present discrete case the $NSI(b)$ reads as

$$NSI(b) \equiv \frac{\sum_a E(a,b)F(a)}{\sum_a E(a,b)}, \tag{3.9}$$

where $E(a,b)$ and $F(a)$ represents scalogram energy and scalogram frequency, respectively. Note that the energy $E(a,b)$ in the scalogram obtained by $H(L(a)(Wf)(a,b))$ which has been explained in subsection 3.2.1 and the scalogram frequency $F(a)$ is for the corresponding energy $E(a,b)$. Algorithm 2 shows the characterization method in detail of the scalogram over the frequency.

Algorithm 2 Normalized spectrum index (NSI)

Require: Time-frequency scalogram: $(Wf)(a,b)$,
a : scale corresponding to the frequency, b : time
Ensure: $NSI(b)$
1: Load $(Wf)(a,b)$
2: **for** each b **do**
3: Find energy $E(a,b)$
4: **for** each a **do**
5: Find $E(a,b)F(a)$ for the corresponding $E(a,b)$
6: **end for**
7: **end for**
8: Calculate $NSI(b)$ according to Eq.(3.9)

Now we show the graphical representation of NSI for scalogram of SR, PEA, VF, and VT signals (see Figures 3.29, 3.30, 3.31, and 3.32,). Here, the NSI is obtained as a "time series" waveform from scalograms for each signal. In addition, the NSI waveform tends to change periodically and regularly for the scalogram of SR signal, while the changes are irregular for scalograms of PEA, VF, and VT signals. As our objective, we mainly concentrate on the discrimination of the shockable (VF and VT) and non-shockable (PEA) arrhythmias in the abnormal class through the NSI. Hence, the NSI value over time is the primary key here. From the visualiza-

tion, we see that the maximum NSI value of the PEA signal is at the time near five second. On the other hand, the maximum NSI value appears at the time near one second for the VT signal. Inspecting the maximum over time, we get different NSI values for PEA, VF, and VT signals.

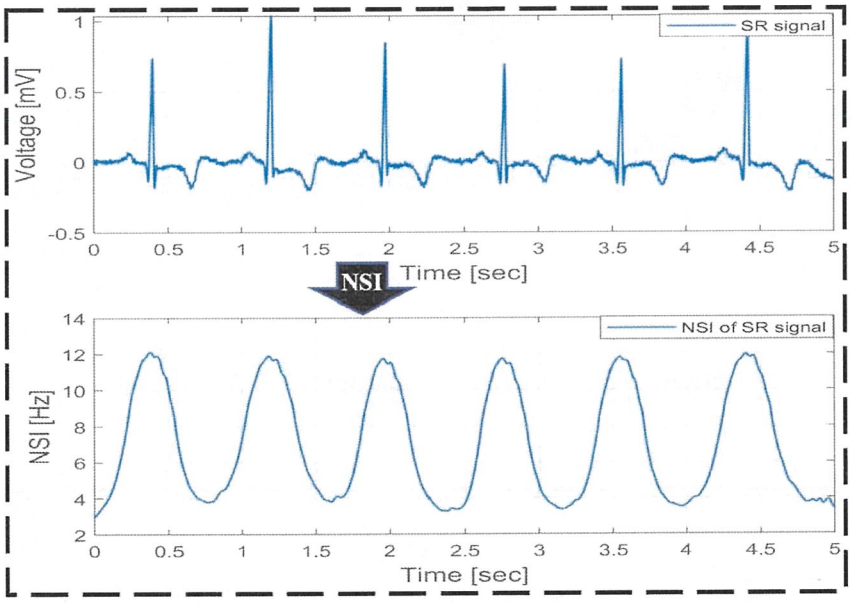

Figure 3.29: $NSI(b)$ for scalogram of SR signal

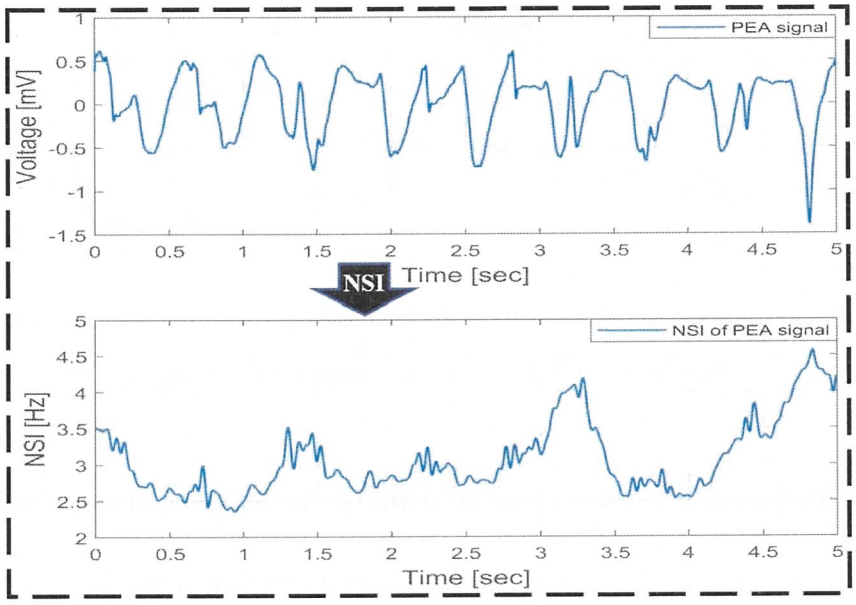

Figure 3.30: $NSI(b)$ for scalogram of PEA signal

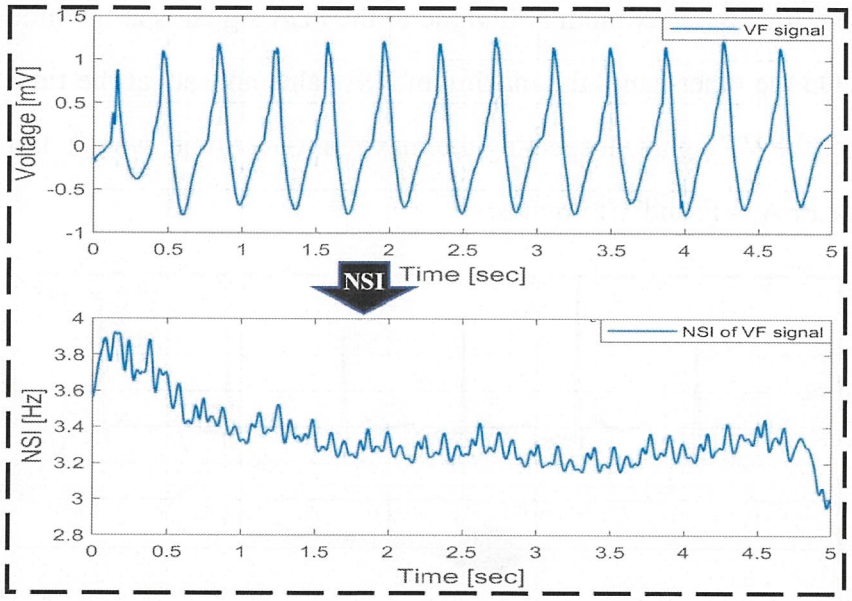

Figure 3.31: $NSI(b)$ for scalogram of VF signal

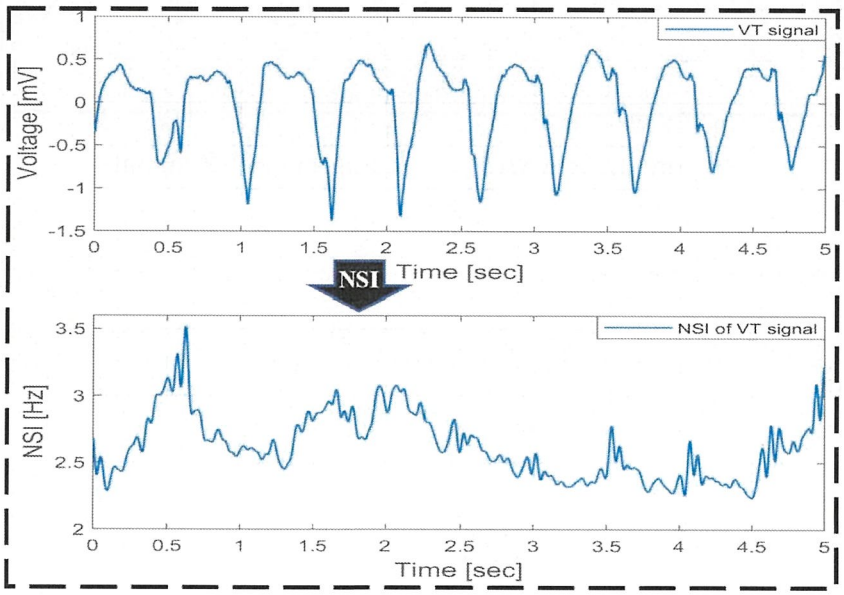

Figure 3.32: $NSI(b)$ for scalogram of VT signal

3.3.1.1 Statistical features extracted from the scalogram through NSI

We deduce statistics of the scalogram by extracting statistical features through NSI. For vector $NSI(b)$ $(b = 1, \cdots, N)$ (where, N is the total number of element), eight statistical features (mean, variance, slope, kurtosis, skewness, entropy, power, and

mode of NSI) are extracted as the feature quantities as follows [149].

- Mean of NSI

$$\mu_{NSI} = \frac{1}{N}\sum_{b=1}^{N} NSI(b)$$

- Variance of NSI

$$V_{NSI} = \frac{1}{N}\sum_{b=1}^{N} (NSI(b) - \mu_{NSI})^2$$

- Slope of NSI

$$S_{NSI} = \frac{1}{N-1}\sum_{b=1}^{N-1} |NSI(b+1) - NSI(b)|$$

- Kurtosis of NSI

$$K_{NSI} = \frac{1}{(V_{NSI})^3}\frac{1}{N}\sum_{b=1}^{N} (NSI(b) - \mu_{NSI})^3$$

- Skewness of NSI

$$SK_{NSI} = \frac{1}{(V_{NSI})^2}\frac{1}{N}\sum_{b=1}^{N} (NSI(b) - \mu_{NSI})^4$$

- Entropy-based index of NSI

$$EBI_{NSI} = -\sum_{b=1}^{N} NSI(b) log_2 NSI(b)$$

- Power of NSI

$$P_{NSI} = \sum_{b=1}^{N} |NSI(b)|^2$$

- Mode of NSI

  The most frequently occurring value in the NSI of the scalogram is calculated by

$$M_{NSI} = mode[NSI(b)]$$

3.3.1.2 A suitable combination of the NSI features

There are eight statistical features are extracted from the scalogram through NSI, and it is not clear which features and combination of feature are effective for the discrimination of shockable and non-shockable arrhythmias. To find out the effectiveness and suitable combination of the NSI features, we first check the effectiveness of individual features with the help of a univariate histogram and look at the effect of all possible feature pairs using eight individual features on the multivariable scatter plot matrix. Therefore, we create a matrix $(8 * 4 * 1079)$ of scatter plots with univariate histograms for each combination of variables (Visualization of the multivariate ECG classes in the different feature spaces), where 1079 samples are grouped into four classes by the grouping variable (see Figure 3.33). The multi-variable plot matrix provides the graphical overview of the relations between all pairs of variables. The Figure shows the pairwise scatter plot in the lower and upper triangular and represents the histogram diagonally from top left to right for all features. From the figure, we see that the univariate histogram for "Mean of NSI" and "Variance of NSI" show the highest separable class and the distribution in the scatter plot for the combination of "Mean of NSI" with all features show good separate class. Precisely, the distribution in the scatter plot for the combination of "Mean of NSI" with "Variance of NSI" shows a better separated class.

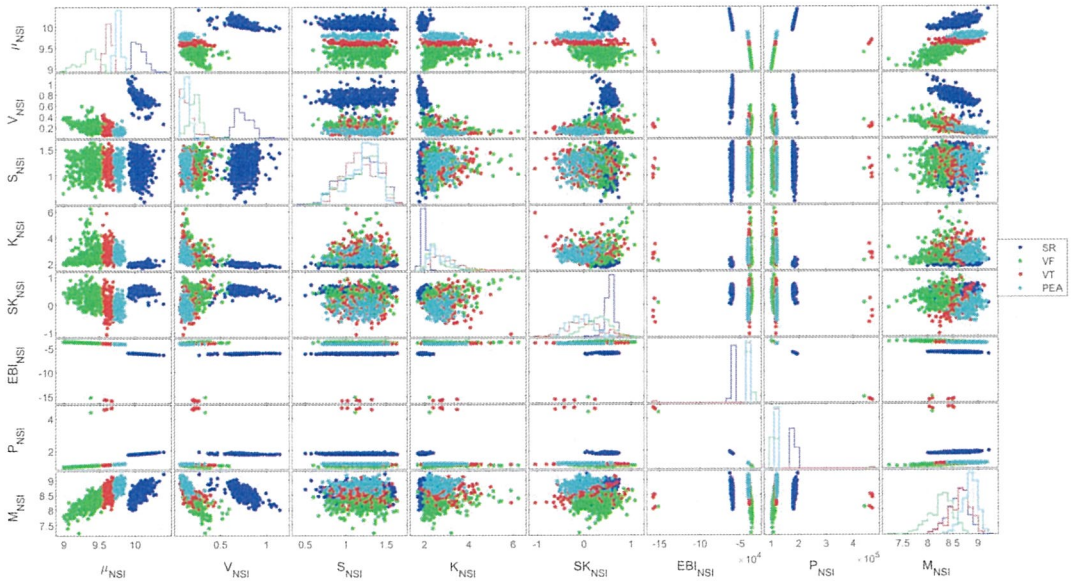

Figure 3.33: Multi-variable scatter plot matrix with univariate histogram for NSI features

3.3.1.3 Discrimination by histogram

We use the histogram as a classifier of the groups to make the decision. The strategy of the histogram method in order to discriminate between the shockable and non-shockable arrhythmia is shown in Figure 3.34, and the detail explanation is as follows.

(i) Let K be the number of groups to be discriminated. Each of the groups corresponds to patients of SR, patients of VF, and so on.

(ii) Suppose that we characterize the groups by using r types of the features.

(iii) Let $x^{(m)} \equiv \left(x_i^{(m)}\right)_{i=1,\ldots,n_m}$ be the data of m-th group for some $n_m \in \mathbb{N}$, for $m = 1, \cdots, K$. Here the i-th data $x_i^{(m)}$ is of the form

$$x_i^{(m)} \equiv (x_{i,1}^{(m)}, \ldots, x_{i,r}^{(m)}).$$

(iv) Now, let $x_{max,p}^{(m)}$ and $x_{min,p}^{(m)}$ be maximum and minimum value in the p-th feature (cf. (ii)), respectively, for $p = 1, \ldots, r$. That is,

$$x_{max,p}^{(m)} \equiv \max_{1 \le i \le n_m} \left\{ x_{i,p}^{(m)} \right\}$$

and

$$x_{min,p}^{(m)} \equiv \min_{1 \le i \le n_m} \left\{ x_{i,p}^{(m)} \right\}.$$

(v) Then, for each of the group, we take the bin width $d_p^{(m)}$ of the histogram,

$$d_p^{(m)} \equiv \frac{1}{n_m} [x_{max,p}^{(m)} - x_{min,p}^{(m)}], \qquad m = 1, \cdots, K.$$

Now, label the frequency between the intervals and compute the histogram $H_p^{(m)}$ for the p-th feature of the m-th group.

(vi) Finally, suppose that we are given a test data, denoted by $x \equiv (x_1, \ldots, x_p)$, and composed with the r number of features. Note that, it is unknown which group the patient test data belongs to. For the given test data x, we determine the successive intervals for each of the group, take the weight values for the corresponding interval and divide the weight value by the size n_m (SR, PEA, VF, and VT) of corresponding group of data, the result of which denoted by $W_p^{(m)}(x)$.

(vii) As the decision by means of the histogram, the test data x is judged to belong to the m_o-th group if $W_p^{(m)}(x)$, $m = 1, \ldots, K$, takes the largest value at $m = m_o$.

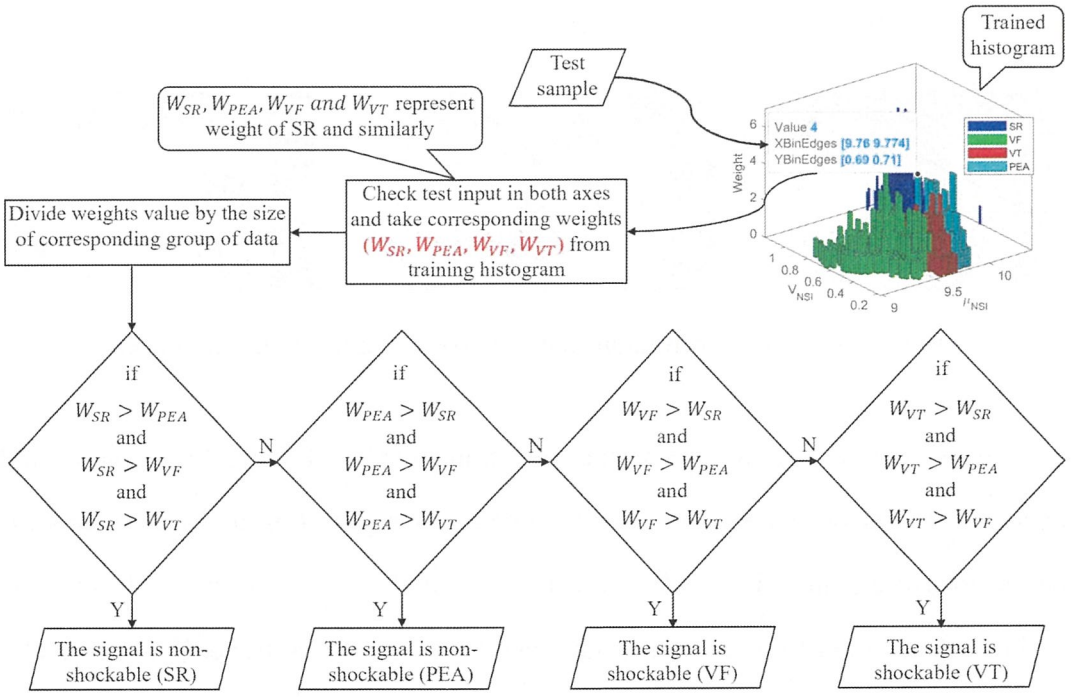

Figure 3.34: Discrimination of shockable and non-shockable arrhythmia by histogram

3.3.1.4 Performance evaluation and discussion

In this section, we explain the evaluation strategy and step-by-step performance result of the proposed method.

3.3.1.4.1 Evaluation matrices

Many evaluation metrics are based on the confusion matrix [150]. The confusion matrix is a cross table that records the number of occurrences between two raters, the true classification, and the predicted classification. Figure 3.35 shows the confusion matrix for the multiclass classification, where TP is a true positive, TN is a true negative, FP is a false positive and FN is a false negative, respectively. If the sample is positive and it is classified as positive, i.e., correctly classified positive sample, it is considered as a TP, if it is classified as negative, i.e., misclassified sample, it is considered as a FN. If the sample is negative and it is classified as negative, i.e., correctly classified negative sample, it is considered as a TN, if it is classified as

positive, i.e., misclassified sample, it is considered as false FP.

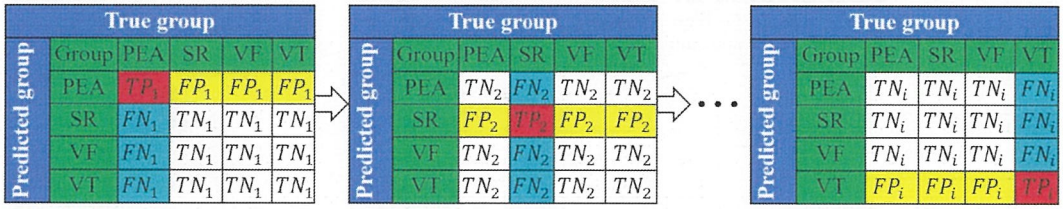

Figure 3.35: The confusion matrices for multiclass classification

We use macro-and micro-average precision, recall, F1-score (F-measure) and accuracy, as performance indices which are commonly used in multi-class classification measurement [151, 152]. The F-measure is the harmonic mean of precision and recall. In order to obtain macro-average F1 score, we compute F-measure (F_i) for each class and then take their average of F-measure over all classes as:

$$F_i = 2\frac{P_i * R_i}{P_i + R_i}, \quad Macro - avg.F1 = \frac{1}{c}\sum_{i=1}^{c} F_i,$$

where c is total number of classes and the precision (P_i) and recall (R_i) for class i are defined as follows:

$$P_i = \frac{TP_i}{TP_i + FP_i}, \quad R_i = \frac{TP_i}{TP_i + FN_i}.$$

Here TP_i, FP_i, and FN_i are true positive, false positive, and false negative in the *ith* class, respectively.

The macro average precision (P_{macro}) and the macro average recall (R_{macro}) are the averages of individual precision and recall respectively:

$$P_{macro} = \frac{1}{c}\sum_{i=1}^{c} \frac{TP_i}{TP_i + FP_i}, \quad R_{macro} = \frac{1}{c}\sum_{i=1}^{c} \frac{TP_i}{TP_i + FN_i}.$$

On the other hand the micro-average F1 score is given as follows:

$$Micro - avg.F1 = 2\frac{P_{micro} * R_{micro}}{P_{micro} + R_{micro}},$$

where micro average precision (P_{micro}) and micro average recall (R_{micro}) are computed by summing individual precision and recall as follows

$$P_{micro} = \frac{\sum_{i=1}^{c} TP_i}{\sum_{i=1}^{c}(TP_i + FP_i)}, \quad R_{micro} = \frac{\sum_{i=1}^{c} TP_i}{\sum_{i=1}^{c}(TP_i + FN_i)}.$$

The group-wise accuracy is the ratio of correctly predicted observation to the total observation, that is:

$$Accuracy_i = \frac{TP_i + TN_i}{TP_i + FP_i + FN_i + TN_i}.$$

When the value of precision, recall, and F-measure is close to 1.0, then the classification performance is considered high. when they are almost 0.0, then it is considered very low performance.

3.3.1.4.2 Evaluation process

Cross-validation is a statistical approach used to get an accurate assessment of the accuracy of a model [153]. It is a technique to evaluate predictive models by partitioning the original sample into a training set to train the model, and a test set to evaluate it. There are several types of methods for cross validation. Among the methods, the K-fold cross-validation method is the most popular and widely used method for the accurate assessment of a model [154, 155]. The K-fold cross-validation procedure has a single parameter called K which refers to the number of groups that a given dataset is to be split into K number of groups. Therefore, the procedure is often called K-fold cross-validation. For using the K-fold method there are no strict rules to set the value of K; that means there is no fixed value of K. The

value of K is set by the user.

In our study, we have performed k-fold cross validation for stabilizing the performance of our proposed method. We have performed 4-fold cross validation that means four times iteration totally. The discrimination results of each iteration for the 1079 samples are in Figures 3.37, 3.38, 3.39, and 3.40, and Tables (3.6-3.9), respectively. We have $\mathcal{Z}_{total} = 1079$ samples where (SR (Non-shockable) $\mathcal{Z}^{SR}_{total} = 491$), (PEA (Non-shockable) $\mathcal{Z}^{PEA}_{total} = 134$), (VF (Shockable) $\mathcal{Z}^{VF}_{total} = 299$) and (VT (Shockable) $\mathcal{Z}^{VT}_{total} = 155$). Since, we performed 4-fold cross-validation, so the total of ($\mathcal{Z}_{total} = 1079$) samples are randomly partitioned into 4 sub-samples of equal size. A single sub-sample, denoted by $\mathcal{T}$, is used as the validation data for testing the model, and the remaining ($\mathcal{Z}_{total} - \mathcal{T}$) sub-samples are used as training data. Here, the $\mathcal{T}$ samples are also selected randomly for each type of ECG signals. The cross-validation process is repeated 4 times and the process is shown in Figure 3.36.

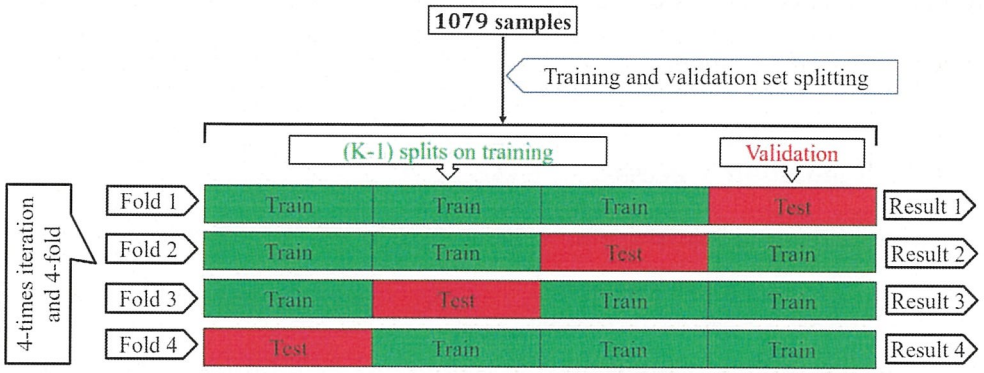

Figure 3.36: Schematic illustration of four-fold cross validation approach

3.3.1.4.3 Performance results

The performance results of the proposed method are evaluated for four class categories using four fold cross validation approach (see subsection 3.3.1.4.2) based on the evaluation matrices (see subsection 3.3.1.4.1). The confusion matrix plots with the performance results for shockable (VF, VT) and non-shockable (SR, PEA)

arrhythmias are shown in Figures 3.37, 3.38, 3.39, and 3.40 respectively. The confusion matrix is generated through the proposed setting $L(a) = \frac{1}{a}$ with $H(\cdot) = |\cdot|^{\frac{1}{4}}$ by using the combination of the "Mean of NSI" with "Variance of NSI" features.

In Figures 3.37, 3.38, 3.39, and 3.40, the rows correspond to the predicted class and the columns correspond to the true class. The diagonal cells correspond to observations that are correctly classified. The off-diagonal cells correspond to incorrectly classified observations. Both the number of observations and the percentage of the total numbers of observations are shown in each cell. The values on the far right column (green, and red color), and the row at the bottom (green, and red color) of each figure show the percentages of the correct predictions and the incorrect predictions, respectively. The cell in the bottom right of the plot shows the overall correct and incorrect accuracy.

For example, on the Figure 3.37, 285 data, which is composed by 42 of PEA, 124 of SR, 80 of VF and 39 of VT, are tested. The first column shows that the 38 PEA data within the actual 42 test data are correctly identified and the rest of the data are incorrectly identified where 1 data is miss judged as VF, and 3 data are miss judged as VT. Similarly, the second column shows that the actual 124 SR test data are correctly identified, and none of them is miss judged as others, i.e., PEA, VF, or VT. Similarly, the fourth column explains that, within the actual 39 number of VT data, 34 are correctly identified but 2 data are miss judged as VF, and 3 data are miss judged as PEA. 12.8% incorrect result given in the bottom of the fourth column, indicated as the red color, is calculated from $(3+2)/(3+2+34) = 5/39$.

On the other hand, the row concern, the first row of the same figure shows that 38 numbers of PEA data are exactly identified as PEA, but in addition 1 of VF, and 3 of VT are miss judged as PEA. The far-right component 90.5% corrected result of the first row, indicated as the green color, is calculated from $38/(38+1+3)$. Similarly, the fourth row shows that 34 VT data are identified correctly, but in addition 5 of VF and 3 of PEA are miss judged as VT. Therefore, 81.0% correct (green color)

and 19.0% (red color) incorrect results are calculated from $34/(34+5+3)$ and $(5+3)/(34+5+3)$ which are shown in the far-right of the fourth row. The cell in the bottom right of the plot of the same figure shows the overall 94.7% correct and 5.3% incorrect accuracy.

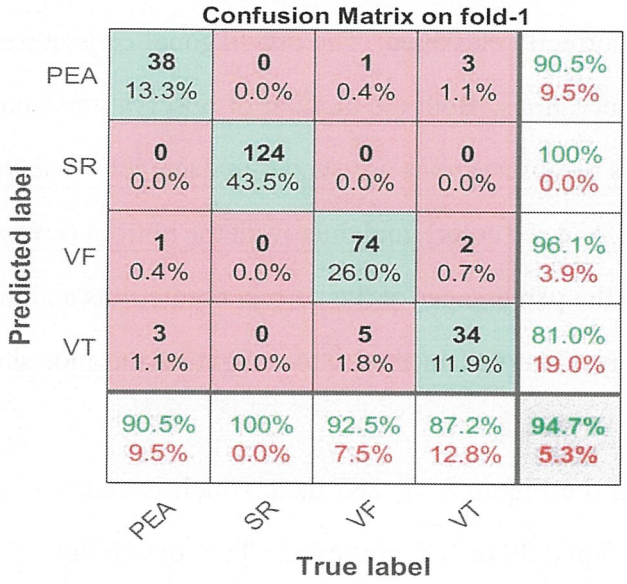

Figure 3.37: Confusion matrix with performance for shockable and non-shockable arrhythmias on fold-1, (μ_{NSI} and V_{NSI} case)

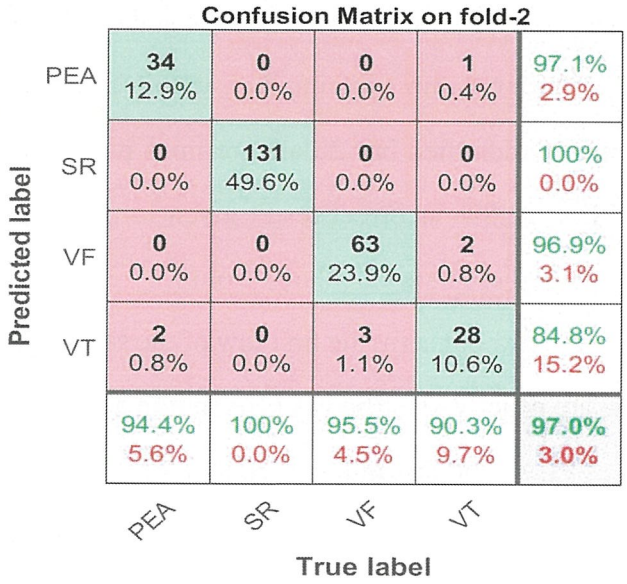

Figure 3.38: Confusion matrix with performance for shockable and non-shockable arrhythmias on fold-2, (μ_{NSI} and V_{NSI} case)

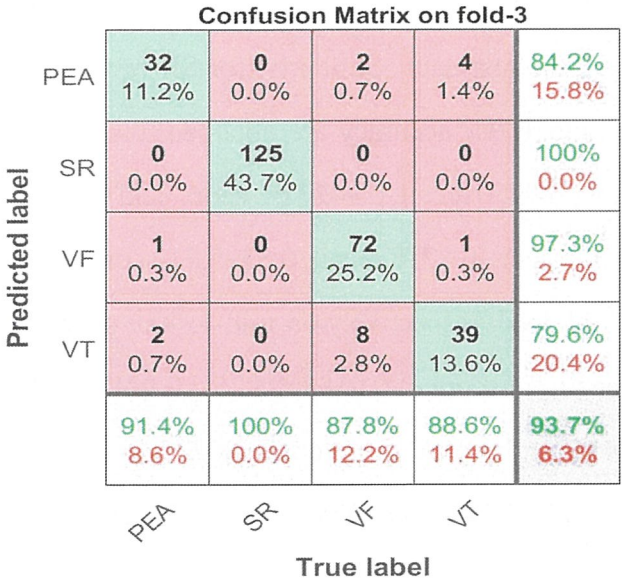

Figure 3.39: Confusion matrix with performance for shockable and non-shockable arrhythmias on fold-3, (μ_{NSI} and V_{NSI} case)

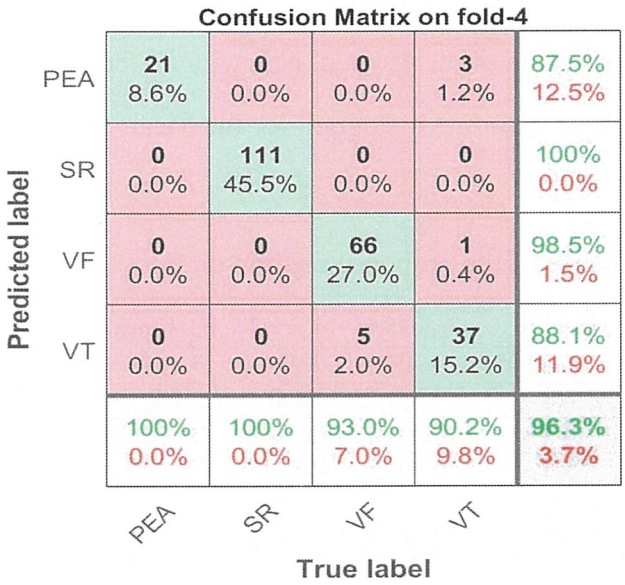

Figure 3.40: Confusion matrix with performance for shockable and non-shockable arrhythmias on fold-4, (μ_{NSI} and V_{NSI} case)

The detailed performance analysis (fold-wise and group-wise) presented in the Tables (3.6-3.9), which corresponding to Figures 3.37, 3.38, 3.39, and 3.40. The table shows individual precision, recall, F1-score, and accuracy for each group, and shows overall macro and micro average precision, recall, and F1-score. For

example, Table 3.6 presents 0.9048 precision, 0.9048 recall, 0.9048 F1-score, and 97.19% accuracy for PEA test data. Similarly, for SR test data 1.0 precision, 1.0 recall, 1.0 F1-score, and 100% accuracy are obtained, respectively. On the other hand, 0.9610 precision, 0.9250 recall, 0.9427 F1-score, and 96.84% accuracy for VF test data and 0.8095 precision, 0.8718 recall, 0.8395 F1-score, and 95.43% accuracy for VT test data are obtained, respectively on fold-1. The overall macro and micro average precision, recall, F1-score of 0.9188, 0.9254, 0.9217, and 0.9474 on fold-1, 0.9473, 0.9506, 0.9486, and 0.9697 on fold-2, 0.9027, 0.9197, 0.9096, and 0.9371 on fold-3, 0.9353, 0.9580, 0.9454, and 0.9631 on fold-4, respectively are shown in Tables (3.6-3.9).

From the experimental results, we observe that the classification accuracy of the PEA, VF, and VT is relatively low. Because the PEA, VF, and VT signals belong to the abnormal class, and the distribution of the abnormal class signals is closed distance for the combination of the Mean of NSI with all features and showing high inter-dependence in the univariate histogram for the Mean of NSI feature as shown in Figure 3.33.

Table 3.6: Performance of the proposed method on fold-1, (μ_{NSI} and V_{NSI} case)

Fold no.	Group	Precision	Recall	F1-score	Accuracy (%)
Fold-1	PEA	0.9048	0.9048	0.9048	97.19
	SR	1.0	1.0	1.0	100.0
	VF	0.9610	0.9250	0.9427	96.84
	VT	0.8095	0.8718	0.8395	95.43
	Macro avg.	0.9188	0.9254	0.9217	
	Micro avg.	0.9474	0.9474	0.9474	

Table 3.7: Performance of the proposed method on fold-2, (μ_{NSI} and V_{NSI} case)

Fold no.	Group	Precision	Recall	F1-score	Accuracy (%)
Fold-2	PEA	0.9714	0.9444	0.9577	98.86
	SR	1.0	1.0	1.0	100.0
	VF	0.9692	0.9545	0.9618	98.10
	VT	0.8485	0.9032	0.8750	96.96
	Macro avg.	0.9473	0.9506	0.9486	
	Micro avg.	0.9697	0.9697	0.9697	

Table 3.8: Performance of the proposed method on fold-3, (μ_{NSI} and V_{NSI} case)

Fold no.	Group	Precision	Recall	F1-score	Accuracy (%)
Fold-3	PEA	0.8421	0.9143	0.8767	96.85
	SR	1.0	1.0	1.0	100.0
	VF	0.9730	0.8780	0.9231	95.80
	VT	0.7959	0.8864	0.8387	94.75
	Macro avg.	0.9027	0.9197	0.9096	
	Micro avg.	0.9371	0.9371	0.9371	

Table 3.9: Performance of the proposed method on fold-4, (μ_{NSI} and V_{NSI} case)

Fold no.	Group	Precision	Recall	F1-score	Accuracy (%)
Fold-4	PEA	0.8750	1.0	0.9333	98.77
	SR	1.0	1.0	1.0	100.0
	VF	0.9851	0.9296	0.9565	97.54
	VT	0.8810	0.9024	0.8916	96.31
	Macro avg.	0.9353	0.9580	0.9454	
	Micro avg.	0.9631	0.9631	0.9631	

3.3.2 Characterization of scalogram along with the time

We also adopt new quality parameter normalized time index (NTI) for an additional analysis of scalogram along the time direction. The NTI gives the center of gravity of energies over time of the scalogram. The NTI for SR, PEA, VF, and VT signals are shown in Figure 3.41, 3.42, 3.43, and 3.44. Here, the NTI is obtained as a waveform over frequencies from scalogram. In the figures, we observe that, the NTI value is different for all classes inspecting over frequency. The different NTI value for the different signals lead to a good discrimination in the decision algorithm. The definition of the NTI is given by

$$NTI(a) \equiv \frac{\sum_b E(a,b)T(b)}{\sum_b E(a,b)}, \tag{3.10}$$

where $E(a,b)$ and $T(b)$ represent scalogram energy and scalogram time, respectively. Note that the energy $E(a,b)$ in the scalogram obtained by $H(L(a)(Wf)(a,b))$ which has been explained in subsection 3.2.1 and the time $T(b)$ is for the corresponding energy $E(a,b)$. The algorithm 3 shows the procedure to characterize the

scalogram along the time direction.

Algorithm 3 Normalized time index (NTI)

Require: Time-frequency scalogram: $(Wf)(a,b)$,
a : scale corresponding to the frequency, b : time
Ensure: $NTI(a)$
1: Load $(Wf)(a,b)$
2: **for** each a **do**
3: Find energy $E(a,b)$
4: **for** each b **do**
5: Find $E(a,b)T(b)$ for the corresponding $E(a,b)$
6: **end for**
7: **end for**
8: Calculate $NTI(a)$ according to Eq.(3.10)

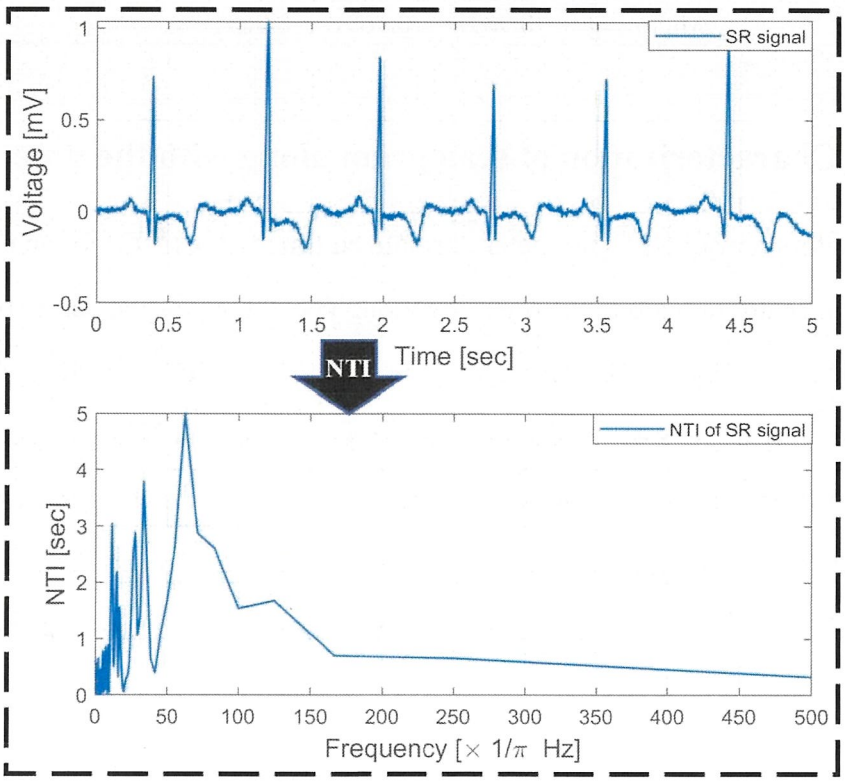

Figure 3.41: $NTI(a)$ for scalogram of SR signal

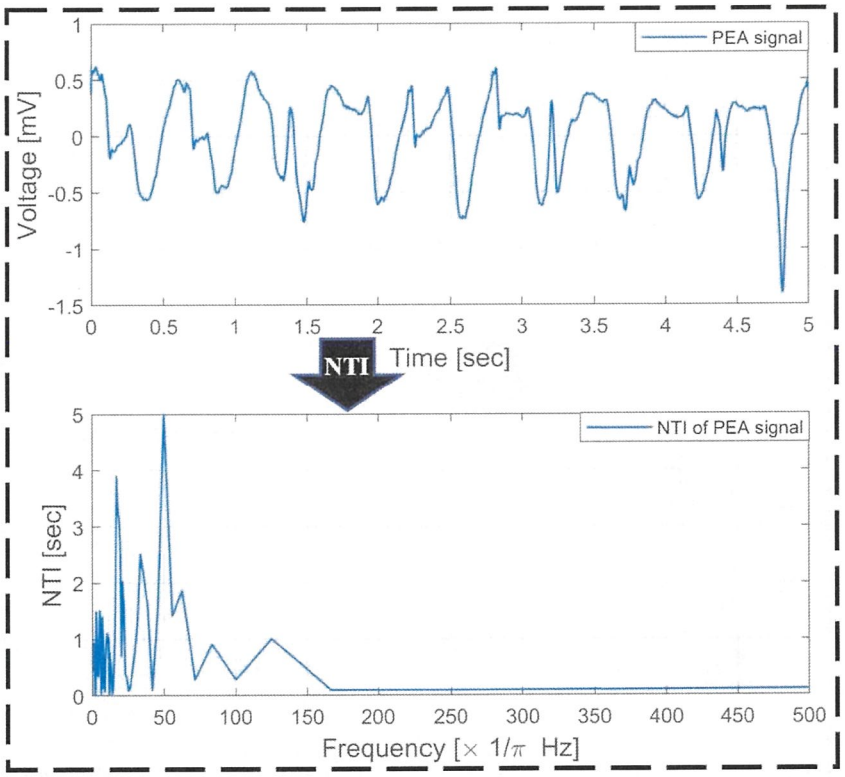

Figure 3.42: $NTI(a)$ for scalogram of PEA signal

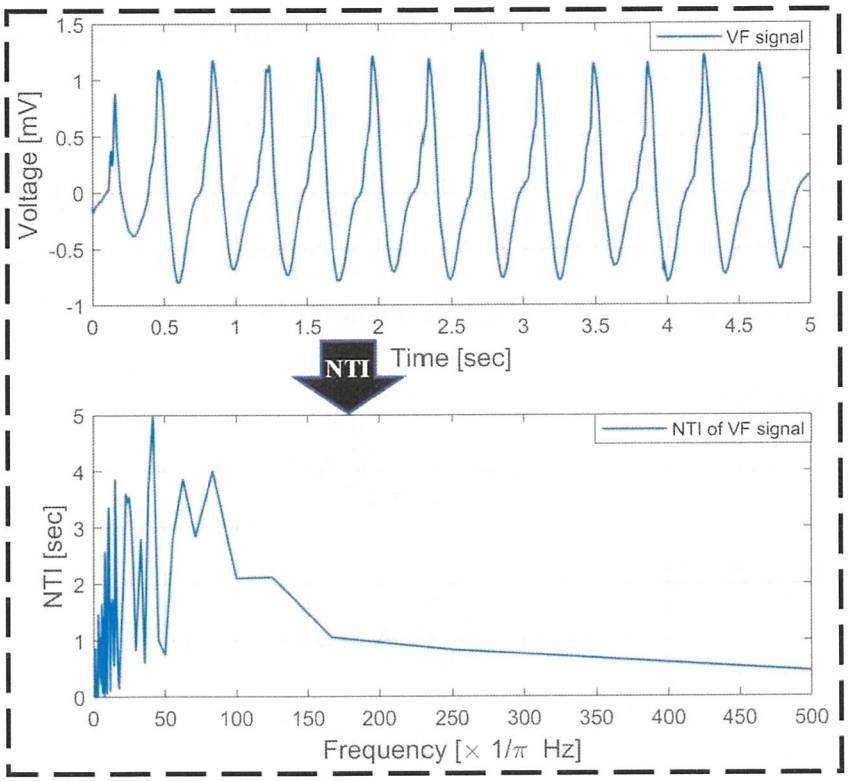

Figure 3.43: $NTI(a)$ for scalogram of VF signal

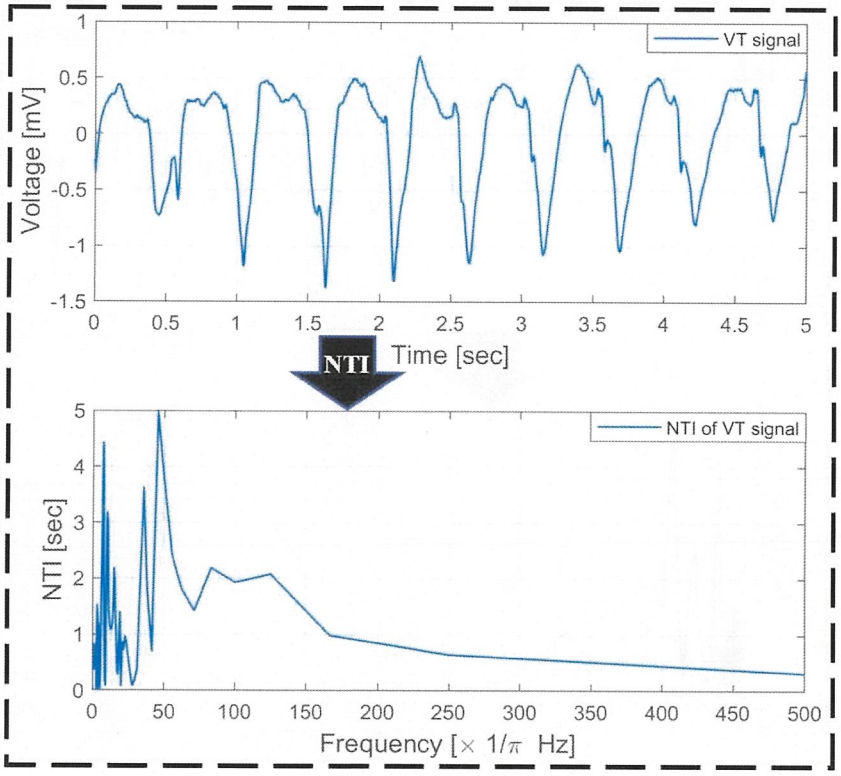

Figure 3.44: $NTI(a)$ for scalogram of VT signal

3.3.2.1 Statistical features extracted from the scalogram through NTI

We deduce statistics of the scalogram by extracting statistical features through NSI. For vector $NTI(a)$ $(a = 1, \cdots, N)$ (where, N is the total number of element), eight statistical features (mean, variance, slope, kurtosis, skewness, entropy, power, and mode of NSI) are extracted as the feature quantities as follows [149].

- Mean of NTI

$$\mu_{NTI} = \frac{1}{N}\sum_{a=1}^{N} NTI(a)$$

- Variance of NTI

$$V_{NTI} = \frac{1}{N}\sum_{a=1}^{N} (NTI(a) - \mu_{NTI})^2$$

- Slope of NTI

$$S_{NTI} = \frac{1}{N-1}\sum_{a=1}^{N-1} |NTI(a+1) - NTI(a)|$$

- Kurtosis of NTI

$$K_{NTI} = \frac{1}{(V_{NTI})^3}\frac{1}{N}\sum_{a=1}^{N} (NTI(a) - \mu_{NTI})^3$$

- Skewness of NTI

$$SK_{NTI} = \frac{1}{(V_{NTI})^2}\frac{1}{N}\sum_{a=1}^{N} (NTI(a) - \mu_{NTI})^4$$

- Entropy-based index of NTI

$$EBI_{NTI} = -\sum_{a=1}^{N} NTI(a) log_2 NTI(a)$$

- Power of NTI

$$P_{NTI} = \sum_{a=1}^{N} |NTI(a)|^2$$

- Mode of NTI

  The most frequently occurring value in the NTI of the scalogram is calculated by

$$M_{NTI} = mode[NTI(a)]$$

3.3.2.2 A suitable combination of the NSI and NTI features

The sixteen statistical features are derived from the scalograms through the NSI and NTI, and a matrix $(16 * 4 * 1079)$ of scatter plots with univariate histograms is created (see Figure 3.45), where 1079 samples are grouped into four classes by the grouping variable. The Figure shows the pairwise scatter plot in the lower and upper

triangular and represents the histogram diagonally from top left to right. From the figure, we see that the univariate histogram for "Mean of NSI" shows the highest separable class. Also, the univariate histogram for "Mean of NTI", and "Variance of NSI" show almost the same level separable class. In addition, The scatter plots of the combination of "Mean of NSI" with all features show good distribution for the four types of arrhythmias. Among them, the scatter plots of the combination of "Mean of NSI" with "Variance of NSI" and the "Mean of NSI" with "Mean of NTI" show better separated class and the distribution is very much scattered among the different groups of arrhythmias.

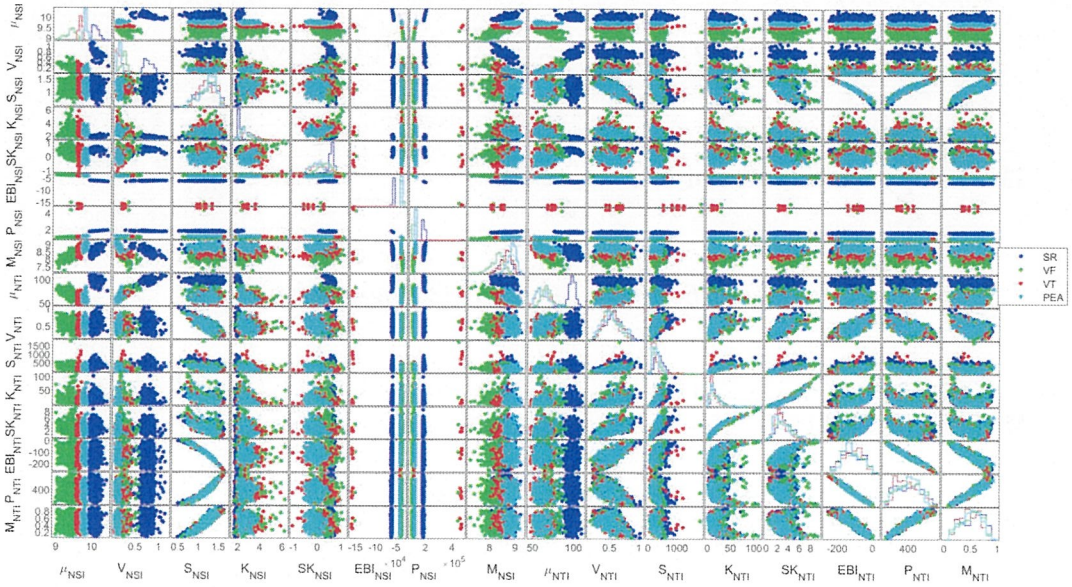

Figure 3.45: Multi-variable scatter plot matrix with univariate histogram for NSI and NTI features

3.3.2.3 Performance evaluation and discussion

In this section, we explain step-by-step performance results and compare the results with existing "Mean of NSI" and "Variance of NSI" results.

3.3.2.3.1 Performance results

We evaluate our proposed method for four class categories using four fold cross validation approach (see subsection 3.3.1.4.2) based on the evaluation matrices (see

subsection 3.3.1.4.1). The confusion matrix plots with the performance results for shockable (VF, VT) and non-shockable (SR, PEA) arrhythmias for the "Mean of NSI" and "Mean of NTI" are shown in Figures 3.46, 3.47, 3.48, and 3.49 respectively. The confusion matrix is generated through the proposed setting $L(a) = \frac{1}{a}$ with $H(\cdot) = |\cdot|^{\frac{1}{4}}$ by using the combination of the "Mean of NSI" with "Mean of NTI" features.

In Figures 3.46, 3.47, 3.48, and 3.49, the rows correspond to the predicted class and the columns correspond to the true class. The diagonal cells correspond to observations that are correctly classified. The off-diagonal cells correspond to incorrectly classified observations. Both the number of observations and the percentage of the total numbers of observations are shown in each cell. The values on the far right column (green, and red color), and the row at the bottom (green, and red color) of each figure show the percentages of the correct predictions and the incorrect predictions, respectively. The cell in the bottom right of the plot shows the overall correct and incorrect accuracy.

For example, on the Figure 3.46, 283 data, which is composed by 35 of PEA, 138 of SR, 70 of VF and 40 of VT, are tested. The first column shows that the 34 PEA data within the actual 35 test data are correctly identified and the rest of the data are incorrectly identified where 1 data is miss judged as VT. Similarly, the second column shows that the actual 138 SR test data are correctly identified, and none of them is miss judged as others, i.e., PEA, VF, or VT. Similarly, the fourth column explains that, within the actual 40 number of VT data, 36 are correctly identified but 1 data is miss judged as VF, and 3 data are miss judged as PEA. 10.0% incorrect result given in the bottom of the fourth column, indicated as the red color, is calculated from $(1+3)/(1+3+36) = 4/40$.

On the other hand, the row concern, the first row of the same figure shows that 34 numbers of PEA data are exactly identified as PEA, but in addition 3 of VT are miss judged as PEA. The far-right component 91.9% corrected result of the first row,

indicated as the green color, is calculated from $34/(34+3)$. Similarly, the fourth row shows that 36 VT data are identified correctly, but in addition 3 of VF and 1 of PEA is miss judged as VT. Therefore, 90.0% corrected (green color) and 10.0% (red color) incorrect results are calculated from $36/(36+3+1)$ and $(3+1)/(36+3+1)$ which are shown in the far-right of the fourth row. The cell in the bottom right of the plot of the same figure shows the overall 97.2% correct and 2.8% incorrect accuracy.

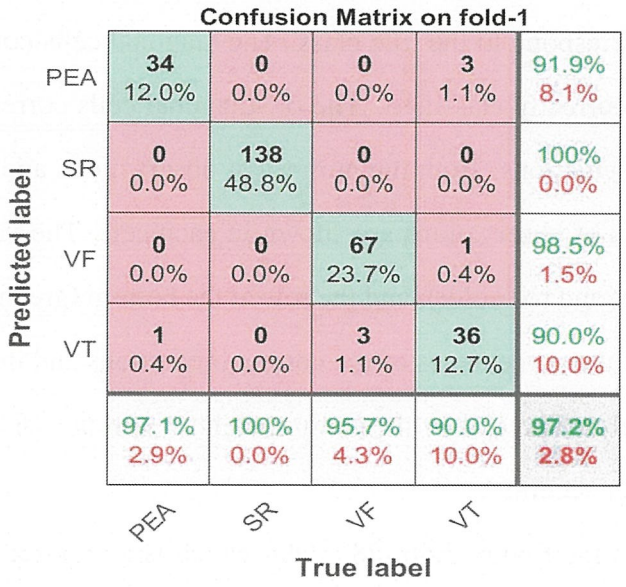

Figure 3.46: Confusion matrix with performance for shockable and non-shockable arrhythmias on fold-1, (μ_{NSI} and μ_{NTI} case)

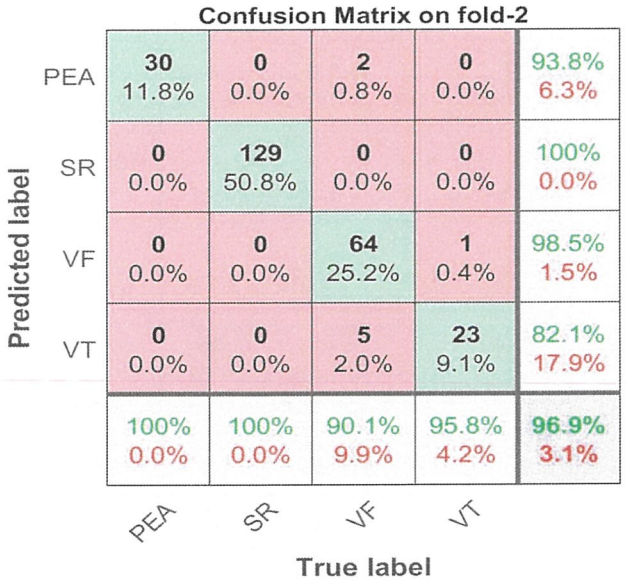

Figure 3.47: Confusion matrix with performance for shockable and non-shockable arrhythmias on fold-2, (μ_{NSI} and μ_{NTI} case)

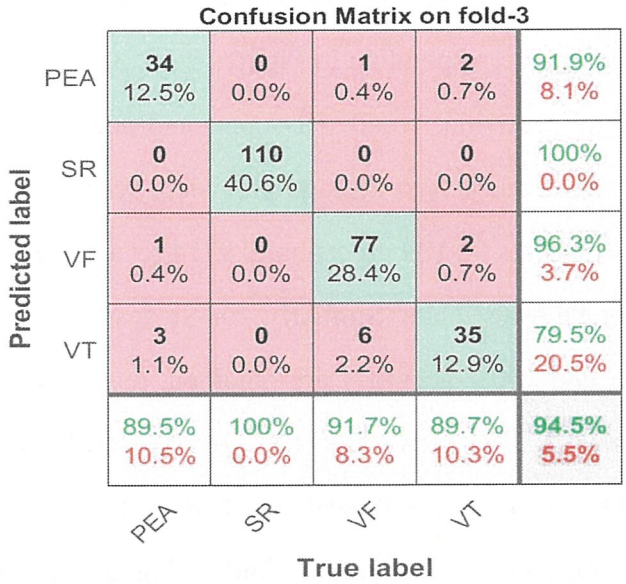

Figure 3.48: Confusion matrix with performance for shockable and non-shockable arrhythmias on fold-3, (μ_{NSI} and μ_{NTI} case)

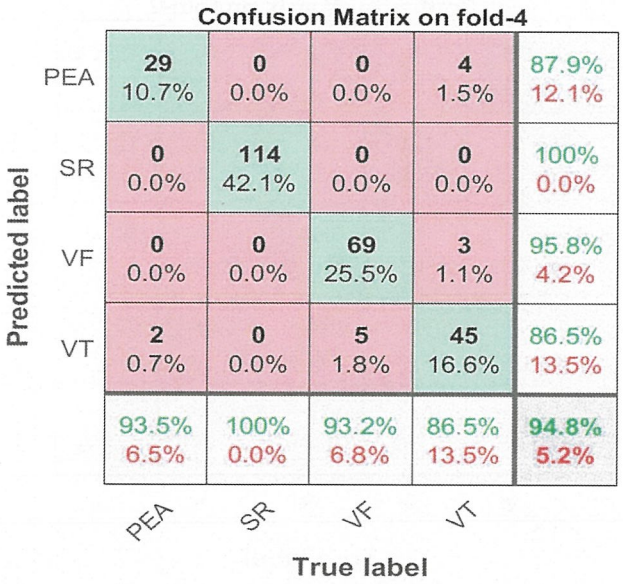

Figure 3.49: Confusion matrix with performance for shockable and non-shockable arrhythmias on fold-4, (μ_{NSI} and μ_{NTI} case)

The detailed performance analysis (fold-wise and group-wise) presented in the Tables (3.10-3.13), which corresponding to Figures 3.46, 3.47, 3.48, and 3.49. The table shows individual precision, recall, F1-score, and accuracy for each group, and shows overall macro and micro average precision, recall, and F1-score. For example, Table 3.10 presents 0.9189 precision, 0.9714 recall, 0.9444 F1-score, and 98.58% accuracy for PEA test data. Similarly, for SR test data 1.0 precision, 1.0 recall, 1.0 F1-score, and 100% accuracy are obtained, respectively. On the other hand, 0.9853 precision, 0.9571 recall, 0.9710 F1-score, and 98.58% accuracy for VF test data and 0.900 precision, 0.900 recall, 0.900 F1-score, and 97.17% accuracy for VT test data are obtained, respectively on fold-1. The overall macro and micro average precision, recall, F1-score of 0.9511, 0.9571, 0.9539, and 0.9717 on fold-1, 0.9359, 0.9649, 0.9484, and 0.9685 on fold-2, 0.9192, 0.9272, 0.9223, and 0.9446 on fold-3, 0.9256, 0.9333, 0.9292, and 0.9483 on fold-4, respectively are shown in Tables (3.10-3.13).

From the experimental results, we observe that the classification accuracy of the PEA, VF, and VT is relatively low. Because the PEA, VF, and VT signals belong

to the abnormal class, and the distribution of the abnormal class signals is closed distance for the combination of the Mean of NSI with all features and showing high inter-dependence in the univariate histogram for the Mean of NSI feature as shown in Figure 3.45.

Table 3.10: Performance of the proposed method on fold-1, (μ_{NSI} and μ_{NTI} case)

Fold no.	Group	Precision	Recall	F1-score	Accuracy (%)
Fold-1	PEA	0.9189	0.9714	0.9444	98.58
	SR	1.0	1.0	1.0	100.0
	VF	0.9853	0.9571	0.9710	98.58
	VT	0.900	0.900	0.900	97.17
	Macro avg.	0.9511	0.9571	0.9539	
	Micro avg.	0.9717	0.9717	0.9717	

Table 3.11: Performance of the proposed method on fold-2, (μ_{NSI} and μ_{NTI} case)

Fold no.	Group	Precision	Recall	F1-score	Accuracy (%)
Fold-2	PEA	0.9375	1.0	0.9677	99.21
	SR	1.0	1.0	1.0	100.0
	VF	0.9846	0.9014	0.9412	96.85
	VT	0.8214	0.9583	0.8846	97.63
	Macro avg.	0.9359	0.9649	0.9484	
	Micro avg.	0.9685	0.9685	0.9685	

Table 3.12: Performance of the proposed method on fold-3, (μ_{NSI} and μ_{NTI} case)

Fold no.	Group	Precision	Recall	F1-score	Accuracy (%)
Fold-3	PEA	0.9189	0.8947	0.9067	97.41
	SR	1.0	1.0	1.0	100.0
	VF	0.9625	0.9167	0.9390	96.31
	VT	0.7955	0.8974	0.8434	95.20
	Macro avg.	0.9192	0.9272	0.9223	
	Micro avg.	0.9446	0.9446	0.9446	

Table 3.13: Performance of the proposed method on fold-4, (μ_{NSI} and μ_{NTI} case)

Fold no.	Group	Precision	Recall	F1-score	Accuracy (%)
Fold-4	PEA	0.8788	0.9355	0.9063	97.78
	SR	1.0	1.0	1.0	100.0
	VF	0.9583	0.9324	0.9452	97.04
	VT	0.8654	0.8654	0.8654	94.83
	Macro avg.	0.9256	0.9333	0.9292	
	Micro avg.	0.9483	0.9483	0.9483	

3.3.2.3.2 Discussion

A goal of this experiment is to check the effectiveness of our proposed method (Mean of NSI with Mean of NTI) and to compare the existing results (Mean of NSI with Variance of NSI) for different group of arrhythmias discrimination, i.e., VF, VT, PEA, and SR. Table 3.14 shows that the present NSI and NTI based features method keeps the better performance of the discrimination than the only NSI based features method. For example, in the table, one can see that the precision, recall, F1-score, and accuracy of the PEA case for the "Mean of NSI" with "Variance of NSI" is 0.8993, 0.9328, 0.9158, and 97.86% while the present "Mean of NSI" with "Mean of NTI" feature based method increase the precision, recall, F1-score, and accuracy to 0.9137, with 1.44% gain, 0.9478, with 1.5% gain, 0.9304, with 1.46% gain and 98.23% with 0.37% gain. Similarly, the precision, recall, F1-score, and accuracy are increased for all group arrhythmia. On the other hand, the overall macro and micro average precision, recall, and F1-score are increased to 0.77%, 0.70%, 0.75% and 0.46% for the "Mean of NSI" with "Mean of NTI" feature case.

The performance is improved of the proposed method for the combination of NSI and NTI-based features than for the combination of only NSI-based features. This is because the combination of "Mean of NSI" with "Mean of NTI" presents good separation corresponding to the abnormal class signals, and class-wise distribution is more isolated than the combination of "Mean of NSI" with "Variance of NSI". Also, the histogram of the abnormal class is less interdependent with each other for the combination of "Mean of NSI" with "Mean of NTI", while more interdependent with each other for the combination of "Mean of NSI" with "Variance of NSI" (see Figure 3.45).

Table 3.14: Overall group-wise performance comparison between (μ_{NSI} with μ_{NTI}) and (μ_{NSI} with V_{NSI})

Features	Group	Precision	Recall	F1-score	Accuracy (%)
μ_{NSI} with μ_{NTI}	PEA	0.9137	0.9478	0.9304	98.23
	SR	1.0	1.0	1.0	100.0
	VF	0.9719	0.9264	0.9486	97.21
	VT	0.8476	0.8968	0.8715	96.20
	Macro avg.	0.9333	0.9427	0.9376	
	Micro avg.	0.9583	0.9583	0.9583	
μ_{NSI} with V_{NSI}	PEA	0.8993	0.9328	0.9158	97.86
	SR	1.0	1.0	1.0	100.0
	VF	0.9717	0.9197	0.9450	97.03
	VT	0.8313	0.8903	0.8598	95.82
	Macro avg.	0.9256	0.9357	0.9301	
	Micro avg.	0.9537	0.9537	0.9537	

3.4 Summary

In this chapter, we have proposed a method based on the Gabor wavelet transform with pseudo-differential like operators and non-linear transformation for the extraction of accurate information (derivation of the scalogram) from the ECG signals. Note that, the major challenge for AED is to extract accurate information from the abnormal class signals for the application of reliable shock therapy. Therefore, we have derived many scalograms using the setting of various pseudo-differential like operators with non-linear transformation function to show the delicate distinction between shockable and non-shockable arrhythmia in the abnormal classes (see Figures 3.3-3.20). After that, we demonstrate an intrinsic effect of different settings of pseudo-differential operators and non-linear transformation function. The qualitative and quantitative evaluation is performed to select the best pair of pseudo-differential operator with non-linear transformation function (see Figures 3.21-3.28 and Table 3.5). From the scalographic representation and numerical experiments, it is shown that the application of pseudo-differential like operators and non-linear transformation function to the GWT is effective for the distinction of shockable and

non-shockable arrhythmias.

In addition, we have added a new approach to analyze the scalogram where we can observe the insights of the scalogram and deduce the statistical features of the scalogram effective for the discrimination (see section 3.3). After that, we have shown the graphical representation of the different combinations of features to select the best combination of the features (see Figure 3.45). Our algorithm followed the cross-validation method and has been validated on the well-known Physio-bank arrhythmia database. Also, we have compared the experimental results of the proposed method with the Gabor wavelet transform-based method, and the proposed method keeps the better performance for the distinction between shockable (VF and VT) and non-shockable (PEA) arrhythmia in the abnormal class signals.

4

Design of the AED shock and non-shock advice algorithm

4.1 Introduction

The automated external defibrillator (AED) is used for the sudden cardiac arrest patients for first aid, and it plays a vital role in saving the life. The rapid and accurate decision by the AED is important to improve the survival rate. It is worth mentioning that the correct information from the ECG signal helps to get an accurate decision by the AED. On the other hand, as for the quickness the survival rate decreases from 7% to 10% per minute according to the statistics of the American

heart association and resuscitation academy [10, 11]. In the first stage of the AED operation, extracting accurate information from the abnormal class ECG signals is crucially important. This issue is addressed by the novel method briefly explained in chapter 3, where the wavelet transform with pseudo-differential like operators was applied to observe statistics on the scalogram of the ECG signals. Second, an accurate and rapid decision-making method for the AED shock and non-shock advice algorithm is the ultimate demand to use the scalogram information properly. The decision algorithm determines if the patient has a life-threatening arrhythmia and makes a shock or no-shock decision. Therefore the decision algorithm is a crucial factor in the safety and performance of an AED.

Many researchers apply the different types of decision algorithms (e.g., Mahalanobis distance, nearest neighbor, etc.) to distinguish the arrhythmias in the decision stage [17, 18]. However, blindly use of such general methods are not the best for considering our problems. For example, the classification through the Mahalanobis distance depends on the concept of an approximation by means of the Gaussian distributions. Although the nearest neighbor is a non-parametric method, works in a small dataset, and evaluation is performed by the Euclidean distance, but this Euclidean metric function-based decision method has an issue for selecting the number of neighbors of the test sample. For example, in figure 4.4, if we consider the three nearest neighbors of the test sample, then the test sample is classified under the group of PEA, and if we consider the seven nearest neighbors, then the test sample is classified under the group of VT. Therefore, the decision becomes changed for selecting the number of the nearest neighbors of the test sample. Also, overfitting and underfitting occur for selecting the number of one nearest neighbor or the total number of data of nearest neighbors of the test sample. We can mitigate this issue by adopting adequate topology (a new metric function) to the space of the scatter plot (see Figure 4.4). In addition, researchers use machine learning classifier in the discrimination stage (A large number of the dataset is required) to separate

features of shockable and non-shockable arrhythmias [19, 20, 21, 22]. Their focus is put mainly on increasing the precision while the classifier adjusts various parameter values, but not on the quickness. A substantial length of computation time may be taken to generate the optimal feature model from the high dimensional parameter space. For a viable solution to the above issues, we develop a simple decision method (Design of the AED shock and non-shock advice algorithm) that guarantees high distinction with a low computational amount.

The rest of this chapter is organized as follows: in section 4.2, we discuss our proposed AED shock and non-shock advice algorithm. After that, the performance results and the discussion is presented in section 4.3. Finally, the summary of this chapter is drawn in section 4.4

4.2 Methodology

The flow chart of the proposed method for shockable and non-shockable arrhythmia distinction is shown in Figure 4.1. In the figure, step 1, we consider four types of data: SR, PEA, VF, and VT and we characterize the group of data by using the f number of features, $X = \left\{X_{N,f}^{(SR)}, X_{N',f}^{(VF)}, X_{N'',f}^{(PEA)}, X_{N''',f}^{(VT)}\right\}$, where $N, N', N'', N''' =$ number of samples of each group and $f =$ number of different statistical features. In this case, such features correspond to statistical features that are derived from the scalogram through NSI and NTI. Note that the scalogram is generated by using the Gabor wavelet transform with pseudo-differential like operators and non-linear transformation function which has been explained in chapter 3. In order to understand the general notations (sub-scripts) for the different types of data with their

different types of features, we give the description as a concise way.

$$X_{N,f}^{(SR)} = \left\{ \begin{pmatrix} X_{1,1}^{(SR)} \\ X_{1,2}^{(SR)} \\ \vdots \\ X_{1,f}^{(SR)} \end{pmatrix}, \begin{pmatrix} X_{2,1}^{(SR)} \\ X_{2,2}^{(SR)} \\ \vdots \\ X_{2,f}^{(SR)} \end{pmatrix}, \cdots, \begin{pmatrix} X_{N,1}^{(SR)} \\ X_{N,2}^{(SR)} \\ \vdots \\ X_{N,f}^{(SR)} \end{pmatrix} \right\} = \left\{ X_{1,\cdot}^{(SR)}, \cdots, X_{N,\cdot}^{(SR)} \right\},$$

$$X_{N',f}^{(VF)} = \left\{ \begin{pmatrix} X_{1,1}^{(VF)} \\ X_{1,2}^{(VF)} \\ \vdots \\ X_{1,f}^{(VF)} \end{pmatrix}, \begin{pmatrix} X_{2,1}^{(VF)} \\ X_{2,2}^{(VF)} \\ \vdots \\ X_{2,f}^{(VF)} \end{pmatrix}, \cdots, \begin{pmatrix} X_{N',1}^{(VF)} \\ X_{N',2}^{(VF)} \\ \vdots \\ X_{N',f}^{(VF)} \end{pmatrix} \right\} = \left\{ X_{1,\cdot}^{(VF)}, \cdots, X_{N',\cdot}^{(VF)} \right\},$$

Similarly for PEA and VT case, $X_{N'',f}^{(PEA)} = \left\{ X_{1,\cdot}^{(PEA)}, \cdots, X_{N'',\cdot}^{(PEA)} \right\}$, and $X_{N''',f}^{(VT)} = \left\{ X_{1,\cdot}^{(VT)}, \cdots, X_{N''',\cdot}^{(VT)} \right\}$.

In step 2, we check the discrimination capabilities of individual features for the different groups of data. The detailed description to find the effectiveness of the features which are derived through the NSI and NTI is presented in section 4.2.1. Following the strategy of the features selection, we define the effective features set for the four groups of data,

$$X = \left\{ X_{N,r}^{(SR)}, X_{N',r}^{(VF)}, X_{N'',r}^{(PEA)}, X_{N''',r}^{(VT)} \right\}, \tag{4.1}$$

where r = number of effective features. Again we give the description of effective features set in order to avoid the confusion about the notations.

$$X_{N,r}^{(SR)} = \left\{ \begin{pmatrix} X_{1,1}^{(SR)} \\ X_{1,2}^{(SR)} \\ \vdots \\ X_{1,r}^{(SR)} \end{pmatrix}, \begin{pmatrix} X_{2,1}^{(SR)} \\ X_{2,2}^{(SR)} \\ \vdots \\ X_{2,r}^{(SR)} \end{pmatrix}, \cdots, \begin{pmatrix} X_{N,1}^{(SR)} \\ X_{N,2}^{(SR)} \\ \vdots \\ X_{N,r}^{(SR)} \end{pmatrix} \right\} = \left\{ X_{1,\cdot}^{(SR)}, \cdots, X_{N,\cdot}^{(SR)} \right\},$$

$$X_{N',r}^{(VF)} = \left\{ \begin{pmatrix} X_{1,1}^{(VF)} \\ X_{1,2}^{(VF)} \\ \vdots \\ X_{1,r}^{(VF)} \end{pmatrix}, \begin{pmatrix} X_{2,1}^{(VF)} \\ X_{2,2}^{(VF)} \\ \vdots \\ X_{2,r}^{(VF)} \end{pmatrix}, \cdots, \begin{pmatrix} X_{N',1}^{(VF)} \\ X_{N',2}^{(VF)} \\ \vdots \\ X_{N',r}^{(VF)} \end{pmatrix} \right\} = \left\{ X_{1,\cdot}^{(VF)}, \cdots, X_{N',\cdot}^{(VF)} \right\},$$

Similarly for PEA and VT case, $X_{N'',f}^{(PEA)} = \left\{ X_{1,\cdot}^{(PEA)}, \cdots, X_{N'',\cdot}^{(PEA)} \right\}$, and $X_{N''',f}^{(VT)} = \left\{ X_{1,\cdot}^{(VT)}, \cdots, X_{N''',\cdot}^{(VT)} \right\}$.

In step 3, the resulting effective features dataset is divided into the testing dataset, $X_{T,r} = \left\{ X_{T,r}^{(SR)}, X_{T,r}^{(VF)}, X_{T,r}^{(PEA)}, X_{T,r}^{(VT)} \right\}$, where $X_{T,r} \in X$, and X is defined by equation 4.1, and the training dataset, $X_{L,r}^{G} = \left\{ X_{L,r}^{(SR)}, X_{L,r}^{(VF)}, X_{L,r}^{(PEA)}, X_{L,r}^{(VT)} \right\}$, where $X_{L,r}^{G} \in X$, and X is defined by equation 4.1. It is worth mentioning that the training dataset carries four types of data while the testing dataset contain mixture of the group data, and we have followed the K-fold cross-validation procedure which has been explained in subsection 3.3.1.4.2 in chapter 3. The training dataset where we give the concise description,

$$X_{L_n,r}^{(SR)} = \left\{ \begin{pmatrix} X_{L_1,1}^{(SR)} \\ X_{L_1,2}^{(SR)} \\ \vdots \\ X_{L_1,r}^{(SR)} \end{pmatrix}, \begin{pmatrix} X_{L_2,1}^{(SR)} \\ X_{L_2,2}^{(SR)} \\ \vdots \\ X_{L_2,r}^{(SR)} \end{pmatrix}, \cdots, \begin{pmatrix} X_{L_n,1}^{(SR)} \\ X_{L_n,2}^{(SR)} \\ \vdots \\ X_{L_n,r}^{(SR)} \end{pmatrix} \right\} = \left\{ X_{L_1,\cdot}^{(SR)}, \cdots, X_{L_n,\cdot}^{(SR)} \right\},$$

$$X_{L_{n'},r}^{(VF)} = \left\{ \begin{pmatrix} X_{L_1,1}^{(VF)} \\ X_{L_1,2}^{(VF)} \\ \vdots \\ X_{L_1,r}^{(VF)} \end{pmatrix}, \begin{pmatrix} X_{L_2,1}^{(VF)} \\ X_{L_2,2}^{(VF)} \\ \vdots \\ X_{L_2,r}^{(VF)} \end{pmatrix}, \cdots, \begin{pmatrix} X_{L_{n'},1}^{(VF)} \\ X_{L_{n'},2}^{(VF)} \\ \vdots \\ X_{L_{n'},r}^{(VF)} \end{pmatrix} \right\} = \left\{ X_{L_1,\cdot}^{(VF)}, \cdots, X_{L_{n'},\cdot}^{(VF)} \right\},$$

similarly for PEA and VT training dataset case, $X_{L_{n''},r}^{(PEA)} = \left\{ X_{L_1,\cdot}^{(PEA)}, \cdots, X_{L_{n''},\cdot}^{(PEA)} \right\}$, and $X_{L_{n'''},r}^{(VT)} = \left\{ X_{L_1,\cdot}^{(VT)}, \cdots, X_{L_{n'''},\cdot}^{(VT)} \right\}$, where $n, n', n'', n''' =$ number of training samples of each group.

On the other hand, for the testing dataset where,

$$X_{T_m,r} = \left\{ \begin{pmatrix} X_{T_1,1} \\ X_{T_1,2} \\ \vdots \\ X_{T_1,r} \end{pmatrix}, \begin{pmatrix} X_{T_2,1} \\ X_{T_2,2} \\ \vdots \\ X_{T_2,r} \end{pmatrix}, \cdots, \begin{pmatrix} X_{T_m,1} \\ X_{T_m,2} \\ \vdots \\ X_{T_m,r} \end{pmatrix} \right\} = \{X_{T_1,\cdot}, \cdots, X_{T_m,\cdot}\},$$

where, m is the number of testing samples.

In step 4, we adopt a new metric function, which is defined through adequately chosen topology for the space of the scatter plots (see equation 4.8). The topology of the scatter plot on D dimensional euclidean space about metric function is shown in Figure 4.4, and the detailed description of the topology of the scatter plot on D dimensional euclidean space (about new metric function) is presented in section 4.2.2. Suppose that we are given a scatter plot of training dataset $X^G_{L,\cdot}$ and test dataset, $X_{T,\cdot} = \{X_{T_1,\cdot}, \cdots, X_{T_m,\cdot}\}$. Then, we calculate the group wise minimum distance using the proposed metric function, $\rho_{(SR),(PEA),(VF),(VF)} = min\Big\{\lambda_1|X_{T,1} - X^{(G)}_{L,1}|^{p_1} + \cdots + \lambda_D|X_{T,r} - X^{(G)}_{L,r}|^{p_D}\Big\}$ where λ_j, $j = 1,\ldots,D$ and p_j, $j = 1,\ldots,D$ are given positive numbers. In our experiment, we put $r = 3$, $D = 3$ and through the experiment, we choose λ_j, $j = 1,2,3$ and p_j, $j = 1,2,3$ as follows: $\lambda_1 = 6, \lambda_2 = 1, \lambda_3 = 1, and\, p_1 = 1, p_2 = 1, p_3 = 1$. Then, we store the group wise minimum distance $(\rho_{SR}, \rho_{PEA}, \rho_{VF}, \rho_{VT})$ for each of the test sample. Finally, as the decision we make the comparison of the group distances and the test sample is classified base on minimum distance. Note that our method (see Figure 4.1) is restricted to the four groups of data where we considered SR, VF, PEA, and VT. We can easily generalize the proposed method. Namely, we can substitute the notations $X = \left\{X^{(SR)}_{N,f}, X^{(VF)}_{N',f}, X^{(PEA)}_{N'',f}, X^{(VT)}_{N''',f}\right\}$, given in step 1, by generalized $X^G_{N,f} = \left\{X^{(1)}_{N,f}, X^{(2)}_{N,f}, \cdots, X^{(C)}_{N,f}\right\}$, for C number of group data. In addition, algorithm 4 shows implementation of the proposed design of the AED shock and non-shock advice al-

gorithm.

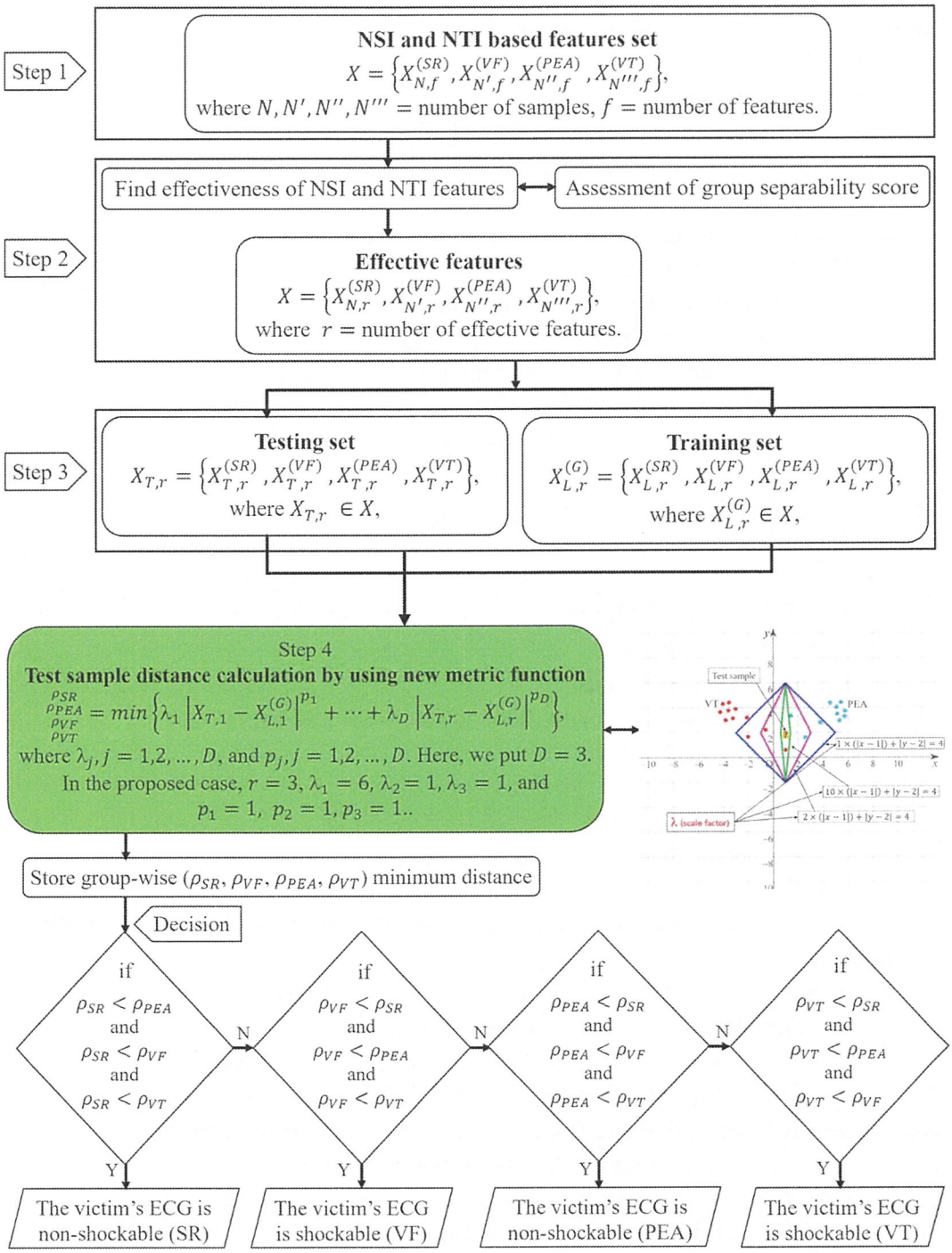

Figure 4.1: Proposed design of the AED shock and non-shock advice algorithm

Algorithm 4 Implementation of the proposed design of the AED shock and non-shock advice algorithm

Require: Dataset "M" containing input features.

Load M
Select best three features from M.
Initialize k_fold=4, Training set TR=[], Test set TE=[].
Generate uniformly distributed random integer equal to size(M) in the range of k_fold.
for $c = 1$ to class **do**
    for $K = 1$ to k_fold **do**
        for rand_idx $i = 1$ to size(M) **do**
            if $i == K$ **then**
                Store value in TE from M
            else
                Store value in TR from M
            end if
        end for
    end for
end for
// START VALIDATION //
for $m = 1$ to size(TE) **do**
    for $n = 1$ to size(TR) **do**
        Calculate the following distance according to Eq. 4.8
            (i) $\rho_{SR}(\mathbf{x},\mathbf{y})$
            (ii) $\rho_{PEA}(\mathbf{x},\mathbf{y})$
            (iii) $\rho_{VF}(\mathbf{x},\mathbf{y})$
            (iv) $\rho_{VT}(\mathbf{x},\mathbf{y})$
    end for
    Store group-wise (ρ_{SR}, ρ_{PEA}, ρ_{VF}, ρ_{VT}) minimum distance for each test sample
    if $\rho_{SR} < \rho_{PEA}$ and $\rho_{SR} < \rho_{VF}$ and $\rho_{SR} < \rho_{VT}$ **then**
        The victim's ECG is "Non-shockable (SR)"
    else if $\rho_{VF} < \rho_{SR}$ and $\rho_{VF} < \rho_{PEA}$ and $\rho_{VF} < \rho_{VT}$ **then**
        The victim's ECG is "Shockable (VF)"
    else if $\rho_{PEA} < \rho_{SR}$ and $\rho_{PEA} < \rho_{VF}$ and $\rho_{PEA} < \rho_{VT}$ **then**
        The victim's ECG is "Non-shockable (PEA)"
    else if $\rho_{VT} < \rho_{SR}$ and $\rho_{VT} < \rho_{PEA}$ and $\rho_{VT} < \rho_{VF}$ **then**
        The victim's ECG is "Shockable (VT)"
    end if
end for

4.2.1 Find effectiveness of the NSI and NTI features

Based on the NSI and NTI of the scalogram, the total sixteen statistical features are derived. Table 4.1 shows the features extracted from the scalogram through NSI and NTI. The detailed description of the NSI and NTI-based different types of features have been presented in chapter 3. Here, it is not clear that which features are effective for the discrimination of shockable and non-shockable arrhythmias. Therefore, it is necessary to find out the discriminatory abilities of features. In order to find out the effective features, we watch at each of the generated features independently and test their discriminatory capabilities by using the class separability technique such as scatter matrices [156]. This technique helps us to select the best feature from the set of features. Algorithm 5 shows a detailed process to find the effective feature.

Suppose that we have an n-dimensional feature vector $\bar{x} = [x_1, x_2, \ldots, x_n]$ assigned to c different classes $(i = 1, 2, \ldots, c)$. The definition of within-class scatter matrix S_w and between-class scatter matrix S_b are given by, respectively:

$$S_w = \sum_{i=1}^{c} \sum_{x \in D_i} P_i (x - \mu_i)(x - \mu_i)^T, \tag{4.2}$$

$$S_b = \sum_{i=1}^{c} P_i (\mu_i - \mu)(\mu_i - \mu)^T, \tag{4.3}$$

where D_i is the ith class, and P_i is a priori probability for class D_i. That is $P_i = n_i/N$, where n_i is the number of samples in class D_i, out of a total of N samples. The classwise mean μ_i and the overall mean μ are defined by:

$$\mu_i = \frac{1}{n_i} \sum_{x \in D_i} x, \tag{4.4}$$

$$\mu = \frac{1}{N} \sum_{D} x, \tag{4.5}$$

respectively, where D is the set of all classes. By following the equations 4.2 and

4.3, we calculate the multiclass separability score $f_x = \frac{S_b}{S_w}$. The scatter matrices value in figure 4.2 provides us with an insight how the separation among the four different arrhythmias are using the individual features. In the figure, we see that the feature "mean of NSI" on its own has the highest scatter matrices value, which indicates that this feature has the best discriminatory capabilities. Also, we see that the "mean of NTI" and "variance of NSI" have the second-best discriminatory capability, whereas the rest of the features are less than a satisfactory level. The selected best three features are visualized by 3D scatter plot that displays the separation of four different arrhythmias (see Figure 4.3). In the figure we see that the trivariate combination presents good separation corresponding to the abnormal groups, and the group-wise distribution is very much scattered.

Considering the characteristics of our actual scatter plot, it is not clever to use the circle that is the Euclidean metric function. Therefore, the Euclidean metric function is not suitable for the separation of the different groups of arrhythmias. This is because there has a high possibility to occurred misclassification of the test samples since many neighbors of the different groups of arrhythmias are belongs to the circle (see Figure 4.3). On the other hand, in order to get a good separation of the different groups of arrhythmias, we should choose an adequate topology for our actual scatter plot. Therefore, I have applied a sharp metric function with scale factor. The proposed metric function, where we can give different scales to select the best area on the scatter plot (see Figure 4.3). Therefore, the highest accuracy is achieved for the test samples since open neighbors of the same groups of arrhythmias are belongs to the sharp box.

Table 4.1: List of features derived through $NSI(b)$ and $NTI(a)$

No.	Feature Name	Symbol
1	Mean of NSI	μ_{NSI}
2	Variance of NSI	V_{NSI}
3	Slope of NSI	S_{NSI}
4	Kurtosis of NSI	K_{NSI}
5	Skewness of NSI	SK_{NSI}
6	Entropy based Index of NSI	EBI_{NSI}
7	Power of NSI	P_{NSI}
8	Mode of NSI	M_{NSI}
9	Mean of NTI	μ_{NTI}
10	Variance of NTI	V_{NTI}
11	Slope of NTI	S_{NTI}
12	Kurtosis of NTI	K_{NTI}
13	Skewness of NTI	SK_{NTI}
14	Entropy based Index of NTI	EBI_{NTI}
15	Power of NTI	P_{NTI}
16	Mode of NTI	M_{NTI}

Algorithm 5 Effective feature search

Require: Feature set: $\bar{x} = [x_1, x_2, \ldots, x_n]$.
Ensure: Effective feature: EF

1: Load $\bar{x}$
2: Initialize $\bar{f} = [\,]$
3: Initialize class number $c = 4$
4: Calculate overall mean μ according to Eq.(4.5)
5: **for** $i = 1$ to c **do**
6: Calculate class wise mean μ_i according to Eq.(4.4)
7: Calculate S_w and S_b according to Eq.(4.2), (4.3)
8: Calculate score $f_x = \frac{S_b}{S_w}$
9: **end for**
10: Store f_x into $\bar{f}$ and arrange in descending order.
11: EF= Select the top three features from $\bar{f}$.

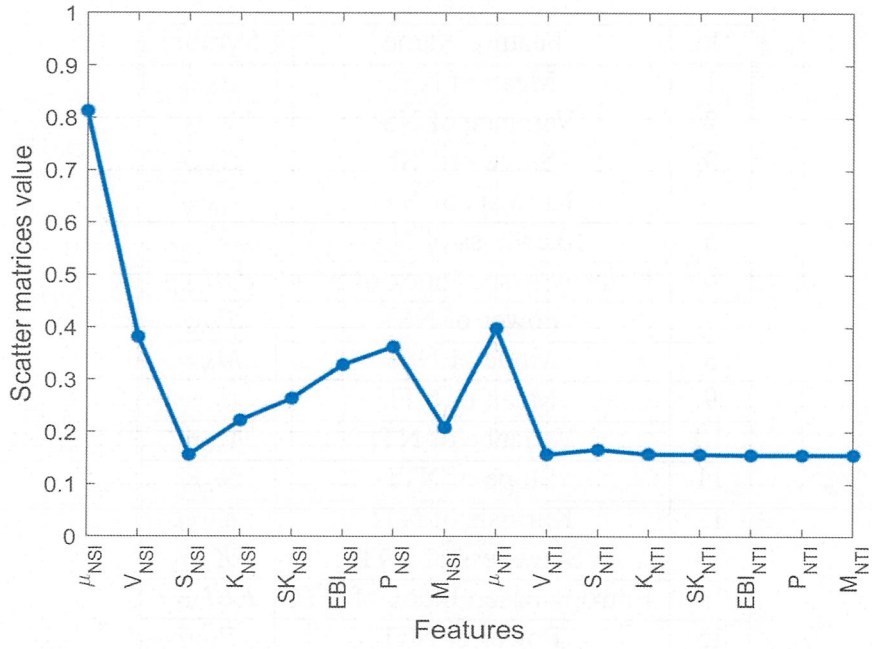

Figure 4.2: Discriminatory capabilities of individual features for multi-class separation

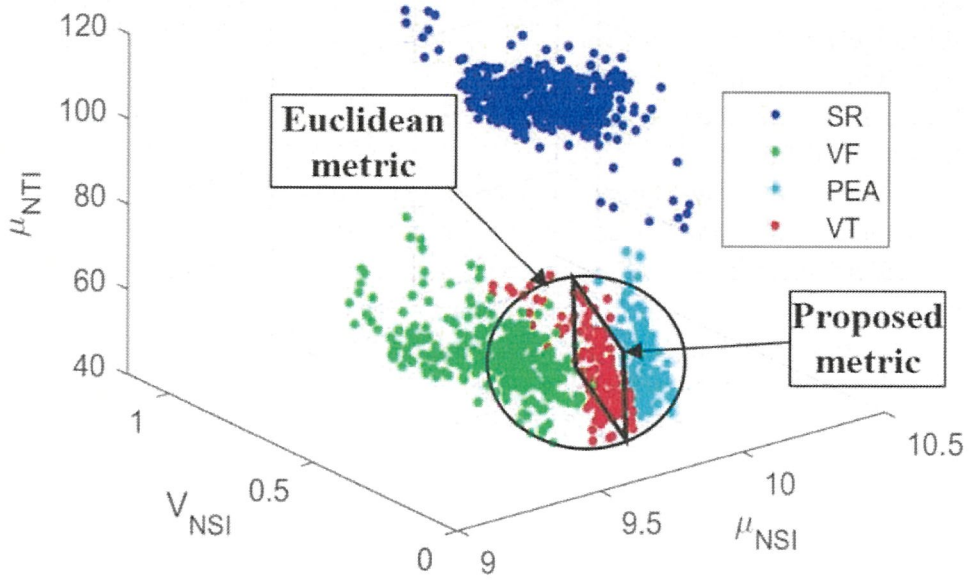

Figure 4.3: 3D scatter plot of the best three features

4.2.2 Topology of the scatter plot on D dimensional Euclidean space

We explain the concept of the topology of scatter plot (see Figure 4.3), through which we are able to get a high accuracy distinction among the different groups of the arrhythmias. We give the corresponding mathematical description as a concise way, and do not go further into the mathematics [157] (General topology) for the corresponding mathematics. Recall that our objective is to give a high accuracy distinction procedure by making use of the informations available from the scatter plot. For this purpose, we should choose an adequate topology of the given scatter plot. In the theory of statistics and corresponding mathematical software, there exist several provided methods of the classification, e.g., the Mahalanobis distance, (general) nearest neighbor evaluation. However, such methods would not always be optimal for each problem in consideration. For example, in case when we are given a scatter plot on D dimensional Euclidean space, then the Mahalanobis distance is defined through the covariance matrix of the scatter plot of training data of a given group, e.g., the group of the ECG signals of SR etc., which is a real symmetric non-negative definite $D \times D$ matrix by which we can define a multi-variable Gaussian distribution. Hence, the classification through the Mahalanobis distance depends on the concept of an approximation by means of the Gaussian distributions. Also, a nearest neighbor evaluation is performed by the Euclidean distance, which we can choose more adequately for each problem in consideration.

Now, suppose that we are given a non negative function $\rho(\mathbf{x},\mathbf{y})$ on the product space of D dimensional Euclidean space $\mathbb{R}^D \times \mathbb{R}^D$, $\mathbb{R} \equiv (-\infty,\infty)$ the real line, that satisfies the following:

$$\rho(\mathbf{x},\mathbf{y}) = \rho(\mathbf{y},\mathbf{x}) \geq 0, \quad \text{for any } \mathbf{x} \in \mathbb{R}^D, \mathbf{y} \in \mathbb{R}^D,$$

$$\rho(\mathbf{x},\mathbf{y}) = 0 \qquad \text{if and only if} \quad \mathbf{x} = \mathbf{y}.$$

We note that here we do not ask ρ to be a function that satisfies the triangle inequality such that $\rho(\mathbf{x},\mathbf{y}) \leq \rho(\mathbf{x},\mathbf{z}) + \rho(\mathbf{z},\mathbf{y})$ for any $\mathbf{x}, \mathbf{y}, \mathbf{z} \in \mathbb{R}^D$, and the ρ does not a metric function in general. For each $\mathbf{x} \in \mathbb{R}^D$ and $r > 0$, let us define an open neighborhood of the point $\mathbf{x} \in \mathbb{R}^D$ as follows:

$$\mathcal{O}(\mathbf{x};r) \equiv \{\mathbf{y} \in \mathbb{R}^D : \rho(\mathbf{x},\mathbf{y}) < r\}. \tag{4.6}$$

Then, we can define a new topology on $\mathbb{R}^D \times \mathbb{R}^D$, which is generated by the open base such that

$$\{\mathcal{O}(\mathbf{x};r) : \mathbf{x} \in \mathbb{R}^D, r > 0\}, \tag{4.7}$$

i.e., the family of the open neighbourhood $\mathcal{O}(\mathbf{x};r)$ defined by equation (4.6).

Our distinction procedure adopted here is as follows: Suppose that we are given a scatter plot of training data (see Figure 4.3), and a test data (we do not know to which group of arrhythmias it belongs), denoted by $\mathbf{x}$. Take the largest $r > 0$ by which $\mathcal{O}(\mathbf{x};r)$ include only one training data, say $\mathbf{y}$, namely $\mathbf{y}$ is the nearest point to the test data $\mathbf{x}$ evaluated by ρ. Then we decide that the test data $\mathbf{x}$ is a same group as the one of $\mathbf{y}$ (see Figure 4.4). For some special cases where the nearest points of $\mathbf{x}$ evaluated by ρ are not only one point, we may prepare an adequate algorithm by which we can avoid the ambiguity. As an example, we can take ρ as follows:

$$\rho(\mathbf{x},\mathbf{y}) \equiv \lambda_1 |x_1 - y_1|^{p_1} + \cdots + \lambda_D |x_D - y_D|^{p_D},$$
$$\text{for} \quad \mathbf{x} = (x_1,\ldots,x_D), \mathbf{y} = (y_1,\ldots,y_D) \in \mathbb{R}^D, \tag{4.8}$$

where λ_j, $j = 1,\ldots,D$ and p_j, $j = 1,\ldots,D$ are given positive numbers. More gen-

erally, we can take ρ as follows:

$$\rho(\mathbf{x},\mathbf{y}) \equiv w(\mathbf{x},\mathbf{y})\, A\, {}^t w(\mathbf{x},\mathbf{y}), \quad with \quad w(\mathbf{x},\mathbf{y}) \equiv \left(|x_1 - y_1|^{\frac{p_1}{2}}, \ldots, |x_D - y_D|^{\frac{p_D}{2}} \right), \tag{4.9}$$

where ${}^t w(\mathbf{x},\mathbf{y})$ is the transpose of the vector $w(\mathbf{x},\mathbf{y})$, and A is a real symmetric positive-definite $D \times D$ matrix:

$$A = \begin{pmatrix} a_{11} & \ldots & a_{1D} \\ \ldots & \ldots & \ldots \\ a_{D1} & \ldots & a_{DD} \end{pmatrix},$$

with real $a_{ij} = a_{ji}$, $i, j = 1, \ldots, D$. In particular, by taking A as the diagonal matrix of which diagonal elements satisfy $a_{ii} = \lambda_i$, $i = 1, \ldots, D$, then equation (4.9) is reduced to (4.8). Note that for the ρ satisfying the equation (4.9), the topology defined through (4.6), and (4.7) is equivalent to the one defined through the Euclidean metric $d(\mathbf{x},\mathbf{y}) = \sqrt{(x_1 - y_1)^2 + \cdots + (x_D - y_D)^2}$, but we evaluate the distance between $\mathbf{x}$ and $\mathbf{y}$ by $\rho(\mathbf{x},\mathbf{y})$, not by $d(\mathbf{x},\mathbf{y})$.

In short, by several λ we can give the different scales to the space of the scatter plots. Therefore, we have different distances ρ. We should choose a ρ that is adequate to the present distinction problem. In the experiment, we put $D = 3$ and through the experiment, we choose λ_j, $j = 1,2,3$ and p_j, $j = 1,2,3$ as follows:

$$\lambda_1 = 6, \quad \lambda_2 = 1, \quad \lambda_3 = 1, \quad and \quad p_1 = 1, \quad p_2 = 1, \quad p_3 = 1.$$

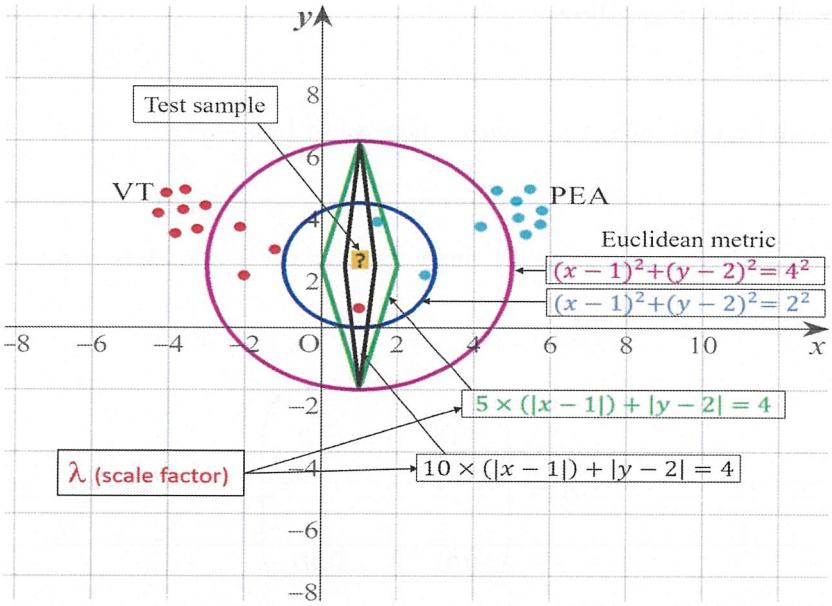

Figure 4.4: Decision strategy based on open neighbourhood topology (Scatter point of training data and neighbourhood of test data in two-dimensional case.)

4.3 Performance evaluation and discussion

Here, we present step by step performance result of our proposed method and compare with shockable and non-shockable state-of the-art methods.

4.3.1 Performance results

The performance results of the proposed method are evaluated for four class categories using four fold cross validation approach (see subsection 3.3.1.4.2 in chapter 3) based on the evaluation matrices (see subsection 3.3.1.4.1 in chapter 3). The confusion matrix plots with the performance results for shockable (VF, VT) and non-shockable (SR, PEA) arrhythmias are shown in Figures 4.5, 4.6, 4.7, and 4.8 respectively. The confusion matrix is generated through the proposed metric function-based decision method with the scale factor, $\lambda_1 = 6, \lambda_2 = 1, \lambda_3 = 1$, by using the combination of the "Mean of NSI", "Variance of NSI", and "Mean of NTI" features. In Figures 4.5, 4.6, 4.7, and 4.8, the rows correspond to the predicted class and the

columns correspond to the true class. The diagonal cells correspond to observations that are correctly classified. The off-diagonal cells correspond to incorrectly classified observations. Both the number of observations and the percentage of the total numbers of observations are shown in each cell. The values on the far right column (green, and red color), and the row at the bottom (green, and red color) of each figure show the percentages of the correct predictions and the incorrect predictions, respectively. The cell in the bottom right of the plot shows the overall correct and incorrect accuracy.

For example, on the Figure 4.5, 270 data, which is composed by 33 of PEA, 123 of SR, 75 of VF and 39 of VT, are tested. The first column shows that the 32 PEA data within the actual 33 PEA test data are correctly identified and 1 PEA test data is miss judged as VT. Similarly, the second column shows that the actual 123 SR test data are correctly identified and non of them is miss judged as others, i.e., PEA, VF, or VT. Similarly, the fourth column explains that, within the actual 39 number of VT, 36 are correctly identified but 1 data is miss judged as VF, and 2 data are miss judged as PEA. Therefore, 7.7% incorrect result given in the bottom of the fourth column, indicated as the red color, is calculated from $(1+2)/(1+2+36) = 3/39$.

On the other hand, the row concern, the first row of the same figure shows that 32 number of PEA are exactly identified as PEA, but in addition 2 of VT are miss judged as PEA, and the far-right component 94.1% of this row, indicated as the green color, is calculated from $32/(32+2)$. Similarly, the fourth row shows that 36 VT data are identified correctly, but in addition 1 of PEA data is miss judged as VT. Therefore, 97.3% corrected (green color) and 2.7% (red color) incorrect results are calculated from $36/(36+1)$ and $1/(36+1)$ which are shown in the far-right of the fourth row. The cell in the bottom right of the plot of the same figure shows the overall 98.5% correct and 1.5% incorrect accuracy.

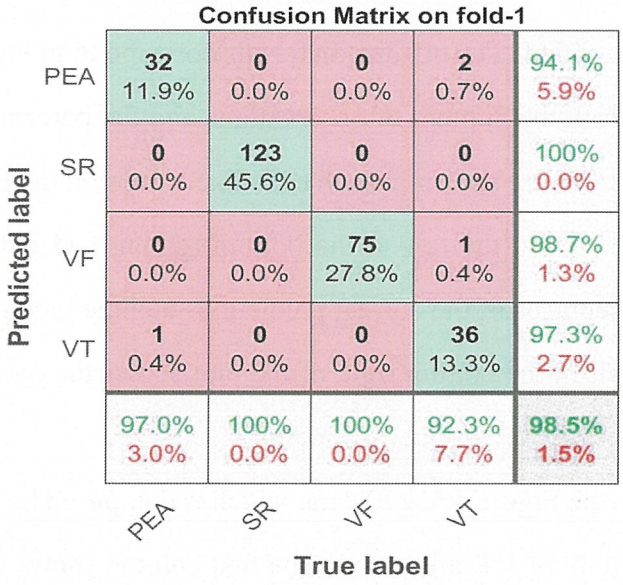

Figure 4.5: Confusion matrix with performance for shockable and non-shockable arrhythmias on fold-1, (μ_{NSI}, V_{NSI} and μ_{NTI}, and scale factor, $\lambda_1 = 6, \lambda_2 = 1, \lambda_3 = 1$ cases)

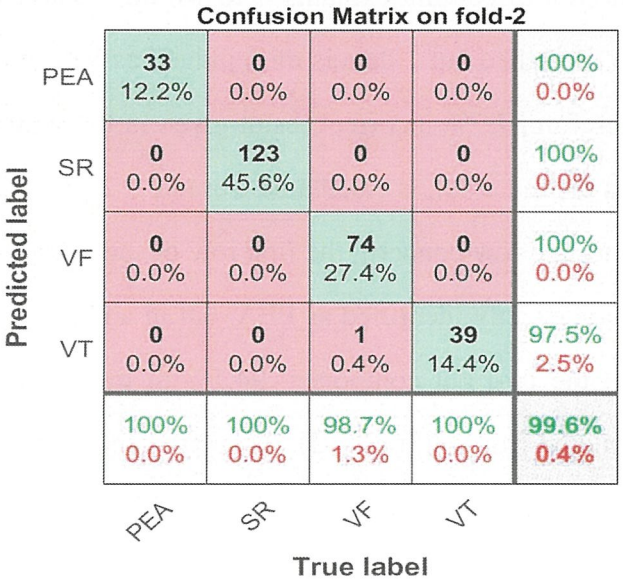

Figure 4.6: Confusion matrix with performance for shockable and non-shockable arrhythmias on fold-2, (μ_{NSI}, V_{NSI} and μ_{NTI}, and scale factor, $\lambda_1 = 6, \lambda_2 = 1, \lambda_3 = 1$ cases)

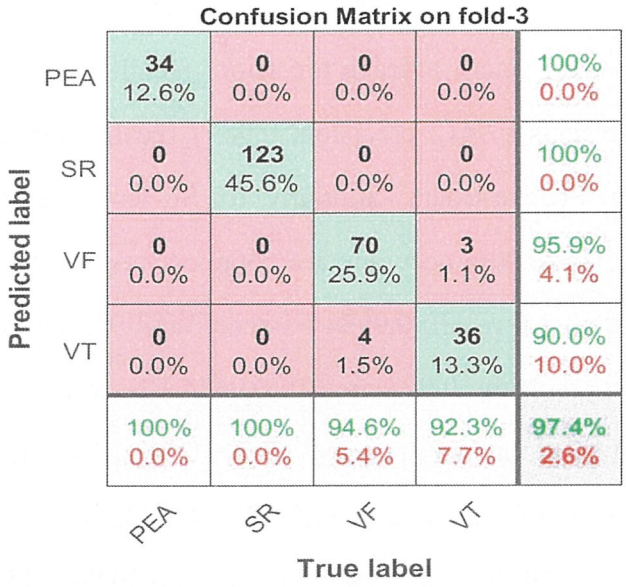

Figure 4.7: Confusion matrix with performance for shockable and non-shockable arrhythmias on fold-3, (μ_{NSI}, V_{NSI} and μ_{NTI}, and scale factor, $\lambda_1 = 6, \lambda_2 = 1, \lambda_3 = 1$ cases)

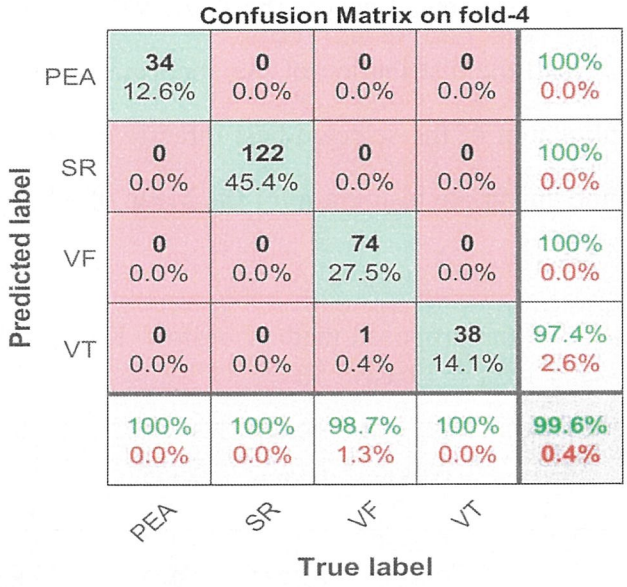

Figure 4.8: Confusion matrix with performance for shockable and non-shockable arrhythmias on fold-4, (μ_{NSI}, V_{NSI} and μ_{NTI}, and scale factor, $\lambda_1 = 6, \lambda_2 = 1, \lambda_3 = 1$ cases)

The detailed performance analysis (fold-wise and group-wise) presented in the Tables (4.2-4.5), which corresponding to Figures 4.5, 4.6, 4.7, and 4.8. The ta-

ble shows individual precision, recall, F1-score, and accuracy for each group, and shows overall macro and micro average precision, recall, and F1-score. For example, Table 4.2 presents 0.9412 precision, 0.9697 recall, 0.9552 F1-score, and 98.88% accuracy for PEA test data. Similarly, for SR test data 1.0 precision, 1.0 recall, 1.0 F1-score, and 100% accuracy are obtained, respectively. On the other hand, 0.9868 precision, 1.0 recall, 0.9934 F1-score, and 99.62% accuracy for VF test data and 0.9730 precision, 0.9231 recall, 0.9474 F1-score, and 98.51% accuracy for VT test data are obtained, respectively on fold-1. The overall macro and micro average precision, recall, F1-score of 0.9752, 0.9732, 0.9740, and 0.9852 on fold-1, 0.9938, 0.9967, 0.9952, and 0.9963 on fold-2, 0.9647, 0.9673, 0.9659, and 0.9741 on fold-3, 0.9936, 0.9967, 0.9951, and 0.9963 on fold-4, respectively are shown in Tables (4.2-4.5).

From the experimental results, we observe that the classification accuracy of the PEA, VF, and VT is relatively low. Because the PEA, VF, and VT signals belong to the abnormal class, and the distribution of the abnormal class signals is closed distance for the combination of the selected best three features and showing high inter-dependence in the univariate histogram for the Mean of NSI feature as shown in Figure 4.3.

Table 4.2: Performance of the proposed method on fold-1, (μ_{NSI}, V_{NSI}, μ_{NTI}, and scale factor, $\lambda_1 = 6, \lambda_2 = 1, \lambda_3 = 1$ cases)

Fold no.	Group	Precision	Recall	F1-score	Accuracy (%)
Fold-1	PEA	0.9412	0.9697	0.9552	98.88
	SR	1.0	1.0	1.0	100.0
	VF	0.9868	1.0	0.9934	99.62
	VT	0.9730	0.9231	0.9474	98.51
	Macro avg.	0.9752	0.9732	0.9740	
	Micro avg.	0.9852	0.9852	0.9852	

Table 4.3: Performance of the proposed method on fold-2, (μ_{NSI}, V_{NSI}, μ_{NTI}, and scale factor, $\lambda_1 = 6, \lambda_2 = 1, \lambda_3 = 1$ cases)

Fold no.	Group	Precision	Recall	F1-score	Accuracy (%)
Fold-2	PEA	1.0	1.0	1.0	100.0
	SR	1.0	1.0	1.0	100.0
	VF	1.0	0.9867	0.9933	99.62
	VT	0.9750	1.0	0.9873	99.62
	Macro avg.	0.9938	0.9967	0.9952	
	Micro avg.	0.9963	0.9963	0.9963	

Table 4.4: Performance of the proposed method on fold-3, (μ_{NSI}, V_{NSI}, μ_{NTI}, and scale factor, $\lambda_1 = 6, \lambda_2 = 1, \lambda_3 = 1$ cases)

Fold no.	Group	Precision	Recall	F1-score	Accuracy (%)
Fold-3	PEA	1.0	1.0	1.0	100.0
	SR	1.0	1.0	1.0	100.0
	VF	0.9589	0.9459	0.9524	97.40
	VT	0.900	0.9231	0.9114	97.40
	Macro avg.	0.9647	0.9673	0.9659	
	Micro avg.	0.9741	0.9741	0.9741	

Table 4.5: Performance of the proposed method on fold-4, (μ_{NSI}, V_{NSI}, μ_{NTI}, and scale factor, $\lambda_1 = 6, \lambda_2 = 1, \lambda_3 = 1$ cases)

Fold no.	Group	Precision	Recall	F1-score	Accuracy (%)
Fold-4	PEA	1.0	1.0	1.0	100.0
	SR	1.0	1.0	1.0	100.0
	VF	1.0	0.9867	0.9933	99.62
	VT	0.9744	1.0	0.9870	99.62
	Macro avg.	0.9936	0.9967	0.9951	
	Micro avg.	0.9963	0.9963	0.9963	

We have derived the detailed performance results of the proposed metric function-based decision method for the different scale factor and compared with the Euclidean metric function-based decision method. Tables (4.6-4.12) show group-wise individual precision, recall, F1-score (F-measure) and accuracy and macro-and micro-average precision, recall, F1-score for the different scale factor. As shown in the Tables, for SR test data, 1.0 precision, 1.0 recall, 1.0 F1-score, and 100% accuracy are obtained for the different scale factors while the precision, recall, F1-score, and accuracy are different for the PEA, VF, and VT test data. The Figure 4.9 illustrates the summary of the performance of the proposed metric function-based

decision method in term of the different scale factor. It is observed from the figure that the highest accuracy 98.79% is obtained at λ_1 = 6, 7, 8, λ_2 = 1, λ_3 = 1, and the performance is repeated for the different scale factor. For example, the accuracy 98.51% is obtained at λ_1 = 3, 4, 5, 12, λ_2 = 1, λ_3 = 1, and the accuracy 98.79%, 98.60%, 98.42%, 98.05%, 97.96%, and 97.86% is obtained at λ_1 = 6, 7, 8, λ_2 = 1, λ_3 = 1, at λ_1 =9, 10, 11, λ_2 = 1, λ_3 = 1, at λ_1=13 to 19, λ_2 = 1, λ_3 = 1, at λ_1= 25 to 33, λ_2 = 1, λ_3 = 1, at λ_1= 34 to 40, λ_2 = 1, λ_3 = 1, and at λ_1= 41 to 50, λ_2 = 1, λ_3 = 1, respectively. The accuracy is at its peak for the different scale factor because the proposed metric function fitted well on the scatter plot by adopting different scale factor (see Figure 4.3). Therefore, there is a high possibility of occurred correct classification of the test samples since open neighbors of the same groups of arrhythmias belong to the proposed metric function.

In addition, Table 4.13 shows the detailed performance (group-wise and different distinction schemes) comparison of the proposed metric function-based decision method and the Euclidean metric function-based decision method. As shown in the Table, the ratio of the successful discrimination between normal signals (SR) and abnormal signals (PEA, VF, and VT) is 100% for both methods. On the other hand, 94.72% accuracy is achieved by the Euclidean metric function-based decision method, while the proposed metric function-based decision method increases the accuracy to 97.78%, with 3.06% gain for the shockable (VF, VT) versus non-shockable (PEA) arrhythmia cases.

The performance is improved of the proposed metric function-based decision method for shockable vs non-shockable cases because we can select the best area of the scatter plot by adopting different scales of the proposed metric function. On the other hand, the performance is low of the Euclidean metric function-based decision method for shockable vs non-shockable cases because the Euclidean metric function is not suitable for the separation of the different groups of arrhythmias due to the characteristics of our actual scatter plot. This is because there has a high possi-

bility to occurred misclassification of the test samples since many neighbors of the different groups of arrhythmias are belongs to the circle (see Figure 4.3).

Table 4.6: Overall group-wise performance of the proposed method for the different scale factor

Scale factor	Group	Precision	Recall	F1-score	Accuracy (%)
$\lambda_1 = 1, \lambda_2 = 1, \lambda_3 = 1$ (without scale)	PEA	0.9699	0.9627	0.9663	99.16
	SR	1.0	1.0	1.0	100.0
	VF	0.9603	0.9699	0.9651	98.05
	VT	0.9085	0.8968	0.9026	97.21
	Macro avg.	0.9597	0.9573	0.9585	
	Micro avg.	0.9722	0.9722	0.9722	
$\lambda_1 = 2, \lambda_2 = 1, \lambda_3 = 1$	PEA	0.9852	0.9925	0.9888	99.72
	SR	1.0	1.0	1.0	100.0
	VF	0.9670	0.9799	0.9734	98.51
	VT	0.9533	0.9226	0.9377	98.23
	Macro avg.	0.9764	0.9738	0.9750	
	Micro avg.	0.9824	0.9824	0.9824	
$\lambda_1 = 3, \lambda_2 = 1, \lambda_3 = 1$	PEA	0.9925	0.9925	0.9925	99.81
	SR	1.0	1.0	1.0	100.0
	VF	0.9672	0.9866	0.9768	98.70
	VT	0.9664	0.9290	0.9474	98.51
	Macro avg.	0.9815	0.9770	0.9792	
	Micro avg.	0.9852	0.9852	0.9852	
$\lambda_1 = 4, \lambda_2 = 1, \lambda_3 = 1$	PEA	0.9925	0.9925	0.9925	99.81
	SR	1.0	1.0	1.0	100.0
	VF	0.9703	0.9833	0.9767	98.70
	VT	0.9603	0.9355	0.9477	98.51
	Macro avg.	0.9808	0.9778	0.9792	
	Micro avg.	0.9852	0.9852	0.9852	
$\lambda_1 = 5, \lambda_2 = 1, \lambda_3 = 1$	PEA	0.9852	0.9925	0.9888	99.72
	SR	1.0	1.0	1.0	100.0
	VF	0.9767	0.9799	0.9783	98.79
	VT	0.9542	0.9419	0.9481	98.51
	Macro avg.	0.9790	0.9786	0.9788	
	Micro avg.	0.9852	0.9852	0.9852	
$\lambda_1 = 6, \lambda_2 = 1, \lambda_3 = 1$	PEA	0.9852	0.9925	0.9888	99.72
	SR	1.0	1.0	1.0	100.0
	VF	0.9865	0.9799	0.9832	99.07
	VT	0.9551	0.9613	0.9582	98.79
	Macro avg.	0.9817	0.9834	0.9826	
	Micro avg.	0.9880	0.9880	0.9880	
$\lambda_1 = 7, \lambda_2 = 1, \lambda_3 = 1$	PEA	0.9852	0.9925	0.9888	99.72
	SR	1.0	1.0	1.0	100.0
	VF	0.9865	0.9799	0.9832	99.07
	VT	0.9551	0.9613	0.9582	98.79
	Macro avg.	0.9817	0.9834	0.9826	
	Micro avg.	0.9880	0.9880	0.9880	

Table 4.7: Overall group-wise performance of the proposed method for the different scale factor (continue)

Scale factor	Group	Precision	Recall	F1-score	Accuracy (%)
$\lambda_1 = 8, \lambda_2 = 1, \lambda_3 = 1$	PEA	0.9852	0.9925	0.9888	99.72
	SR	1.0	1.0	1.0	100.0
	VF	0.9865	0.9799	0.9832	99.07
	VT	0.9551	0.9613	0.9582	98.79
	Macro avg.	0.9817	0.9834	0.9826	
	Micro avg.	0.9880	0.9880	0.9880	
$\lambda_1 = 9, \lambda_2 = 1, \lambda_3 = 1$	PEA	0.9852	0.9925	0.9888	99.72
	SR	1.0	1.0	1.0	100.0
	VF	0.9832	0.9766	0.9799	98.88
	VT	0.9487	0.9548	0.9518	98.60
	Macro avg.	0.9793	0.9810	0.9801	
	Micro avg.	0.9861	0.9861	0.9861	
$\lambda_1 = 10, \lambda_2 = 1, \lambda_3 = 1$	PEA	0.9852	0.9925	0.9888	99.72
	SR	1.0	1.0	1.0	100.0
	VF	0.9832	0.9766	0.9799	98.88
	VT	0.9487	0.9548	0.9518	98.60
	Macro avg.	0.9793	0.9810	0.9801	
	Micro avg.	0.9861	0.9861	0.9861	
$\lambda_1 = 11, \lambda_2 = 1, \lambda_3 = 1$	PEA	0.9852	0.9925	0.9888	99.72
	SR	1.0	1.0	1.0	100.0
	VF	0.9864	0.9732	0.9798	98.88
	VT	0.9430	0.9613	0.9521	98.60
	Macro avg.	0.9787	0.9818	0.9802	
	Micro avg.	0.9861	0.9861	0.9861	
$\lambda_1 = 12, \lambda_2 = 1, \lambda_3 = 1$	PEA	0.9925	0.9851	0.9888	99.72
	SR	1.0	1.0	1.0	100.0
	VF	0.9864	0.9699	0.9781	98.79
	VT	0.9317	0.9677	0.9494	98.51
	Macro avg.	0.9776	0.9807	0.9791	
	Micro avg.	0.9852	0.9852	0.9852	
$\lambda_1 = 13, \lambda_2 = 1, \lambda_3 = 1$	PEA	0.9925	0.9851	0.9888	99.72
	SR	1.0	1.0	1.0	100.0
	VF	0.9863	0.9666	0.9764	98.70
	VT	0.9259	0.9677	0.9464	98.42
	Macro avg.	0.9762	0.9798	0.9779	
	Micro avg.	0.9842	0.9842	0.9842	
$\lambda_1 = 14, \lambda_2 = 1, \lambda_3 = 1$	PEA	0.9925	0.9851	0.9888	99.72
	SR	1.0	1.0	1.0	100.0
	VF	0.9863	0.9666	0.9764	98.70
	VT	0.9259	0.9677	0.9464	98.42
	Macro avg.	0.9762	0.9798	0.9779	
	Micro avg.	0.9842	0.9842	0.9842	

Table 4.8: Overall group-wise performance of the proposed method for the different scale factor (continue)

Scale factor	Group	Precision	Recall	F1-score	Accuracy (%)
$\lambda_1 = 15, \lambda_2 = 1, \lambda_3 = 1$	PEA	0.9925	0.9851	0.9888	99.72
	SR	1.0	1.0	1.0	100.0
	VF	0.9863	0.9666	0.9764	98.70
	VT	0.9259	0.9677	0.9464	98.42
	Macro avg.	0.9762	0.9798	0.9779	
	Micro avg.	0.9842	0.9842	0.9842	
$\lambda_1 = 16, \lambda_2 = 1, \lambda_3 = 1$	PEA	0.9925	0.9851	0.9888	99.72
	SR	1.0	1.0	1.0	100.0
	VF	0.9863	0.9666	0.9764	98.70
	VT	0.9259	0.9677	0.9464	98.42
	Macro avg.	0.9762	0.9798	0.9779	
	Micro avg.	0.9842	0.9842	0.9842	
$\lambda_1 = 17, \lambda_2 = 1, \lambda_3 = 1$	PEA	0.9925	0.9851	0.9888	99.72
	SR	1.0	1.0	1.0	100.0
	VF	0.9863	0.9666	0.9764	98.70
	VT	0.9259	0.9677	0.9464	98.42
	Macro avg.	0.9762	0.9798	0.9779	
	Micro avg.	0.9842	0.9842	0.9842	
$\lambda_1 = 18, \lambda_2 = 1, \lambda_3 = 1$	PEA	0.9925	0.9851	0.9888	99.72
	SR	1.0	1.0	1.0	100.0
	VF	0.9863	0.9666	0.9764	98.70
	VT	0.9259	0.9677	0.9464	98.42
	Macro avg.	0.9762	0.9798	0.9779	
	Micro avg.	0.9842	0.9842	0.9842	
$\lambda_1 = 19, \lambda_2 = 1, \lambda_3 = 1$	PEA	0.9925	0.9851	0.9888	99.72
	SR	1.0	1.0	1.0	100.0
	VF	0.9863	0.9666	0.9764	98.70
	VT	0.9259	0.9677	0.9464	98.42
	Macro avg.	0.9762	0.9798	0.9779	
	Micro avg.	0.9842	0.9842	0.9842	
$\lambda_1 = 20, \lambda_2 = 1, \lambda_3 = 1$	PEA	0.9925	0.9851	0.9888	99.72
	SR	1.0	1.0	1.0	100.0
	VF	0.9829	0.9632	0.9730	98.51
	VT	0.9198	0.9613	0.9401	98.23
	Macro avg.	0.9738	0.9774	0.9755	
	Micro avg.	0.9824	0.9824	0.9824	
$\lambda_1 = 21, \lambda_2 = 1, \lambda_3 = 1$	PEA	0.9925	0.9851	0.9888	99.72
	SR	1.0	1.0	1.0	100.0
	VF	0.9796	0.9632	0.9713	98.42
	VT	0.9193	0.9548	0.9367	98.14
	Macro avg.	0.9728	0.9758	0.9742	
	Micro avg.	0.9815	0.9815	0.9815	

Table 4.9: Overall group-wise performance of the proposed method for the different scale factor (continue)

Scale factor	Group	Precision	Recall	F1-score	Accuracy (%)
$\lambda_1 = 22, \lambda_2 = 1, \lambda_3 = 1$	PEA	0.9851	0.9851	0.9851	99.62
	SR	1.0	1.0	1.0	100.0
	VF	0.9796	0.9632	0.9713	98.42
	VT	0.9188	0.9484	0.9333	98.05
	Macro avg.	0.9709	0.9742	0.9724	
	Micro avg.	0.9805	0.9805	0.9805	
$\lambda_1 = 23, \lambda_2 = 1, \lambda_3 = 1$	PEA	0.9851	0.9851	0.9851	99.62
	SR	1.0	1.0	1.0	100.0
	VF	0.9763	0.9632	0.9697	98.33
	VT	0.9182	0.9419	0.9299	97.96
	Macro avg.	0.9699	0.9726	0.9712	
	Micro avg.	0.9796	0.9796	0.9796	
$\lambda_1 = 24, \lambda_2 = 1, \lambda_3 = 1$	PEA	0.9851	0.9851	0.9851	99.62
	SR	1.0	1.0	1.0	100.0
	VF	0.9763	0.9632	0.9697	98.33
	VT	0.9182	0.9419	0.9299	97.96
	Macro avg.	0.9699	0.9726	0.9712	
	Micro avg.	0.9796	0.9796	0.9796	
$\lambda_1 = 25, \lambda_2 = 1, \lambda_3 = 1$	PEA	0.9851	0.9851	0.9851	99.62
	SR	1.0	1.0	1.0	100.0
	VF	0.9764	0.9666	0.9714	98.42
	VT	0.9241	0.9419	0.9329	98.05
	Macro avg.	0.9714	0.9734	0.9724	
	Micro avg.	0.9805	0.9805	0.9805	
$\lambda_1 = 26, \lambda_2 = 1, \lambda_3 = 1$	PEA	0.9851	0.9851	0.9851	99.62
	SR	1.0	1.0	1.0	100.0
	VF	0.9764	0.9666	0.9714	98.42
	VT	0.9241	0.9419	0.9329	98.05
	Macro avg.	0.9714	0.9734	0.9724	
	Micro avg.	0.9805	0.9805	0.9805	
$\lambda_1 = 27, \lambda_2 = 1, \lambda_3 = 1$	PEA	0.9851	0.9851	0.9851	99.62
	SR	1.0	1.0	1.0	100.0
	VF	0.9764	0.9666	0.9714	98.42
	VT	0.9241	0.9419	0.9329	98.05
	Macro avg.	0.9714	0.9734	0.9724	
	Micro avg.	0.9805	0.9805	0.9805	
$\lambda_1 = 28, \lambda_2 = 1, \lambda_3 = 1$	PEA	0.9851	0.9851	0.9851	99.62
	SR	1.0	1.0	1.0	100.0
	VF	0.9764	0.9666	0.9714	98.42
	VT	0.9241	0.9419	0.9329	98.05
	Macro avg.	0.9714	0.9734	0.9724	
	Micro avg.	0.9805	0.9805	0.9805	

Table 4.10: Overall group-wise performance of the proposed method for the different scale factor (continue)

Scale factor	Group	Precision	Recall	F1-score	Accuracy (%)
$\lambda_1 = 29, \lambda_2 = 1, \lambda_3 = 1$	PEA	0.9851	0.9851	0.9851	99.62
	SR	1.0	1.0	1.0	100.0
	VF	0.9764	0.9666	0.9714	98.42
	VT	0.9241	0.9419	0.9329	98.05
	Macro avg.	0.9714	0.9734	0.9724	
	Micro avg.	0.9805	0.9805	0.9805	
$\lambda_1 = 30, \lambda_2 = 1, \lambda_3 = 1$	PEA	0.9851	0.9851	0.9851	99.62
	SR	1.0	1.0	1.0	100.0
	VF	0.9764	0.9666	0.9714	98.42
	VT	0.9241	0.9419	0.9329	98.05
	Macro avg.	0.9714	0.9734	0.9724	
	Micro avg.	0.9805	0.9805	0.9805	
$\lambda_1 = 31, \lambda_2 = 1, \lambda_3 = 1$	PEA	0.9852	0.9925	0.9888	99.72
	SR	1.0	1.0	1.0	100.0
	VF	0.9731	0.9666	0.9698	98.33
	VT	0.9295	0.9355	0.9325	98.05
	Macro avg.	0.9719	0.9736	0.9728	
	Micro avg.	0.9805	0.9805	0.9805	
$\lambda_1 = 32, \lambda_2 = 1, \lambda_3 = 1$	PEA	0.9852	0.9925	0.9888	99.72
	SR	1.0	1.0	1.0	100.0
	VF	0.9731	0.9666	0.9698	98.33
	VT	0.9295	0.9355	0.9325	98.05
	Macro avg.	0.9719	0.9736	0.9728	
	Micro avg.	0.9805	0.9805	0.9805	
$\lambda_1 = 33, \lambda_2 = 1, \lambda_3 = 1$	PEA	0.9852	0.9925	0.9888	99.72
	SR	1.0	1.0	1.0	100.0
	VF	0.9731	0.9666	0.9698	98.33
	VT	0.9295	0.9355	0.9325	98.05
	Macro avg.	0.9719	0.9736	0.9728	
	Micro avg.	0.9805	0.9805	0.9805	
$\lambda_1 = 34, \lambda_2 = 1, \lambda_3 = 1$	PEA	0.9852	0.9925	0.9888	99.72
	SR	1.0	1.0	1.0	100.0
	VF	0.9730	0.9632	0.9681	98.23
	VT	0.9236	0.9355	0.9295	97.96
	Macro avg.	0.9704	0.9728	0.9716	
	Micro avg.	0.9796	0.9796	0.9796	
$\lambda_1 = 35, \lambda_2 = 1, \lambda_3 = 1$	PEA	0.9852	0.9925	0.9888	99.72
	SR	1.0	1.0	1.0	100.0
	VF	0.9730	0.9632	0.9681	98.23
	VT	0.9236	0.9355	0.9295	97.96
	Macro avg.	0.9704	0.9728	0.9716	
	Micro avg.	0.9796	0.9796	0.9796	

Table 4.11: Overall group-wise performance of the proposed method for the different scale factor (continue)

Scale factor	Group	Precision	Recall	F1-score	Accuracy (%)
$\lambda_1 = 36, \lambda_2 = 1, \lambda_3 = 1$	PEA	0.9852	0.9925	0.9888	99.72
	SR	1.0	1.0	1.0	100.0
	VF	0.9730	0.9632	0.9681	98.23
	VT	0.9236	0.9355	0.9295	97.96
	Macro avg.	0.9704	0.9728	0.9716	
	Micro avg.	0.9796	0.9796	0.9796	
$\lambda_1 = 37, \lambda_2 = 1, \lambda_3 = 1$	PEA	0.9852	0.9925	0.9888	99.72
	SR	1.0	1.0	1.0	100.0
	VF	0.9730	0.9632	0.9681	98.23
	VT	0.9236	0.9355	0.9295	97.96
	Macro avg.	0.9704	0.9728	0.9716	
	Micro avg.	0.9796	0.9796	0.9796	
$\lambda_1 = 38, \lambda_2 = 1, \lambda_3 = 1$	PEA	0.9852	0.9925	0.9888	99.72
	SR	1.0	1.0	1.0	100.0
	VF	0.9730	0.9632	0.9681	98.23
	VT	0.9236	0.9355	0.9295	97.96
	Macro avg.	0.9704	0.9728	0.9716	
	Micro avg.	0.9796	0.9796	0.9796	
$\lambda_1 = 39, \lambda_2 = 1, \lambda_3 = 1$	PEA	0.9852	0.9925	0.9888	99.72
	SR	1.0	1.0	1.0	100.0
	VF	0.9730	0.9632	0.9681	98.23
	VT	0.9236	0.9355	0.9295	97.96
	Macro avg.	0.9704	0.9728	0.9716	
	Micro avg.	0.9796	0.9796	0.9796	
$\lambda_1 = 40, \lambda_2 = 1, \lambda_3 = 1$	PEA	0.9852	0.9925	0.9888	99.72
	SR	1.0	1.0	1.0	100.0
	VF	0.9730	0.9632	0.9681	98.23
	VT	0.9236	0.9355	0.9295	97.96
	Macro avg.	0.9704	0.9728	0.9716	
	Micro avg.	0.9796	0.9796	0.9796	
$\lambda_1 = 41, \lambda_2 = 1, \lambda_3 = 1$	PEA	0.9852	0.9925	0.9888	99.72
	SR	1.0	1.0	1.0	100.0
	VF	0.9729	0.9599	0.9663	98.14
	VT	0.9177	0.9355	0.9265	97.86
	Macro avg.	0.9689	0.9720	0.9704	
	Micro avg.	0.9787	0.9787	0.9787	
$\lambda_1 = 42, \lambda_2 = 1, \lambda_3 = 1$	PEA	0.9852	0.9925	0.9888	99.72
	SR	1.0	1.0	1.0	100.0
	VF	0.9729	0.9599	0.9663	98.14
	VT	0.9177	0.9355	0.9265	97.86
	Macro avg.	0.9689	0.9720	0.9704	
	Micro avg.	0.9787	0.9787	0.9787	

Table 4.12: Overall group-wise performance of the proposed method for the different scale factor (continue)

Scale factor	Group	Precision	Recall	F1-score	Accuracy (%)
$\lambda_1 = 43, \lambda_2 = 1, \lambda_3 = 1$	PEA	0.9852	0.9925	0.9888	99.72
	SR	1.0	1.0	1.0	100.0
	VF	0.9729	0.9599	0.9663	98.14
	VT	0.9177	0.9355	0.9265	97.86
	Macro avg.	0.9689	0.9720	0.9704	
	Micro avg.	0.9787	0.9787	0.9787	
$\lambda_1 = 44, \lambda_2 = 1, \lambda_3 = 1$	PEA	0.9852	0.9925	0.9888	99.72
	SR	1.0	1.0	1.0	100.0
	VF	0.9729	0.9599	0.9663	98.14
	VT	0.9177	0.9355	0.9265	97.86
	Macro avg.	0.9689	0.9720	0.9704	
	Micro avg.	0.9787	0.9787	0.9787	
$\lambda_1 = 45, \lambda_2 = 1, \lambda_3 = 1$	PEA	0.9852	0.9925	0.9888	99.72
	SR	1.0	1.0	1.0	100.0
	VF	0.9729	0.9599	0.9663	98.14
	VT	0.9177	0.9355	0.9265	97.86
	Macro avg.	0.9689	0.9720	0.9704	
	Micro avg.	0.9787	0.9787	0.9787	
$\lambda_1 = 46, \lambda_2 = 1, \lambda_3 = 1$	PEA	0.9852	0.9925	0.9888	99.72
	SR	1.0	1.0	1.0	100.0
	VF	0.9729	0.9599	0.9663	98.14
	VT	0.9177	0.9355	0.9265	97.86
	Macro avg.	0.9689	0.9720	0.9704	
	Micro avg.	0.9787	0.9787	0.9787	
$\lambda_1 = 47, \lambda_2 = 1, \lambda_3 = 1$	PEA	0.9852	0.9925	0.9888	99.72
	SR	1.0	1.0	1.0	100.0
	VF	0.9729	0.9599	0.9663	98.14
	VT	0.9177	0.9355	0.9265	97.86
	Macro avg.	0.9689	0.9720	0.9704	
	Micro avg.	0.9787	0.9787	0.9787	
$\lambda_1 = 48, \lambda_2 = 1, \lambda_3 = 1$	PEA	0.9852	0.9925	0.9888	99.72
	SR	1.0	1.0	1.0	100.0
	VF	0.9729	0.9599	0.9663	98.14
	VT	0.9177	0.9355	0.9265	97.86
	Macro avg.	0.9689	0.9720	0.9704	
	Micro avg.	0.9787	0.9787	0.9787	
$\lambda_1 = 49, \lambda_2 = 1, \lambda_3 = 1$	PEA	0.9852	0.9925	0.9888	99.72
	SR	1.0	1.0	1.0	100.0
	VF	0.9729	0.9599	0.9663	98.14
	VT	0.9177	0.9355	0.9265	97.86
	Macro avg.	0.9689	0.9720	0.9704	
	Micro avg.	0.9787	0.9787	0.9787	

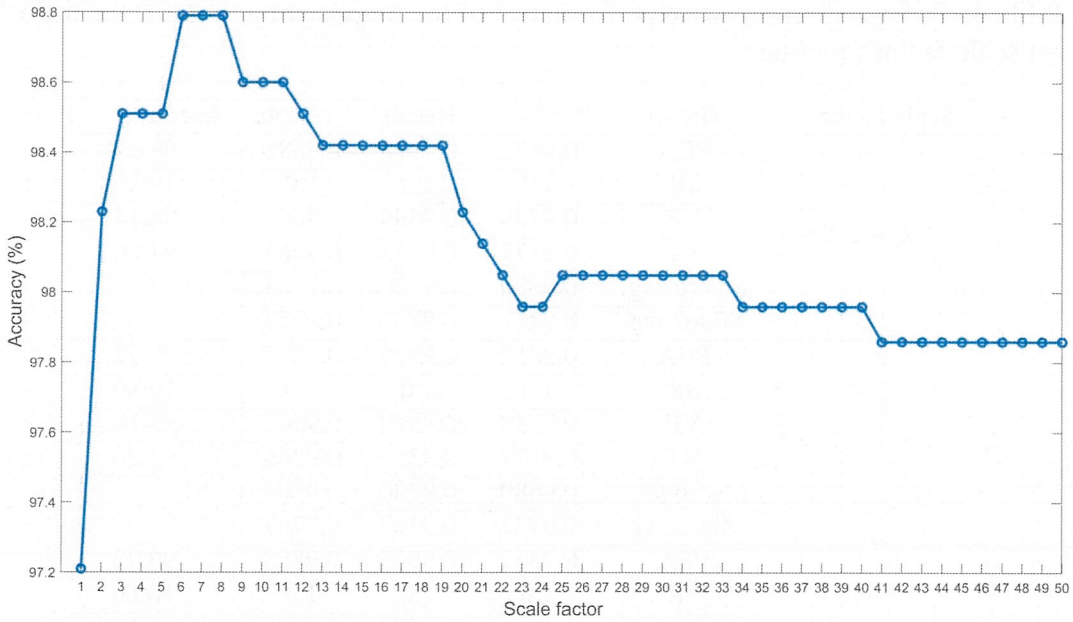

Figure 4.9: Accuracy for the different scale factor

Table 4.13: Performance comparison of the proposed metric function with the Euclidean metric function

Method	Group	Precision	Recall	F1-score	Group-wise accuracy (%)	*Distinction scheme	Accuracy(%)
Proposed metric function-based decision method	PEA	0.9852	0.9925	0.9888	99.72	SR vs (PEA, VF, VT)	100.0
	SR	1.0	1.0	1.0	100.0		
	VF	0.9865	0.9799	0.9832	99.07		
	VT	0.9551	0.9613	0.9582	98.79	PEA vs (VF, VT)	97.78
	Macro avg.	0.9817	0.9834	0.9826			
	Micro avg.	0.9880	0.9880	0.9880			
Euclidean metric function-based decision method	PEA	0.9697	0.9552	0.9624	99.07	SR vs (PEA, VF, VT)	100.0
	SR	1.0	1.0	1.0	100.0		
	VF	0.9572	0.9732	0.9652	98.05		
	VT	0.9079	0.8903	0.8990	97.12	PEA vs (VF, VT)	94.72
	Macro avg.	0.9587	0.9547	0.9567			
	Micro avg.	0.9713	0.9713	0.9713			

* Normal (SR) vs Abnormal (PEA, VF and VT) and non-shockable (PEA) vs Shockable (VF, VT).

4.3.2 Discussion

The objective of this experiment is to certify the effectiveness of our proposed method as an absolute sense, and to compare relatively the performance with the existing state-of-the-art shockable and non-shockable arrhythmia discrimination methods. Table 4.14, and 4.15 show the performance results where several factors have been considered to compare the proposed method with other methods. For example,

i have compared the proposed method with other distance-based decision methods (e.g., Euclidean distance, Mahalanobis distance), and baseline methods where the same strategy was used for the information extraction from the signals. I further compared the proposed method with other existing state-of-the-art methods, those exactly followed the same databases, the same distinction scheme, and included the same arrhythmia types.

First, we compare the proposed method with the existing state-of-the-art method that exactly followed the same strategy for the information extraction from the signals. For example, Rahman et al. [24] represented a method to derive the scalogram in the time-frequency domain. In this paper, the authors presented various experimental scalograms of the electrocardiograms using wavelet transform with various pseudo differential-like operators and non-linear transformation functions. Then, the scalogram is analyzed only in the frequency direction, and calculated statistical features from the scalogram. Finally, the histogram is used in the decision stage to distinguish shockable and non-shockable arrhythmia. The authors achieved 100% accuracy for normal (SR) versus abnormal (PEA, VF, and VT) signals, while 91.58% accuracy was achieved for the shockable (VF, and VT) versus non-shockable (PEA) of the abnormal class signals. On the other hand, the proposed work followed the same strategy for the derivation of the scalogram from the signals and analyzed the scalogram along frequency direction. In addition, the scalogram is analyzed along the time direction which is a new addition in our research. Also, in this proposed work I have designed a simple distance-based decision method with a scale factor where the highest accuracy achieved. However, the proposed work achieved 100% accuracy for normal (SR) versus abnormal (PEA, VF, and VT) signals, while 97.78% accuracy was achieved for the shockable (VF, and VT) versus non-shockable (PEA) of the abnormal class signals at scale factor $\lambda_1 = 6$, $\lambda_2 = 1$, $\lambda_3 = 1$.

We further compare our proposed method with other distance-based decision

methods. From the Tables 4.14, and 4.15, it is clear that the proposed metric function-based decision method performed better than the other distance-based decision methods. For example, in [162, 168], they used the Euclidean metric function-based decision method to distinguish arrhythmias. There it is mentioned that 91.75% and 91.67% accuracy have been obtained, while the proposed metric function-based decision method increases the accuracy to 97.78% with 6.03% and 6.11% gain. In addition, Okai et al. [29] showed the detailed performance results of shockable versus non-shockable arrhythmia recognition algorithms by analyzing different spectrum feature parameters. They applied the Gabor wavelet transform to extract the information from the ECG signal, and used the Mahalanobis distance in their decision stage. Note that, the classification through the Mahalanobis distance depends on the concept of an approximation by means of the Gaussian distributions. The Mahalanobis metric function-based decision method achieves 100% accuracy for the distinction between normal (SR) and abnormal (PEA, VF, and VT) cases, and 86.03% accuracy for the shockable (VF, VT) and non-shockable (PEA) arrhythmias in abnormal class signals, while the proposed metric function-based decision method achieves 100% accuracy for the distinction between normal (SR) and abnormal (PEA, VF, and VT) cases and increases the accuracy to 97.78% with 11.75% gain for the shockable (VF, VT) and non-shockable (PEA) arrhythmias in abnormal class signals.

We also further compare our proposed method with other existing state-of-the-art methods those exactly followed the same types of distinction scheme and included PEA arrhythmia. Sharma et al. [165] employed five-level decomposition of the signal, extracted fuzzy entropy (FE), renyi entropy (RE) features, and then fed features into various machine-learning based classifiers for the shockable and non-shockable classification. They achieved 97.8% accuracy for the Shockable (VF, VT) versus non-shockable (NSR, PEA, others), while the proposed method achieves 97.78%. The accuracy is slightly high for the existing method since the evaluation

Table 4.14: Comparison of the proposed method with other state-of-the-art methods

References (year)	Methods	Dataset used	Sample length	Group wise sample number	Distinction scheme	Performance
Tripathy et al. [158] 2016	VMD, RF classifier	MITDB, VFDB, CUDB	5s	†NSR, VF, VT, others=1250	Shockable (VF, VT) vs non-shockable (NSR, others)	Acc=97.23%
Cheng et al. [159] 2017	Personalized features, SVM	MITDB, VFDB, CUDB	8s	VA=1047, non-VA=15517	VA vs Non-VA, excluded PEA	Acc=95.46%
Acharya et al. [160] 2018	Pre-processing, CNN	MITDB, VFDB, CUDB	2s	†NSR, PEA, others=48095, VF,VT=6001	Shockable (VF, VT) vs non-shockable (NSR, PEA, others)	Acc=93.18%
Tripathy et al. [161] 2018	DTFT, LS-SVM	VFDB, CUDB	5s	†NSR, others=4144, VF,VT=2072	Shockable (VF, VT) vs non-shockable (NSR, others), VF vs non-VF	Acc=83.63% Acc=89.81%
Resiandi et al. [162] 2018	Preprocessing, features, KNN (K=1 to 11)	MITDB-AFBD, NSRDB	10s	NSR=1280, AF=2500	Normal vs AF	Acc=91.75% to 78.0%
Xie et al. [163] 2019	SVM and Opt-AMSA	MITDB, VFDB	1s	NSR=50, VF=40, VT=58	Shockable (VF, VT) vs non-shockable (NSR)	Acc=94.9%
Li et al. [164] 2019	Markov model	MITDB, VFDB, CUDB	5s	†Shockable and non-shockable=1670	VA vs non-VA excluded PEA	*Acc=90.03%

* The accuracy has been calculated according their predicted result.
† Mentioned shockable and non-shockable sample numbers.

Table 4.15: Comparison of the proposed method with other state-of-the-art methods (continue)

References (year)	Methods	Dataset used	Sample length	Group wise sample number	Distinction scheme	Performance
Sharma et al. [165] 2020	Wavelet based features, (FE, RE), SVM	MITDB, VFDB, CUDB	2s	†NSR, PEA, VF, VT, others=500	Shockable (VF, VT) vs non-shockable (NSR, PEA, others)	Acc=97.8%
Okai et al. [29] 2020	GWT, spectrum features, Mahalanobis distance	AHA, MITDB, CUDB, KUH	5s	SR=552, PEA=224, VF,VT=356	Shockable (VF, VT) vs non-shockable (PEA), SR vs ,PEA,VF,VT	*Acc=86.03% *Acc=100.0%
Hajeb et al. [166] 2021	Filtering, Machine learning (BP)	MITDB, VFDB, CUDB, SDDB	14s	†NSR, others=2600, VF,VT=2340	Shockable (VT, VF) vs non-shockable (NSR, others)	Acc=89.2%
Hammad et al. [167] 2021	Preprocessing, Features, PCA, SVM	MITDB, VFDB, CUDB	2s, 5s	†PEA, others=6210, VF,VT=5794	Shockable (VF, VT) vs non-shockable (PEA, others)	Acc=87.95% Acc=90.14%
Toulni et al. [168] 2021	DWT, Features, KNN (K=1 to 7)	MITDB	1m	-	Normal vs abnormal	Acc=91.67% to 66.67%
Rahman et al. [24] 2022	Wavelet transform pseudo differential like operators, NSI, Histogram	MITDB, VFDB, CUDB	5s	SR=491, PEA=134, VF=299,VT=155	Shockable (VF, VT) vs non-shockable (PEA), SR vs PEA,VF,VT	Acc=91.58% Acc=100.0%
Proposed approach 2022	Wavelet transform pseudo differential like operators, NSI, NTI, Open neighbourhood topology	MITDB, VFDB, CUDB	5s	SR=491, PEA=134, VF=299,VT=155	Shockable (VF, VT) vs non-shockable (PEA), SR vs PEA,VF,VT	Acc=97.78% Acc=100.0%

* The accuracy has been calculated according their predicted result (See part A of section III in [29]).
† Mentioned shockable and non-shockable sample numbers.
- Not mentioned the sample number.

was performed on around five hundred samples where non-shockable samples (e.g., NSR samples) numbers are relatively higher than the shockable samples. In addition, we observe from Tables 4.14, and 4.15, that the methods as [158, 159, 160, 161, 163, 164, 166], and [167] achieved the high-performance results for shockable versus non-shockable arrhythmia distinction, but PEA arrhythmia is not individually considered there. As has been explained in the introduction the discrimination of PEA arrhythmia is particularly important in the abnormal classes regarding the actual application of AED. From the Tables, we see that our proposed method obtains an accuracy comparable to or greater than the above methods with respect to the delicate distinction between shockable and non-shockable cases.

Run-time performance evaluation. We evaluate the running time of our proposed method. We use 11^{th} Gen Intel(R) Core(TM) i7-1185G7 @ 3.00GHz CPU, 32 GB of RAM, iRIS-Xe graphics, and a 64-bit Windows 11 operating system in our experiment. We measure feature extraction time (Derivation of the scalogram, and statistical feature calculation), data set separation (training, and testing set) time for cross fold validation, and testing time for 1079 samples. The features extraction phase takes $4.37 * 10^{-2}s$ in average for each test sample. In the training phase, the time it takes $2.89 * 10^{-1}s$ to separate the training data and test data for the 4-fold cross-validation. The testing phase takes $8.90 * 10^{-2}s$ in average for each fold. Hence, our method takes $3.35 * 10^{-4}s$ in average to test each sample. So, our proposed method takes in a total $4.40 * 10^{-2}s$ in average to test each sample.

4.4 Summary

A new shock and non-shock advice algorithm for the AED has been proposed in this chapter. The algorithm is designed for two important guiding principles: first, increasing the shockable and non-shockable arrhythmias distinction accuracy for the application of reliable shock therapy by the AED. Second, the rapid decision by

the AED is important to increase the survival rate of the patients. The proposed design of the algorithm is based on a set of effective features and adopts a new metric function, which is defined through an adequately chosen topology for the space of scatter plots. We can give the different scales of the metric function to the space of the scatter plot through which we can choose the open neighbor of the test sample (see Figure 4.4). As a consequence, the proposed method gives the highest accuracy and rapid decision between shockable and non-shockable arrhythmias. Note that the performance of the proposed method is generally affected by the different scale factors; therefore we have verified the variation in the performance of the proposed method by changing the scale factor from 1 to 50 (See Tables (4.6-4.12), and Figure 4.9). On the other hand, the effectiveness of the features is measured through the assessment of the group separability score (see Figure 4.2) and by following the effective features set, the three-dimensional scatter plot is derived to visualize the separation of the four different groups (see Figure 4.3). Note that the features correspond to statistical features, which are derived from the scalogram through two quality parameters and the scalogram is derived by using the Gabor wavelet transform with pseudo-differential like operators and non-linear transformation function. The proposed shock and non-shock advice algorithm followed the cross-validation process and has been validated on the well-known physio-bank arrhythmia database.

We conducted a comparative performance analysis of our proposed algorithm with other state-of-the-art approaches, and the Euclidean metric function-based decision method and it is shown that the proposed algorithm has the highest accuracy of the distinction between abnormal shockable (VT, VF) and abnormal non-shockable (PEA) arrhythmias (see the comparison Tables 4.13, 4.14, and 4.15). Also we have measured the run time performances of the proposed method, which is explained in the discussion section. In the next chapter, we will provide the conclusions of our whole work in this dissertation and will discuss the future work in detail.

5

Conclusions

5.1 Thesis summary

This thesis investigates the arrhythmia diagnosis system of the AED to find the significant issues, and propose a structure of the arrhythmia diagnosis system to overcome the existing issues through the analysis of ECG signals with engineering methods and generalized function theories. In the arrhythmia diagnosis system, two methods have been proposed: first, the core idea is to derive exact information (derivation of the scalogram) from the abnormal classes of ECG signals which leads to the decision algorithm for getting a better distinction between shockable and non-shockable arrhythmias. Following the information, the new quality param-

eter is adopted to get more information by quantizing the statistical features on the scalogram. Second, design a simple decision algorithm (design of the AED shock and non-shock advice algorithm) by following this information for improving the precision and rapid decision in order to increase the survival rate.

The first approach, namely derivation of the scalogram explained in chapter 3. To derive an accurate scalogram for the shockable and non-shockable arrhythmias of the abnormal ECG classes, we proposed a method based on the Gabor wavelet transform with pseudo-differential like operators and non-linear transformation function. Through the pseudo-differential like operators, we can get much more enlarged fruitful information (fractional order of differentiation of the signal) on the original signals. Moreover, by applying the non-linear transformation functions to the transformed signals, we can make balanced and bigger the part of the transformed signals which has relatively small energy and amplitude. Through these, we are able to generate different energies over time in the scalogram and different energies over time lead to get the best discrimination in the decision stage, while the same level of energies over time in the scalogram is generated by using the conventional approach. The same level of energies over time gives a barrier to distinguishing in the decision algorithm. In addition, we have introduced a new quality parameter to explore the insights of the scalogram. Through the quality parameter, we can draw out more information from the scalograms, which is useful for better discrimination. The proposed method has been evaluated against 1079 samples from the physio bank database. We have demonstrated an intrinsic effect of the different settings of pseudo differential like operators with non-linear transformation functions by using qualitative evaluation, and performed numerical experiments in terms of individual precision, recall, F1-score (F-measure) and group-wise accuracy, and macro-and micro-average precision, recall, F1-score, to find how the application of the pseudo differential like operators is powerful to the delicate distinctions of shockable and non-shockable arrhythmias in abnormal classes ECG signals. The experimental re-

sult of the proposed method was also compared with the Gabor wavelet transform-based method, and the proposed method keeps the better performance for the distinction between shockable (VF and VT) and non-shockable (PEA) arrhythmia in the abnormal class signals.

The second approach, namely the design of the AED shock and non-shock advice algorithm explained in chapter 4. The algorithm is designed for two important guiding principles: first, increasing the shockable and non-shockable arrhythmias distinction accuracy for the application of reliable shock therapy by the AED. Second, the rapid decision by the AED is essential to increase the survival rate of the patients. The proposed design of the algorithm is based on a set of effective features and adopts a new metric function, which is defined through an adequately chosen topology for the space of scatter plots. We can give the different scales of the metric function to the space of the scatter plot through which we can choose the open neighborhood of the test sample. As a consequence, the proposed method gives the highest accuracy and rapid decision between shockable and non-shockable arrhythmias. The method followed the cross validation approach for stabilizing the performance and the experimental results, individual precision, recall, F1-score (F-measure) and group-wise accuracy, and macro-and micro-average precision, recall, F1-score, that tested on physio bank arrhythmia databases are used to evaluate the proposed method. The results of the proposed method are also compared with other formally published methods and the Euclidean metric function-based decision method and show high performance for the distinction of shockable and non-shockable arrhythmias in the abnormal classes. Moreover, we have measured the run-time performances of the proposed method.

Overall, the main contribution of this thesis is to enhance the arrhythmia diagnosis system in the AED in order to increase the survival rate from sudden cardiac arrest. The proposed arrhythmia diagnosis system is general and could be applied for the distinction of different arrhythmia-based applications. Also, each contribu-

tion to the arrhythmia diagnosis system could be used independently in different applications.

5.2 Future work

There are several types of arrhythmias, depending on what part of the heart is affected (upper chambers of the heart or lower chambers of the heart). Among these arrhythmias, some are fatal arrhythmias, and some are non-fatal arrhythmias. Usually, the four possible fatal arrhythmias (e.g., PEA, VF, VT, and asystole) exist in an unresponsive patient. They can be categorized into shockable (defibrillation effective) and non-shockable (defibrillation should not be used) arrhythmias. Note that the asystole signal where there is no heartbeat and treated as a flat line and easily identifiable. Also, it is worth mentioning that the conventional arrhythmia diagnosis system uses the four types (e.g., SR, PEA, VF, and VT) of arrhythmias for classification. Therefore, in this thesis, we have considered four types of arrhythmias (e.g., SR, PEA, VF, and VT) to evaluate our proposed arrhythmias diagnosis system, which comes from fatal and non-fatal arrhythmias. In addition, it is important to classify all types of arrhythmias so that the clinician can prevent and treat the life-threatening arrhythmias. This is because there are some non-fatal arrhythmias (e.g., AF, LBBBB, etc.) that could be precursors for the creation of fatal arrhythmias. Therefore, in our future work, all types of arrhythmias will be considered to validate our arrhythmias diagnosis system. Besides, the current stage of our arrhythmias diagnosis system still stays at the software algorithms level. Therefore, the final aim of our work is to design a hardware platform that can be integrated with the AED to prevent sudden cardiac death caused by fatal arrhythmia. In this case, it is possible to translate the proposed algorithms (e.g., derivation of the scalogram, analysis of the scalogram, design of the AED shock non-shock advice algorithm) into a single hardware framework.

References

[1] Pereira-Junior, P.P., Marocolo, M., Rodrigues, FP., Medei, E., and Nascimento, JH., Noninvasive method for electrocardiogram recording in conscious rats: feasibility for heart rate variability analysis, *Anais da Academia Brasileira de Ciências*, pp. 431-437, 2010.

[2] WHO/Cardiovascular diseases (CVDs) in the world, *https://www.who.int/news-room/fact-sheets/detail/cardiovascular-diseases-(cvds)*

[3] Japanese society of emergency medicine cardiopulmonary resuscitation for citizens, *http://aed.jaam.jp/sudden_death.html*

[4] WHO/Cardiovascular diseases (CVDs) in the USA, *https://www.cdc.gov/heartdisease/facts.htm*

[5] WHO/Cardiovascular diseases (CVDs) in the europe, *https://ehnheart.org/cvd-statistics.html*

[6] Highlights of the American Heart Association's Guidelines for CPR and AED, *https://cpr.heart.org/media/cpr-files/cpr-guidelines-fi-les/highlights/hghlghts_2020_ecc_guidelines_english.pdf*

[7] American Heart Association in collaboration with the International Liaison Committee on Resuscitation and others: The automated external defibrillator:Guidelines 2000 for cardiopulmonary resuscitation and emergency cardiovascular care, *circulation*, 102, 2000.

[8] Deakin, C.D., Nolan, J.P., Sunde, K., and Koster, R.W., European Resuscitation Council Guidelines for Resuscitation Section 3. Electrical therapies: automated external defibrillators, defibrillation, cardioversion and pacing, *Resuscitation*, 81, pp. 1293-1304, 2010.

[9] Littmann, L., Bustin, D.J., and Haley, M.W., A simplified and structured teaching tool for the evaluation and management of pulseless electrical activity, *Medical Principles and Practice*, 23, pp. 1-6, 2014.

[10] Field, J.M., Hazinski, M.F., Sayre, M.R., Chameides, L., Schexnayder, S.M., Hemphill, R., Samson, R.A., Kattwinkel, J., Berg, R.A., Bhanji, F., and Cave, D.M., Part 1: executive summary: American Heart Association guidelines for cardiopulmonary resuscitation and emergency cardiovascular care, *Circulation*, pp. 640-656, 2010.

[11] Strategies to Improve Cardiac Arrest Survival: A Time to Act, *http://www.resuscitationacademy.org/downloads/RA-35-Strategies-to-Improve-CA-Survival.pdf*

[12] Larsen, M.P., Eisenberg, M.S., Cummins, R.O., and Hallstrom, A.P., Predicting survival from out-of-hospital cardiac arrest: a graphic model, *Annals of emergency medicine*, pp. 1652-1658, 1993.

[13] Valenzuela, T.D., Roe, D.J., Cretin, S., Spaite, D.W., and Larsen, M.P., Estimating effectiveness of cardiac arrest interventions: a logistic regression survival model, *Circulation*, pp. 3308-3313, 1997.

[14] Marenco, J.P., Wang, P.J., Link, M.S., Homoud, M.K., and Estes, N.M., Improving survival from sudden cardiac arrest: the role of the automated external defibrillator, *Jama*, pp. 1193-1200, 2001.

[15] Okai, T., Hirata, S., Oya, H., Hoshi, Y., Nakano, K., Yamaguchi, Y., Igarashi, T., and Miyauchi, H., A New Recognition Algorithm for Shockable Arrhythmias and Its Performance Analysis, *The 44th Annual Conference of the IEEE Industrial Electronics Society*, pp. 2671-2676, 2018.

[16] Okai, T., Oya, H., Hoshi, Y., Ogino, Y., Nakano, K., Yamaguchi, Y., and Miyauchi, M., A recognition algorithm for electrocardiogram based on wavelet transform and feature selection, *Proceedings of the IASTED International Conference on Modelling, Identification and Control*, pp. 125-132, 2017.

[17] Babiloni, F., Bianchi, L., Semeraro, F., del, R., Millan, J., Mouriño, J., Cattini, A., Salinari, S., Marciani, M.G., and Cincotti, F., Mahalanobis distance-based classifiers are able to recognize EEG patterns by using few EEG electrodes, *In 2001 Conference Proceedings of the 23rd Annual International Conference of the IEEE Engineering in Medicine and Biology Society*, vol. 1, pp. 651-654, 2001.

[18] Park, J., Lee, K., and Kang, K., Arrhythmia detection from heartbeat using k-nearest neighbor classifier, *IEEE International Conference on Bioinformatics and Biomedicine*, pp. 15-22, 2013.

[19] Nguyen, M.T., Van Nguyen, B., and Kim, K., Deep feature learning for sudden cardiac arrest detection in automated external defibrillators, *Scientific reports*, 8, pp. 1-2, 2018.

[20] Ming, Y., Taihu, W., Pengcheng, Y., Meng, L., Guang, Z., and Feng, C., Detection of Shockable Rhythm during Chest Compression based on Machine Learning, *IEEE 8th Joint International Information Technology and Artificial Intelligence Conference*, pp. 365-370, 2019.

[21] Kumar, A., and Kumar, R., Time-frequency analysis and support vector machine in automatic detection of defect from vibration signal of centrifugal pump, *Measurement*, pp. 119-133, 2017.

[22] Jambukia, S.H., Dabhi, V.K., and Prajapati, H.B., Classification of ECG signals using machine learning techniques: A survey *IEEE International Conference on Advances in Computer Engineering and Applications*, pp. 714-721, 2015.

[23] Rahman, M.M., Kagawa, T., Kawasaki, S., Nagai, S., Okai, T., Oya, H., Yahagi, Y., and Yoshida, M.W., An analysis of electrocardiograms through the wavelet transform with pseudo-differential operator like operators, *Numerical harmonic analysis and signal processing*, the JSST International Conference on Simulation Technology, pp.63-66, 2021.

[24] Rahman, M.M., Kagawa, T., Kawasaki, S., Nagai, S., Okai, T., Oya, H., Yahagi, Y., and Yoshida, M.W., Various scalographic representation of electrocardiograms through wavelet transform with pseudo-differential operator like operators, *Journal of Advanced Simulation in Science and Engineering*, vol. 9, issue 1, pp. 96-112, 2022.

[25] Sejdic, E., Djurovic, I., and Stankovic, L., Quantitative performance analysis of scalogram as instantaneous frequency estimator, *IEEE Transactions on Signal Processing*, vol. 56, issue 8, pp. 3837-3845, 2008.

[26] Carmona, R.A., Hwang, W.L., and Torrésani, B., Characterization of signals by the ridges of their wavelet transforms, *IEEE transactions on signal processing*, vol. 45, issue 10, pp. 2586-2590, 1997.

[27] Rahman, M.M., Albeverio, S., Kagawa, T., Kawasaki, S., Okai, T., Oya, H., Yahagi, Y., and Yoshida, M.W., Improvement of arrhythmias distinction accuracy using suitable combination of features of the Electrocardiograms, *Numerical harmonic analysis and signal processing*, the JSST International Conference on Simulation Technology, pp.40-43, 2022.

[28] Rahman, M.M., Albeverio, S., Kagawa, T., Kawasaki, S., Okai, T., Oya, H., Yahagi, Y., and Yoshida, M.W., High accuracy distinction of shockable and non-shockable arrhythmias in abnormal classes through wavelet transform with pseudo differential like operators, *Scientific Reports Journal, Springer Nature*, Passed revision, January 03 2023.

[29] Okai, T., Hirata, S., Oya, H., Hoshi, Y., Nakano, K., Yamaguchi, Y., Igarashi, T., and Miyauchi, H., Detailed Performance Analysis of Recognition Algorithm Based on Spectrum Feature Parameters for Electrocardiogram, *International Conference on Signal Processing and Communication Systems (ICSPCS)*, IEEE, pp. 1-6, 2020.

[30] How the heart works, *https://www.nhlbi.nih.gov/health/heart*

[31] What is an arrhythmia, *https://www.nhlbi.nih.gov/health/arrhythmias*

[32] Carrara, M., Carozzi, L., Moss, T.J., Pasquale, M., Cerutti, S., Ferrario, M., Lake, D.E., and Moorman, J.R., Heart rate dynamics distinguish among atrial

fibrillation, normal sinus rhythm and sinus rhythm with frequent ectopy *Physiological measurement*, 2015.

[33] Myerburg. R.J., Halperin, H., Egan, D.A., Boineau, R., Chugh, S.S., Gillis, A.M., Goldhaber, J.I., Lathrop, D.A., Liu, P., Niemann, J.T., and Ornato, J.P., Pulseless electric activity: definition, causes, mechanisms, management, and research priorities for the next decade: report from a National Heart, Lung, and Blood Institute workshop, *Circulation*, pp. 2532-2541, 2013.

[34] Harris, P., and Lysitsas, D., Ventricular arrhythmias and sudden cardiac death, *BJA Education*, pp. 221-229, 2016.

[35] Physio-bank.org database, *https://archive.physionet.org/cgi-bin/atm/ATM*

[36] MIT-BIH arrhythmia database (MITDB), *https://physionet.org/content/mitdb/*

[37] MIT-BIH malignant ventricular ectopy database (VFDB), *https://physionet.org/content/vfdb/*

[38] Creighton university ventricular tachyarrhythmia database (CUDB), *https://physionet.org/content/cudb/*

[39] Canan, S., Ozbay, Y., and Karlik, B., A method for removing low varying frequency trend from ECG signal, *IEEE Proceedings of the international conference biomedical engineering*, pp. 144-146, 1998.

[40] Dinakarrao, S.M., Jantsch, A., and Shafique, M., Computer-aided arrhythmia diagnosis with bio-signal processing: A survey of trends and techniques, *ACM Computing Surveys (CSUR)*, vol. 52, no. 2, pp. 1-37, 2019.

[41] Berkaya, S.K., Uysal, A.K., Gunal, E.S., Ergin, S., Gunal, S., and Gulmezoglu, M.B., A survey on ECG analysis, *Biomedical Signal Processing and Control*, vol. 43, no. 1, pp. 216-235, 2018.

[42] Camm, J., Task Force of the European Society of Cardiology and the North American Society of Pacing and Electrophysiology. Heart Rate Variability: Standarts of measurement, physiological interpretation and clinical use, *Circulation*, 93, pp. 1043-1065, 1996.

[43] Chakroborty, S., and Patil, M.A., Real-time arrhythmia classification for large databases, *The Annual International Conference of the IEEE Engineering in Medicine and Biology Society*, IEEE, pp. 1448-1451, 2014.

[44] Murugappan, M., Murukesan, L., Omar, I., Khatun, S., and Murugappan, S., Time domain features based sudden cardiac arrest prediction using machine learning algorithms, *Journal of Medical Imaging and Health Informatics*, vol. 5, no. 6 pp. 1267-1271, 2015.

[45] Arafat, M.A., Chowdhury, A.W., and Hasan, M., A simple time domain algorithm for the detection of ventricular fibrillation in electrocardiogram, *Signal, Image and Video Processing*, vol. 5, no. 1, pp. 1-10, 2011.

[46] Zhou, S., Zhang, Z., and Gu, J., Time-domain ECG signal analysis based on smart-phone, *Annual International Conference of the IEEE Engineering in Medicine and Biology Society*, IEEE, pp. 2582-2585, 2011.

[47] Mazomenos, E.B., Chen, T., Acharyya, A., Bhattacharya, A., Rosengarten, J., and Maharatna, K., A time-domain morphology and gradient based algorithm for ECG feature extraction, *IEEE International conference on industrial technology*, IEEE, pp. 117-122, 2012.

[48] Seong, K.W., Na, S.D., Park, Y.S., Park, H.J., Kim, M.N., Cho, J.H., and Lee, J.H., Implementation of automatic external defibrillator using real time ventricular fibrillation detecting algorithm based on time domain analysis, *Computer Assisted Surgery*, pp. 86-92, 2017.

[49] Park, J., Lee, S., and Kang, K., Arrhythmia detection using amplitude difference features based on random forest, *Annual International Conference of the IEEE Engineering in Medicine and Biology Society (EMBC)*, pp. 5191-5194, 2015.

[50] Tian, L., and Tompkins, W.J., Time domain based algorithm for detection of ventricular fibrillation. Proceedings of the 19th Annual International Conference of the IEEE Engineering in Medicine and Biology Society, *Magnificent Milestones and Emerging Opportunities in Medical Engineering*, vol. 1, pp. 374-377, 1997.

[51] Tsipouras, M.G., and Fotiadis, D.I., Automatic arrhythmia detection based on time and time–frequency analysis of heart rate variability, *Computer methods and programs in biomedicine*, pp. 95-108, 2004.

[52] Thakor, N.V., and Pan, K., Tachycardia and fibrillation detection by automatic implantable cardioverter-defibrillators: sequential testing in time domain, *IEEE Engineering in Medicine and Biology Magazine*, pp. 21-24, 1990.

[53] Schuckers, S.C., Xu, X., Schuckers, M.E., and Jenkins, J.M., Ventricular arrhythmia detection using time-domain template algorithms, *In Proceedings of the IEEE 24th Annual Northeast Bioengineering Conference*, pp. 21-23, 1998.

[54] Zhang, X.S., Zhu, Y.S., Thakor, N.V., and Wang, Z.Z., Detecting ventricular tachycardia and fibrillation by complexity measure, *IEEE Transactions on biomedical engineering*, vol. 46, no. 5, pp. 548-555, 1999.

[55] Anuradha, B., Kumar, K.S., and Reddy, V.V., Classification of cardiac signals using time domain methods, *ARPN journal of engineering and applied sciences*, no. 3, pp. 7-12, 2008.

[56] Sivanantham, A., and Devi, S.S., Cardiac arrhythmia detection using linear and non-linear features of HRV signal, *IEEE International Conference on Advanced Communications, Control and Computing Technologies*, IEEE, pp. 795-799, 2014.

[57] Monte, G.E., Scarone, N.C., Liscovsky, P.O., and Rotter, P., A novel time-domain signal processing algorithm for real time ventricular fibrillation detection, *Journal of Physics*, vol. 332, no. 1, pp. 012015, 2011.

[58] Dicarlo, L.A., Throne, R.D., and Jenkins, J.M., A time-domain analysis of intracardiac electrograms for arrhythmia detection, *Pacing and Clinical Electrophysiology*, no. 2, pp. 329-336, 1991.

[59] Lee, S.H., and Lim, J.S., Detection of ventricular fibrillation based on time domain analysis, *International Conference on Information Science and Applications*, IEEE, pp. 1-3, 2013.

[60] Roberts, F.M., Povinelli, R.J., and Ropella, K.M., Identification of ECG arrhythmias using phase space reconstruction, *European Conference on Principles of Data Mining and Knowledge Discovery*, pp. 411-423, Springer, Berlin, Heidelberg, 2001.

[61] Amann, A., Tratnig, R., and Unterkofler, K., Detecting ventricular fibrillation by time-delay methods, *IEEE Transactions on Biomedical Engineering*, pp. 174-177, 2006.

[62] Anas, E.M., Lee, S.Y., and Hasan, M.K., Sequential algorithm for life threatening cardiac pathologies detection based on mean signal strength and EMD functions, *Biomedical engineering online*, no. 1, pp. 1-22, 2010.

[63] Othman, M.A., Safri, N.M., Ghani, I.A., and Harun, F.K., Characterization of ventricular tachycardia and fibrillation using semantic mining, *Computer and Information Science*, pp. 35, 2012.

[64] Povinelli, R.J., Roberts, F.M., Johnson, M.T., and Ropella, K.M., Are nonlinear ventricular arrhythmia characteristics lost, as signal duration decreases?, *Computers in Cardiology*, IEEE, pp. 221-224, 2002.

[65] Romero, I., and Serrano, L., ECG frequency domain features extraction: A new characteristic for arrhythmias classification, *Proceedings of the 23rd Annual International Conference of the IEEE Engineering in Medicine and Biology Society*, vol. 2, pp. 2006-2008, 2001.

[66] Temelkov, G., and Gusev, M., A Method to Detect Ventricular Fibrillation in Electrocardiograms, *44th International Convention on Information, Communication and Electronic Technology*, IEEE, pp. 334-339, 2021.

[67] Jekova, I., and Krasteva, V., Real time detection of ventricular fibrillation and tachycardia, *Physiological measurement*, p. 1167, 2004.

[68] Lin CH., Frequency-domain features for ECG beat discrimination using grey relational analysis based classifier, *Computers and Mathematics with Applications*, pp. 680-690, 2008.

[69] Lin, C.H., Du, Y.C., Chen, Y.F., and Chen, T.S., Multiple ECG beats recognition in the frequency domain using grey relational analysis, *International Conference of the IEEE Engineering in Medicine and Biology Society*, IEEE, pp. 2154-2158, 2006.

[70] Minami, K.I., Nakajima, H., and Toyoshima, T., Real-time discrimination of ventricular tachyarrhythmia with Fourier-transform neural network, *IEEE transactions on Biomedical Engineering*, pp. 179-185, 1999.

[71] Chen, K.C., and Chien, P.C., A fast ECG diagnosis using frequency-based compressive neural network, *IEEE 6th Global Conference on Consumer Electronics*, IEEE, pp. 1-2, 2017.

[72] Gothwal, H., Kedawat, S., and Kumar, R., Cardiac arrhythmias detection in an ECG beat signal using fast fourier transform and artificial neural network, *Journal of Biomedical Science and Engineering*, pp. 289-296, 2011.

[73] Nolle, F.M., Bowser, R.W., Badura, F.K., Catlett, J.M., Guadapati, R.R., Hee, T.T., Mooss, A.N., and Sketch, M.H., Evaluation of a frequency-domain algorithm to detect ventricular fibrillation in the surface electrocardiogram, *Computers in Cardiology*, IEEE, pp. 337-340, 1988.

[74] Ming, Y., Taihu, W., Pengcheng, Y., Meng, L., Guang, Z., and Feng, C., Detection of Shockable Rhythm during Chest Compression based on Machine Learning, *IEEE 8th Joint International Information Technology and Artificial Intelligence Conference*, pp. 365-370, 2019.

[75] Aramendi, E., Gauna, S.R., Irusta, U., Ruiz, J., Arcocha, M.F., and Ormaetxe, J.M., Detection of ventricular fibrillation in the presence of cardiopulmonary resuscitation artefacts, *Resuscitation*, pp. 115-123, 2007.

[76] Widman, L.E., Mead, C.N., and Pierce, B.L., Frequency domain characterization of artifact and tachyarrhythmias in the surface electrocardiogram, *Proceedings Computers in Cardiology*, pp. 453-456, 1990.

[77] Parsi, A., Loughlin, D., Glavin, M., and Jones, E., Heart rate variability analysis to predict onset of ventricular tachyarrhythmias in implantable cardioverter defibrillators, *41st Annual International Conference of the IEEE Engineering in Medicine and Biology Society*, pp. 6770-6775. 2019.

[78] Aubert, A.E., Goldreyer, B.N., Wyman, M.G, Kurth, P.A, Ector, H., and Geest, H., Power spectrum analysis of endocardial electrograms during automatic defibrillator implantation, *In Computers in Cardiology*, IEEE, pp. 61-64, 1994.

[79] Clayton, R.H., Murray, A., and Campbell, R.W., Changes in the surface ECG frequency spectrum during the onset of ventricular fibrillation, *In Proceedings Computers in Cardiology*, IEEE, pp. 515-518, 1990.

[80] Mironovova, M., and Bíla, J., Fast fourier transform for feature extraction and neural network for classification of electrocardiogram signals, *The Fourth International Conference on Future Generation Communication Technology*, IEEE, pp. 1-6, 2015.

[81] Huikuri, H.V., Valkama, J.O., Airaksinen, K.E., Seppänen, T., Kessler, K.M., Takkunen, J.T., and Myerburg, R.J., Frequency domain measures of heart rate variability before the onset of nonsustained and sustained ventricular tachycardia in patients with coronary artery disease, *Circulation*, pp. 1220-1228, 1993.

[82] Ropella, K.M., Baerman, J.M., Sahakian, A.V., and Swiryn, S., Differentiation of ventricular tachyarrhythmias, *Circulation*, pp. 2035-2043, 1990.

[83] Minami, K., Ohkuma, Y., Nakajima, H., and Toyoshima, T., Real-time ventricular arrhythmia detection with Fourier analysis and neural network, *In Computers in Cardiology*, IEEE, pp. 545-548, 1996.

[84] Hadhoud, M.M., Eladawy, M.I., and Farag, A., Computer aided diagnosis of cardiac arrhythmias, *International Conference on Computer Engineering and Systems*, IEEE, pp. 262-265, 2006.

[85] Owis, M.I., Youssef, A., and Kadah, Y.M., Characterisation of electrocardiogram signals based on blind source separation, *Medical and Biological Engineering and Computing*, pp. 557-564, 2002.

[86] Afonso, V.X., and Tompkins, W.J., Detecting ventricular fibrillation, *IEEE Engineering in Medicine and Biology Magazine*, pp. 152-159, 1995.

[87] Jones, D.L., and Parks, T.W., A resolution comparison of several time-frequency representations, *In International Conference on Acoustics, Speech, and Signal Processing*, IEEE, pp. 2222-2225, 1989

[88] Rankine, L., Stevenson, N., Mesbah, M., and Boashash, B., A quantitative comparison of non-parametric time-frequency representations, *European Signal Processing Conference*, IEEE, pp. 1-4, 2005.

[89] Bialasiewicz, J.T., Application of wavelet scalogram and coscalogram for analysis of biomedical signals, *In Proceedings of the World Congress on Electrical Engineering and Computer Systems and Science*, vol. 333, 2015.

[90] Andreev, D.A., Bozhokin, S.V., Venevtsev, I.D., and Zhunusov, K.T., Gabor transform and continuous wavelet transform for model pulsed signals, *Technical Physics*, pp. 1428-1433, 2014.

[91] Mena-Chalco, J., Carrer, H., Zana, Y., and Cesar, R.M., Identification of protein coding regions using the modified Gabor-wavelet transform, *IEEE Transactions on Computational Biology and Bioinformatics*, pp. 198-207, 2008.

[92] Hidetoshi, O., Kosuke, T., Katsuhiro, H., Kazushi, N., Yoshihiro, Y., and Hiroshi M., A wavelet transform-based detection algorithm for electrocardiogram, *IEEE International Conference on Signal Processing, Communication and Computing*, pp. 768-773, 2012.

[93] Balasundaram, K., Masse, S., Nair, K., Farid, T., Nanthakumar, K., and Umapathy, K., Wavelet-based features for characterizing ventricular arrhythmias in optimizing treatment options, *Annual International Conference of the IEEE Engineering in Medicine and Biology Society*, pp. 969-972, 2011.

[94] Meng, O., Xia, D.E., Zhang, Q.I., and Zhang, Z.A., Detection ventricular tachycardia and fibrillation using the lempel-ziv complexity and wavelet transform, *WSEAS Transactions on information science and applications*, pp. 118-125, 2016.

[95] Zhou, X., and Lim, J.S., Improved Ventricular Fibrillation/Tachycardia Detection using NEWFM for Automated External Defibrillators, *International Journal of Bio-Science and Bio-Technology*, pp. 33-42, 2015.

[96] Al-Abdi, R.M., and Jarrah, M., Cardiac disease classification using total variation denoising and morlet continuous wavelet transformation of ECG signals, *IEEE International Colloquium on Signal Processing and Its Applications (CSPA)*, pp. 57-60, 2018.

[97] Onishi, Y., Oya, H., Nishida, Y., Ogino, Y., Nakano, K., Yamaguchi, Y., Miyauchi, H., and Okai, T., An wavelet transform-based discrimination algorithm for electrocardiogram, *In Signal and Information Processing Association Annual Summit and Conference (APSIPA)*, pp. 1-7, 2014.

[98] Kheder, G., Kachouri, A., and Samet, M., HRV analysis using wavelet package transform and least square support vector machine, *International Journal of Circuits, System, Signal Process*, 2008.

[99] Sinha, A., Singh, G., and Kashyap, M., Feature Extraction for Detection of Ventricular Tachycardia and Ventricular Fibrillation using WAVELET Decomposition, *International Journal of Computer Applications*, 2015.

[100] Daqrouq, K., and Abu-Isbeih, IN., Arrhythmia detection using wavelet transform, *The International Conference on Computer as a Tool*, IEEE, pp. 122-126, 2007.

[101] Balasundaram, K., Masse, S., Nair, K., and Umapathy, K., Automated signal pattern detection in ECG during human ventricular arrhythmias, *Annual International Conference of the IEEE Engineering in Medicine and Biology Society*, IEEE, pp. 1029-1032, 2013.

[102] Sun, Y., Chan, K.L., and Krishnan, S.M., Life-threatening ventricular arrhythmia recognition by nonlinear descriptor, *BioMedical Engineering OnLine*, 2005.

[103] Balasundaram, K., Masse, S., Nair, K., and Umapathy, K., A classification scheme for ventricular arrhythmias using wavelets analysis, *Medical and biological engineering and computing*, vol. 51, issue. 1, pp. 153-164, 2013.

[104] Namarvar, H.H., Shahidi, A.V., Cardiac arrhythmias predictive detection methods with wavelet-svd analysis and support vector machines, *The 26th Annual International Conference of the IEEE Engineering in Medicine and Biology Society*, IEEE, vol. 1, pp. 365-368, 2004.

[105] Lai, D., Fan, X., Zhang, Y., and Chen, W., Intelligent and efficient detection of life-threatening ventricular arrhythmias in short segments of surface ECG signals, *IEEE Sensors Journal*, pp. 14110-14120, 2020.

[106] Shilla, W., and Wang, X., Wavelet Transform and Convolutional Neural Network Based Techniques in Combating Sudden Cardiac Death, *EMITTER International Journal of Engineering Technology*, pp. 377-389, 2021.

[107] Jang, S.W., and Lee, S.H., Detection of ventricular fibrillation using wavelet transform and phase space reconstruction from ECG signal, *Journal of Mechanics in Medicine and Biology*, pp. 2140036, 2021.

[108] Khadra, L., Al-Fahoum, A.S., and Al-Nashash, H., Detection of life-threatening cardiac arrhythmias using the wavelet transformation, *Medical and Biological Engineering and Computing*, pp. 626-632, 1997.

[109] Sumathi, S., Beaulah, H.L., and Vanithamani, R., A wavelet transform based feature extraction and classification of cardiac disorder, *Journal of medical systems*, vol. 38, pp. 1-11, 2014.

[110] Mjahad, A., Rosado-Muñoz, A., Guerrero-Martínez, J.F., Bataller-Mompeán, M., Francés-Villora, J.V., and Dutta, M.K., Detection of ventricular fibrillation using the image from time-frequency representation and combined classifiers without feature extraction, *Applied Sciences*, pp. 2057, 2018.

[111] Werther, T., Klotz, A., Kracher, G., Baubin, M., Feichtinger, H.G., Gilly, H., and Amann, A., CPR artifact removal in ventricular fibrillation ECG signals using Gabor multipliers, *IEEE Transactions on Biomedical Engineering*, pp. 320-327, 2008.

[112] Zhang, Z.X., Tian, X.W., and Lim, J.S., Real-time algorithm for a mobile cardiac monitoring system to detect life-threatening arrhythmias, *International Conference on Computer and Automation Engineering*, IEEE, vol. 4, pp. 232-236, 2010.

[113] Karthika, J.S., Thomas, J.M., and Kizhakkethottam, J.J., Detection of life-threatening arrhythmias using temporal, spectral and wavelet features, *IEEE International Conference on Computational Intelligence and Computing Research*, IEEE, pp. 1-4, 2015.

[114] Jung, Y., and Tompkins, W.J., Detecting and classifying life-threatening ECG ventricular arrythmias using wavelet decomposition, *Proceedings of the 25th Annual International Conference of the IEEE Engineering in Medicine and Biology Society*, IEEE, vol. 3, pp. 2390-2393, 2003.

[115] Hoher, M., Kestler, H.A., Bauer, S., Weismuller, P., Palm, G., and Hombach, V., Neural network based analysis of the signal-averaged electrocardiogram, *In Computers in Cardiology*, IEEE, pp. 257-260, 1995.

[116] Nambiar, V.P., Khalil-Hani, M., and Marsono, M.N., Evolvable Block-based Neural Networks for real-time classification of heart arrhythmia From ECG signals, *IEEE-EMBS Conference on Biomedical Engineering and Sciences*, pp. 866-871, 2012.

[117] Kohli, N., Verma, N.K., and Roy A., SVM based methods for arrhythmia classification in ECG, *IEEE international conference on computer and communication technology*, pp. 486-490, 2010.

[118] Mustaqeem, A., Anwar, S.M., and Majid, M., Multiclass classification of cardiac arrhythmia using improved feature selection and SVM invariants, *Computational and mathematical methods in medicine*, 2018.

[119] Bruser, C., Diesel, J., Zink, M.D., Winter, S., Schauerte, P., and Leonhardt, S., Automatic detection of atrial fibrillation in cardiac vibration signals, *IEEE journal of biomedical and health informatics*, pp. 162-171, 2012.

[120] Kutlu, Y., and Kuntalp, D., A multi-stage automatic arrhythmia recognition and classification system, *Computers in biology and medicine*, pp.37-45, 2011.

[121] Huang, Y.P., and Chen, S.R., A fuzzy approach to discriminating heartbeat types and detecting arrhythmia, *IEEE international conference on Fuzzy Theory and Its Applications*, pp. 327-332, 2012.

[122] Acharya, U.R., Fujita, H., Oh, S.L., Hagiwara, Y., Tan, J.H., and Adam, M., Application of deep convolutional neural network for automated detection of myocardial infarction using ECG signals, *Information Sciences*. pp. 190-198, 2017.

[123] Joo, S., Choi, K.J., and Huh, S.J., Prediction of ventricular tachycardia by a neural network using parameters of heart rate variability, *Computing in Cardiology*, IEEE, pp. 585-588, 2010.

[124] Rai, H.M., Trivedi, A., Shukla, S., and Dubey, V., ECG arrhythmia classification using daubechies wavelet and radial basis function neural network, *Nirma University International Conference on Engineering*, IEEE, pp. 1-6, 2012.

[125] Ghongade, R., Deshmukh, M., and Joshi, D., Arrhythmia classification using morphological features and probabilistic neural networks, *Innovative Applications of Computational Intelligence on Power, Energy and Controls with their impact on Humanity*, IEEE, pp. 80-84, 2014

[126] Suotsalo, K., and Särkkä, S., Detecting malignant ventricular arrhythmias in electrocardiograms by Gaussian process classification, *IEEE International Workshop on Machine Learning for Signal Processing*, IEEE, pp. 1-5, 2017.

[127] Alonso-Atienza, F., Morgado, E., Fernandez-Martinez, L., García-Alberola, A., and Rojo-Alvarez, J.L., Detection of life-threatening arrhythmias using feature selection and support vector machines, *IEEE Transactions on Biomedical Engineering*, pp. 832-840, 2013.

[128] Jayagopi, G., and Pushpa, S., On the classification of arrhythmia using supplementary features from tetrolet transforms, *International Journal of Electrical and Computer Engineering*, val. 9, no. 6, 2019.

[129] Bayasi, N., Tekeste, T., Saleh, H., Mohammad, B., Khandoker, A., and Ismail, M., Low-power ECG-based processor for predicting ventricular arrhythmia, *IEEE Transactions on Very Large Scale Integration (VLSI) Systems*, IEEE, pp. 1962-1974, 2015.

[130] Lashgari, E., Jahed, M., and Khalaj, B., Manifold learning for ECG arrhythmia recognition, *The 20th Iranian Conference on Biomedical Engineering*, IEEE, pp. 126-131, 2013.

[131] Ahmed, A.F., Owis, M.I., and Yassine, I.A., Novel Bayesian classifier discriminant function optimization strategies for arrhythmia classification, *In IEEE-EMBS International Conference on Biomedical and Health Informatics*, IEEE, pp. 693-696, 2014.

[132] Abbas, R., Aziz, W., and Arif, M., Prediction of ventricular tachyarrhythmia in electrocardiograph signals using neural network and modified nearest neighbour method, *In Student Conference On Engineering, Sciences and Technology*, IEEE, pp. 1-6, 2004.

[133] Zuo, W.M., Lu, W.G., Wang, K.Q, and Zhang, H., Diagnosis of cardiac arrhythmia using kernel difference weighted KNN classifier, *Computers in Cardiology*, IEEE, pp. 253-256, 2008.

[134] Rad, A.B., Eftestøl, T., Kvaløy, J.T., Ayala, U., Kramer-Johansen, J., and Engan, K., Nearest-manifold classification approach for cardiac arrest rhythm interpretation during resuscitation, *IEEE International Conference on Acoustics, Speech and Signal Processing*, IEEE, pp. 3621-3625, 2014.

[135] Picon, A., Irusta, U., Álvarez-Gila, A., Aramendi, E., Alonso-Atienza, F., Figuera, C., Ayala, U., Garrote, E., Wik, L., Kramer-Johansen, J., and Eftestøl, T., Mixed convolutional and long short-term memory network for the detection of lethal ventricular arrhythmia, *PloS one*, no. 5, p.e0216756, 2019.

[136] Jaureguibeitia, X., Zubia, G., Irusta, U., Aramendi, E., Chicote, B., Alonso, D., Larrea, A., and Corcuera, C., Shock decision algorithms for automated external defibrillators based on convolutional networks, *IEEE Access*, pp. 154746-154758, 2020.

[137] Kiranyaz, S., Ince, T., and Gabbouj, M., Real-time patient-specific ECG classification by 1-D convolutional neural networks, *IEEE Transactions on Biomedical Engineering*, IEEE, pp. 664-675, 2015.

[138] Acharya, U.R., Oh, S.L., Hagiwara, Y., Tan, J.H., Adam, M., Gertych, A., and San-Tan, R., A deep convolutional neural network model to classify heartbeats, *Computers in biology and medicine*, pp. 389-396, 2017.

[139] Sugiura, T., Hirata, H., Harada, Y., and Kazui, T., Automatic discrimination of arrhythmia waveforms using fuzzy logic, *In Proceedings of the 20th Annual International Conference of the IEEE Engineering in Medicine and Biology Society*, vol. 20, pp. 108-111, 1998.

[140] Lim, J.S., Finding features for real-time premature ventricular contraction detection using a fuzzy neural network system, *IEEE Transactions on Neural Networks*, IEEE, pp. 522-527, 2009.

[141] Lee, S.Y., Ahn, D.Y., Song, M.H., and Lee, K.J., The classification of electrocardiograph arrhythmia patterns using fuzzy support vector machines, *International Journal of Fuzzy Logic and Intelligent Systems*, pp. 204-210, 2011.

[142] Alliche, A., and Mokrani, K., Higher order statistics and ECG arrhythmia classification, *In Proceedings of the 3rd IEEE International Symposium on Signal Processing and Information Technology*, IEEE, pp. 641-643, 2003.

[143] Ruiz, J., Aramendi, E., De-Gauna, S.R., Lazkano, A., Leturiondo, L.A., and Gutierrez, J.J., Distinction of ventricular fibrillation and ventricular tachycardia using cross correlation, *In Computers in Cardiology*, IEEE, pp. 729-732, 2003.

[144] Ramakrishnan, S., Akshaya, V., Kishor, S., and Thyagarajan, T., Real time implementation of arrhythmia classification algorithm using statistical methods, *The Trends in Industrial Measurement and Automation*, IEEE, pp. 1-4, 2017.

[145] Sharma, M., Singh, S., Kumar, A., San-Tan, R., and Acharya, U.R., Automated detection of shockable and non-shockable arrhythmia using novel wavelet-based ECG features, *Computers in biology and medicine*, 115, pp. 103446, 2019.

[146] Cartas-Rosado, R., Becerra-Luna, B., Martínez-Memije, R., Infante-Vazquez, O., Lerma, C., Pérez-Grovas, H., and Rodríguez-Chagolla, J.M., Continuous wavelet transform based processing for estimating the power spectrum content of heart rate variability during hemodiafiltration, *Biomedical Signal Processing and Control*, pp. 102031, 2020.

[147] Mizohata S., The theory of partial differential equations, *CUP Archive*, 1973.

[148] Kumano-Go H., Pseudo-differential operators, *the MIT Press*, Cambridge, 1982.

[149] Yousefi, M.R., Khezri, M., Bagheri, R. and Jafari, R., Automatic detection of premature ventricular contraction based on photoplethysmography using chaotic features and high order statistics, *IEEE International Symposium on Medical Measurements and Applications*, pp. 1-5, 2018.

[150] Maria-Navin, J.R., and Pankaja, R., Performance analysis of text classification algorithms using confusion matrix, *International Journal of Engineering and Technical Research (IJETR)*, pp. 75-78, 2016.

[151] Grandini, M., Bagli, E., and Visani, G., Metrics for multi-class classification: an overview. *arXiv preprint*, 2020.

[152] Tharwat A., Classification assessment methods, *Applied Computing and Informatics*, Emerald Publishing Limited, 2020.

[153] Stone M., Cross-validation: A review. Statistics, *A Journal of Theoretical and Applied Statistics*, pp. 127-139, 1978.

[154] Raschka S., Model evaluation, model selection, and algorithm selection in machine learning, *arXiv preprint*, 1811.12808, 2018.

[155] Anguita, D., Ghelardoni, L., Ghio, A., Oneto, L., and Ridella, S., The 'K'in K-fold cross validation, *In20th European Symposium on Artificial Neural Networks, Computational Intelligence and Machine Learning (ESANN)*, pp. 441-446, 2012.

[156] Theodoridis, S., and Koutroumbas, K., Pattern recognition 4th edition, *Academic press*, New York.

[157] Kelley, J.L., General topology, *Dover Publications*, New York, 2017.

[158] Tripathy, R.K., Sharma, L.N., and Dandapat, S., Detection of shockable ventricular arrhythmia using variational mode decomposition, *Journal of medical systems*, 40, 2016.

[159] Cheng, P., and Dong, X., Life-threatening ventricular arrhythmia detection with personalized features, *IEEE access*, pp. 14195-14203, 2017.

[160] Acharya, U.R., Fujita, H., Oh, S.L., Raghavendra, U., Tan, J.H., Adam, M., Gertych, A., and Hagiwara, Y., Automated identification of shockable and non-shockable life-threatening ventricular arrhythmias using convolutional neural network, *Future Generation Computer Systems*, pp. 952-959, 2018.

[161] Tripathy, R.K., Zamora-Mendez, A., Serna, J.A., Paternina, M.R., Arrieta, J.G., and Naik, G.R., Detection of life threatening ventricular arrhythmia using digital Taylor Fourier transform, *Frontiers in physiology*, pp. 722, 2018.

[162] Resiandi, K., Adiwijaya, and Utama, D.Q., Detection of atrial fibrillation disease based on electrocardiogram signal classification using RR interval and K-nearest neighbor, *IEEE International Conference on Information and Communication Technology*, pp. 501-506, 2018.

[163] Xie, Z., Yang, Q., Yang, Y., Li, W., and Yang Z., A Decision-making Method for Defibrillation Based on SVM and Opt-AMSA, *The Chinese Control Conference (CCC)*, IEEE, pp. 3497-3501, 2019.

[164] Li, Z., Derksen, H., Gryak, J., Hooshmand, M., Wood, A., Ghanbari, H., Gunaratne, P., and Najarian, K., Markov models for detection of ventricular arrhythmia, *The 41st Annual International Conference of the IEEE Engineering in Medicine and Biology Society (EMBC)*, pp. 1488-1491, 2019.

[165] Sharma, M., Tan, R.S., and Acharya, U.R., Detection of shockable ventricular arrhythmia using optimal orthogonal wavelet filters, *Neural Computing and Applications*, pp. 15869-15884, 2020.

[166] Hajeb-Mohammadalipour, S., Cascella, A., Valentine, M., and Chon, K.H., Automated Condition-Based Suppression of the CPR Artifact in ECG Data to Make a Reliable Shock Decision for AEDs during CPR, *Sensors*, pp. 8210, 2021.

[167] Hammad, M., Rajesh, K.N., Abdelatey, A., Abdar, M., Zomorodi-Moghadam, M., San-Tan, R., Acharya, U.R., Pławiak, J., Tadeusiewicz, R., Makarenkov, V., and Sarrafzadegan, N., Automated detection of Shockable ECG signals: A Review, *Information Sciences*, 2021.

[168] Toulni, Y., Belhoussine Drissi, T. and Nsiri, B., ECG signal diagnosis using Discrete Wavelet Transform and K-Nearest Neighbor classifier, *International Conference on Networking, Information Systems and Security*,pp. 1-6, 2021.

A

Appendix

A.1 Comparison of NTI with the Fourier transform frequency spectrum

This section compares the NTI generated from the scalogram and the Fourier transform frequency spectrum. Note that the scalogram is generated using the proposed Gabor wavelet transform with pseudo-differential-like operators and a non-linear transformation function. It is known that the wavelet transform method does not return the frequency directly from the signal, whereas the Fourier transform does. The NTI and Fourier transform frequency spectrum for normal SR and abnormal PEA signals are in Figures A.1, A.2, A.3, and A.4. It is observed from Figure A.1 that we get the NTI ripples up to 200 scales (Equivalent frequency is 60 (Hz)) of the scalogram for the normal SR signal that is equivalent to the Fourier transform frequency spectrum shown in Figure A.2. Similarly from Figure A.3, we get the NTI ripples up to 60 scales (Equivalent frequency is 18 (Hz)) of the scalogram for the abnormal PEA signal that is equivalent to the Fourier transform frequency spectrum shown in Figure A.4.

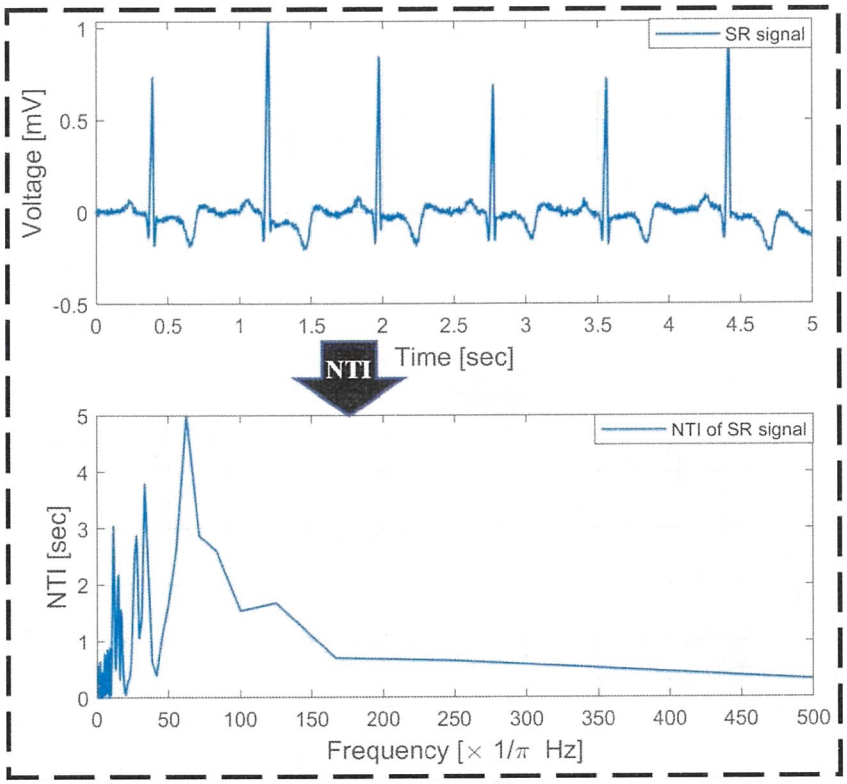

Figure A.1: NTI for scalogram of SR signal

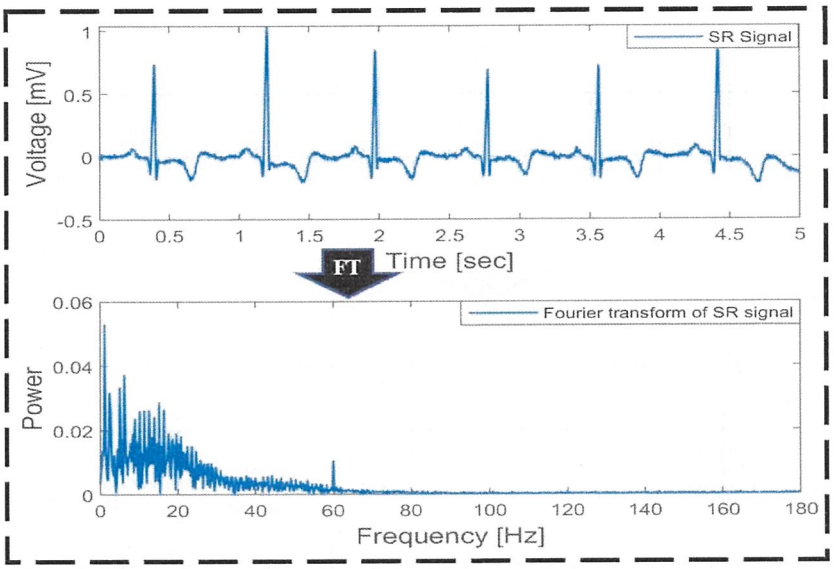

Figure A.2: Fourier spectrum of SR signal

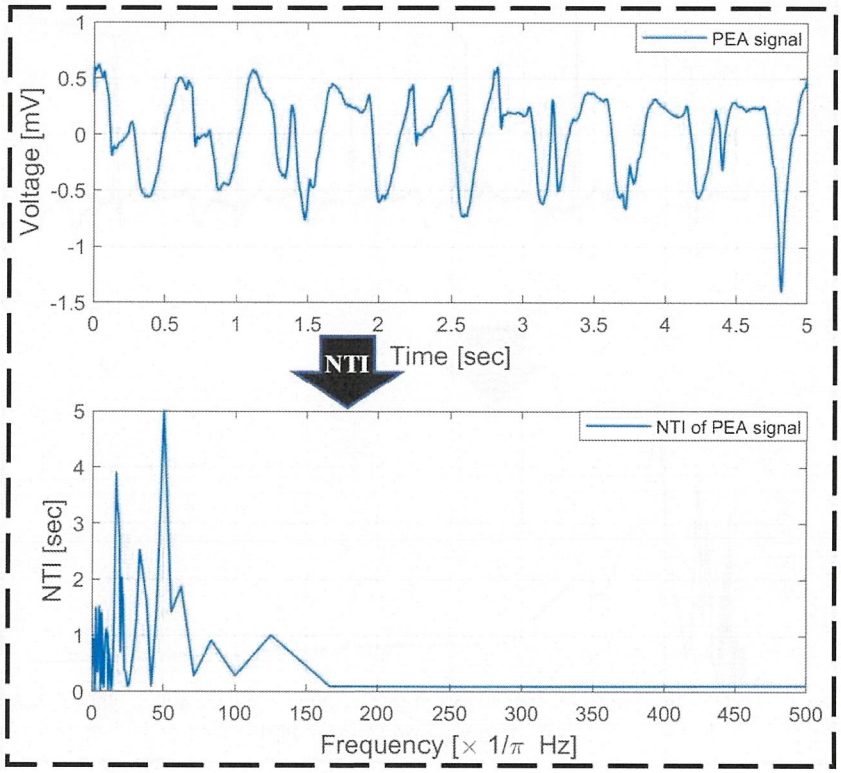

Figure A.3: NTI for scalogram of PEA signal

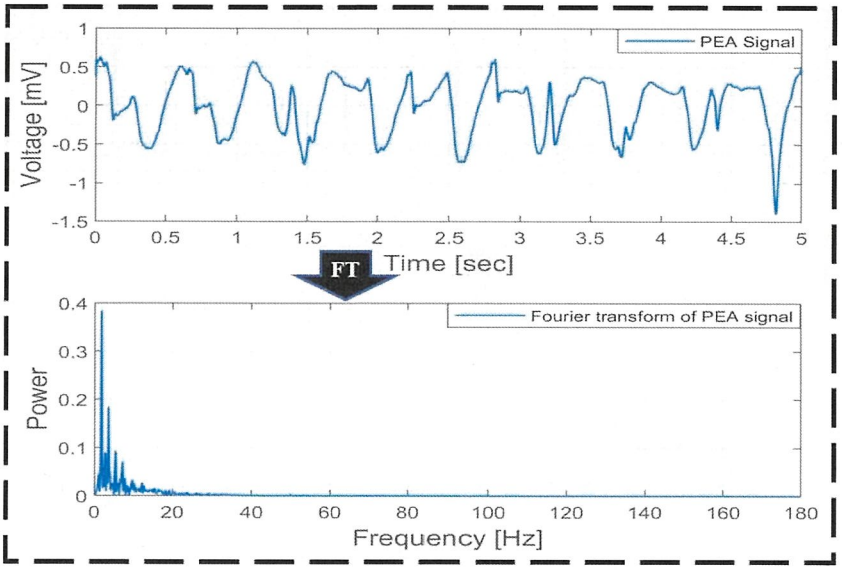

Figure A.4: Fourier spectrum of PEA signal

A.2 Dataset preparation, and implementation of the proposed arrhythmia diagnosis system

PhysioBank database contains over 90,000 recordings, over 4 terabytes of digitized physiologic signals and time series, organized in over 80 databases. This section explains how to download digitized ECG data from the Pysiobank database and prepare dataset with five second signal segments through a programming environment using MATLAB. In order to download digitized time series data from the database, we install the WFDB Toolbox into the MATLAB. Here, we use the commands 'rdsamp' and 'rdann' to download the ECG data pro-grammatically. The specific procedure for installing WFDB Toolbox is as follows:

- Start MATLAB.
- Go to the directory where we want to install WFDB Toolbox.
- Type the following command into the MATLAB.

```
[old_path]=which('rdsamp');
if( isempty(old_path)) rmpath(old_path(1:end-8));
end
wfdb_url='https://physionet.org/physiotools/matlab/...
wfdb-app-matlab/wfdb-app-toolbox-0-10-0.zip';
[filestr, status]= urlwrite(wfdb_url,'wfdb-app-toolbox-0-10-0.zip');
unzip('wfdb-app-toolbox-0-10-0.zip');
cd mcode
addpath(pwd)
savepath
```

```
1  ============================================================
2                        Dataset preparation
3  ============================================================
4  function DLMITDB()
5      fileID = fopen('mitdb_record_num_list.txt');
6      num_list_c = textscan(fileID, '%d');
7      num_list = cell2mat(num_list_c);
8      fclose(fileID);
9      [n_size, ~] = size(num_list);
10     for i=1:n_size
11         fprintf('%d / %d\n', i, n_size);
```

```
        num = num_list(i);
        db_url = ['mitdb/' num2str(num)];
        %[ann, an_type] = rdann(db_url, 'atr', [],[],[],
            r_tag);
        [ann, an_type] = rdann(db_url, 'atr');
        dir_path='mitdb';
        if ~exist(dir_path,'dir')
            mkdir(dir_path);
        end
        [signal,Fs,tm]=rdsamp(db_url);
        save(['.\mitdb\' num2str(num) '.mat'], 'signal', '
            Fs', 'tm', 'ann', 'an_type');
    end
end
function Split()
    mit_data = load('.\mitdb\100.mat');
    for i=1:360
        start_idx = 1 + (i-1)*(360*5);
        end_idx =  start_idx + (360*5);
        data = mit_data.signal(start_idx:end_idx, 1);
        time = mit_data.tm(start_idx:end_idx, 1);
        mat = [time, data];
        dlmwrite(['.\data\reclass\mitdb_100_1' num2str(i)
            '.mat' ], mat)
    end
end
============================================================
    Implementation of the arrhythmia diagnosis system
============================================================
function obj = CreateFeaturesMat(obj)
        tic;
    for l=1:4
        switch l
            case 1
                target_name = 'VF';
            case 2
                target_name = 'PEA';
            case 3
                target_name = 'VT';
```

```
48              case 4
49                  target_name = 'SR';
50          end
51          files = dir(['.\data\reclass\' target_name]);
52          [f1_size, ~] = size(files);
53          f1_feature_v = [];
54  %       nsi_str = cell();
55          nsi_str = struct([]);
56          nti_str = struct([]);
57          snr = 1;
58          for i=1:f1_size
59              fprintf('createfeaturematrix %s ... %d / %d\n'
                    , target_name, i, f1_size);
60              fp = [char(files(i).folder) '\' char(files(i).
                    name)];
61              mat_v = load(fp);
62              d = mat_v.data_t;
63              data = [mat_v.time_t , d];
64              wvl = Wavelet(data);
65              wvl = m_gwt(wvl);
66              ft = Features(fp, wvl, target_name);
67              ft = ft.NSI();
68              ft = ft.NTI();
69              ft = ft.NSI_Features_All();
70              ft = ft.NTI_Features_All();
71              nsi_str = [nsi_str; ft.nsi_features_struct];
72              nti_str = [nti_str; ft.nti_features_struct];
73          end
74          file_name = ['features\' target_name '
                _features_all.mat'];
75          save(file_name, 'nsi_str', 'nti_str');
76      end
77      time=toc;
78  end
79  classdef Wavelet
80      properties (SetAccess = public)
81          original_wave
82          scalogram
83          time_sweep
```

```
84          scalo_power_ser
85          scalo_amp_max
86          scalo_amp_width
87          freq
88          target_type = '' % SR,VF,PEA, VT
89          file_name = ''
90      end
91      properties (SetAccess = private)
92          time  % original_wave
93          data  % original_wave
94          fs  %
95          ext_sec = 5
96      end
97      methods
98          function obj = Wavelet(data)
99              obj.original_wave = data;
100             obj.time = obj.original_wave(:,1);
101             obj.time = obj.time - obj.time(1);
102             obj.data = obj.original_wave(:,2);
103             if (obj.time(2) - obj.time(1))==0
104                 obj.fs = 360;
105 %               obj.fs = 250;
106             else
107                 obj.fs = 1/(obj.time(2) - obj.time(1));
108             end
109 %           if (obj.fs * obj.ext_sec) > length(obj.time)
110 %               obj.ext_sec = length(obj.time) / obj.fs;
111 %           end
112         end
113         function value = get.ext_sec(obj)
114             value = obj.ext_sec;
115         end
116         function value = get.fs(obj)
117             value = obj.fs;
118         end
119         obj = m_gwt(obj)
120         obj = m_gwt_nn(obj)
121         obj = wvl_feature(obj)
122         obj = scalo(obj)
```

```
123     end
124 end
125 classdef Features
126     properties (SetAccess = public)
127         file_name
128         wvl
129         category
130         nsi
131         nti
132         nsi_features_struct
133         nti_features_struct
134         signal_features_struct
135         scalogram_features_struct
136         vt_features_struct
137         calc_feature_time
138         scalo_nsi_struct
139         scalo_amp_width
140     end
141     methods
142         function obj = Features(file_name, in_wvl, ctg)
143             obj.file_name = file_name;
144             obj.wvl = in_wvl;
145             obj.category = ctg;
146         end
147         function obj = Calc(obj)
148             tic;
149             obj = obj.NSI();
150             obj = obj.NTI();
151             obj = obj.NSI_Features_All();
152             obj = obj.NTI_Features_All();
153             obj.calc_feature_time = toc;
154             obj = obj.Signal_Features();
155         end
156         function obj = PreCalc(obj)
157             obj = obj.NSI();
158             obj = obj.NTI();
159         end
160         function obj = CalcNSIF(obj)
161             obj = obj.NSI_Features();
```

```
162         end
163          function obj = CalcNTIF(obj)
164              obj = obj.NTI_Features();
165          end
166         obj = NSI_Features_OneLoop(obj, i);
167         obj = NTI_Features_OneLoop(obj, i);
168         obj = ScaloPeakNSI(obj, i);
169         obj = ScaloPeakNTI(obj, i);
170         function obj = Calc_s(obj)
171             tic;
172             obj = obj.NSI();
173             obj = obj.NTI();
174             obj = obj.NSI_Features_s();
175             obj = obj.NTI_Features_s();
176             obj.calc_feature_time = toc;
177             obj = obj.Signal_Features();
178         end
179         function obj = Calc_vt(obj)
180             obj = obj.VF_Features();
181         end
182         obj = NSI(obj)
183         obj = NTI(obj)
184         obj = NSI2(obj)
185         obj = NSI3(obj)
186         obj = TimeSweep(obj);
187         obj = Signal_Features(obj);
188         obj = Signal_Features_All(obj);
189         obj = NSI_Features_All(obj);
190         obj = NTI_Features_All(obj);
191         obj = Scalogram_Features_All(obj);
192         obj = NSI_Features_master(obj);
193         obj = NTI_Features_master(obj);
194         obj = Signal_Features_master(obj);
195         obj = NSI_Features(obj)
196         obj = scalo(obj)
197         slope = H03_slope_func(obj, signal,Fs)
198         [ ER ] = energy_ratio( obj, vector, alpha, beta )
199     end
200     methods(Static)
```

```
201             CreateFeatures()
202         end
203     end
204     function obj = m_gwt(obj)
205         T = length(obj.data);
206         opol = 6;
207         [p,mu] = polyfit(obj.time,obj.data,opol);
208         f_y = polyval(p,obj.time,[],mu);
209         demean_signal_f = obj.data - f_y;
210         sigma = 0.5;
211         omega_0 = 2*pi;
212         N = 200;
213     %   N=500;
214         dt = 1/ obj.fs;
215         ext_points = round(obj.ext_sec * obj.fs) - 1;
216         loop_num = floor(length(demean_signal_f) / ext_points)
                ;
217         %all_range_scalo = zeros(T, length(obj.data));
218         all_range_scalo = zeros(T, ext_points+1, loop_num);
219         f_signal = zeros(ext_points+1, loop_num);
220         for i = 1:loop_num
221             start_idx = (i-1)*ext_points+1;
222             if i>1
223                 start_idx = start_idx - 1;
224             end
225             target = demean_signal_f(start_idx : start_idx +
                    ext_points);
226             f_signal(:,i) = target;
227             len_t = length(target);
228             YY = zeros(len_t, T);
229             for j = 1:N
230                 omega = 0.2*pi*j;
231     %           omega = 0.2*j;
232                 a = omega_0 / omega;
233                 wvl_time = sigma * a;
234                 t = -wvl_time/2 : dt : wvl_time/2;
235                 t = t./a;
236     %           t = t./(4*a);
237     %           t = t./(a/4);
```

```
238 %           t = t./(sqrt(a));
239             gauss = exp((-t.^2)/(2*sigma^2)) / sqrt((2*pi*
                    sigma^2));
240 %           psi = gauss .* (exp(1i * omega_0 * t) - exp
    (-1/2*sigma^2*omega_0^2));
241             psi = gauss .* (exp(1i * omega_0 * t) - exp
                    (-1/2*sigma^2*omega_0^2)).* (1/a);
242 %           psi = gauss .* (exp(1i * omega_0 * t) - exp
    (-1/2*sigma^2*omega_0^2)).* ((1/a).^2);
243 %           psi = gauss .* (exp(1i * omega_0 * t) - exp
    (-1/2*sigma^2*omega_0^2)).* sqrt(1/a);
244 %           psi = gauss .* (exp(1i * omega_0 * t) - exp
    (-1/2*sigma^2*omega_0^2)).* a;
245 %           psi = gauss .* (exp(1i * omega_0 * t) - exp
    (-1/2*sigma^2*omega_0^2)).* (a.^2);
246 %           psi = gauss .* (exp(1i * omega_0 * t) - exp
    (-1/2*sigma^2*omega_0^2)).* 4*a;
247 %           psi = gauss .* (exp(1i * omega_0 * t) - exp
    (-1/2*sigma^2*omega_0^2)).* (sqrt(a));
248 %           psi = gauss .* (exp(1i * omega_0 * t) - exp
    (-1/2*sigma^2*omega_0^2)).* (1/(4*a));
249 %           psi = gauss .* (exp(1i * omega_0 * t) - exp
    (-1/2*sigma^2*omega_0^2)).* (1/(sqrt(a)));
250 %           psi = 1/sqrt(4*a)*psi;
251 %           psi = 1/sqrt(a/4)*psi;
252             psi = 1/sqrt(a)*psi;
253 %           psi = 1/sqrt(sqrt(a))*psi;
254             Y = abs(conv(target, psi)) * dt;
255             f_len = length(psi);
256             rem_v = rem(f_len, 2);
257             f_len = f_len + rem_v;
258             Y(1:f_len/2) = [];
259             Y(len_t+1 : len_t+f_len/2-rem_v-1) = [];
260             YY(:,j) = Y;
261         end
262         %%
263         XX = YY';
264         %MAX = zeros(len_t, 1);
265         sum_time_ser = zeros(len_t, 1);
```

```
266             for j=1:len_t
267                 [mz, idx] = max(XX(:, j));
268                 %MAX(j) = idx*0.1;
269                 sum_time_ser(j) = sum(XX(:, j));
270                 XX(:,j) = XX(:,j) ./ mz;
271             end
272 %           XX = XX.^2;
273 %           XX = XX.^4;
274 %           XX = XX.^(1/2);
275             XX = XX.^(1/4);
276 %           XX = XX.^(1/8);
277 %           all_range_scalo(:, start_idx : start_idx +
    ext_points) = XX;
278             all_range_scalo(:,:,i) = XX;
279             %%
280             if obj.target_type ~= ''
281                 folder_path = ['.\images\scalo_power\' obj.
                    target_type];
282                 if ~exist(folder_path, 'dir')
283                     mkdir(folder_path);
284                 end
285                 path = [folder_path '\' obj.file_name '.png'];
286                 x_ser = 0:1/obj.fs:obj.ext_sec;
287                 x_ser = x_ser';
288                 x_ser = x_ser(1:len_t);
289                 f = figure;
290                 plot(x_ser, sum_time_ser);
291                 xlabel('sec');
292                 ylabel('Scalogram Power');
293                 %ylim([-10, 10]);
294                 grid on;
295                 saveas(f, path);
296                 delete(f);
297 %               saveas(f, path);
298             end
299             obj.scalo_power_ser = sum_time_ser;
300             obj.scalo_amp_max = max(sum_time_ser);
301         end
302         obj.freq = Y;
```

```
303         obj.scalogram = all_range_scalo;
304         %obj.filtered_signal = f_signal;
305     end
306     function obj = NSI(obj)
307         [N, len_t, loop_num] = size(obj.wvl.scalogram);
308         FSMN = zeros(len_t, loop_num);
309         for i=1:loop_num
310             %FSMN = zeros(1,len_t-1);
311             AF = zeros(N,len_t);
312             Af = zeros(N,len_t);
313             AFa = zeros(1,len_t);
314             Afa = zeros(1,len_t);
315             for k = 1:1:len_t
316                 xx = obj.wvl.scalogram(:,k,i);
317                 for f = 1:1:N
318                     AF(f,k) = xx(f)*(f);
319                     Af(f,k) = xx(f);
320                 end
321                 AFa(1,k) = sum(AF(:,k));
322                 Afa(1,k) = sum(Af(:,k));
323             end
324             FSMN(:,i) = AFa./Afa;
325             %nsi = FSMN;
326         end
327         obj.nsi = FSMN;
328     end
329     function obj = NTI(obj)
330         [N, len_t, loop_num] = size(obj.wvl.scalogram);
331         FTMN = zeros(N, loop_num);
332         for i=1:loop_num
333             AF = zeros(len_t,N);
334             Af = zeros(len_t,N);
335             AFa = zeros(1, N);
336             Afa = zeros(1, N);
337             for k = 1:1:N
338                 xx = (obj.wvl.scalogram(k,:,i))';
339                 for f = 1:1:len_t
340                     AF(f,k) = xx(f)*(f);
341                     Af(f,k) = xx(f);
```

```
342                 end
343                 AFa(1,k) = sum(AF(:,k));
344                 Afa(1,k) = sum(Af(:,k));
345             end
346             FTMN(:,i) = AFa./Afa;
347         end
348         obj.nti = FTMN;
349     end
350     function [slope] = H03_slope_func(obj, signal,Fs)
351         dt = 1/Fs;
352         [y x]=size(signal);
353         if y<x
354             signal=signal';
355         end
356         ziku1 = 1:2:length(signal)-1;
357         ziku2 = ziku1+1;
358         normal_signal = (signal - mean(signal)) .*max(abs(
                signal));
359         slope = (normal_signal(ziku2) - normal_signal(ziku1))
                ./dt;
360         slope = mean(abs(slope));
361     end
362     function [obj] = NSI_Features_All(obj)
363         fs = obj.wvl.fs;
364         Signal = obj.nsi;
365         [LONGS, ~] = size(Signal);
366         str = struct([]);
367     %   Signal ========================================
368         one_struct.name = 'NSI Mean';
369         one_struct.value = 1/LONGS*sum(Signal);
370         str = [str, one_struct];
371     %   Signal ========================================
372     %   one_struct.name = 'NSI std';
373     %   one_struct.value = std(Signal);
374     %   str = [str, one_struct];
375     %   Signal ========================================
376         one_struct.name = 'NSI Var';
377         one_struct.value = var(Signal);
378         str = [str, one_struct];
```

```
%    Signal ==========================================
     one_struct.name = 'NSI Slope';
     one_struct.value = obj.H03_slope_func(Signal,fs);
     str = [str, one_struct];
%    Signal ==========================================
     one_struct.name = 'NSI kurtosis';
     one_struct.value = kurtosis(Signal);
     str = [str, one_struct];
     % Signal==========================================
     one_struct.name = 'NSI skewness';
     one_struct.value = skewness(Signal);
     str = [str, one_struct];
%    Signal ==========================================
     one_struct.name = 'NSI EBI';
     one_struct.value = -sum(Signal.*log2(Signal));
     str = [str, one_struct];
%    Signal==========================================
     one_struct.name = 'NSI energy';
     Signal_energy_t = Signal.^2;
     one_struct.value = sum(Signal_energy_t);
     str = [str, one_struct];
%    Signal ==========================================
     one_struct.name = 'NSI mode';
     one_struct.value = mode(Signal);
     str = [str, one_struct];
%    Signal ==========================================
%    one_struct.name = 'Signal median';
%    one_struct.value = median(Signal);
%    str = [str, one_struct];
     obj.nsi_features_struct = str;
end
function [obj] = NTI_Features_All(obj)
     fs = obj.wvl.fs;
     Signal = obj.nti;
     [LONGS, ~] = size(Signal);
     str = struct([]);
%    Signal ==========================================
     one_struct.name = 'NTI Mean';
     one_struct.value = 1/LONGS*sum(Signal);
```

```
418         str = [str, one_struct];
419 %       Signal ==========================================
420 %       one_struct.name = 'NTI std';
421 %       one_struct.value = std(Signal);
422 %       str = [str, one_struct];
423 %       Signal ==========================================
424         one_struct.name = 'NTI Var';
425         one_struct.value = var(Signal);
426         str = [str, one_struct];
427 %       Signal ==========================================
428         one_struct.name = 'NTI Slope';
429         one_struct.value = obj.H03_slope_func(Signal,fs);
430         str = [str, one_struct];
431 %       Signal ==========================================
432         one_struct.name = 'NTI kurtosis';
433         one_struct.value = kurtosis(Signal);
434         str = [str, one_struct];
435 %       Signal==========================================
436         one_struct.name = 'NTI skewness';
437         one_struct.value = skewness(Signal);
438         str = [str, one_struct];
439 %       Signal ==========================================
440         one_struct.name = 'NSI EBI';
441         one_struct.value = -sum(Signal.*log2(Signal));
442         str = [str, one_struct];
443 %       Signal==========================================
444         one_struct.name = 'NTI energy';
445         Signal_energy_t = Signal.^2;
446         one_struct.value = sum(Signal_energy_t);
447         str = [str, one_struct];
448 %       Signal ==========================================
449         one_struct.name = 'NTI mode';
450         one_struct.value = mode(Signal);
451         str = [str, one_struct];
452 %       Signal ==========================================
453 %       one_struct.name = 'Signal median';
454 %       one_struct.value = median(Signal);
455 %       str = [str, one_struct];
456         obj.nti_features_struct = str;
```

```
457 end
458 function decision()
459     tic;
460     pea_mat = load('features\PEA_features_all.mat');
461     sr_mat = load('features\SR_features_all.mat');
462     vf_mat = load('features\VF_features_all.mat');
463     vt_mat = load('features\VT_features_all.mat');
464     [size_pea, ~] = size(pea_mat.nsi_str);
465     [size_sr, ~] = size(sr_mat.nsi_str);
466     [size_vf, ~] = size(vf_mat.nsi_str);
467     [size_vt, ~] = size(vt_mat.nsi_str);
468     pea_fp = GetStructureValue(pea_str);
469     sr_fp = GetStructureValue(sr_str);
470     vf_fp = GetStructureValue(vf_str);
471     vt_fp = GetStructureValue(vt_str);
472     fp_all=[pea_fp; sr_fp; vf_fp; vt_fp];
473     pea_label = GetStructureLabel1(pea_str);
474     sr_label = GetStructureLabel2(sr_str);
475     vf_label = GetStructureLabel3(vf_str);
476     vt_label = GetStructureLabel4(vt_str);
477     true_label=[pea_label; sr_label; vf_label; vt_label];
478     fp_score=scattermat(fp_all,true_label);
479     features_idx = [fp_score];
480     [size_f_idx, ~] = size(features_idx);
481     k_fold = 4;
482     pea_rnd_idx = randi(4, size_pea, 1);
483     sr_rnd_idx = randi(4, size_sr, 1);
484     vf_rnd_idx = randi(4, size_vf, 1);
485     vt_rnd_idx = randi(4, size_vt, 1);
486     pea_str = [pea_mat.nsi_str, pea_mat.nti_str];
487     sr_str = [sr_mat.nsi_str, sr_mat.nti_str];
488     vf_str = [vf_mat.nsi_str, vf_mat.nti_str];
489     vt_str = [vt_mat.nsi_str, vt_mat.nti_str];
490     pea_distance_k = cell(4,1);
491     sr_distance_k = cell(4,1);
492     vf_distance_k = cell(4,1);
493     vt_distance_k = cell(4,1);
494     for k=1:k_fold
495         learn_f_pea = [];
```

```
496         valid_f_pea = [];
497         learn_f_sr = [];
498         valid_f_sr = [];
499         learn_f_vf = [];
500         valid_f_vf = [];
501         learn_f_vt = [];
502         valid_f_vt = [];
503         [learn_f_pea, valid_f_pea] = Learning(pea_rnd_idx,
                k, features_idx, pea_str);
504         [learn_f_sr, valid_f_sr] = Learning(sr_rnd_idx, k,
                features_idx, sr_str);
505         [learn_f_vf, valid_f_vf] = Learning(vf_rnd_idx, k,
                features_idx, vf_str);
506         [learn_f_vt, valid_f_vt] = Learning(vt_rnd_idx, k,
                features_idx, vt_str);
507         training=toc;
508         pea_d = Valid(learn_f_pea, learn_f_sr, learn_f_vf,
                learn_f_vt, valid_f_pea);
509         sr_d = Valid(learn_f_pea, learn_f_sr, learn_f_vf,
               learn_f_vt, valid_f_sr);
510         vf_d = Valid(learn_f_pea, learn_f_sr, learn_f_vf,
               learn_f_vt, valid_f_vf);
511         vt_d = Valid(learn_f_pea, learn_f_sr, learn_f_vf,
               learn_f_vt, valid_f_vt);
512         testing=toc;
513         pea_distance_k{k,1} = pea_d;
514         sr_distance_k{k,1} = sr_d;
515         vf_distance_k{k,1} = vf_d;
516         vt_distance_k{k,1} = vt_d;
517     end
518         PEA_test=pea_distance_k{1};
519         for m = 2:size(pea_distance_k,1)
520         PEA_test = [PEA_test;pea_distance_k{m}];
521         end
522         colidx = sum(cumprod(cellfun(@isempty, PEA_test),
               2),2) + 1;
523         PEA_output = PEA_test(sub2ind(size(PEA_test), (1:
               size(PEA_test,1)).', colidx));
524         SR_test=sr_distance_k{1};
```

```
525         for m = 2:size(sr_distance_k,1)
526         SR_test = [SR_test;sr_distance_k{m}];
527         end
528         colidx = sum(cumprod(cellfun(@isempty, SR_test),
               2),2) + 1;
529         SR_output = SR_test(sub2ind(size(SR_test), (1:size
               (SR_test,1)).', colidx));
530         VF_test=vf_distance_k{1};
531         for m = 2:size(vf_distance_k,1)
532         VF_test = [VF_test;vf_distance_k{m}];
533         end
534         colidx = sum(cumprod(cellfun(@isempty, VF_test),
               2),2) + 1;
535         VF_output = VF_test(sub2ind(size(VF_test), (1:size
               (VF_test,1)).', colidx));
536         VT_test=vt_distance_k{1};
537         for m = 2:size(vt_distance_k,1)
538         VT_test = [VT_test;vt_distance_k{m}];
539         end
540         colidx = sum(cumprod(cellfun(@isempty, VT_test),
               2),2) + 1;
541         VT_output = VT_test(sub2ind(size(VT_test), (1:size
               (VT_test,1)).', colidx));
542         predicted_result=[PEA_output; SR_output; VF_output
               ; VT_output];
543         micro_macro_PR(true_label , predicted_result);
544         plotconfusion(categorical(true_label),categorical(
               predicted_result));
545         fh = gcf;
546         ax = gca;
547         ax.FontSize = 10;
548         set(fh,'Position',[0 0 350 350]);
549         set(findobj(ax,'type','test'),'fontsize',3);
550         ah = fh.Children(2);
551         ah.XLabel.String = 'True label';
552         ah.YLabel.String = 'Predicted label';
553 %       title('Confusion Matrix for Euclidean Metric', '
    Fontsize',10)
554 %       title('Confusion Matrix for fold-1', 'Fontsize
```

```
    ',10)
555         title('Confusion Matrix for \lambda=6', 'Fontsize'
                ,10)
556         set(gcf,'color','w');
557         hold on
558 end
559 function [learn_f, valid_f] = Learning(rnd_idx, k, f_idx,
        f_str)
560     learn_f = [];
561     valid_f = [];
562     [size_file, ~] = size(rnd_idx);
563     [size_f_idx, ~] = size(f_idx);
564     for i=1:size_file
565         if rnd_idx(i) ~= k
566             l_f = zeros(1, size_f_idx);
567             for f=1:size_f_idx
568                 l_f(1,f) = f_str(i, f_idx(f)).value;
569             end
570             learn_f = [learn_f; l_f];
571         else
572             v_f = zeros(1, size_f_idx);
573             for f=1:size_f_idx
574                 v_f(1,f) = f_str(i, f_idx(f)).value;
575             end
576             valid_f = [valid_f; v_f];
577         end
578     end
579 end
580 function [distance] = Valid(learn_f_pea, learn_f_sr,
        learn_f_vf, learn_f_vt, valid_f)
581     [size_v, ~] = size(valid_f);
582     distance = cell(size_v, 4);
583     lamda=6;
584     for i=1:size_v
585         test(i,:) = valid_f(i,:);
586         for j=1:size(learn_f_sr)
587             dis_sr(j,1) = lamda*(abs(test(i,1)-learn_f_sr(j,1)
                    ))+abs(test(i,2)-learn_f_sr(j,2))+abs(test(i,3)
                    -learn_f_sr(j,3));
```

```
588 %         dis_sr(j,1) = sqrt((test(i,1)-learn_f_sr(j,1))
    ^2+(test(i,2)-learn_f_sr(j,2))^2+(test(i,3)-learn_f_sr(
    j,3))^2);
589         end
590          d_sr=min(dis_sr);
591         for j=1:size(learn_f_vf)
592          dis_vf(j,1) = lamda*(abs(test(i,1)-learn_f_vf(j,1)
                ))+abs(test(i,2)-learn_f_vf(j,2))+abs(test(i,3)
                -learn_f_vf(j,3));
593 %         dis_vf(j,1) = sqrt((test(i,1)-learn_f_vf(j,1))
    ^2+(test(i,2)-learn_f_vf(j,2))^2+(test(i,3)-learn_f_vf(
    j,3))^2);
594         end
595          d_vf=min(dis_vf);
596         for j=1:size(learn_f_pea)
597          dis_pea(j,1) = lamda*(abs(test(i,1)-learn_f_pea(j
                ,1)))+abs(test(i,2)-learn_f_pea(j,2))+abs(test(
                i,3)-learn_f_pea(j,3));
598 %         dis_pea(j,1) = sqrt((test(i,1)-learn_f_pea(j,1))
    ^2+(test(i,2)-learn_f_pea(j,2))^2+(test(i,3)-
    learn_f_pea(j,3))^2);
599         end
600          d_pea=min(dis_pea);
601         for j=1:size(learn_f_vt)
602          dis_vt(j,1) = lamda*(abs(test(i,1)-learn_f_vt(j,1)
                ))+abs(test(i,2)-learn_f_vt(j,2))+abs(test(i,3)
                -learn_f_vt(j,3));
603 %         dis_vt(j,1) = sqrt((test(i,1)-learn_f_vt(j,1))^2+(
    test(i,2)-learn_f_vt(j,2))^2+(test(i,3)-learn_f_vt(j,3)
    )^2);
604         end
605          d_vt=min(dis_vt);
606          if d_sr<d_vf && d_sr<d_pea && d_sr<d_vt
607 %                distance(i,1) = d_sr;
608                 distance{i,1} = 'SR';
609                 fprintf('The signal is SR (Non-Shockable)\
                       n');
610             elseif d_vf<d_sr && d_vf<d_pea && d_vf<d_vt
611 %                distance(i,2) = d_vf;
```

```
612                 distance{i,2} = 'VF';
613                 fprintf('The signal is VF (Shockable)\n');
614             elseif d_pea<d_sr && d_pea<d_vf && d_pea<d_vt
615 %               distance(i,3) = d_pea;
616                 distance{i,3} = 'PEA';
617                 fprintf('The signal is PEA (Non-Shockable)\
                        n');
618             elseif d_vt<d_sr && d_vt<d_vf && d_vt<d_pea
619 %               distance(i,4) = d_vt;
620                 distance{i,4} = 'VT';
621                 fprintf('The signal is VT (Shockable)\n');
622         end
623     end
624 end
625 function [score_idx]=scattermat(data,Y)
626     [~, l]=size(data);
627      clases=unique(Y);
628     tot_clases=length(clases);
629     [total_length, ~]=size(data);
630     S_b=zeros(l,l);
631     S_w=zeros(l,l);
632     overallmean=mean(data);
633      for i=1:tot_clases
634         clasei = find(Y==clases(i));
635         xi=data(clasei,:);
636         mci=mean(xi);
637         xi=xi-repmat(mci,length(clasei),1);
638         S_w=S_w+((length(clasei)./total_length)*(xi'*xi));
639         S_b=S_b+((length(clasei)./total_length)*(mci-
               overallmean)'*(mci-overallmean));
640      end
641     sw=diag(S_w);
642     sb=diag(S_b);
643     score=sb/sw;
644     [~,score_idx] = maxk(score,3);
645     score = sort(score,'descend');
646     plot(score, '-*', 'linewidth',2);
647     xticks([1 2 3 4 5 6 7 8 9 10 11 12 13 14 15 16])
648     xticklabels({'\mu_{NSI}','V_{NSI}','S_{NSI}','K_{NSI}'
```

```
        ,'SK_{NSI}','EBI_{NSI}','P_{NSI}','M_{NSI} ','\mu_{
        NTI}','V_{NTI}','S_{NTI}','K_{NTI}','SK_{NTI}','
        EBI_{NTI}','P_{NTI}','M_{NTI}'});
    xlabel('Features', 'FontSize',12);
    ylabel('Scatter matrices value', 'FontSize',12);
    grid on
end
function vs = GetStructureValue(str)
    [r, c] = size(str);
    vs = zeros(r,c);
    for i=1:r
        for j=1:c
            vs(i,j) = str(i,j).value;
        end
    end
end
function ls1 = GetStructureLabel1(str)

    [ro, ~] = size(str);
    ls1 = cell(ro,1);
    for i=1:ro
            ls1{i,:} = 'PEA';
    end
end
function ls2 = GetStructureLabel2(str)
    [ro, ~] = size(str);
    ls2 = cell(ro,1);
    for i=1:ro
            ls2{i,:} = 'SR';
    end
end
function ls3 = GetStructureLabel3(str)

    [ro, ~] = size(str);
    ls3 = cell(ro,1);
    for i=1:ro
            ls3{i,:} = 'VF';
    end
end
```

```
function ls4 = GetStructureLabel4(str)
    [ro, ~] = size(str);
    ls4 = cell(ro,1);
    for i=1:ro
            ls4{i,:} = 'VT';
    end
end
function m_display()
    sr_mat = load('features\SR_features_all.mat');
    vf_mat = load('features\VF_features_all.mat');
    pea_mat = load('features\PEA_features_all.mat');
    vt_mat = load('features\VT_features_all.mat');
    [size_sr, ~] = size(sr_mat.nsi_str);
    [size_vf, ~] = size(vf_mat.nsi_str);
    [size_pea, ~] = size(pea_mat.nsi_str);
    [size_vt, ~] = size(vt_mat.nsi_str);
    sr_str = [sr_mat.nsi_str, sr_mat.nti_str];
    vf_str = [vf_mat.nsi_str, vf_mat.nti_str];
    pea_str = [pea_mat.nsi_str, pea_mat.nti_str];
    vt_str = [vt_mat.nsi_str, vt_mat.nti_str];
    pea_fp = GetStructureValue(pea_str);
    sr_fp = GetStructureValue(sr_str);
    vf_fp = GetStructureValue(vf_str);
    vt_fp = GetStructureValue(vt_str);
    fp_all=[pea_fp; sr_fp; vf_fp; vt_fp];
    pea_label = GetStructureLabel1(pea_str);
    sr_label = GetStructureLabel2(sr_str);
    vf_label = GetStructureLabel3(vf_str);
    vt_label = GetStructureLabel4(vt_str);
    true_label=[pea_label; sr_label; vf_label; vt_label];
    X=[fp_all(:,1),fp_all(:,2),fp_all(:,3),fp_all(:,4),
       fp_all(:,5),fp_all(:,6),fp_all(:,7),fp_all(:,8),
       fp_all(:,9),fp_all(:,10),fp_all(:,11),fp_all(:,12),
       fp_all(:,13),fp_all(:,14),fp_all(:,15),fp_all(:,16)
       ];
    varNames = {'\mu_{NSI}'; 'V_{NSI}'; 'S_{NSI}'; 'K_{NSI
       }';'SK_{NSI}'; 'EBI_{NSI}'; 'P_{NSI}'; 'M_{NSI} ';'
       \mu_{NTI}'; 'V_{NTI}'; 'S_{NTI}'; 'K_{NTI}';'SK_{
       NTI}'; 'EBI_{NTI}'; 'P_{NTI}'; 'M_{NTI} ';};
```

```
717     gplotmatrix(X,[],true_label,[],[],10);
718     text([.01 .07 .14 .20 .26 .32 .38 .46 .52 .57 .64 .71
            .77 .83 .90 .96], repmat(-.06,1,16), varNames, '
            FontSize',10);
719     text(repmat(-.04,1,16), [.96 .88 .82 .77 .70 .63 .57
            .51 .45 .37 .32 .26 .19 .12 .065 .01], varNames, '
            FontSize',10, 'Rotation',90);
720     x=fp_all(:,1);
721     y=fp_all(:,2);
722     z=fp_all(:,9);
723     group = cell2mat(true_label);
724     uniqueGroups = unique(group);
725         view(3)
726         grid on
727         hold on
728         for k = 1:length(uniqueGroups)
729               ind = group==uniqueGroups(k);
730               if k==1
731                   plot3(x(ind),y(ind),z(ind),'.','Color','
                        b','markersize',10);
732               elseif k==2
733                   plot3(x(ind),y(ind),z(ind),'.','Color','
                        g','markersize',10);
734               elseif k==3
735                   plot3(x(ind),y(ind),z(ind),'.','Color','
                        c','markersize',10);
736                 elseif k==4
737                   plot3(x(ind),y(ind),z(ind),'.','Color','
                        r','markersize',10);
738               end
739          end
740         xlabel('\mu_{NSI}');
741         ylabel('V_{NSI}')
742         zlabel('\mu_{NTI}')
743         legend('SR','VF','PEA','VT')
744  end
745 function scalo()
746     f = figure;
747     set(f,'Position',[0 0 800 700]);
```

```
    [~, LONGS, ~] = size(scalogram);
    mesh(scalogram);
    grid('off');
    az = 0;
    el = 90;
    view( az, el);
    set(gca,'XTickLabel',0:1:5,'XTick',1:round(LONGS/5):
       LONGS,'FontSize',12);
    set(gca,'YTickLabel',0:1:20,'YTick',1:10:200,'FontSize
       ',12);
    colorbar;
    colormap( 'jet');
    shading( 'interp');
    xlim( [0 LONGS]);
    xlabel('Time [sec]','FontSize',16);
    ylabel('Frequency [Hz]','FontSize',16);
 end
function [micro, macro] = micro_macro_PR(orig_label ,
   pred_label)
    mat=confusionmat(orig_label, pred_label);
    len=size(mat,1);
    TP=zeros(len,1);
    FP=zeros(len,1);
    FN=zeros(len,1);
    Pre=zeros(len,1);
    Re=zeros(len,1);
    F1_score=zeros(len,1);
    total = sum(sum(mat));
        for i=1:len
            subtotal=0;
            TP(i)=mat(i,i);
            FP(i)=sum(mat(:, i))-mat(i,i);
            FN(i)=sum(mat(i,:))-mat(i,i);
            subtotal=subtotal+sum(FP(i)+FN(i));
            cla=total-subtotal;
            classwiseAcc(i)=100*cla/total;
            Pre(i)=TP(i)/(TP(i)+FP(i));
            Re(i)=TP(i)/(TP(i)+FN(i));
            F1_score(i)=2*Pre(i)*Re(i)/(Pre(i)+Re(i));
```

```
784             end
785             total_correct = 0;
786             total1 = 0;
787             for i =1:len
788                 total_correct = total_correct+ mat(i,i);
789                 total1 = total1 + sum(mat(:,i));
790             end
791         overall_accuracy = 100*total_correct/total1;
792         macro.precision=mean(Pre);
793         macro.recall=mean(Re);
794         macro.fscore=mean(F1_score);
795         micro.precision=sum(TP)/(sum(TP)+sum(FP));
796         micro.recall=sum(TP)/(sum(TP)+sum(FN));
797         micro.fscore=2*micro.precision*micro.recall/(micro.
               precision+micro.recall);
798 end
```